eman ta zabal zazu

Universidad del País Vasco
Euskal Herriko Unibertsitatea

Departamento de Química Inorgánica

Development of surface treatments to improve the behavior of Ti6Al4V in orthopedic applications

Doctoral Thesis

Virginia Sáenz de Viteri Gimeno

January 2016

Universidad del País Vasco
Euskal Herriko Unibertsitatea

Departamento de Química Inorgánica

Development of protective coatings to improve the Ti6Al4V alloy behavior in orthopedic applications

Submitted for the Doctoral degree certificate at the University of the Basque Country (UPV/EHU)

Presented by

Virginia Sáenz de Viteri Gimeno

Supervisors

Dra. Gotzone Barandika Argoitia

Dra. Amaya Igartua Aranzabal

Leioa, January 2016

A mis padres, hermana, marido e hijos

Podría decir que este apartado es uno de los que más me ha costado realizar. En estos años que ha durado mi tesis, tengo tanto que agradecer que resulta complicado no dejarse a alguien sin mencionar.

En primer lugar y con especial cariño, quiero agradecer a mis directoras de tesis, la Dra. Gotzone Barandika, Profesora Titular de Química Inorgánica, y a la Dra. Amaya Igartua, Directora de la Unidad de Tribología, haberme guiado en esta etapa de mi vida. Me gustaría agradecer a Amaya la oportunidad que me brindó en su momento. Sin ella, a día de hoy, no estaría donde estoy. Por otro lado, dar millones de gracias a una de mis amigas más queridas por su apoyo constante y por haber estado a mi lado en todo momento, tanto nivel profesional como personal. En estos años hemos pasado mucho, tanto bueno como malo, y espero que nos quede mucho por pasar. Sé que el fin de esta tesis no será un punto y final en nuestra amistad. We can, Gotzone!

Me gustaría hacer especial mención a los miembros del tribunal de la tesis por haber aceptado evaluar mi trabajo. Grandes profesionales a los que tengo especial cariño y que han aceptado acompañarme en la recta final de esta etapa. Todo un placer para mí. ¡Gracias!

A mis compañeros de la unidad de tribología, mil gracias por haberme apoyado en todo momento. Raquel, gracias por tu apoyo e introducirme en el mundo de la tribocorrosión. Elena, uno de mis mayores pilares en Tekniker, ¡eres como una madre! Eskerrik asko! Xana, Gemma, me gustaría agradeceros la ayuda ofrecida con parte de la caracterización de las muestras.

A mis compañeros de mesa, que aunque no han estado directamente relacionados con mi tesis, me alegran los días. ¡Cristina, Ainara, Olatz y Francesco, mila esker por todas las risas y complicidad que tenemos! ¡¡Francesquito, eres único!!

Al grupo de Física de Superficies, no sé cómo agradeceros todos los conocimientos que me habéis transmitido y todos los procesos de deposición de capas que habéis realizado para que mi tesis pudiese seguir adelante. ¡Gracias chic@s!

Eva Urbistondo, millones de gracias por cuidar de mí y por todas las alegrías que me has dado al detectar yodo mediante fluorescencia de rayos X cuando yo misma no daba ni un duro. Javi Arzamendi, te has preocupado de mí como muy pocos lo han

hecho, no sabes cuánto te lo agradezco... No puedo olvidarme de Iban. Tu apoyo en Tekniker ha sido continuo. ¡Gracias!

Al resto de compañeros de IK4-Tekniker que me han apoyado y acompañado, mil gracias. Y en especial a ti, Unai, por ser uno de mis mayores apoyos. Pase lo que pase, siempre estás ahí. Benetan, eskerrik asko!

Al Departamento de Microbiología Clínica de la Fundación Jiménez Díaz, muchísimas gracias por llevar a cabo los ensayos de adherencia bacteriana en las muestras que os envié en su momento. Sin vuestra ayuda, habría resultado difícil darle sentido a este estudio. Jaime, quisiera agradecerte de todo corazón haberme guiado en mi tesis y haberme brindado tu ayuda en todo momento. Me aconsejaste ir a por el yodo, y sin pensármelo dos veces te hice caso. Moncho, en especial a ti, me gustaría darte las gracias por todo lo que me has ayudado. Te deseo lo mejor en Finlandia. Conchita, gracias también por haber continuado con los ensayos.

Fernando Agullo-Rueda del ICMM-CSIC, gracias por descubrirme la espectroscopia Raman. Será un placer poder coincidir contigo en un futuro.

Quiero hacer especial mención a los técnicos de los Servicios Generales de Investigación de la Universidad del País Vasco UPV/EHU (SGIker) por realizar los estudios de difracción de rayos X.

Y en cuanto a mi familia... Qué decir... Con un "gracias" me quedo corta. Siempre han estado ahí, han sido mi mayor apoyo y los que más han sufrido. Aita, ama, sois el mejor ejemplo a seguir. Apoyo incondicional. Gran parte de esta tesis os la debo a vosotros. Os quiero! Mai, mi hermana favorita, siempre a mi lado, eres la mejor, enana! Love U! Y a ti Dani, gracias, gracias y gracias por quererme de manera ilimitada y por caminar a mi lado en todo momento, mi gran compañero de viaje. Sin ti, no lo habría conseguido. Y sobre todo, gracias por darme a Javier y a Martín, mis dos soles, ¡mis Cum Laude! ¡Os quiero mis chicos! Al resto de ti@s y prim@s, gracias por animarme en todo momento. Quiero hacer especial mención a mi prima Clau. Esta tesis también va por ti.

Y por último, expresar mi más sincero agradecimiento a IK4-Tekniker por la financiación y por darme la oportunidad de realizar mi trabajo de tesis, y a la Fundación Iñaki Goenaga por concederme la beca que me permitió iniciar este estudio.

Summary

Biomaterials are of great importance in medicine due to the ability to treat, improve, or replace damaged organs or body functions. Orthopedics is one of the sectors in which the biomaterials are widely used, improving the quality of life of millions of patients. Even so, there are some problems that must be highlighted: i.e. the premature wear, the lack of osseointegration and the appearance of a bacterial infection.

In order to solve the above mentioned problems, a great effort has been devoted to the development of both new materials and surface treatments.

In the implants´ manufacture, the Ti6Al4V alloy is one of the most common biomaterials; in particular, for knee and hip prosthesis. This alloy exhibits excellent properties, such as corrosion resistance and suitable mechanical properties. Unfortunately, it has a poor tribological behavior with a low wear resistance.

With the aim of improving the behavior of the Ti6Al4V alloy and increase the lifetime of knee and hip implants, two types of coatings have been developed and characterized in this doctoral thesis.

The first approach is focused on knee implants and consists of the development of Ti-C-N coatings deposited by Physical Vapor Deposition (PVD), through the cathodic arc method. All the developed coatings exhibit better wear resistance than the bare Ti6Al4V. Additionally, one of them presents an outstanding tribocorrosion performance.

In the case of hip stem, TiO_2 coatings have been developed via Plasma Electrolytic Oxidation (PEO). With the aim of improving the osseointegration, cell-proliferation agents like Ca and P were added. The as-developed coatings have higher roughness than the Ti6Al4V substrate. Besides, they are porous and present higher wear resistance than the substrate.

Additionally, both Ti-C-N and TiO_2 coatings were doped with biocide agents. In the first case, a thin film of Ag was deposited on Ti-C-N layers by magnetron sputtering technique. In the second case, iodine was introduced into the PEO coatings. All the developed coatings have been confirmed to exhibit biocidal properties.

In conclusion, a significant improvement in the wear and corrosion behavior of the Ti6Al4V alloy has been achieved through the developed coatings. Additionally, antibacterial properties have been provided to them.

These findings are part of the work developed in the framework of the FUNCOAT project (CSD2008-00023) financed by the Spanish Minister under the CONSOLIDER INGENIO-2010 program, and by the Basque Government under the EMAITEK program.

Los biomateriales son de gran importancia en medicina debido a la capacidad que tienen de tratar, mejorar, o sustituir órganos o funciones del cuerpo dañados. Uno de los campos en los que se hace un amplio uso de los biomateriales es en ortopedia, mejorando la calidad de vida de millones de pacientes. Aun así, hay algunos problemas que deben ser resaltados: esto es, el desgaste prematuro, la falta de oseointegración y la aparición de infecciones bacterianas.

Con el fin de solventar los problemas mencionados anteriormente, se ha dedicado un gran esfuerzo al desarrollo tanto de nuevos materiales como de tratamientos superficiales.

En la fabricación de implantes, la aleación de Ti6Al4V es uno de los biomateriales más comunes; en particular, para las prótesis de rodilla y cadera. Esta aleación presenta unas excelentes propiedades, como resistencia a corrosión y propiedades mecánicas adecuadas. Desafortunadamente, posee un pobre comportamiento tribológico con una baja resistencia al desgaste.

Con el objetivo de mejorar el comportamiento de la aleación de Ti6Al4V y aumentar el tiempo de vida de los implantes de rodilla y cadera, en esta tesis doctoral se han desarrollado y caracterizado dos tipos de recubrimientos.

El primer enfoque se centra en los implantes de rodilla y consiste en el desarrollo de recubrimientos de Ti-C-N depositados por Deposición Física en Fase Vapor (PVD), mediante el método de arco catódico. Todos los recubrimientos desarrollados en esta tesis doctoral presentan una mejor resistencia al desgaste que el Ti6Al4V sin recubrir. Además, uno de ellos presenta un destacable rendimiento a tribocorrosión.

En el caso de los vástagos de cadera, se han desarrollado recubrimientos de TiO_2 mediante la Electro Oxidación por Plasma (PEO). Con la intención de mejorar la oseointegración, se han añadido agentes que fomentan la proliferación celular, como el Ca y P. Los recubrimientos así desarrollados tienen una mayor rugosidad que el sustrato de Ti6Al4V. Además, son porosos y presentan una mayor resistencia al desgaste que el sustrato.

Asímismo, tanto las capas de Ti-C-N como las de TiO_2 se doparon con agentes

biocidas. En el primer caso, se depositó una fina película de Ag sobre el recubrimiento de Ti-C-N mediante la técnica de magnetrón sputtering. En el segundo caso, se introdujo yodo en los recubrimientos de TiO_2. Se ha confirmado que todas las capas desarrolladas muestran propiedades biocidas.

En conclusión, mediante los recubrimientos desarrollados se ha logrado una mejora significativa en el comportamiento a desgaste y a corrosión de la aleación de Ti6Al4V. Además, se le ha proporcionado propiedades antibacterianas.

Estos hallazgos son parte del trabajo desarrollado en el marco del proyecto FUNCOAT (CSD2008-00023) financiado por el Ministerio Español bajo el programa CONSOLIDER INGENIO-2010, y por el Gobierno Vasco bajo el programa EMAITEK.

GLOSSARY

Symbol	Description	Units
Ø	Nominal diameter	µm
A_0	Total sample area in contact with the electrolyte	cm^2
A_{act}	Active area of the wear track	cm^2
a-C	Amorphous carbon	
B	Constant	mV
CAE	Cathodic Arc Evaporation	
CFU	Colony-forming units	
CVD	Chemical Vapor Deposition	
d	Density	g/cm^3
DLC	Diamond Like Carbon	
DRI	Device-related infection	
e	Coating thickness	µm
EDS	Energy Dispersive Spectroscopy	
EDTA	Ethylenediaminetetraacetic acid	
EIS	Electrochemical Impedance Spectroscopy	
ELI	Extra Low Interstitial	
ESB	European Society of Biomaterials	
F	Faraday constant	C/mol
FBS	Fetal Bovine Serum	
FUNCOAT	Surface Functionalisation of Materials for High Added Value Applications	

Glossary

FWHM	Full Width at Half Maximum	
GD-OES	Glow Discharge Optical Emission Spectroscopy	
h_r	Residual deep of the indentation	µm
h_t	Maximum penetration deep under load	µm
HV	Vickers Hardness	kg/mm^2
i_{act}	Current density due to corrosion	A
ICP-OES	Inductive Coupled Plasma Optical Emission Spectroscopy	
L	Length of the wear track	mm
LAFAD	Large Area Filtered Arc Deposition	
M	Molecular weight	g/mol
n	Number of electrons involved in the process	
N	Number of cycles	
nc-G	Nanocrystalline graphite	
OCP	Open Circuit Potential	
P	Total applied load	mN
PA-CVD	Plasma Assisted Chemical Vapor Deposition	
PBS	Phosphate Buffered Saline	
PEO	Plasma Electrolytic Oxidation	
PVD	Physical Vapor Deposition	
r_{act}	Specific polarization resistance of the active area	$ohm.cm^2$
R_{act}	Polarization resistance of the active area	ohm
r_p	Specific polarization resistance of the passive surface	$ohm.cm^2$

R_p	Polarization resistance	ohm
R_{pass}	Polarization resistance of the passive area outside the wear track	ohm
R_{ps}	Polarization resistance during sliding process	ohm
S	Cross section area of the wear track	cm^2
SEM	Scanning Electron Microscope	
t_{lat}	Period between two successive cycles	s
UHMWPE	Ultra High Molecular Weight Polyethylene	
W^c_{act}	Material loss due to electrochemical effect	cm^3
W_E	Energy invested in the deformation and elastically recovered	J
W^m_{act}	Material loss due to mechanical effect	cm^3
W_T	Total energy invested in the deformation (plastic + elastic)	J
W_{tr}	Material loss due to tribocorrosion effect	cm^3
XRD	X-ray Diffraction	
XRF	X-ray Fluorescence	

Chapter 1 1

INTRODUCTION

Chapter 2 39

HYPOTHESIS

Chapter 3 45

OBJECTIVES

Chapter 4 49

METHODOLOGY

Chapter 5 55

THESIS OVERVIEW

Chapter 6 67

RESULTS AND DISCUSSION

6.1. Contribution 1 69

Ti-C-N coatings developed by PVD technique pre-selection of Ti-C-N coatings

6.2. Contribution 2 95

Ti-C-N coatings developed by PVD technique: tribological and bacterial adhesion behavior of the selected coatings

6.3. Contribution 3 131

TiO_2 coatings developed by PEO technique: tribocorrosion and bacterial adhesion characterization

Chapter 7 161

CONCLUSIONS

Chapter 8 165

FUTURE PERSPECTIVES

ANNEX A 169

Instrumental Techniques

ANNEX B 199

Bibliography

ANNEX C 221

Publications and Dissamination

Chapter 1

INTRODUCTION

The field of biomaterials is on a continuous growing due to the high demand of an aging population as well as the increasing average weight of people. For example, according to Consumers Union, in 2011, in the United States there are estimations that predict that in 2030, 4 million of hip and knee prosthesis will be needed[1]. This is due to the fact that human joints suffer from degenerative diseases such as osteoarthritis (inflammation in the bone joints), osteoporosis (weakening of the bones) and trauma leading to pain or loss in function. The degenerative diseases lead to degradation of the mechanical properties of the bone due to excessive loading or absence of normal biological self-healing process.

Biomaterials can be the solution to these problems, and the surgical implantation of these artificial biomaterials of suitable shapes helps the recovery of the structure's function. However, not only the replacement surgeries have increased. Simultaneously, the revision surgeries of implants have also been incremented. These revision surgeries which cause pain for the patients are very expensive and also their success rate is rather small. The target of present researches is to develop biomaterials or surface treatments to produce implants that can serve for much longer period to cover their full lifetime without failure or revision surgery[2]. Thus, appropriate materials or treatments have to be developed that provide higher longevity, superior corrosion resistance in body environment, excellent combination of high strength and low modulus, high fatigue and wear resistance, high ductility and excellent biocompatibility, avoiding citotoxicity[3, 4].

1.1. Biomaterials: definition, applications and classification

1.1.1. Definition

The first definition of "biomaterial" obtained by consensus was conducted in 1986 by the different International Societies of Biomaterials[5]. This definition has been refined until obtaining today a biomaterial definition established by the European

[1] Vallet Regí, M., *Qué sabemos de?: Biomateriales*, Los libros de la CATARATA, Madrid, Spain, **2013**.
[2] Geetha, M.; Singh, A. K.; Asokamani, R.; Gogia, A. K., *Prog Mater Sci.* **2009**, 54, 397-425.
[3] Long, M.; Rack, H. J., *Biomaterials.* **2008**, 19, 1621-1639.
[4] Wang, K., *Mat Sci Eng A-Struct.* **1996**, 213, 134-137.
[5] Clavijo, D.; Orjuela, J.; Cardozo, C.; Torrado, A.; Covarrubias, A., *Rev Col Or Tra.* **2010**, 24, 168-

Society of Biomaterials (ESB), in which a biomaterial is defined as **a material destined to interact with the biological systems to evaluate, treat, increase or replace some tissue, organ or body function**.

1.1.2. Applications and classification

Biomaterials applications

Due to their special properties, biomaterials can be used in different applications:

- Stents, prostheses and implants
- Tools and auxiliary material in contact with living tissue
- Transport system and drug delivery
- Adhesives, sealants, cements, suture material
- Culture medium and cell proliferation

Classification of biomaterials

Concerning the different types of biomaterial, they can be classified according to their composition in three main groups:

- Polymers
- Ceramics
- Metals

In general, polymeric materials are commonly used because of their suitable flexibility and stability, but have also been utilized for low friction articulating surfaces. Ceramic biomaterials are generally used due to their hardness and wear resistance in applications such as articulating surfaces, in joints and teeth, as well as bone bonding surfaces in implants. Metallic biomaterials are used for load carrying bearing applications and must have sufficient fatigue strength to endure the rigors of daily activity (e.g. walking, chewing)[6].

177.
[6] Czenuszka, J., *Mater World.* **1996**, 4, 452-453.

Polymers

Polymers are materials consisting of large molecules (macromolecules) formed by the polymerization or union of small molecules (called monomers). Biopolymer can be both natural and synthetic. There are biostable formulations (with permanent character, particularly useful for partial or total replacement of tissues or of damaged or destroyed organs) and biodegradable formulations (with temporarily character: that is, with a proper functionality during a limited time, the necessary while the problem persists).

The main polymers used in medical and pharmacological applications are summarized in table 1.1:

Table 1.1.
Main polymers and their applications in biomaterials.

Synthetic Polymers	**Application**
Methacrylate	Contact lenses
Silicone	Breast implants, contact lenses, knuckles replacements
Polyethylene	Parts of joint prostheses
Polyethylene terephthalate	Artificial heart valves
Polyethylene glycol	Fillings, wound dressings
Polycaprolactone	Drug delivery systems, sutures
Teflon	Vascular grafts, sutures
Poly(lactic acid)	Scaffolds for tissue engineering, delivery systems

Natural Polyners	Application
Alginate	Wound dressings
Chitosan	Wound dressings
Collagen	Mold for nerve repair, scaffolds for tissue engineering
Fibrin	Haemostatic products, products for sealing tissue

Figure 1.1 shows an example of a temporary total artificial heart with different polymeric components.

Fig. 1.1. Temporary total artificial heart with polymeric components.
Source: https://en.wikipedia.org/wiki/Artificial_heart (CC BY-SA 3.0)

Ceramics

Ceramics are inorganic materials formed by metallic and non-metallic components joined by ionic and covalent bonds. Ceramics have high chemical stability against oxygen, water, acid, alkaline and saline environments, as well as organic solvents. They offer high wear resistance and they generally behave as good thermal and electrical insulators.

The main materials within this category and their more typical applications can be

seen in table 1.2:

Table 1.2.
Main ceramics and their applications in biomaterials.

Ceramic	Application
Alumina (Aluminum oxide)	Components for artificial joints, coatings for implants, dentures
Bioactive glasses	Coatings for orthopedic and dental implants, components for facial reconstruction, bone grafts
Calcium phosphate	Coatings for orthopedic and dental implants, material for dentures, material for bone grafts, bone cements

Figure 1.2 shows the crown of a dental implant made of a ceramic material.

Fig. 1.2. Dental implant.
Source: https://en.wikipedia.org/wiki/Dental_implant (CC BY-SA 3.0)

Metals

Overall, the number of metallic elements used in the manufacture of implants is very limited.

Among the main metallic materials and their most common applications, the following ones can be highlighted (Table 1.3):

Table 1.3.
Main metals and their applications in biomaterials.

Metal	Application
Cobalt-Chromium alloys	Artificial heart valves, dentures, orthopedic plates, components of artificial joints, stents
Gold and platinum	Dental fillings, electrodes for cochlear implants
Silver-tin-copper alloys	Dental amalgams
Stainless steel	Dentures, orthopedic plates, stents
Titanium alloys	Artificial heart valves, dentures, components for artificial joints, orthopedic screws, housing for pacemakers

Figure 1.3 is an example of a bare-metal stent.

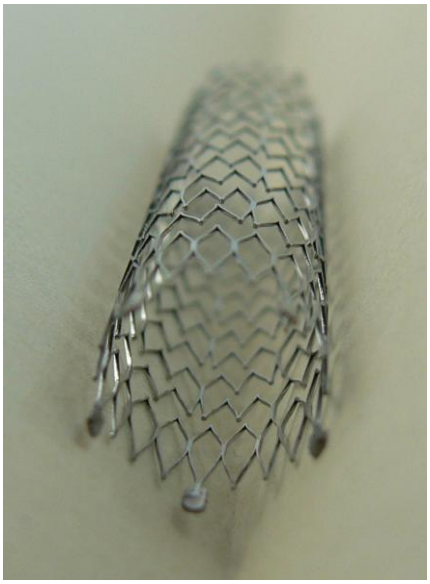

Fig. 1.3. Bare-metal stent.
Source: https://en.wikipedia.org/wiki/Bare-metal_stent (CC BY-SA 4.0)

Metallic Biomaterials

In orthopedic applications, metallic materials are the most commonly used biomaterials.

Pure metals do not have the resistance, elasticity, ductility and purity required by the different types of implants, currently used in orthopedics. For that reason, it turns to the addition of one or more metals to the base element with the aim to modify and improve their properties.

The major families of alloys most commonly used are:

- Stainless steels
- Cobalt-chromium alloys
- Titanium and titanium alloys

Stainless Steels

The most used stainless steels in implants, and more specifically in orthopedics applications, is the AISI 316L. This type of stainless steel is an iron-carbon alloy, with elements as chromium, nickel and molybdenum, and with small amounts of magnesium, phosphorous, sulfur and silicon.

The stainless steels have good corrosion resistance due to the chromium content. They have the capacity to form a spontaneous oxide layer (Cr_2O_3) on the surface when the chromium is in contact with the oxygen. Even so, these steels can be corroded in low oxygen environments because their passivation depends on this element. For this reason, these materials are appropriate for temporal implants as screws or plates.

Cobalt-chromium alloys

The ease of manufacture and the wide range of properties available for cobalt alloys, make them ideal for an extensive number of orthopedic applications. The chromium content of these alloys provides an excellent corrosion resistance (superior to that of the stainless steel). Besides, their biocompatibility makes them exceptional for prolonged clinical use. Two are the most typical cobalt-chromium alloys:

- Forged CoNiCrMo alloy: it presents good corrosion resistance, and is used in dental restorations and artificial joints.

- CoCrMo moldable alloy (obtained by casting): it presents high corrosion resistance in saline medium and under load, and is used especially in heavily loaded stems in knee and hip implants[7].

Titanium and titanium alloys

Titanium is one of the few materials that naturally matches the requirements for implantation in the human body. Among all pure titanium grades and its alloys, the mainly used materials in medical field are the commercially "pure" titanium (Ti cp, grades 1-4, purity ›99%) and Ti6Al4V (grade 5) alloy[8, 9, 10].

Titanium possesses a hexagonal closely packed crystal structure α up to a temperature of 882.5 °C. Titanium transforms into a body centered cubic structure β above this temperature[11]. Titanium alloys may be classified as α, near-α, α + β, metastable β, or stable β depending upon the room temperature microstructure[12]. The α and near-α titanium alloys exhibit superior corrosion resistance but have limited low temperature strength. In contrast, the α + β alloys exhibit higher strength due to the presence of both the α and β phases. The properties of the materials depend on the chemical composition, relative proportions of the α and β phases, thermal treatment, and thermo-mechanical processing conditions. The β alloys also offer the unique characteristic of low elastic modulus and superior corrosion resistance[13, 14]. The alloying elements for titanium, fall into three

[7] Park, B. J.; Bronzino J. D., *Biomaterials: Principles and Applications*, CRC Press, Boca Raton, Florida, USA, **2002**.
[8] Luo, Y., Biotribology of Titanium Alloys, in: Davim, P. (Ed), *Biotribology*, John Wiley & Sons, Inc, Hoboken, NJ, USA, **2013**.
[9] Pretucci, R. H.; Hardwood, W. S., *Química General: Principios y aplicaciones modernas*, PRENTICE HALL IBERIA, Madrid, Spain, **1999**.
[10] Bhushan, B.; Gupta, B. K., *Handbook of Tribology: Materials, coatings, and surface treatments*, McGraw-Hill, New York, USA, **1991**.
[11] Collings, E. W., The physical metallurgy of titanium alloys, in: Gegel, H. L. (Ed), *ASM Series in Metal Processing*, Edward Arnold Publications, Cleveland, Metal Park, OH, USA, **1984**.
[12] Polmear, J. J., *"Titanium alloys", in Light Alloys*, Edward Arnold Publications, London, UK, **1981**.
[13] Bania, P. J., Beta titanium alloys and their role in the titanium industry, in: Eylon, D.; Boyer, R. R.; Koss, D. A. (Eds), *Beta Titanium Alloys in the 1990´s*, The Minerals, Metals and Materials Society: Warrendale, Pennsylvania, USA, **1999**.
[14] Schutz, R. W., An overview of beta titanium alloy environmental behavior, in: Eylon, D.; Boyer, R. R.; Koss, D. A. (Eds), *Beta Titanium Alloys in the 1990´s*, The Minerals, Metals and Materials Society: Warrendale, Pennsylvania, USA, **1999**.

categories: (1) α-stabilizers (Al, O, N, C); (2) β-stabilizers (Mo, V, Nb, Ta, Fe, W, Cr, Si, Co, Mn, H); and (3) neutrals (Zr).

Chemical composition of the most important titanium and titanium alloys is presented in the following table (Table 1.4)[15]:

Table 1.4.
Chemical composition of main titanium and titanium alloys.

Alloy	Chemical composition (nominal wt. % max.)							
	Al	C	Fe	H	N	O	V	Ti
Ti cp-1 (α)	0	0.10	0.20	0.015	0.03	0.18	0	balance
Ti cp-2 (α)	0	0.10	0.30	0.015	0.03	0.25	0	balance
Ti cp-3 (α)	0	0.10	0.30	0.015	0.05	0.35	0	balance
Ti cp-4 (α)	0	0.10	0.50	0.015	0.05	0.40	0	balance
Ti6Al4V (α/β)	6.0	0.10	0.20	0.015	0.03	0.13	4.0	balance

Ti cp is used in dental implants because of its excellent osseointegration capacity, biocompatibility and corrosion resistance. On the other hand, Ti6Al4V alloy is the most used one between all titanium alloys for medical applications; this is due to the fact that has superior mechanical properties, corrosion resistance and biocompatibility[16, 17].

1.2. Biomaterials for orthopedic applications

The main properties that a material must have to be considered as a biomaterial for orthopedic applications are the following: to be biocompatible, not carcinogenic

[15] Textor, M.; Freese, H. L.; Volas, M. G.; Wood, J. R., Titanium and its alloys in biomedical engineering, in: Buschow, K. H. J.; Cahn, R. W.; Flemings, M. C.; Ilscher, B.; Kramer, E. J.; Mahajan, S. (Eds.), *Encyclopedia of Materials: Science and Technology*, Elsevier, Oxford, UK, **2001**.
[16] Gil, F. J.; Ginebra, M. P.; Planell, J. A., *Biomecánica*. **1999**, 13, 73-78.
[17] Ratner, J. B. B. D.; Hoffman, A. S.; Shoen, F. J.; Lemons, J. E., *Biomaterials Science: An Introduction to Materials in Medicine*, Academic Press, Altham, MA, USA, **1996**.

and chemically stable, to have appropriate mechanical properties, excellent wear and corrosion resistance, suitable size and shape, to ensure proper osseointegration, and to be reproducible and affordable.

A **biocompatible** material should not produce toxic or negative effects to the body. The materials used as implants are expected to be highly non toxic and should not cause any inflammatory or allergic reactions into human body. The success of the biomaterials is mainly dependent on the reaction of the human body to the implant[18]. The two main factors that influence the biocompatibility of a material are the host response induced by the material and the materials degradation in the body environment.

The different possible reactions of an organism against a biomaterial depend on different factors: type of material, chemical properties of the surface, porosity and hydrophobic/hydrophilic nature.

In relation to **not carcinogenic** character of the biomaterial, it is worth mentioning that there are two routes to produce the cell transformation or mutation: the chemical and the foreign-body ones. In the chemical route, the carcinogenic stimuli are given by hydrocarbon based molecules. And the foreign body route depends on the caused pain in the implantation and on the size of the implant[19].

Chemical stability means that the biomaterial must not be degraded after implantation into the body. The release of elements (ions or particles) from the implant to the surrounding tissue can provoke catastrophic effects.

The most important **mechanical properties** that help to decide the type of material are hardness, tensile and compressive strength, young modulus, fatigue strength and elongation. An implant fracture due to a mechanical failure is related to a biomechanical incompatibility. For this reason, it is expected that the material employed to replace one tissue or bone of the body has adequate mechanical properties[20, 21].

[18] Williams, D. F., *Biomaterials*. **2008**, 29, 2941-2953.
[19] Temenoff, J. S.; Mikos, A. G., *Biomaterials: The intersection of Biology and Materials Science*, Pearson/Prentice Hall, New Jersey, USA, **2008**.
[20] Black, J.; Hastings, G. W., *Handbook of biomaterials propertie,* Champan and Hall, London, UK, **1998**.
[21] Lawrence Katz, J., *Nature*. **1980**, 283, 106-107.

Wear always occurs in the articulation of artificial joints as a result of a mixed lubrication regime. The movement of an artificial hip or knee joint produces billions of microscopic particles that are rubbed off during cutting motions. These particles are trapped inside the tissues of the joint capsule and may lead to unwanted foreign body reactions. Histocytes and giant cells phagocytose "digest" the released particles and form granulomas or granuloma-like tissues. At the boundary layer between the implant and bone, they interfere with the transformation process of the bone leading to osteolysis.

Therefore, the material should have a high wear resistance and exhibit a low friction coefficient when sliding against body tissues. An increase in friction coefficient or a decrease in wear resistance can cause failure of the implant.

Regarding to biological **corrosion resistance**, it is known that all metallic implants electrochemically corrode to some extent. This is disadvantageous due to two main reasons: (1) the process of degradation reduces the structural integrity and (2) degradation products may react unfavorably with the host. Metallic implant degradation results from both electrochemical dissolution and wear, but most frequently occurs through a synergistic combination of the two[22,23]. Electrochemical corrosion process includes both generalized dissolution uniformly affecting the entire surface and localized areas of a component.

Metal implant corrosion is controlled by (1) the extent of the thermodynamic driving forces which cause corrosion (oxidation/reduction reactions) and (2) physical barriers which limit the corrosion kinetics. In practice, these two parameters, that mediate the corrosion of orthopedic biomaterials, can be broken down into a number of variables: geometric variables (e.g., taper geometry in modular component hip prostheses), metallurgical variables (e.g., surface micro-structure, oxide structure and composition), mechanical variables (e.g., stress and/or relative motion) and solution variables (e.g., pH, solution proteins and enzymes)[24].

The corrosion characteristics of an alloy are greatly influenced by the passive film

[22] Black, J., *Orthopaedic Biomaterials in Research and Practice*, Churchill Livingstone, New York, USA, 1988.
[23] Jacobs, J. J.; Gilbert, J. L.; Urban, R. M., *J Bone Joint Surg [Am]*. **1998**, 80, 268-282.
[24] Hallab, N. J.; Urban, R. M.; Jacobs, J. J., Corrosion and Biocompatibility of Orthopedic Implants, in: Yaszemski, M. J.; Trantolo, D. J.; Lewandrowski K-U.; Hasirci, V.; Altobelli D. E.;

formed on the surface of the alloy and the presence of the alloying elements.

On the other hand, a non **suitable size and shape** can cause failure of the implant due to an overload or fatigue. Therefore, the design of an implantable device has to be sufficiently developed.

Osseointegration is the capacity for joining with bone and other tissue being another important aspect of the use of metallic alloys in bone applications (Fig. 1.4). A good integration of implant with the bone is essential to ensure the safety and efficacy of the implant over its useful life. The inability of an implant surface to integrate with the adjacent bone and other tissues due to micromotions, results in implant loosening[25]. It has been shown in previous studies[26], that enhancement of the bone response to implant surfaces can be achieved by increasing the roughness or by other surface treatments[27]. Although the precise molecular mechanisms are not well understood, it is clear that the chemical and physical properties of the surface play a major role in the implant–surface interactions through modulation of cell behavior, growth factor production and osteogenic gene expression[28, 29, 30].

Wise, D. L. (Eds.), *Biomaterials in Orthopedics,* Marcel Dekker, New York, USA, **2004**.
[25] Viceconti, M.; Muccini, R.; Bemakiewicz, M.; Baleani, M.; Cristofolini, L., *J Biomech.* **2000**, 33, 1611-1618.
[26] Wennerberg, A., On surface roughness and implant incorporation. Göteborg, Sweden: Biomaterials/Handicap Research; Doctoral thesis, Institute of Surgical Sciences, Göteborgs Universitet, 1996.
[27] Carlsson, L. V.; Macdonald, W.; Magnus Jacobsson, C.; Albrektsson, T., Osseointegration Principles in Orthopedics: Basic Research and Clinical Applications, in: Yaszemski, M. J.; Trantolo, D. J.; Lewandrowski K-U.; Hasirci, V.; Altobelli D. E.; Wise, D. L. (Eds.), *Biomaterials in Orthopedics*, Marcel Dekker, New York, USA, **2004**.
[28] Junker, R.; Dimakis, A.; Thoneick, M.; Jansen, J. A., *Clin Oral Implan Res.* **2009**, 20, 185-206.
[29] Kim, H. J.; Kim, S. H.; Kim, M. S.; Lee, E. J.; Oh, H. G.; Oh, W. M.; Park, S. W.; Kim, W. J.; Lee, G. J.; Choi, N. G.; Koh, J. T.; Dinh, D. B.; Hardin, R. R.; Johnson, K.; Sylvia, V. L.; Schmitz, J. P.; Dean. D. D., *J Biomed Mater Res A.* **2005**, 74, 366-373.
[30] Vlacic-Zischke, J.; Hamlet, S. M.; Friis, T.; Tonetti, M. S.; Ivanovski, S., *Biomaterials.* **2011**, 32, 665-671.

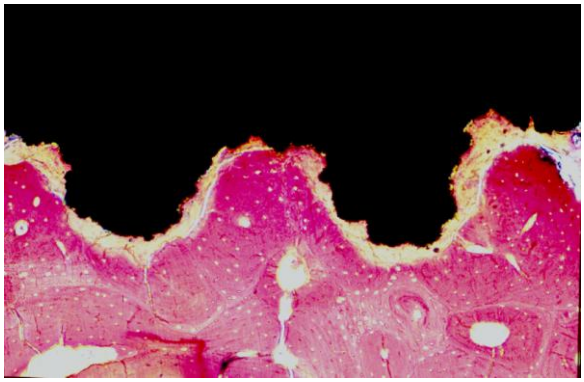

Fig.1. 4. Microscopic histological section of bone (in red) integrated to the titanium surface (in black).
Source: https://en.wikipedia.org/wiki/Osseointegration Public Domain.

Finally and not less important, the biomaterial has to be easily **reproducible** to show always the same behavior. Additionally, for economical reasons, the biomaterial should be also **affordable**. Due to the high demand of prosthesis in the last years and the predictions for the next future, the price is one factor to be taken into account when selecting a biomaterial.

1.3. Titanium-based alloys: Ti6Al4V

Ti6Al4V is the most commonly used titanium alloy in orthopedic applications. It is as strong as steel and twice as strong as aluminum, but it is 45% lighter than steel and only 60% heavier than aluminum[8].

Ti6Al4V is widely used as hard–tissue replacements in artificial bones and joints because of their outstanding characteristics such as high strength, low density, high immunity to corrosion, complete inertness to body environment, enhanced compatibility, relatively low Young´s modulus and high capacity to join with bone or other tissues. Its lower modulus, superior biocompatibility and better corrosion resistance in comparison with conventional stainless steels and cobalt-based alloys, make it an ideal choice for bio-applications[31]. However, the most important limitation of this alloy is its poor tribological behavior.

[31] Liu, X.; Chu, P. K.; Ding, C., *Mater Sci Eng R.* **2004**, 47, 49-121.

1.3.1. Properties of Ti6Al4V

Some of the main properties of Ti6Al4V alloy are described in more detail:

Wear resistance in Ti6Al4V

The fundamental drawback of Ti6Al4V alloy which limits wider use of this material include, as commented previously, its lack of wear resistance and poor tribological properties[32, 33], because of its low hardness[34]. This behavior is characterized by high coefficient of friction, severe adhesive wear with a strong tendency to seizing and low abrasion resistance[35]. Ti6Al4V biomaterial tends to undergo severe wear when it is rubbed between itself or in contact with other materials. Additionally, Ti6Al4V has tendency for moving or sliding parts to gall (severe adhesive wear) and eventually seize. This causes a more intensive wear as a result of creation of adhesion couplings and mechanical instability of passive layer of oxides, particularly in presence of third bodies (Fig. 1.5). Owing to this effect, in cases of total joint replacements made of Ti6Al4V head and polymer cup, the 10-20% of joints needs to be replaced within 15-20 years and the aseptic loosening accounts for approximately 80% of the revisions[36]. The reason for the failure of the implants is due to the high friction coefficient of this material that can lead to the release of wear debris from the implant into the bloodstream that results in an inflammation of the surrounding tissue and gives rise to the bone resorption (osteolysis)[37, 38], which ultimately leads to loosening of the implant and hence the implant has to be replaced by a new one.

[32] Fraczek, T.; Olejnik, M.; Tokarz, A., *Metalurgija*. **2009**, 48, 83-86.
[33] Kustas, F. M.; Misra, M. S., Friction and Wear of Titanium Alloys, in: Blau, P. J. (Ed.), *ASM Metals Handbook, Friction, Lubrication and Wear Technology*, ASM International, USA, **1992**.
[34] Freese, H. L.; Volas, M. G.; Wood, J. R., Metallurgy and technological properties of titanium and titanium alloys, in: Brunette, D. M.; Tengvall, P.; Textor, M.; Thomsen, P. (Eds.), *Titanium in Medicine: Material Science, Surface Science, Engineering, Biological Responses, and Medical Applications*, Springer, Berlin, Germany, **2001**.
[35] Yerokhin, A. L.; Niea, X.; Leyland, A.; Matthew, A., *Surf Coat Technol.* **2000**, 130, 195-206.
[36] Malchau, H.; Herberts, P., Revision and re-revision rate in THR: a revisión-risk study in 148.359 primary operations. Scientific exhibition. 65th annual meeting of the AAOS, New-Orlands, USA, **1998**.
[37] Chandra, A.; Ryu, J. J.; Karra, P.; Shrotriya, P.; Tvergaard, V.; Gaisser, M.; Weik, T., *J Mech Behav Biomed.* **2011**, 4, 1990-2001.
[38] Wolford, L. M., *Proc (Bayl Univ. Med. Cent.)*. **2006**, 19, 232-238.

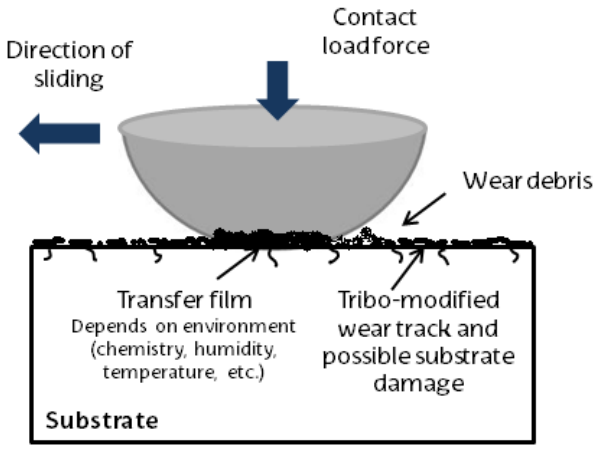

Fig. 1.5. Schematic representation of a sliding tribological coating with the presence of third bodies[39].

Corrosion behavior of Ti6Al4V

All metals and alloys are subjected to corrosion when they are in contact with body fluid. This body environment is very aggressive owing to the presence of chloride ions and proteins. A variety of chemical reactions occurs on the surface of a surgically implanted alloy. The metallic components of the alloy are oxidized to their ionic forms and dissolved oxygen is reduced to hydroxide ions. Metal ions that are released can be incorporated easily into the bloodstream, which can be very detrimental[40, 41]. This degradation of the surface of the metallic biomaterial affects various physiological processes leading to the release of proinflammatory cytokines involved in loosening of prosthesis, allergic reactions and toxicity.

The high corrosion resistance of Ti6Al4V alloy makes it the most promising biomaterials for implants. This effect is due to the fact that Ti6Al4V in general rely on the spontaneously formed extremely thin, adherent and protective titanium oxide film, which separates the metal from its environment[42, 43]. Typically, the

[39] Zabinski, J. S.; Veovodin, A. A., Ceramic and other hard coatings, in: Vizintin, J.; Kalin, M.; Dohda, K.; Jahanmir, S. (Eds.), *Tribology of Mechanical Systems: A Guide to Present and Future Technologies*, ASME Press, New York, USA, **2004**.
[40] Dunstan, E.; Ladon, D.; Whittingham-Jones, P.; Carrington, R.; Briggs, T. W., *J Bone Joint Surg (Am)*. **2008**, 90,517-522.
[41] Pandit, H.; Glyn-Jones, S.; McLardy-Smith, P.; Gundle, R.; Whitwell, E.; Gibbons, C. L. M.; Ostlere, S.; Athanasou, N.; Gill, H. S.; Murray, D., *J Bone Joint Surg Br.* **2008**, 90, 847-851.
[42] Landolt, D., *Corrosion and Surface Chemistry of Metals*, EPFL Press, Lausanne, Switzerland, **2007**.
[43] Hallab, N. J.; Urban, R. M.; Jacobs, J. J., Corrosion and Biocompatibility of Orthopedic Implants, in: Yaszemski, M. J.; Trantolo, D. J.; Lewandrowski K-U.; Hasirci, V.; Altobelli D. E.; Wise, D. L. (Eds.), *Biomaterials in Orthopedics*, Marcel Dekker, New York, USA, **2004**.

thickness of this film formed on these metals during the passivation or repassivation process, is about 3-10 nm[44]. It is known that the protective and stable oxides on titanium surface (TiO_2) are able to provide favorable osseointegration and is the major criterion for the excellent biocompatibility of Ti6Al4V alloy. The stability of the oxide depends strongly on the composition, the microstructure and thickness of the film[45, 46, 47, 48, 49].

However, the overall reaction of the human body on an implant is a system property that includes many different aspects, such as surface chemistry, implant movement, biodegradation and surgical aspects. For this reason, high corrosion resistance is required for the material to use in this biological environment. Moreover, wear debris produced from joint movement can lead to wear-corrosion causing biodegradation.

The relatively poor tribological properties and possible corrosion problems have led to the development of surface treatments to effectively increase near-surface strength, improving the hardness and abrasive/adhesive wear resistance thereby reducing the coefficient of friction as well as avoiding or reducing the transference of ions from the surface or bulk material to the surrounding tissue.

1.3.2. Applications of Ti6Al4V

Concerning the medical applications of titanium and its alloys, the use of cp Titanium is more limited to the dental implants because of its limited mechanical properties. In cases where good mechanical characteristics are required as in hip or knee implants, bone screws, and plates, Ti6Al4V alloy is being used[50, 51]. One of the most common applications of Ti6Al4V alloy is artificial hip joints that consist of an

[44] Neoh, K. G.; Hu, X.; Zheng, D.; Tang Kang, E., *Biomaterials.* **2012**, 33, 2813-2822.
[45] Zhu, X.; Chen, J.; Scheideler, L. R.; Reichl, R.; Geis-Gerstorfer, J., *Biomaterials*, **2004**, 25, 4087-4103.
[46] Williams, J. M.; Bucharan, R. A., *Mater Sci Eng.* **1985**, 69, 237-246.
[47] Magaziner, R. S.; Jain, V. K.; Mall, S., *Wear.* **2009**, 267, 368-373.
[48] Everitt, N. M.; Ding, J.; Bandak, G.; Shipway, P. H.; Leen, S. B.; Williams, E. J., *Wear.* **2009**, 267, 238-291.
[49] Dalmaglio, M.; Schaaff, P.; Holzwarth, U.; Chiesa, R.; Rondelli, G., *J Biomed Mater Res A.* **2008**, 86B, 407-416.
[50] Stadlinger, B.; Ferguson, S. J.; Eckelt, U.; Mai, R.; Lode, A. T.; Loukota, R.; Sclotting, F., *Brit J Oral Max Surg.* **2012**, 50, 74-79.
[51] Subramani, K.; Mathew, R. T., Titanium Surface Modification. Techniques for Dental Implants – From Microscale to Nanoscale, in: Subramani, K.; Ahmed, W. (Eds.), *Emerging Nanotechnologies in Dentistry: Materials, Processes and Applications*, William Andrew, Elsevier, Oxford, UK, **2012**.

articulating bearing (femoral head and cup) and stem[52] (Fig. 1.6), where metallic cup and hip stem components are made of titanium. As well, they are also often used in knee joint replacements, which consist of a femoral and tibial component made of titanium and a high molecular weight polyethylene articulating surface.

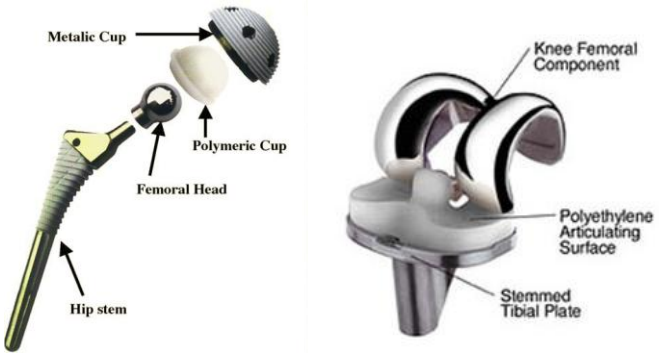

Fig. 1.6. Schematic diagram of artificial hip joint (left) and knee implant[53] (right).

1.4. Most common failure reasons in artificial joints

Bone and its several associated elements – cartilage, connective tissue, vascular elements and nervous components – act as functional organs. They provide support and protection for soft tissues and act together with skeletal muscles to make body movements possible. Bones are relatively rigid structures and their shapes are closely related to their functions. Bone metabolism is mainly controlled by the endocrine, immune and neurovascular systems, and its metabolism and response to internal and external stimulations are still under assessment[54].

Long bones of the skeletal system are prone to injury, and internal or external fixation is a part of their treatment. Joint replacement is another major intervention where the bone is expected to host biomaterials. Response of the bone to biomaterial intervenes in the regeneration process. Materials implanted into the bone will cause local and systemic biological responses even if they are known to be inert. Host responses with joint replacement and fixation materials will initiate

[52] Jacobs, J. J.; Gilbert, J. L.; Urban, R. M., *J Bone Joint Surg (Am)*. **1998**, 80, 268-282.
[53] http://www.hss.edu/conditions_arthritis-of-the-knee-total-knee-replacement.asp.
[54] Korkusuz, P.; Korkusuz, F., Hard Tissue – Biomaterial Interactions, in: Yaszemski, M. J.; Trantolo, D. J.; Lewandrowski K-U.; Hasirci, V.; Altobelli D. E.; Wise, D. L. (Eds.), *Biomaterials in Orthopedics,* Marcel Dekker, New York, USA, **2004**.

an adaptive and reactive process[55].

Artificial biomaterials are the solution to these problems and the surgical implantation of these artificial biomaterials of suitable shapes helps to restore the function of the otherwise functionally compromised structures. However, not only the replacement surgeries have increased, simultaneously the revision surgery of hip and knee implants have also increased. Thus, development of appropriate material or surface treatment with improved properties, in terms of wear, corrosion and osseointegration is highly essential.

In this sense, the most typical problems in joints are described below.

1.4.1. Wear

In the human body, there are tribological contacts created due to locomotion that contributes to the accelerated degradation of the biomaterial[56, 57, 58]. This can lead to crack initiation, wear debris release from the implant into bloodstream or early implant fracture, as well as serious inflammatory reactions, osteolysis or allergies, which can significantly shorten the life in service of the implanted device[59, 60, 61, 62].

A very common tribological effect in orthopedic implants is that, apart from the loads that have to support, they are subjected to another wear process produced by vibration, called fretting. This effect occurs when two surfaces that are in contact suffer reciprocated micro-movements of very low amplitude (‹150 microns). This type of wear takes place, for example, in knee implants, producing the elimination of mounts of polyethylene and Ti6Al4V alloy debris[63] due to the wear produced between the backside of the ultra-high molecular weight polyethylene (UHMWPE) patellar component and the tibial tray of fixed bearing tibial component made of Ti6Al4V. And in non-cemented hip implants, where the thick coating of calcium

[55] Santavirta, S.; Gristina, A.; Konttinen, Y. T., *Acta Orthop Scand.* **1992**, 63, 225-232.
[56] Manhabosco, T. M.; Tamborim, S. M.; dos Santos, C. B.; Müller, I. L., *Corros Sci.* **2011**, 53, 1786-1793.
[57] Diomidis, N.; Mischler, S.; More N. S.; Manish, R., *Acta Biomater.* **2012**, 8, 852-859.
[58] Niinomi, M., *J Mech Behav Biomed.* **2008**, 1, 30-42.
[59] Diomidis, N.; Mischler, S., *Tribol Int.* **2011**, 44, 1452-1460.
[60] Williams, S.; Tipper, J. L.; Ingham, E.; Stone, M. H.; Fisher, J., *P I Mech Eng H.* **2003**, 217, 155-163.
[61] Contu, F.; Elsener, B.; Böhni, H., *Electrochim Acta*, **2004**, 50, 33-41.
[62] Chandra, A.; Ryu, J. J.; Karra, P.; Shrotriya, P.; Tvergaard, V.; Gaisser, M.; Weik, T., *J Mech Behav Biomed.* **2011**, 4, 1990-2001.
[63] Billi, F.; Sangiorgio, S. N.; Aust, S.; Ebramzadeh, E., *J Biomech.* **2010**, 43, 1310-1315.

phosphate, hydroxyapatite, glasses, and other materials[64, 65, 66] deposited on the stem, may delaminate or fail under fatigue, leading to a potential source of a third-body wear phenomenon generating a possible loosening of the implant (Fig. 1.7).

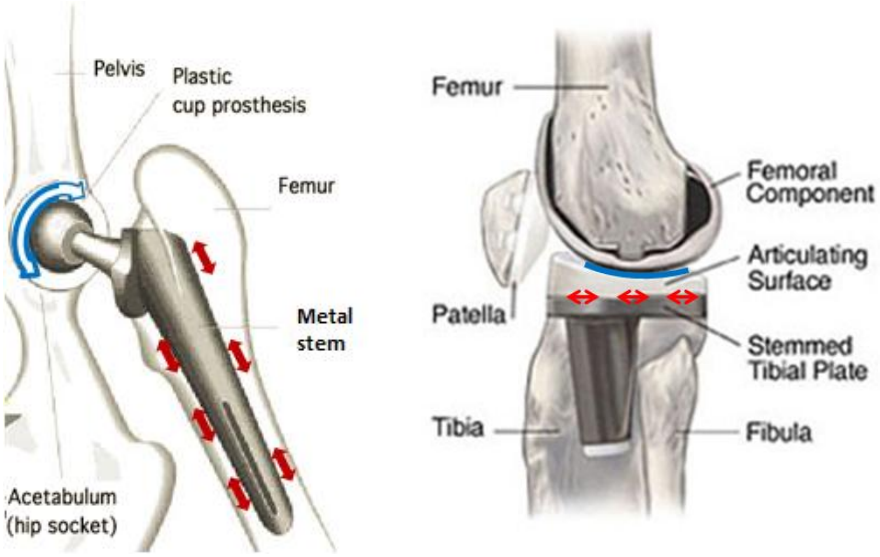

Fig. 1.7. Wear problems in joint (left) and knee[67] (right) implants.

As well, the presence of tribological effects in a corrosive media like the human fluids give rise to a phenomenon called tribocorrosion. Tribocorrosion can be defined as a form of solid surface alteration that involves the joint action of relatively moving mechanical contact with chemical reaction in which the result may be different in effect that either process acting separately[68]. In other words, tribocorrosion is a term used to refer to material degradation resulting from a combination of tribological and corrosion processes[69]. Degradation products, as metal ions and wear particles removed during tribocorrosion effect, can affect on the surrounding body tissue and cause a significant impact on the lifetime of implants.

[64] Jacobs, J. J.; Goodman, S. B.; Sumner, D. R.; Hallab, N. J., Biologic response to orthopaedic implants, in: Buckwalter, J. A.; Einhorn, T. A.; Simon, S. R. (Eds.), *Orthopaedic Basic Science*, Rosemont, IL, American Academy of Orthopaedic Surgeons, **2000**.
[65] Goosen, J. H.; Kums, A. J.; Kollen, B. J.; Verheyen, C. C., *Arch Orthop Trauma Surg.* **2008**, 129, 1165-1169.
[66] Pilliar, R.M., *Orthop Clin North Am.* **2005**, 36, 113-119.
[67] https://www.hss.edu/conditions_understanding-implants-in-knee-and-hip-replacement.asp.
[68] ASTM G40-13, Standard Terminology Relating to Wear and Erosion.
[69] Azzi, M.; Klemberg-Sapieha, J. E., Tribocorrosion test protocols for sliding contacts, in: Landolt, D.; Mischler, S. (Eds.), *Tribocorrosion of Passive Metals and Coatings*, Woodhead Publishing Limited, Oxford, UK, **2011**.

1.4.2. Bacterial adhesion

Post-operative prosthesis infection is a severe complication of joint replacements surgery that needs large-scale, typically two stage, revision surgeries and long-term antibiotic treatments[70, 71, 72]. Most of the purulent prosthesis infections that develop

very early, less than 1 month after the surgery, are caused by virulent bacteria (e.g. *Staphylococcus aureus* and *Staphylococcus epidermidis*). On the other hand, delayed infections occur 3-24 months after implantation as late chronic infections. It can be estimated that approximately 1/3 of deep device-related infections occur as early infections, and most of the rest as late infections[73].

A device-related infection (DRI) is an infection in a patient with a device that was in use for at least 48 hours before the onset of infection[74, 75]. The presence of an implanted device significantly reduces the number of bacteria required to produce infection, owing to the creation of an immunologically compromised zone adjacent to the implant. Within this zone, the ability of the host to clear not desired bacteria may be complicated, and this can lead to biofilm formation on the surface of the biomaterial. This is observed for all medical devices, ranging from fracture fixation implants and prosthetic joints to catheters, shunts, stents, and prosthetic heart valves[76]. Often the only solution to an infected implanted device is its surgical removal[77].

The diagnosis and treatment of prosthetic joint infections is further complicated by the development of a bacterial biofilm. This structure allows bacteria to resist antimicrobial agents and immune responses. Patients with this type of infection

[70] Zimmerli, W.; Trampuz, A.; Ochsner, P. E., *N Engl J Med.* **2004**, 351, 1645-1654.
[71] Jämsen, E.; Furnes, O.; Engesaeter, L. B.; Konttinen, Y. T.; Odgaard, A.; Stefánsdóttir, A.; Lidgren L., *Acta Orhtop.* **2010**, 81, 660-666.
[72] Pajarinen, J.; Mackiewiez, Z.; Pöllänen, R.; Takagi, M.; Epstein, N. J.; Ma, T.; Goodman, S. B.; Konttinen, Y. T., *J Biomed Mater Res.* **2010**, 92A, 1528-1537.
[73] Takakubo, Y.; Berce, A.; Trebse, R.; Tamaki, Y.; Milosev, I.; Al- Samadi, A.; Tiainen, V.M.; Konttinen, Y. T., Wear and corrosion in the loosening of total joint replacements (TJRs), in: Yan, Y. (Ed.), *Bio-tribocorrosion in biomaterials and medical implants*, Woodhead Publishing Limited, Oxford, UK, **2013**.
[74] Singhai, M.; Malik, A.; Shahid, M.; Malik, M. A.; Goyal, R., *J Glob Infect Dis.* **2012**, 4, 193-198.
[75] Garner, J. S.; Jarvis, W. R.; Emori, T. G.; Horan, T. C.; Hughes, J. M., *Am. J Infect Control.* **1988**, 16, 128-140.
[76] Rochford, E. T.; Richards, R. G.; Moriarty, T. F., *Cli. Microbiol Infect.* **2012**, 18, 1162-1167.
[77] Katsikogianni, M.; Missirlis, Y. F., *Eur Cell Mater.* **2004**, 8, 37-57.

require a longer period of antibiotic therapy and repeated surgical procedures[78].

The adherence process depends largely on the surface and near-surface atomic structure and composition of implanted biomaterials[79, 80, 81]. Factors influencing the bacteria adherence to a biomaterial surface include chemical composition of the

material, surface charge, hydrophobicity, as well as surface topography (roughness) and/or physical configuration. It would be desirable to develop biomedical coatings for implants which are repellent to bacteria to minimize the colonization of the implant surface with circulating planktonic bacteria that can lead to biofilm development[82, 83].

1.4.3. Lack of osseointegration

The chemical composition of bone depends on the location, age, eating background and illnesses. In general, the mineral or inorganic phase constitutes the 60-70% of the tissue, basically composed of hydroxyapatite; contains between 10% and 20% of water; and most of the rest is an organic phase. This last is composed of 90-96% of collagen and 5% of cellular components[84]. The mineral phase is the responsible of providing hardness and resistance to the bone.

The hydroxyapatite, $Ca_{10}(PO_4)_6(OH)_2$, is the most stable form of calcium phosphate. It has a Ca:P ratio of 1.67, whereas the bone mineral itself has Ca:P ratios ranging from 1.37-1.87[85].

There are four types of cells in bone (Fig. 1.8): osteoprogenitor, osteoblast, osteocyte and osteoclast. Osteoprogenitor cells are divided themselves to produce additional cells. Some of these produced daughter cells differentiate into osteoblasts, the cells that produce bone matrix. Once the osteoblasts cannot

[78] Perez-Tanoira, R.; Perez-Jorge, C.; Endrino, J. L.; Gomez-Barrena, E.; Horwat, D.; Pierson, J. F.; Esteban, J., *J Biomed Mater Res A.* **2012**, 100, 1521-1528.
[79] Cordero, J.; Munuera, L.; Folgueira, M.D., *Injury.* **1996**, 27, SC34-7.
[80] Gristina, A. G., *Science.* **1987**, 237, 1588-1595.
[81] An, Y. H.; Friedman, R. J., *J Biomed Mater Res.* **1998**, 43, 338-348.
[82] Perez-Jorge, C.; Conde, A.; Arenas, M. A.; Perez-Tanoira, R.; Matykina, E.; de Damborenea, J. J.; Gómez-Barrena, E.; Esteban, J., *J Biomed Mater Res. A.* **2012**, 100, 1696-1705.
[83] Perez-Tanoira, R.; Isea-Pena, M. C.; Celdran, A.; Garcia-Vasquez, C.; Esteban, J., *Surg Infect (Larchmt).* **2014**, 15, 90-93.
[84] Kaplan, F. S.; Hayes, W.; Keaveny, T.; Boskey, A.; Einhorn, T.; Iannotti, J., Forma y función del hueso., in: Simon, S. R. (Ed.), *Ciencias básicas en ortopedia*, America Academy of Orthopaedic Surgeons, 135-191, **1997**.

produce more bone matrix, they become osteocytes, which maintain bone. Just as the human body has the ability to make bone matrix, it also has the ability to degrade bone matrix. The cell that degrades bone matrix is the osteoclast[86].

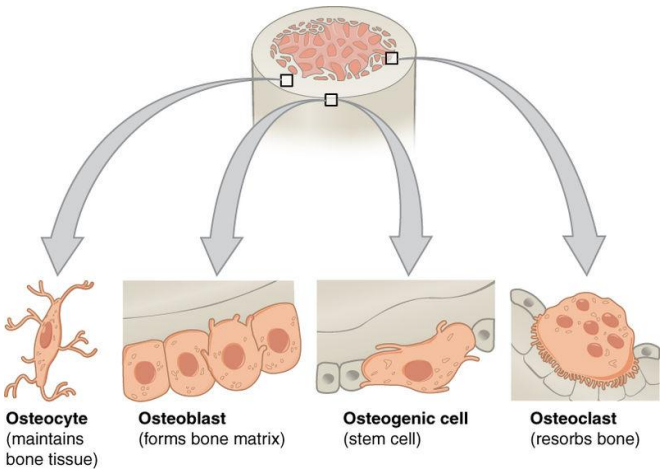

Fig. 1.8. Type of cells in bone.
Source: http://cnx.org/content/col11496/1.6/ (CC BY 3.0)

When an implant is surgically placed within bone, there are numerous biological, physical, chemical, thermal and other factors functioning that determine whether or not osseointegration will occur.

It is of great interest to ensure a good osseointegration between the implant and the tissue because the higher the mechanical stability, the lower the probability of losing the implant. The interaction between the implant and the tissue depends on[87, 88]:

- *Surface topography*: Increased surface roughness and topological features provide increased material surface area for protein adsorption.
- *Chemistry*: The chemical composition of a substrate surface dictates the types of bond between proteins and material surface.

[85] http://www.doitpoms.ac.uk/tlplib/bones/structure.php.
[86] Clark, R. K., *Anatomy and Physiology: Understanding the Human Body*, Jones and Bartlett Learning, Burlington, USA, **2005**.
[87] Dee, K. C.; Puleo, D. A.; Bizios, R. P., Protein-surface interactions, in: Dee, K. C.; Puleo, D. A.; Bizios, R. P. (Eds.), *An introduction to tissue-biomaterial interactions*, John Wiley and Sons, Hoboken, NJ, USA, **2002**.
[88] Horbett, T. A., The role of adsorbed proteins in tissue response to biomaterials, in: Ratner, B. D.; Hoffman, A. S.; Schoen, F.J.; Lemons, J. E. (Eds.), *Biomaterials science*, Elsevier Academic Press, San Diego, USA, **2004**.

- *Hydrophobicity*: Hydrophobic surfaces tend to bind more proteins, while hydrophilic surfaces tend to resist protein adsorption.
- *Heterogeneity*: The lack of uniformity of the surface creates more opportunities for interaction.
- *Charge*: Opposite electric charges between the surface and protein promote increased protein adsorption, while similar charges tend to reduce protein adsorption.

Furthermore, it is known that even if initial implant stability is achieved, the bone may retreat or be isolated from the implant because of different reasons or situations listed below:

- Reaction of the implant with a foreign body as debris from implant component degradation or wear or due to toxic emissions from the implant[89].
- Damage or lesion to the bone through mechanical trauma surgery.
- Imposition of abnormal or unphysiological conditions on the bone, such as fluid pressures or motion against implant components.
- Alteration to the mechanical signals encouraging bone densification; strain reductions or stress-shielding of replaced or adjacent bone.

Titanium and its alloys have been widely used for dental and orthopedic implants under load-bearing conditions because of their good biocompatibility coupled with high strength and fracture toughness. Despite reports of direct bonding to bone, they do not form a chemical bond with bone tissue. For the last decade, various coatings have been attempted to provide titanium and its alloys with bone-bonding ability, which spontaneously bond to living bone. Hydroxyapatite plasma spray coatings are widely used in cementless hip replacement surgery, but the hydroxyapatite coating, although exhibiting a very good biocompatibility, presents some disadvantages including delamination of the coating layer from the substrate, difficulties in controlling the composition of the coating layer and degradation of the coating layer itself, which can release debris becoming a source

[89] Montanaro, L.; Campoccia, D.; Arciola, C. R., *Int J Artif Organs.* **2008**, 31, 771-776.

of third body wear[90].

A strong and durable bone to implant connection can be achieved by the formation of a stable bone tissue at the bone-implant interface by proper implant surface treatments, as can be electrochemical deposition, dipping, physical vapor deposition and plasma electrolytic oxidation techniques[91].

1.5. Surface treatments for Ti6Al4V in orthopedic applications

Surface treatments can play a significant role in extending the performance of orthopedic devices made of Ti6Al4V several times beyond its natural capability.

The main objectives of surface treatments principally consist of the improvement of the tribological behavior, corrosion resistance, biocide capacity and osseointegration of implants. There are coatings for enhanced wear and corrosion resistance by improving the surface hardness or resistance of the material. Some surface modifications techniques that can be applied to achieve these objectives could be surface oxidation, physical deposition methods like ion implantation and plasma spray coatings, as well as thermo-chemical surface treatments such as nitriding, carburizing and boriding[92, 93].

In this work, two surface treatment techniques have been used to develop coatings with different properties, Physical Vapour Deposition (PVD) and Plasma Electrolytic Oxidation (PEO). These two treatments are explained in more detail in the following sections.

1.5.1. Physical Vapor Deposition (PVD)

Vapor techniques are based on the formation of a vapor of the material to be deposited to condense it on the surface of the substrate forming a solid deposit as thin coating. Generally, the process must be carried out in vacuum or in controlled atmosphere to avoid the interaction between the vapor and the air as well as the

[90] Liu, F.; Wang, F.; Shimizu, T.; Igarashi, K.; Zhao, L., *Surf Coat Tech.* **2005**, 199, 220-224.
[91] Kokubo, T.; Kim, H. M.; Miyaji, F.; Nakamura, T., *J Biomed Mater Res.* **1996**, 32, 409-417.
[92] Carapeto, A. P.; Serro, A. P.; Nunes, B. M. F.; Martins, M. C. L.; Todorovic, S.; Duarte, M. T.; André, V.; Colaço, R.; Saramago, B., *Surf Coat Tech.* **2010**, 204, 3451-3458.
[93] Ma, G.; Gong, S.; Lin, G.; Zhang, L.; Sun, G., *Appl Surf Sci.* **2012**, 258, 3045-3050.

adsorption of the gaseous components present in the air on the surface of the substrate.

Figure 1.9 shows a diagram of a deposition process, common to all deposition techniques from the vapor phase. In all of them, the vapor of the material to be deposited is generated from a source and is subsequently condensed on the substrate and on the reactor or chamber walls where the process takes place. The variations among the different techniques lies in the nature of the vapor source (solid, liquid or gas) or in the method used to produce it (chemical reaction, heating, charged particles bombardment, photons, plasma, etc.). This allows classifying the different methods in two large groups[94]:

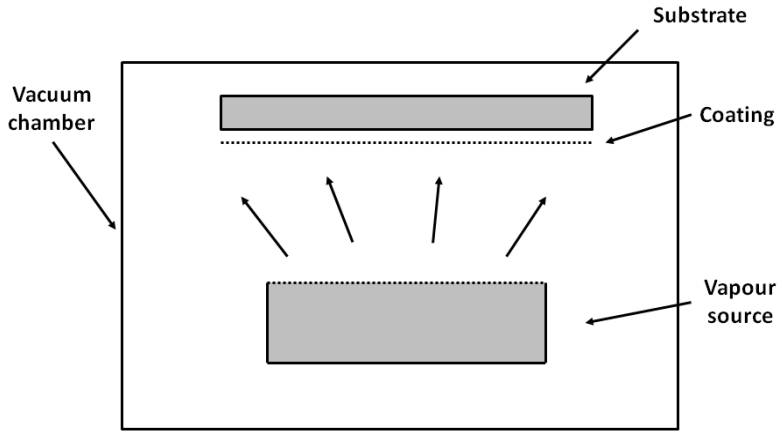

Fig. 1.9. Diagram of the deposition process from the vapor.

- *Chemical techniques* ("Chemical Vapor Deposition" or CVD): It starts directly from gases (sometimes in the liquid form that pass to vapor state) which, by chemical reaction, give a new product that is condensed as a thin film on the substrate.

- *Physical techniques* ("Physical Vapor Deposition" or PVD): It comes from a solid material (the one which is going to be deposited) to turn it into vapor by heating (evaporation) or bombardment with energetic particles (ions, electrons, photons).

In PVD technology, there are different methods: cathodic arc deposition, electron

[94] Albella, J. M., Introducción: Ciencia y tecnología de capas delgadas, in: Albella, J. M. (Ed.), *Láminas delgadas y recubrimientos. Preparación, propiedades y aplicaciones*, CSIC, Madrid, **2003**.

beam physical vapor deposition, pulse laser deposition, and magnetron sputter deposition.

In some biomedical applications, mainly in orthopedics field, continuously sliding contact is required, subjecting the implant to aggressive and corrosive situations. To achieve and maintain higher efficiency and durability under such increasingly more severe sliding and corrosive conditions, protective and/or solid hard coatings are becoming prevalent. One possible alternative to solve tribological and corrosion problems is to protect the alloy surface by means of a biocompatible hard coating as diamond-like carbon (DLC), transition-metal carbides (TiC), nitrides (TiN), or a combination of hard phases, such as TiN and TiC[95, 96, 97, 98] .

"Diamond-Like-Carbon" is a generic term referring to amorphous carbon films, deposited by either Physical Vapor Deposition or Chemical Vapor Deposition. DLC coatings basically consist of a mixture of diamond (sp^3) and graphite (sp^2). The relative amounts of these two phases will determine much of the coating properties. Both, the mechanical and tribological properties of DLC coatings have been studied for about 30 years, and several different types of DLC coatings can currently be found. DLC films are attractive biomedical materials due to their relatively high hardness, low friction coefficient, achieved by the solid lubricant generated by the formation of carbonous transfer layer on the sliding surface due to the graphite and amorphous carbon contents[99, 100], good chemical stability and excellent bio and hemocompatibility[101, 102, 103, 104].

The tribological behavior of DLC films requires a solid background on the chemical and structural nature of these films, which, in turn, depends on the deposition process and/or parameters. The chemical composition, such as the hydrogen

[95] Mändl, S.; Rauschenbach, B., *Surf Coat Technol.* **2002**, 156, 276-283.
[96] Shtansky, D. V.; Levashov, E.A.; Glushankova, N. A.; D´yakonova, N. B.; Kulinich, S. A.; Petrzhik, M. I.; Kiryukhantsev-korneev, F. V.; Rossi, F., *Surf Coat Technol.* **2004**, 182, 101-11.
[97] Hauert, R., *Diamond Relat Mater.* **2003**, 12, 583-589.
[98] Sánchez-López, J. C.; Abad, M. D.; Carvalho, I.; Escobar Galindo, R.; Benito, N.; Ribeiro, S.; Henriques, M.; Cavaleiro, A.; Carvalho, S., *Surf Coat Technol.* **2012**, 206, 2192-2198.
[99] Kustas, F. M.; Misra, M. S., Friction and Wear of Titanium Alloys, in: Blau, P. J. (Ed.), *ASM Metals Handbook, Friction, Lubrication and Wear Technology*, ASM International, USA, **1992**.
[100] Ronkainen, H.; Holmberg, K., *Environmental and Thermal Effects on the Tribological Performance of DLC Coatings*, Springer, Berlin, Germany, **2008**.
[101] Dowling, D. P., *Diam Relat Mater.* **1997**, 6, 390-393.
[102] Ma, G.; Gong, S.; Lin, G.; Zhang, L.; Sun, G., *Appl Surf Sci.* **2012**, 258, 3045-3050.
[103] Zhang, L.; Lv, P.; Huang, Z. Y.; Lin, S. P.; Chen, D. H.; Pan, S. R.; Chen, M., *Diam Relat Mater.* **2008**, 17, 1922.1926.

and/or nitrogen content or the presence of other alloying elements, controls the mechanical and tribological properties of a sliding pair consisting of DLC on one or both sliding surfaces[105]. For example, DLC samples containing different concentrations of titanium have also been examined "in vitro" to obtain a biocompatible surface that is hard, preventing abrasion and scratching[106]. Meanwhile, the nitrogen reduced the internal stresses in DLC coatings[107] and at low concentrations it was proved that reduces the friction coefficient and wear rates[108, 109, 110].

TiN coatings are also used to enhance the surface wear and corrosion properties because of their high hardness, high adhesion strength to the substrate, low friction coefficient, excellent wear resistance and good chemical stability[111, 112, 113].

TiC coatings have a combination of very high hardness, high melting temperature, and excellent thermal stability. Due to its abrasion resistance, it can be used in abutment parts of dental implants and sliding parts of artificial joints[114].

As commented above TiC and TiN films are used as protective coatings, but they can hardly satisfy the requirements under some severe conditions. There are studies that have shown that Ti-C-N coating is a solid solution of TiN and TiC, incorporating the advantages and characteristics of both coatings, like the high hardness of TiC film as well as the high ductility and adhesion strength of TiN layer[115]. Ti-C-N coatings have higher hardness, superior thermal and chemical stability, low friction coefficient and excellent wear resistance (Table 1.5). The

[104] Zheng, Y.; Liu, D.; Liu, X.; Li, L.,*Biomed Mater.* **2008**, 3, 44103-44109.
[105] Fontaine, J.; Donnet, C.; Erdemir, A., *Fundamentals of the Tribology of DLC Coatings*, Springer, Berlin, Germany, **2008**.
[106] Hauert, R.; Knoblauch-Meyer, L.; Francz, G.; Schroeder, A.; Wintermantel, E., *Surf Coat Technol.* **1999**, 120-121, 291-296.
[107] Koskinen, J.; Hirvonen, J. P.; Levoska, J.; Torri, P., *Diam Relat Mater.* **1996**, 5, 669-673.
[108] Grill, A.; Patel, V., *Diam Relat Mater.* **1993**, 2, 1519-1524.
[109] Grill, A.; Patel, V., *Diamond Film Technol.* **1992**, *2, 25-29.*
[110] Prioli, R.; Zanette, S. I.; Caride, A. O.; Franceschini, D. F.; Freire Jr., F. L., *J Vac Sci Technol A.* **1996**, 14, 2351-2355.
[111] Wang, C. T.; Gao, N.; Gee, M. G.; Wood, R. J. K.; Langdon, T. G., *J Mech Behav Biomed Mater.* **2013**, 17, 166-175.
[112] Deng, B.; Tao, Y.; Guo, D., *Appl Surf Sci.* **2012**, 258, 9080-9086.
[113] Lin, N.; Huang, X.; Zhang, X.; Fan, A.; Qin, L.; Tang, B., *Appl Surf Sci.* **2012**, 258, 7047-7051.
[114] Zhu, Y.; Wang, W.; Jia, X.; Akasaka, T.; Liao, S.; Watari, F., *Appl Surf Sci.* **2012**, 262, 15-158.
[115] Erturk, E.; Knotek, O.; Burgmer, W.; Prengel, H.G.; Heuvel, H.J.; Dederichs, H.G.; Stossel, C., *Surf Coat Technol.* **1991**, 46, 39-46.

presence of carbon acts as lubricant decreasing friction and wear[116, 117, 118]. Besides, the TiC provides superior abrasive wear resistance, while TiN reduces wear[119] and resists adhesive wear and built-up edge formation as well as increases oxidation resistance. It also acts as a chemical barrier to diffusion wear[120, 121].

Table. 1.5.

Hardness and friction coefficient of TiN, TiC and TiCN coatings[122].

Property	TiN	TiC	TiCN
Hardness (HV)	2500	3600	3000
Friction coefficient[123]	0.7	0.2	0.25

From a biological point of view, there is a serious clinical problem consisting of the formation of bacterial colonies on metal surfaces of implants. Nowadays, due to the lack of effectiveness of the antibiotics in antibacterial treatments, many bacteria are immune to the antibiotics after treatment. Due to the development of new bacteria strains, resistant to currently used antibiotics[124], the bactericidal properties are the most desired features in implants field. In this sense, silver has been used as antibacterial agent due to its good natural biocide properties[125, 126]. Physical Vapor Deposition is a suitable technique to develop silver thin films.

At the beginning of this thesis work, in which the activity related to the state of the art of coatings is described, the development of Ti-C-N coatings for medical applications is approached by different technologies like CVD (chemical vapor deposition), LAFAD (large area filtered arc deposition) and magnetron sputtering[127,

[116] Hsieh, J. H.; Tan, A. L. K.; Zeng, X. T., *Surf Coat Technol.* **2006**, 201, 4094-4098.
[117] Shan, L.; Wang, Y.; Li, J.; Li, H.; Wu, X.; Chen, J., *Surf Coat Techno*l. **2013**, 226, 40-50.
[118] Wei, C.; Lin, J. F.; Jiang, T. H.; Ai, C. F., *Thin Solid Films.* **2001**, 381, 104-118.
[119] Cozza, R. C., *Surf Coat Technol.* **2013**, 215, 224-233.
[120] George, L.; Wayne, D. K., *Mater Lett.* **1998**, 35, 344-350.
[121] Schneider, J. M.; Voevodin, A.; Rebholz, C.; Matthews, A.; Hogg, J. H. C.; Lewis, D. B.; Ives, M., *Surf Coat Technol.* **1995**, 74-75,312-319.
[122] Stephenson, D. A.; Agapiou, J. S., *Metal Cutting Theory and Practice*, CRC Press, Taylor & Francis Group, Boca Raton, Florida, USA, **2006**.
[123] Zhang, G.; Li, B.; Jiang, B.; Yan, F.; Chen, D., *Appl Surf Sci.* **2009**, 255, 8788-8793.
[124] Kyriacou, S. V.; Brownlow, W. J.; Xu, X. H., *Biochemistry.* **2004**, 43, 140-147.
[125] Bociaga, D.; Komorowski, P.; Batory, D.; Szymanski, W.; Olejnik, A.; Jastrzebski, K.; Jakubowski, W., *Appl Surf Sci.* **2015**, 355, 388-397.
[126] Baba, K.; Hatada, R.; Flege, S.; Ensinger, W.; Shibata, Y.; Nakashima, J.; Sawase, T.; Morimura, T., *Vacuum.* **2013**, 89, 179-184.
[127] Chen, R.; Tu, J. P.; Liu, D. G.; Mai, Y. J.; Gu, C. D., *Surf Coat Technol.* **2011**,205, 5228-5234.

[128, 103]. So far, the use of the cathodic arc technique had been more focused on the machine tool application because of the need to reach high performance[129,130]. This is due to the fact that with cathodic arc method, the discharges require a low voltage and high current power supply. As consequence, the plasma generated has an elevated density of ions leading to a material evaporation in positive ions form. This allows the control of the path of evaporated material to the substrate and the energy of ions with the applications of magnetic and electric fields with proper density. The ions energy adjustment allows the production of coatings with improved density, hardness and adherence properties. Concerning the use of Ti-C-N coatings in orthopedic field, it has been found Ti-C-N coatings deposited on AISI 316L by cathodic arc method for medical applications where the corrosion resistance and *in vitro* compatibility was studied[131].

Besides, there is no knowledge of the existence of knee replacements with this kind of functional protective coatings in the market. So taking into account the hard working conditions of implants, the excellent performance of Ti-C-N coatings and that the most used alloy in orthopedic applications is the Ti6Al4V, within the FUNCOAT project, the develop of Ti-C-N coatings by means of cathodic arc method and their deposition on Ti6Al4V alloy was decided. Concerning the analysis of developed coatings, a thorough characterization arises, studying the effect of wear-corrosion synergy, the response under fretting conditions in an environment close to the real application, and the effect of the Ag film deposited as antibacterial agent was analyzed. Apart from this, a deeply physico-chemical and structural characterization of the coatings was carried out.

1.5.2. Plasma Electrolytic Oxidation (PEO)

Plasma Electrolytic Oxidation[132, 133] technique is an electrochemical process of oxidation where arc micro-discharges are produced at the metal/electrolyte interface. These plasma discharges are initiated at potentials above the breakdown

[128] Cheng, Y. H.; Browne, T.; Heckerman, B.; Meletis, E. I., *Surf Coat Technol.* **2011**, 205, 4024-4029.
[129] Feng, W.; Zhou, H.; Yang, S., *Mater Sci Eng, A.* **2012**, 527, 4767-4770.
[130] Canteli, J. A.; Cantero, J. L.; Marín, N. C.; Gómez, B.; Gordo, E.; Miguélez, M. H., *J Mater ProcessTechnol.* **2010**, 210, 122-128.
[131] Antunes, R. A.; Rodas, A. C. D.; Lima, N. B.; Higa, O. Z.; Costa, I., *Surf Coat Technol.* **2010**, 205, 2074-2081.
[132] Kurze, P.; Krysman, W.; Dittrich, K. H.; Schneider, H. G., *Cryst Res Technol.* **1984**, 19, 973–979.

voltage of the growing oxide film and move rapidly across the anode surface transforming it into a complex ceramic protective matrix, without subjecting the substrate itself to damaging thermal exposure, since they rapidly develop and extinguish (within 10^{-4}-10^{-5} s). The discharges heat the metal substrate to less than 100-150 °C. As the sample is immersed into a bath with an electrolyte, the coating is composed of oxides of both the substrate material and electrolyte-borne modifying elements.

In comparison to other oxidation techniques, such as thermal oxidation or conventional anodic oxidation, the main advantages of PEO technique are:

- Coatings exhibit higher porosity increasing bioactivity and they are thicker improving the wear resistance[134].

- Coatings with uniform thickness produced quickly and easily on components with complex surface geometry.

- It does not involve major health or safety hazards since the electrolytes are environmentally safe and it does not require the use of concentrated acid (e.g. sulphuric acid).

In the case of PEO coatings, both the electrolyte composition and the current density regime have an influence on the phase composition and morphology (porosity size and level) of the anodic oxide layer[135]. A higher spark voltage causes a higher level of discharge energy, which provides a larger pore[136]. Concerning the electrolyte, it can provide different properties to the coating depending on its chemical composition.

Obtained ceramic coating with this technique not only prevents the wear but also provides excellent dielectric insulation for contact metals, helping to protect them against aggressive galvanic corrosion. They have an excellent bonding strength with the substrate and high hardness. Apart from that, PEO technique can be

[133] Kurze, P.; Dittrich, K. H.; Krysman, W.; Schneider, H. G., *Cryst Res Technol.* **1984**, 19, 93–99.
[134] Park, S.; Woo, T. G.; Lee, M. H.; Ahn, S. G.; Park, M. S.; Bae, T. S.; Seol, K. W., *Metals Mater. Int.* **2006**, 12, 505-511.
[135] Yerokhin, A. L.; Nie, X.; Leyland, A.; Matthews, A.; Dowey, S. J., *Surf Coat Technol.* **1999**, 122, 73-93.
[136] Shokuhfar, M.; Dehghanian, C.; Montazeri, M.; Baradaran, A., *Appl Surf Sci.* **2012**, 258, 2416-2423.

considered as an economic, efficiency and ecological friendliness alternative[137, 138, 139]. The electrolyte is an aqueous based solution and the pH is around 7-12.

PEO treatment can be applied in light alloys as aluminum, magnesium and titanium. In this thesis work, Plasma Electrolytic Oxidation (PEO) technique was used for the synthesis of TiO_2 layers.

At the beginning of the study related to the use of plasma electrolytic oxidation technique for the development of TiO_2 coatings, the existence in the market of hip stems coated with hydroxyapatite layers or bioactive glass-coatings was observed. However, in these cases, the coating is deposited on the substrate with the subsequent risk of delamination. With PEO technique, as the coating is a result of a surface transformation in a ceramic matrix, the risk of delamination cannot take place.

A commented before, in biomedical application, titanium is the most employed alloy due to its biocompatibility as an implant material, attributed to surface oxides spontaneously formed in air or in contact with physiological fluids[140]. Cellular behaviors, e.g. adhesion, morphological change, functional alteration, proliferation and differentiation are greatly affected by surface properties, including composition, roughness, hydrophobicity, texture and morphology of the oxide on titanium[141, 142]. The natural oxide is thin (about 3–10 nm in thickness[44]) amorphous and stoichiometrically defective. It is known that the protective and stable oxides on titanium surfaces are able to provide favorable osseointegration[143, 144]. The stability of the oxide depends strongly on the composition structure and thickness of the film[145]. However, contact loads damage this thin native oxide film and cause

[137] Han, I.; Choi, J. H.; Zhao, B. H.; Baik, H. K.; Lee, I., *Curr Appl Phys*, **2007**, 7S1, 23–27.
[138] Matykina, E.; Berkani, A.; Skeldon, P.; Thompson, G. E., *Electrochim Acta.* **2007**, 53, 1987–1994.
[139] Wang, Y.; Lei, T.; Jiang, B.; Guo, L., *Appl Surf Sci.* **2004**, 233, 258–267.
[140] Williams, D.F., Titanium and titanium alloys, in: Williams, D.F. (Ed.), *Biocompatibility of clinical implant materials*, CRC Press, Boca Raton, Florida, USA, **1981**.
[141] Lampin, M.; Warocquier-Clerout, R.; Legris, C.; Degrange, M.; Sigot-Luizard, M. F., *J Biomed Mater Res.* **1997**, 36, 99-108.
[142] Lim, Y. J.; Oshida, Y.; Andres, C. J.; Barco, M. T., *Int J Oral Maxillofac Implants.* **2001**, 16, 333–342.
[143] Keller, J. C.; Stanford, C. M.; Wightman, J. P.; Draughn, R. A.; Zaharias, R., *J Biomed Mater Res.* **1994**, 28, 939–946.
[144] Kieswetter, K.; Schwartz, Z.; Dean, D. D.; Boyan, B. D., *Crit Rev Oral Biol Med.* **1996**, 7, 329–345.
[145] Pouilleau, J.; Devilliers, D.; Garrido, F.; Durand-Vidal, S.; Mahe, E., *Mater Sci Eng.* **1997**, B47, 235–243.

galvanic and crevice corrosion as well as corrosion embrittlement. Moreover, the low wear resistance and high friction coefficient without applying protective coatings on the surface, gravely limit its protective properties. In order to solve it, the production of synthetic TiO_2 coatings could be an alternative.

TiO_2 exists in three polymorphic forms: rutile, anatase and brookite. By means of PEO technique, the percentage of rutile and anatase in the layers can be controlled. The rutile/anatase ratio has influence on the mechanical properties of the coating and in its tribocorrosion properties. Rutile phase has higher density than anatase. It offers more stability, superior hardness, better tribological properties, and consequently, greater wear resistance. Meanwhile, anatase phase is more porous and promotes a better osseointegration of the coated surface with the bone[146, 147].

The biological response to titanium depends on the surface chemical composition and the ability of titanium oxides to absorb molecules and incorporate certain elements[148]. Surface topography plays a fundamental role in regulating cell behavior, e.g. the shape, orientation and adhesion of cells[149, 150]. Concerning the pore size, values between 1 and 20 µm are suitable for cell adhesion[19]. Also, the presence of Ca has been reported to be advantageous to cell growth, and "in vivo" data show that implant surfaces containing both Ca and P enhance bone apposition on the implant surface[151, 152]. This is due to the fact that both elements are presented in hydroxyapatite.

By anodic oxidation, elements such as Ca and P can be incorporated into the titanium oxide coating and its micro-topography can be varied through the adjustment of the chemical composition of the electrolyte, and electrochemical process conditions.

Due to the possibility to introduce different elements by PEO technique, it is possible to provide the coatings with antibacterial properties doping the electrolyte

[146] Han, Y.; Hong, S. H.; Xu, K. W., *Surf Coat Tec.* **2002**, 154, 314–318.
[147] Sollazzo, V.; Pezzetti, F.; Scarano, A.; Piattelli, A.; Massari, L.; Brunelli, G.; Carinci, F., *J Craniofac Surg.* **2007**, 18, 806-810.
[148] Letic-Gavrilovic, A.; Scandurra, R.; Abe, K., *Dent Mater J.* **2000**, 19, 99–132.
[149] Eriksson, C.; Lausmaa, J.; Nygren, H., *Biomaterials.* **2001**, 22, 1987–1996.
[150] Ravanetti, F.; Borghetti, P.; De Angelis, E.; Chiesa, R.; Martini, F. M.; Gabbi, C.; Cacchioli, A., *Acta Biomater.* **2010**, 6, 1014-1024.
[151] Wang, H. Y.; Zhu, R. F.; Lu, Y. P.; Xiao, G. Y.; Zhao, X. C.; He, K.; Yuan, Y. F.; Li, Y.; Ma, X. N., *Mat Sci Eng C.* **2014**, 42, 657-664.
[152] Li, L. H.; Kong, Y. M.; Kim H. W.; Kim, Y. W.; Kim, H. E.; Heo, S. J.; Koak, J. Y., *Biomaterials.*

with biocide elements, like Ag, Cu or F. Most studies have focuses on the incorporation of silver in the TiO_2 layer as a biocide agent[153, 154, 155, 156]. There are also

researchers that have doped TiO_2 coatings with Cu and F[157, 158, 159]. Less known is the use of iodine as biocide element. There are a few studies where they produce TiO_2 coatings with iodine through hydrothermal reactions or using anodizing[160, 161]. References related to iodine doped TiO_2 coatings developed by plasma electrolytic oxidation technology have not been found, despite the iodine is widely used in medicine as antiseptic.

Additionally, even knowing in advance the difficulty of working with iodine due to its ease of sublimation at room temperature, in this research, the use of iodine, as biocide agent, has been studied to provide biocide characteristics to the developed TiO_2 coatings.

1.6. Technological demand framework

For 2030, it is estimated that the number of total hip replacements will rise by 174% (572,000 procedures) and total knee arthroplasties are projected to grow by 673% from the present rate (3.48 million procedures)[162]. In Spain during the period 1997-2012, 430,000 knee implants and 426,000 hip implants were placed, which in turn around 58,000 were reimplanted prosthesis as a consequence of a fault in a first

2004, 25, 2867-2875.
[153] Necula, B. S.; Fratila-Apachitei, L. E.; Zaat, S. A. J.; Apachitei, I.; Duszczyk, J., *Acta Biomater.* **2009**, 5, 3573-3580.
[154] Necula, B. S.; Apachitei, I.; Tichelaar, F. D.; Fratila-Apachitei, L. E.; Duszczyk, J.,*Acta Biomater.* **2011**, 7, 2751-2757.
[155] Necula, B. S.; van Leeuwen, J. P. T. M.; Fratila-Apachitei, L. E.; Zaat, S. A. J.; Apachitei, I.; Duszczyk, J., *Acta Biomater.* **2012**, 8, 4191-4197.
[156] Ando, Y.; Miyamoto, H.; Noda, I.; Sakurai, N.; Akiyama, T.; Yonekura, Y.; Shimazaki, T.; Miyazaki, M.; Mawatari, M.; Hotokebuchi, T., *Mater Sci Eng C.* **2010**, 30, 175-180.
[157] Zhu, W.; Zhang, Z.; Gu, B.; Sun, J.; Zhu, L., *J Mater Sci Technol.* **2013**, 29, 237-244.
[158] Venkateswarlu, K.; Rameshbabu, N.; Sreekanth, D.; Bose, A. C.; Muthupandi, V.; Subramanian, S., *Ceram Int.* **2013**, 39, 801-812.
[159] Arenas, M. A.; Pérez-Jorge, C.; Conde, A.; Matykina, E.; Hernández-López, J. M.; Pérez-Tanoira, R.; de Damborenea, J. J.; Gómez-Barrena, E.; Estaban, J., *Colloid Surface B.* **2013**, 105, 106-112.
[160] Neupane, M. P.; Sankara, T. S. N.; Park, J. E.; Kim, Y. K.; Park, I. S.; Song, K. Y.; Bae, T. S.; Lee, M. H., *World Acad Sci Eng Technol.* **2012**, 70, 795-798.
[161] Shirai, T.; Shimizu, T.; Ohtani, K.; Zen, Y.; Takaya, M.; Tsuchiya, H., *Acta Biomater.* **2011**, 7, 1928-1933.
[162] Kurtz, S.; Ong, K.; Jau, E.; Mowat F.; Halpem, M., *J Bone Joint Surg Am.* **2007**, 89, 780-785.

intervention[1].

In view of all this, at the beginning of this thesis, the need to improve the behavior of Ti6Al4V alloy in hip and knee implants by means of surface treatments was identified. Likewise, the literature review carried out could identify the need to develop wear-corrosion resistant coatings on Ti6Al4V by cathodic arc method and the necessity of more holistic characterization of the coatings, based on laboratory tests that simulate real working conditions of the implants. Moreover, in the literature it has been observed that the use of iodine has not still been explored as biocide agent in combination to plasma electrolytic oxidation coatings to protect orthopedic implants.

These needs were within the objectives of the FUNCOAT project (CSD2008-00023, CONSOLIDER INGENIO-2010 program), and of the EMAITEK program, which are the framework of this thesis.

Chapter 2

HYPOTHESIS

Nowadays, due to the increased life expectancy, the fast rhythm of life and the increasing number of sport practitioners, it is necessary to be active and dynamic longer than ever. This involves a series of problems at articular-bone level (complex lesions, arthritis, osteoarthritis, osteoporosis, etc.) that can limit physical activity of people and reduce their quality of life. Sometimes these complications may lead to the need of a total or partial reconstruction or replacement of a tissue, bone or joint. The use of biomaterials has an important role to achieve all these needs.

So far, the current implants present some limitations, particularly in orthopedics, where devices, especially in some joints, are subjected to high loads and an important daily activity. These limitations, normally related to the restrictions of the actual biomaterials, can shorten the lifespan of prosthesis.

In this context, this work was planned to improve the behavior of Ti6Al4V alloy in the orthopedic field by means of different surface treatments.

In this sense, this study was focused on two applications: knee and hip implants. In knee implants, a premature wear on the tibial plateau can be produced, due to the poor tribological behavior characteristic of the Ti6Al4V alloy. In hip replacements, severe wear on the stem can be generated, as a result of a lack of osseointegration. This effect is more pronounced in cementless hip prostheses.

In addition to the above problems, there is a risk of bacterial infection during or after device implantation. These infections, if not treated in time, can cause serious health problems in the patient. Moreover, in some cases, a second surgery is necessary. The later implies additional risks for the patient, and generates an important economic impact on public health services.

By means of surface treatments proposed in this study, Physical Vapor Deposition (PVD) and Plasma Electrolytic Oxidation (PEO), multifunctional coatings were expected to be produced. Taking into consideration the excellent, previous results of Ti-C-N films generated by cathodic arc method for machine tool applications, the efficiency of Ti-C-N coatings for knee implants was scheduled to be studied, in order to solve the durability problems associated to the Ti6Al4V alloy. Besides, the deposition of a thin layer of Ag on Ti-C-N coating was thought to provide the implant with antibacterial properties. In this way, advanced triborrosion and fretting tests were planned to be performed in order to screen their effectiveness.

To carry out the structual characterization, the following techniques were available: Raman spectroscopy, SEM (scanning electron microscopy), XRD (X-ray diffraction) and ICP-OES (inductive coupled plasma optical emission spectroscopy).

Concerning the hip replacements, TiO_2 coatings were planned to be grown on Ti6Al4V alloy by PEO. Due to the superior hardness conferred by the ceramic nature of TiO_2, a significant increase of the wear resistance was estimated. Additionally, the insertion of Ca and P into the coating was expected to promote the cell attachment and subsequent growth on the surface. On the other hand, in order to minimize the infection risk, insertion of iodine as biocide agent into the coating was also proposed. The selection of iodine was caused by the fact that a scarce number of studies on this element had been found at the beginning of this thesis. Tribocorrosion test were planned to be performed in order to study the wear-corrosion synergy. For the structural characterization, the available techniques were: SEM (scanning electron microscopy), XRD (X-ray diffraction) and XRF (X-ray fluorescence).

Chapter 3

OBJECTIVES

Taking into account the background and context analyzed, the main objective of this study is the improvement of Ti6Al4V alloy behavior by means of the development of different multifunctional coatings, solving in this way the most common problems existent in orthopedic implants.

In this sense, the aim of this work can be divided into the following more specific objectives:

- ✓ To develop protective coatings by Physical Vapor Deposition (PVD) and Plasma Electrolytic Oxidation (PEO) techniques.
- ✓ To modify the chemical composition of the developed layers to provide antibacterial properties and promote the osseointegration.
- ✓ To characterize in depth physico-chemical and structural properties of the coatings.
- ✓ To study the behavior of the developed coatings against tribocorrosion and fretting tests.
- ✓ To establish correlations between the physico-chemical and microstructural properties and the tribological and corrosion response.
- ✓ To analyze the efficiency of the inserted biocide elements into the coatings against bacterial adhesion.

Chapter 4

METHODOLOGY

In this thesis, different technologies and equipments have been used to carry out the coatings development and the characterization.

The different methodologies used can be divided depending on the type of activity or characterization performed. In this section, all these methodologies are summarized; nevertheless, all of them are explained in detail in Annex A – Instrumental techniques.

The technologies required for the development of the protective coatings are:

- *Physical Vapor Deposition* (PVD), where cathodic arc and magnetron sputtering deposition method have been used to deposit Ti-C-N and Ag coatings, respectively.

- *Plasma Electrolytic Oxidation* (PEO) process to transform the titanium in TiO_2 coatings doped with Ca, P and I.

In order to perform the physico-chemical and structural characterization the equipments and methodologies employed are the following ones:

- *Thickness* measurements of coatings were carried out by means of Calotests equipment from CSEM.

- Fischer nanoindenter equipment with Vickers indentor was employed, using the method of Oliver and Pharr to measure the coating *hardness*.

- Surface *roughness* was determined with Perthometer M2 profilometer from Mahr according to ISO 4287 and ISO 4288 standars.

- *Adhesion* of the coatings to the substrate was measured by means of a Rockwell test, evaluating the results following the protocol described in the VDI 3198 indentation test standard.

- The profiles of the *chemical composition* in depth were obtained analyzing the coatings with GD-OES (Glow Discharge Optical Emission Spectroscopy) technology by means of GD-Profiler 2 equipment from Horiba Jobin Yvon.

- *Raman analysis* was carried out to study the microstructure of the coatings.

- *X-ray diffraction (XRD)* characterization was done by means of a PHILIPS

PW1710 powder diffractometer to analyze the phases of the coatings.

- *Microstructure* of different developed coatings was analyzed with Scanning Electron Microscope (SEM), from OXFORD INCA synergy.

- Chemical composition was also analyzed with SEM equipment by EDS (Energy Dispersive Spectroscopy) technique.

- *X-ray Fluorescence Spectroscopy (XRF)* was used to analyze the chemical composition of coatings with S8 TIGER equipment from BRUKER.

- *Hydrophilic/hydrophobia grade* was analyzed by means of measuring the contact angle. This test was carried out in the SURFTENS universal goniometer.

- *Inductive coupled plasma optical emission spectroscopy (ICP-OES)* in ULTIMA 2 HORIBA Jobin Yvon equipment was used to analyze the electrolytes after the tribocorrosion tests for detecting the presence of aluminum, vanadium and titanium released from the coating/substrate during the test.

Concerning the study of tribological and tribocorrosion behavior the following tests were carried out:

- *Fretting tests* were performed in SRV® tribometer under the ball-on-disc configuration.

- *Tribocorrosion tests* were carried out by using the Microtest tribometer with rotatory movement under ball-on-disc configuration, and assisted by an Autolab-Methrom potentiostat PGSTAT302N.

- *Wear tracks* produced in fretting and tribocorrosion tests were analyzed with the confocal microscopy by means of track profiles and topographies, and following the protocol described by N. Diomidis[163].

Bacterial adhesion study was carried out by Staphylococcal adhesion experiments under an established protocol described by T.J. Kinnari and Pérez-Tanoira, and with

[163] Diomidis, N., Towards a standard test for the determination of synergism in tribocorrosion: Design of a protocol for passivating materials, in: Celis, J. P.; Ponthiaux, P. (Eds.), *Testing tribocorrosion of passivating materials supporting research and industrial innovation: Handbook*, Manley Publishing, Leeds, UK, **2012**.

a statistical analysis.

Chapter 5

THESIS OVERVIEW

The research work carried out and presented in this thesis is composed by three scientific contributions presented in this memory in chapter 6[164, 165, 166]. Additionally, a book chapter[167] was published about titanium and its alloys as biomaterials, also included in annex C. This book chapter was used as a general reference for the introduction of this thesis.

In the following lines, a general outlook of the whole study presented in the three scientific contributions is given.

Figure 5.1 is a scheme explaining the work carried out for knee implant by means of the development of Ti-C-N coatings (contributions in sections 6.1 and 6.2).

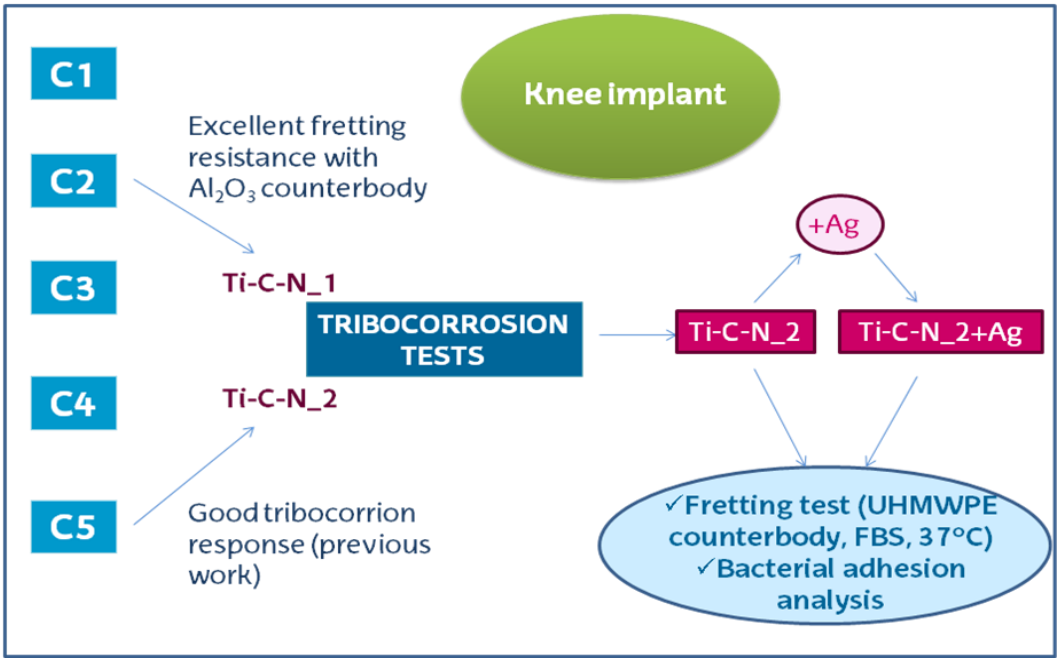

Fig. 5.1. Scheme of the studies carried out on the developed Ti-C-N coatings. Five original coatings were developed, C1-C5, and two were selected, Ti-C-N_1 and Ti-C-N_2, after a previous characterization. A Ag coating was deposited on the best coating (Ti-C-N_2) producing Ti-C-N_2+Ag. Fretting tests and bacterial adhesion analysis were carried out on Ti-C-N_2 and Ti-C-N_2+Ag.

[164] Sáenz de Viteri, V.; Barandika, M. G.; Ruiz de Gopegui, U.; Bayón, R.; Zubizarreta, C.; Fernández, X.; Igartua, A.; Agullo-Rueda, F., *J Inorg Biochem*. **2012**, 117, 359-366.
[165] Sáenz de Viteri, V.; Barandika, G.; Bayón, R.; Fernández, X.; Ciarsolo, I.; Igaruta, A.; Pérez Tanoira, R.; Esteban Moreno, J.; Pérez-Jorge Peremarch, C., *J Mech Behav Biomed*. **2015**, 55, 75-86.
[166] Sáenz de Viteri, V.; Bayón, R.; Igartua, A.; Barandika, G.; Esteban Moreno, J.; Pérez-Jorge Peremarch, C.; Martínez Pérez, M., Submitted to *Appl Surf Sci*. **2015**.
[167] Sáenz de Viteri, V.; Fuentes, E., Titanium and Titnaium alloys as Biomaterials, in: Gegner, J. (Ed.), *Tribology-Fundamentals and advancements*, Intech, Rijeka, Croatia, **2013**.

On the other hand, figure 5.2 represents the activity carried out on the developed TiO_2 coatings for hip implants (contribution in section 6.3).

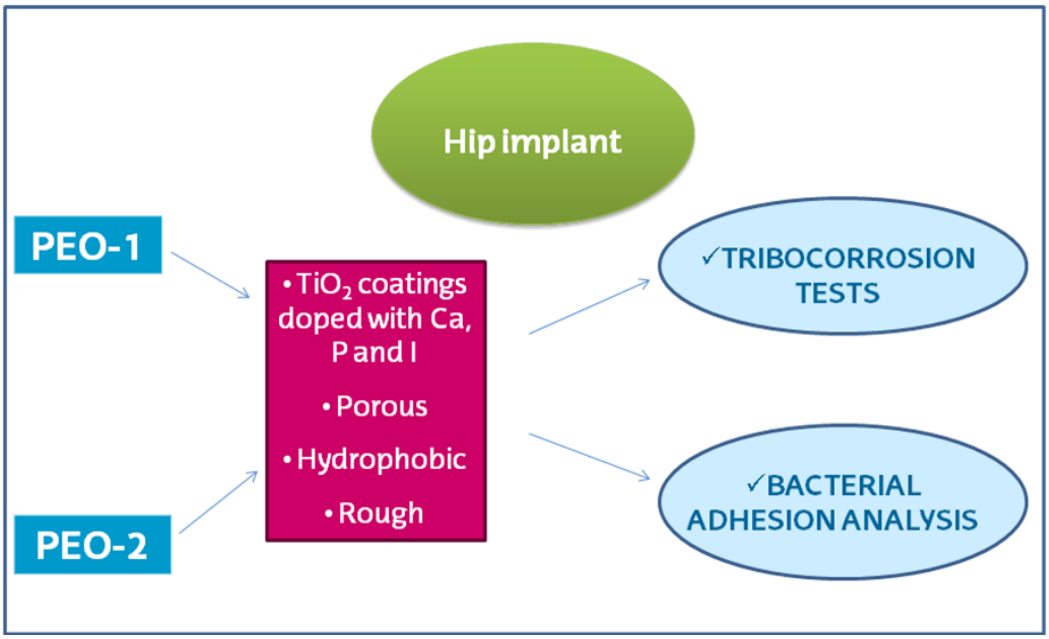

Fig. 5.2. Scheme of the studies carried out on the developed TiO_2 coatings. Two coatings were developed (PEO-1 and PEO-2) and characterized by tribocorrosion tests and bacterial adhesion analysis.

As mentioned before, the main objective of this thesis is to improve the behavior of the Ti6Al4V alloy for orthopedic applications by means of the development of different protective coatings. Two different types of surface treatment techniques have been employed trying to solve, as far as possible, the difficulties presented in artificial implants made of Ti6Al4V alloy, in particular in knee and hip prosthesis.

Among all the possible complications that prosthesis may present, this study has been focused on the presence of an excessive and premature wear, a poor osseointegration between the implant and the bone, and the possibility of contracting a bacterial infection. These drawbacks can lead to a series of complications in the patient being necessary, in some cases, a second surgical intervention and the partial or total replacement of the prosthesis.

In relation to the knee prosthesis, this work has attempted to reduce the wear produced on the tibial plateau, made of Ti6Al4V alloy, due to vibrations (commonly known as fretting effect), produced between the metallic component and the polymeric insert, made of UHMWPE (Ultra High Molecular Weight Polyethylene), as

well as to provide a biocide character to reduce the risk of bacterial infection. For that, the Physical Vapor Deposition (PVD) technology has been used to carry out the development of Ti-C-N coatings capable of improving the tribological response reducing wear, and with biocide features to avoid bacterial adhesion and the subsequent growth (Fig. 5.3).

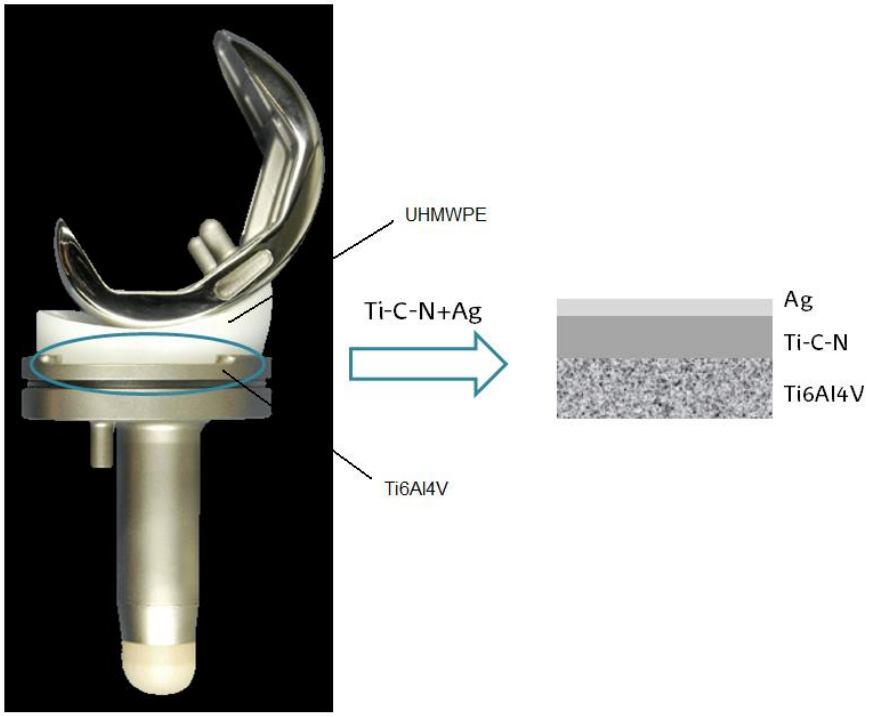

Fig. 5.3. Scheme of the developed solution for knee implant application.
Source: https://en.wikipedia.org/wiki/Knee_replacement (CC BY 3.0)

In the first contribution (section 6.1), the first steps carried out in the search for coatings with high wear resistance are presented. By means of PVD technology with the cathodic arc method, five types of Ti-C-N coatings (Fig. 5.4) have been developed varying the parameters of the deposition process, resulting in layers with different percentages of titanium, carbon and nitrogen, and different physical and microstructural properties.

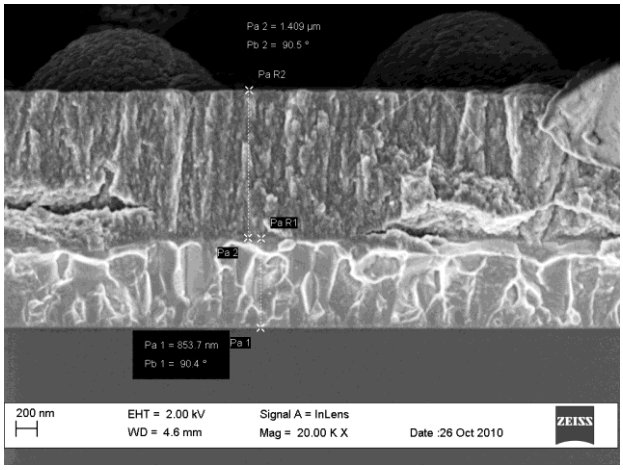

Fig. 5.4. Example of a SEM micrograph for a Ti-C-N coating.

Once the characterization processes of all developed layers and the tribological tests had been performed, the results demonstrated that all the developed coatings improved the tribological response of the Ti6Al4V (Fig. 5.5). The coatings C2 and C5, exhibiting the best wear resistance and lowest coefficient of friction, have been selected in order to go on with further characterization.

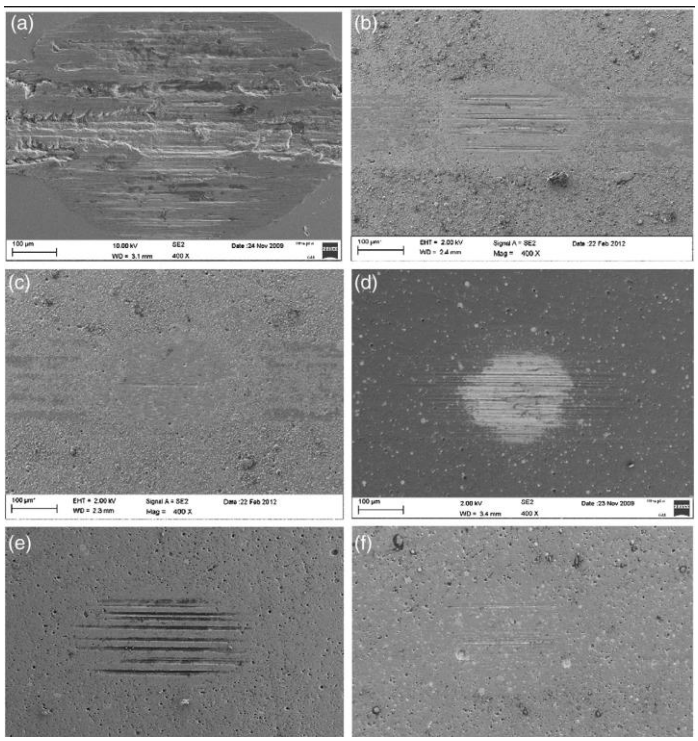

Fig. 5.5. SEM micrographs of the fretting tests wear scars. a) Ti6Al4V, b) C1, c) C2, d) C3, e) C4 and f) C5.

In the second contribution (section 6.2), a holistic characterization of the selected

coatings in the first contribution (named C2 and C5 in the first contribution and renamed as Ti-C-N_1 and Ti-C-N_2 in the second one) has been carried out. In this case, the tribocorrosion behavior of the two selected layers and substrate has been analyzed. The study of the synergy between mechanical wear and electrochemical processes always helps to understand more in depth what happens actually in the human body, when the implant is surrounded by corrosive biological fluids. These tests indicated that just one of the coatings, Ti-C-N_2, satisfactorily outperform the test conditions (Fig. 5.6), with the presence of a minimum wear, good corrosion resistance and an impermeable effect that prevents the migration of ions from the substrate to the outside.

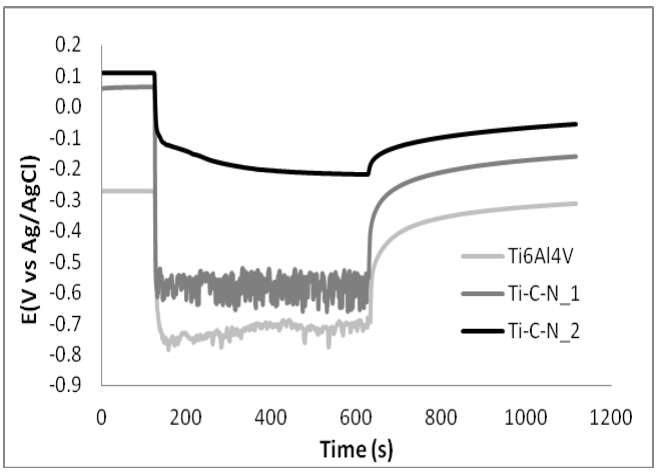

Fig. 5.6. Open circuit potential during sliding process in tribocorrosion test for bare Ti6Al4V and Ti-C-N_1 and Ti-C-N_2 coatings.

After selected the most promising coating, a thin silver film was deposited by means of the magnetron sputtering method in order to provide biocide properties to the Ti-C-N_2 layer (Fig. 5.7). In order to simulate real fretting conditions produced in the tibial plateau, fretting tests with fetal bovine serum and using the current contramaterial (UHMWPE) have been performed. The tribological response of the Ti-C-N_2 coating was very promising, while with silver layer is quite poor. The low hardness of silver seems to be the responsible of its lack of wear resistance.

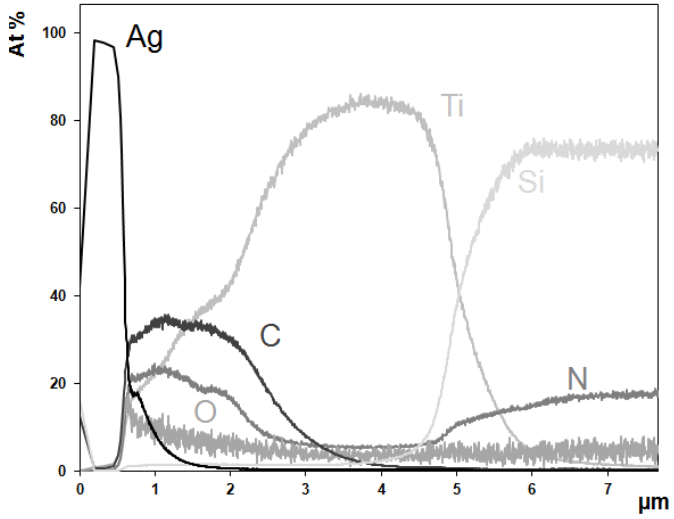

Fig. 5.7. Chemical composition in depth of Ti-C_N_2+Ag obtained by GD-OES analysis.

Concerning the response in bacterial adhesion tests against *Staphylococcus aureus* and *Staphylococcus epidermidis*, the Ag layer has shown an excellent antibacterial behavior (Fig. 5.8). Additionally, taking into account that the higher risk of contracting a bacterial infection occurs in the first hour after the prosthesis implantation, a quick release of the silver, once the device has been implanted into the body, may be desirable.

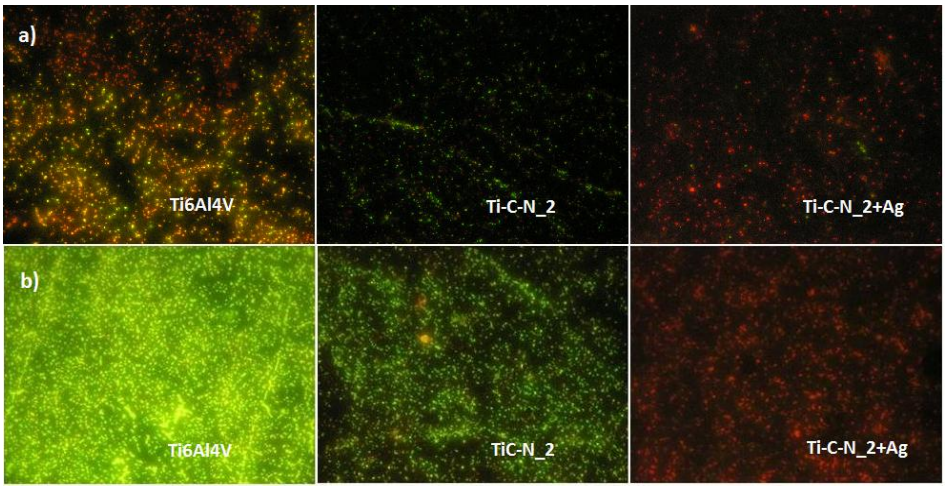

Fig.5.8. Fluorescence microscope images for Ti6Al4V substrate, Ti-C-N_2 surface and Ti-C-N_2+Ag surface covered by *S. aureus* (a) and *S.epidermidis* (b) shown the decrease of bacteria colonization in Ti-C-N_2+Ag.

Over the first two contributions, it has been possible to achieve a biocompatible coating, with great wear resistance, low coefficient of friction, high corrosion resistance, being impermeable, and finally, with antibacterial properties.

Regarding the hip prosthesis, this study has been focused on providing to the surface of the implanted device favorable characteristics to promote the cell growth and enhance the osseointegration of the stem made of Ti6Al4V. In addition, like in the knee device, greater wear resistance and antibacterial properties were desired. For this second application, the Plasma Electrolytic Oxidation (PEO) technique has been used for the development of TiO_2 protective coatings with the aforementioned features (Fig. 5.9).

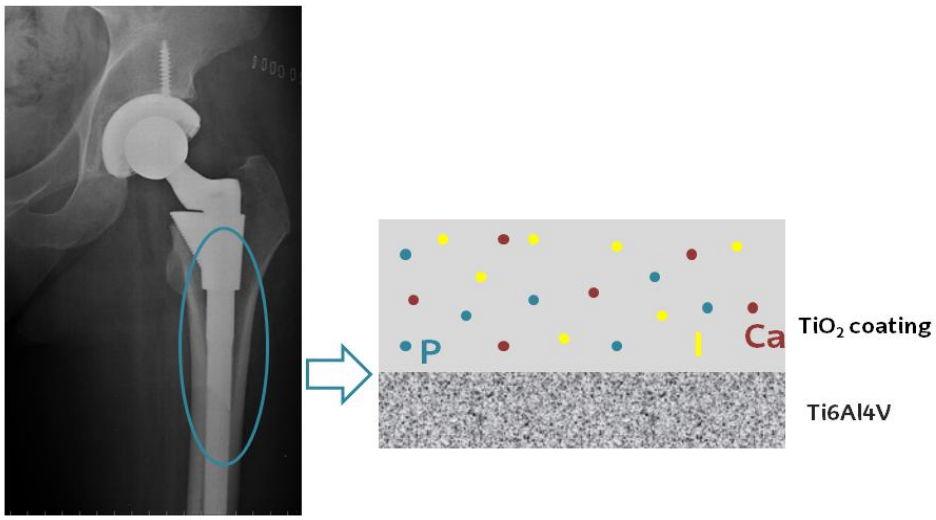

Fig.5.9. Scheme of the developed solution for hip implants application.
Source: "Hip-replacement" by KimvdLinde, https://commons.wikimedia.org/wiki/File:Hip-replacement.jpg#/media/File:Hip-replacement.jpg (CC BY-SA 3.0)

In the work presented in the third contribution (section 6.3), titanium oxide coatings have been developed using the PEO technology (PEO-1 and PEO-2), inserting calcium and phosphorous elements like cell growth promoters. In addition, these coatings have a certain content of TiO_2 in anatase form, a porous and rough microstructure and exhibit more hydrophobicity than the Ti6Al4V. All these features make the developed TiO_2 coatings suitable for the absorption of proteins and posterior cells bind (Fig. 5.10).

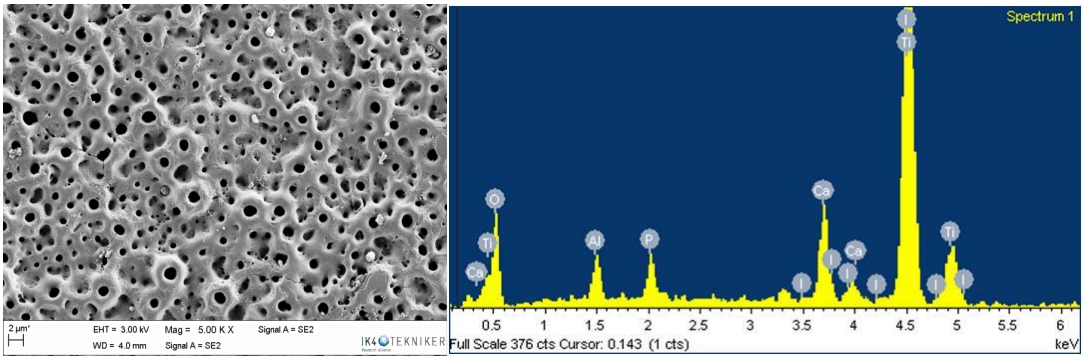

Fig. 5.10. Left) SEM micrograph of one of the developed coatings, where the porous structure can be observed. Right) Spectrum of the chemical composition obtained by EDS analysis.

In tribocorrosion tests, the developed coatings have showed higher friction coefficients than the untreated substrate due to the higher roughness conferred by the presence of pores. Moreover, they have exhibited improved wear resistance in comparison to the bare Ti6Al4V alloy due to its relatively high hardness conferred by its ceramic nature, the chemical stability and better mechanical properties provided by the presence of high ratio of rutile TiO_2 (Fig. 5.11). The corrosion resistance has not been affected in any case by the sliding process.

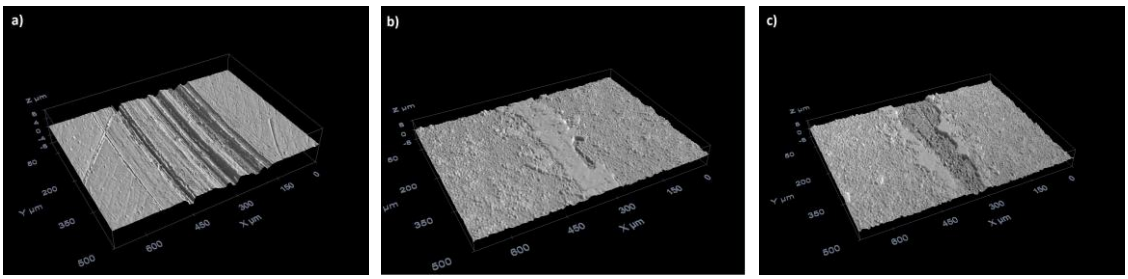

Fig. 5.11. Wear tracks topography: a) Ti6Al4V, b) PEO-1 and c) PEO-2.

In order to provide antibacterial properties to the coatings, iodine was added into the TiO_2 coating as a biocide agent. The results for the bacterial adhesion assays, performed with collection strains, have been positive against *Staphylococcus epidermidis* (Fig. 5.12). However, with *Staphylococcus aureus* strains, the biocidal effect of iodine was not appreciated.

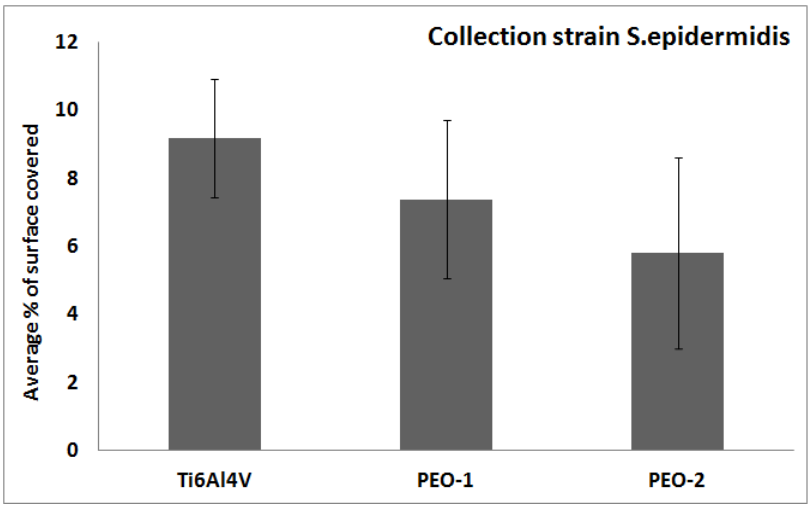

Fig. 5.12. Mean percentage of surface covered by *S. epidermidis.*

As general conclusion of this thesis work, the Ti6Al4V properties for orthopedic implants have been improved by means of the development of two different coating with PVD and PEO techniques. This could be reflected in an increase of the lifetime of the implants due to the higher wear resistance that these coatings possess, and the decrease of the possibility of contracting a bacterial infection as a result of the antibacterial properties conferred with the addition of biocide agents to the coatings.

Chapter 6

RESULTS AND DISCUSSION

Contribution 1

Ti-C-N coatings developed by PVD technique: pre-selection of Ti-C-N coatings

Characterization of Ti-C-N coatings deposited on Ti6Al4V for biomedical applications

Journal of Inorganic Biochemistry. **2012**, 117, 359-366

6.1.1. Introduction 76

6.1.2. Experimental 77

6.1.2.1. Materials 77

6.1.2.2. Coating Deposition Process 78

6.1.2.3. Coatings Characterization 79

6.1.2.4. Fretting tests 80

6.1.3. Results and Discussion 81

6.1.3.1. Chemical and structural characterization 81

6.1.3.2. Raman Spectroscopy 85

6.1.3.3. X-ray diffraction 87

6.1.3.4. Fretting tests 88

6.1.4. Conclusions 92

ABSTRACT

Ti6Al4V alloy is the most commonly employed implant material for orthopedic replacements due to its good mechanical properties close to those of bones, biocompatibility and its good corrosion resistance in biological media. Nevertheless, it does not exhibit good wear resistance, showing friction and wear even with soft tissues. This latter feature can lead to a premature failure of the implant with the subsequent component replacement. Therefore, a system with good tribological resistance is required for several medical applications. One possible alternative to solve tribological problems consists of protecting the alloy surface by means of biocompatible Ti-C-N coatings. In this work, five types of metallic Ti-C-N coatings deposited by physical vapor deposition (PVD) cathodic arc method on Ti6Al4V substrate have been studied. Different deposition conditions have been analyzed, and the superficial properties of films have been characterized. Additionally, tribological response of these films have been determined and compared with the substrate one under fretting conditions in simulated body fluid. The results indicate that Ti-C-N coatings improve the general response of the biomaterial.

6.1.1. Introduction

In total joint replacements, the purpose of the artificial components is to restore the functionality and smooth articulation between the bones[1]. Among all biomaterials, the Ti6Al4V alloy is one of the most used material because, in addition to its excellent biocompatibility, it exhibits low elastic modulus (comparable with that of human bone), good corrosion resistance, high specific strength, and fatigue resistance[2, 3, 4, 5]. In general, the orthopedic bearing is manufactured from highly polished metal alloys with extreme precision that articulate against a metal material (CoCrMo or stainless steel), ceramic material or against a polymeric material, mainly ultra high molecular weight polyethylene (UHMWPE), in case of knee joints.

Major drawback of Ti alloys is their relative low load-carrying capacity and their poor tribological properties as high friction coefficient during dry sliding against numerous important technical materials[6]. In implants, one type of common wear mechanism that takes place on contacting surfaces is named fretting. It occurs when two surfaces are subjected to small amplitude reciprocating motion of micro order. This phenomenon generated by vibration can significantly reduce the contact mechanism life[7]. Moreover, as a result of wear, metallic ions are released with high facility to enter in the bloodstream, leading to inflammation of the surrounding tissues and give rise to bone resorption (osteolysis), causing pain and aseptic loosening of the prosthesis[8, 9]. The wear causes the degradation of the surface with the consequent loss of accuracy and implant failure[10]. Avoiding the failure of the prosthesis is, therefore, one of the goals for these types of materials, and one of the possible approaches consists of minimizing the wear on the surface of the biomaterial. To this purpose, the enhancement of the surface hardness is

[1] Klein, J., *Science*. **2009**, 323, 47-48.
[2] Williams, J. M.; Bucharan, R. A., *Mater Sci Eng*. **1985**, 69, 237-246.
[3] Magaziner, R. S.; Jain, V.K.; Mall, S., *Wear*. **2009**, 267, 368-373.
[4] Everitt, N. M.; Ding, J.; Bandak, G.; Shipway, P. H.; Leen, S. B.; Williams, E.J., *Wear*. **2009**, 267, 283-291.
[5] Dalmiglio, M.; Schaaff, P.; Holzwarth, V.; Chiesa, R.; Rondelli, G.; *J Biomed Mater Res A*. **2008**, 86B, 407-416.
[6] Wendler, B.G.; Pawlak, W.; Achiev, J., *Mater Manuf Eng*. **2008**, 26, 207-210.
[7] Sylvestre, M.; Zaidi, H.; Rivière, J.P.; Eyidi, D.; Doyen, F., *Surf Coat Tech*. **2010**, 205, 1374-1380.
[8] Chandra, A.; Ryu, J. J.; Karra, P.; Shrotriya, P.; Tvergaard, V.; Gaisser, M.; Weik, T., *J Mech Behav.Biomed*. **2011**, 4, 1990-2001.
[9] Wolford, L. M., *Proc (Bayl Univ. Med. Cent.)*. **2006**, 19, 232-238.
[10] Goodman, S. B.; Gómez Barrena, E.; Takagi, M.; Konttinen, Y. T., *J Biomed Mater Res A*. **2008**, 90A, 603-618.

desired as well as the reduction of the friction coefficient between contacting surfaces. Cathodic arc evaporation deposited gradient Ti-C-N coatings exhibiting good adhesion to the Ti6Al4V substrate, and serve as hard intermediate layers between the Ti substrate and the top hard amorphous carbon (a-C) layer. Ti-C-N films are an attractive biomedical material due to their high hardness, low friction coefficient, good chemical stability and excellent hemocompatibility[11, 12, 13, 14]. Thus, Ti-C-N coatings are becoming a successful approach to the improvement of wear resistance of the implant[15]. The purpose of this work is to investigate the potential benefits of protecting the Ti6Al4V medical alloy by means of Ti-C-N coatings. Therefore, we herein present our first results, including significant chemical and structural information. To this purpose, a set of five coated samples has been deeply analyzed. In fact, microstructural characterization has been carried out by means of XRD (X-ray diffraction), SEM (scanning electron microscope), GD-OES (glow discharge optical emission spectroscopy) and RAMAN Spectroscopy techniques. Thickness, hardness, adhesion and roughness of coatings have also been measured. Concerning to the tribological study, fretting tests were conducted in fetal bovine serum (FBS) environment reproducing the characteristics of the biological fluids.

6.1.2. Experimental

6.1.2.1. Materials

Ti6Al4V ELI (extra low interstitial) was selected to be used as substrate. The mechanical properties and composition meet the ASTM F136-02 standard specification for wrought Titanium-6Aluminum-4Vanadium ELI alloy for surgical implant applications (UNS R56401).

Discs of Ti6Al4V with dimensions of 24 mm of diameter and 7.9 mm of height were manufactured. They were mirror polished up to a final roughness of 0.05 µm.

[11] Zheng, Y.; Liu, D.; Liu, X.; Li, L., *Biomed Mater.* **2008,** 3, 44103-44109.
[12] Dowling, D. P., *Diam Relat Mater.* **1997**, 6, 390-393.
[13] Zhang, L.; Lv, P.; Huang, Z. Y.; Lin, S. P.; Chen, D. H.; Pan, S.R.; Chen, M., *Diam Relat Mater.* **2008**, 17, 1922-1926.
[14] Ma, G.; Gong, S.; Lin, G.; Zhang, L.; Sun, G., *Appl Surf Sci.* **2012**, 258, 3045-3050.
[15] Yetim, A. F.; Celik, A.; Alsaran, A., *Surf Coat Tech.* **2010**, 205, 320-324.

6.1.2.2. Coating Deposition Process

Ti-C-N coatings were deposited by physical vapour deposition (PVD) technique using cathodic arc evaporation (CAE) method in the industrial equipment MIDAS 775 designed and manufactured by Tekniker[16]. This system has 12 circular evaporators of 100 mm, working intensity range of 60-200 A, and a 45 kW pulsed DC bias power supply system consisting of two MDX II DC and one SPARC-VS pulsing unit from Advanced Energy.

Prior the coating deposition process, the samples were sprayed with a solvent product, cleaned in an alkaline detergent by means of ultrasounds method and finally rinsed with distilled water and alcohol before drying with hot air. The substrates were wrapped with aluminum foil so as to prevent particles of dirt and dust coming from the air on the surface of the parts. After loading the discs, the vacuum chamber was evacuated up to a pressure of 10^{-4} mbar. Then, they were heated by means of infrared radiant heaters up to a substrate temperature of 500 ºC. After the heating process, a cleanliness step named Glow Discharge was applied to the samples. This process consists of an electrical pulsed DC discharge to create plasma around the samples by using a gas mixture of argon and hydrogen at a pressure of between 0.4 and 0.8 mbar. To ensure the necessary adhesion for the coating a very thin pure titanium layer (around 1 µm thickness) was deposited. This step needs a very high bias voltage up to 1000 V to get very high energy ions bombardment to the substrate. This promotes the adhesion in three ways. First of all, the high-energy-ion bombardment cleans the very top layers of the substrate. Secondly, it is an ion implantation of titanium in the substrate, and finally it is the beginning of the coating. Then, the Ti-C-N coating was completed by adding the necessary reactive gases, nitrogen and acetylene, with a gas flow between 50 to 200 sccm (standard cm^3/min at a pressure of 1 bar). During this step the pressure in the chamber was set value in the range of 2-8 $x10^{-3}$ mbar and the flow of the gases was controlled with a mass flow controller from Bronkhorst High Tech. The arc intensity of the titanium target was set between 70-140 A and the bias voltage between 400-30 V. Therefore, coatings were carried out in two steps for obtaining in this way two layers. The first one was a pure metallic titanium layer that worked as a stress relaxing for a better adhesion of the Ti-C-N coating. The second was the Ti-C-N layer

[16] Goikoetxea, J.; Ruiz de Gopegui, U.; Garmendia, K.; Delgado, A., *Arc evaporator and method for operating the evaporator*: Patent number WO2010072850 A1. Fundación Tekniker, **2010**.

that provided wear and corrosion resistance to the coated system. In this way, five different samples were prepared (C1 to C5) by varying the parameters of the coating process. During the deposition process, the argon flow was constant for all the samples (200 sccm), and the nitrogen flow was 50 sccm for all of them, with the exception of C4, that did not have any. An arc intensity of 100 A was applied for all the samples, with the exception of C5 (for which an intensity of 75 A was applied). Different flows of C_2H_2 were also tried: 100 sccm for C1, 50 sccm for C2, and 200 sccm for C3, C4, and C5. Table 6.1.1 shows the deposition parameters of the coating process for all samples.

Table 6.1.1.
Deposition parameters of the coating process.

Sample	Ar sccm	N_2 sccm	C_2H_2 sccm	I_{arc} A
C1	200	50	100	100
C2	200	50	50	100
C3	200	50	200	100
C4	200	-	200	100
C5	200	50	200	75

In joint replacements, in areas in which two artificial components are in contact and movement takes place, it is necessary to have a very smooth surface to prevent or minimize friction, and therefore wear. A polishing treatment was applied on the surfaces of the coated samples using 1 µm polishing diamond cloths in order to prepare the surface for the characterization process. The final roughness was lower than 0.2 µm, before performing tribological tests.

6.1.2.3. Coatings Characterization

Coatings thickness measurement was made with Calotest equipment from CSEM.

For hardness measurements, Fischer nanoindenter equipment with Vickers indentor was employed, using the method of Oliver and Pharr[17, 18, 19]. A final load of 5

[17] Farhat, Z. N.; King, Y.; Northwood, D. O.; Alpas, A. T., *Mater Sci Eng A.* **1996**, 206, 302-308.
[18] Loubet, J. L.; Georges, J. M.; Meille, G., Vickers indentation curves of elastoplastic materials, in: Blau, P. J.; Lawn, B. R. (Eds.), *Microindentation techniques in materials science and*

mN was applied in 20 steps to determine the coatings hardness profile versus depth.

The profiles of composition in depth were analyzed with GD-OES equipment from Horiba Jobin Yvon. The measurement conditions used were 650 Pa and 35 W, with a copper anode of 4 mm of diameter[20]. For this characterization, coatings deposited on Ti6Al4V samples were employed.

The adhesion of the coating to the substrates was measured by means of a Rockwell test and for discussion of the results the evaluation system employed in the VDI 3198 indentation test standard was followed. This test uses a standard Rockwell hardness tester fitted with a Rockwell "C"-type diamond cone indenter with an applied load of 150 kg. The result is obtained by using an optical microscope and classifying the adhesion as HF 1 to HF 6 according to the level of cracking or coating delamination around the indent. Only indents classified as HF 1 and HF 2 correspond to adequate adhesion. This method provides results rapidly with a minimum of effort.

The roughness measurements were performed according to ISO 4287 and ISO 4288 standards specifications with Mahr Perthometer M2 equipment. Obtained values correspond to the roughness before the polishing process.

Raman spectra were obtained with a Renishaw Ramascope 2000 microspectrometer and an ion argon laser (emission wavelength 514.5 nm) as the excitation light source. A 100× microscope objective was used to focus the laser on the sample and to collect the scattered light. Laser power on the sample was about 3 mW.

X-ray powder diffraction data were collected on a PHILIPS PW1710 powder diffractometer with Cu-Kα radiation in steps of 0.02° over the 5–69.96° 2θ-angular range and a fixed-time counting of 1 s at 25 °C.

6.1.2.4. Fretting tests

For the fretting tests SRV tribometer with ball-on-disc configuration was selected.

engineering, ASTM STP 889, American Society for Testing and Materials, Philadelphia, **1986**.
[19] Oliver, W. C., Pharr, G. M., *J Mater Res.* **1992**, 7, 1564-1583.
[20] Payling, R.; Michler, J.; Aeberhard, M., *Surf Interface Anal.* **2002**, 33, 472-477.

As counterbody balls of Al_2O_3 with a diameter of 10 mm were used. All tests were conducted at a load of 50 MPa, a frequency of 2 Hz (0.6 mm/s) and a stroke of 150 µm. Tests were carried out at 37ºC during 12 minutes (3 tests per sample). Tests were done under lubricated conditions by using fetal bovine serum (FBS) with sodium azide and EDTA, according to ASTM F732-00 standard. Friction and wear response of uncoated and Ti-C-N coated Ti6Al4V alloy was studied and compared.

6.1.3. Results and Discussion

6.1.3.1. Chemical and structural characterization

Ti-C-N coatings developed had a thickness between 2.00 and 3.86 µm. The hardness values registered lie among the typical ones for this kind of coatings (up to 25 GPa)[21, 22] and are displayed in Table 2. It must be pointed out that the highest hardness has been found for C4 (22 GPa) which does not present nitrogen. This could cause a higher sp^3/sp^2 fraction for the carbon that leads to a higher hardness values[23].

Almost all coatings show similar values of the roughness (higher than 0.3 µm), except the C4 in which is approximately twice. These high values of roughness are due to the droplets generated during arc deposition, promoting irregularities on the surface and increasing the roughness. Therefore, all samples should require post-deposition treatment for the rest of the characterization tests. Adhesion measurements indicated that, according to the Rockwell test, all the coatings are classified as HF 1. Therefore, all of them exhibit adequate adherence to the substrate (Table 6.1.2).

[21] Fukui, H., *Surf Coat Tech.* **2004**, 187, 70-76.
[22] Dearnaley, G.; Arps, J. H., *Surf Coat Tech.* **2005**, 200, 2518 – 2524.
[23] Guoqing, L., *Thin Solid Films.* **2005**, 475, 279-282.

Table 6.1.2.

Coatings Characterization. Physical Properties.

Sample	Thickness µm	Hardness GPa	Carbon content C_2H_2 sccm	Roughness Ra, µm	Adhesion HF
C1	2.00	7	100	0.36	HF 1
C2	2.40	10	50	0.36	HF 1
C3	3.28	3	200	0.40	HF 1
C4	3.05	22	200	0.60	HF 1
C5	3.86	8	200	0.42	HF 1

By means of GD-OES technique, the chemical composition profiles in depth are obtained (Fig. 6.1.1). It must be said that the profiles are accurate in thickness but they give us a qualitative idea of the progression in chemical composition. On the right of the graphs, the chemical composition of Ti6Al4V substrate can be seen, and afterwards an increase of the titanium concentration is appreciated due to the first titanium layer. The decrease of titanium accompanied by the presence of nitrogen and carbon indicates that the area corresponds to the Ti-C-N layer. In C3, C4 and C5 the increase of carbon observed is due to the increase of acetylene flow during the coating deposition process. This increase of carbon content, moreover, goes along with the increase of coating thickness, which can be verified with the measurement of thickness done by Calotest equipment, where C3, C4 and C5 are then samples exhibiting the highest thickness.

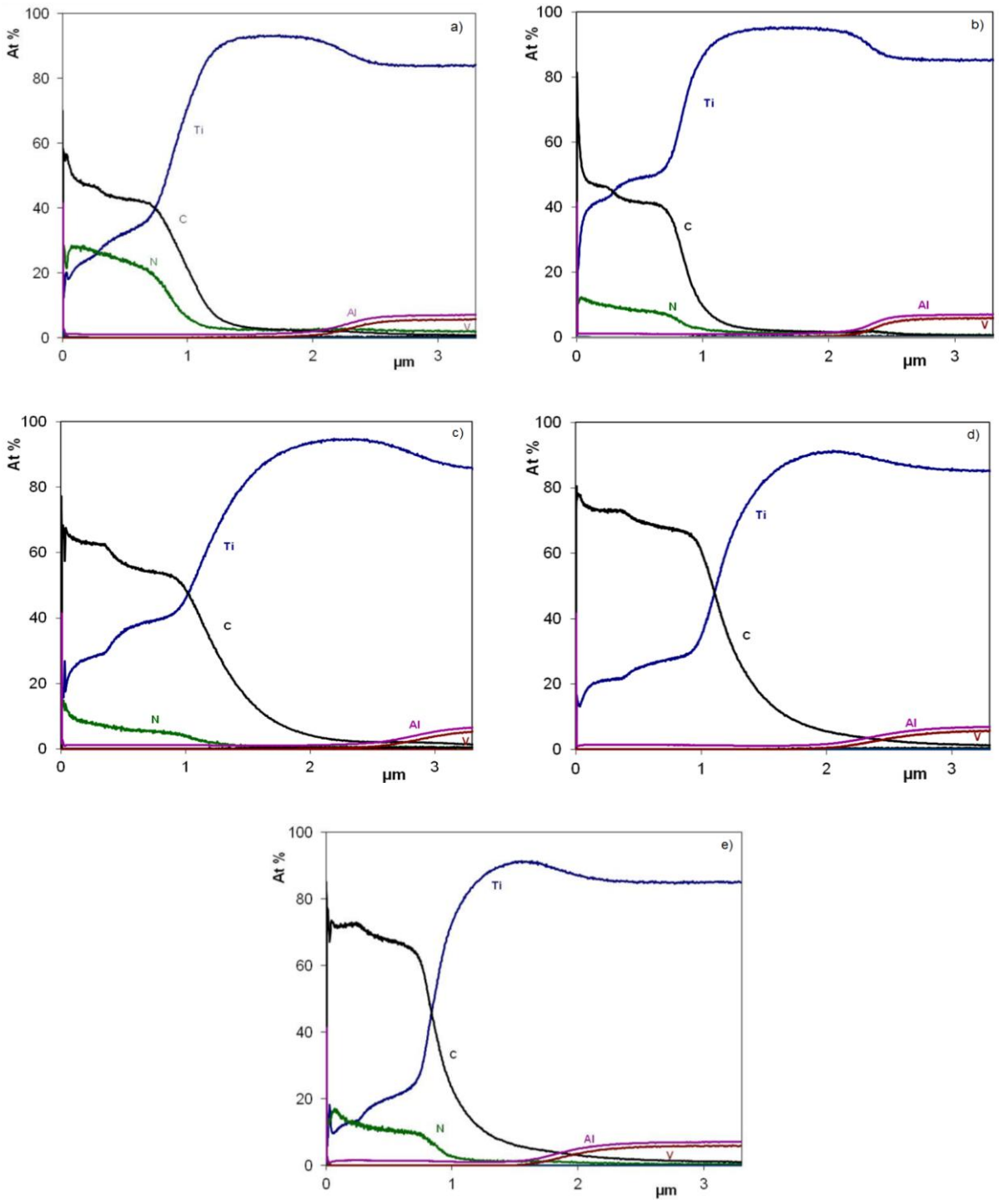

Fig. 6.1.1. Coating composition graphics obtained by GD-OES. a) C1, b) C2, c) C3, d) C4 and e) C5.

SEM micrographies of the transversal section of films deposited onto silicon wafer were taken (Fig. 6.1.2). All coatings showed pure titanium layer and Ti-C-N layer well defined. In all cases the coatings are dense. In the micrographies of C1, C2 and C5, a columnar growth of the layers can be seen. The presence of droplets embedded in

the film while it grows can be also observed. This is due to the fact that for the study of the microstructure by the SEM, the samples were not previously polished.

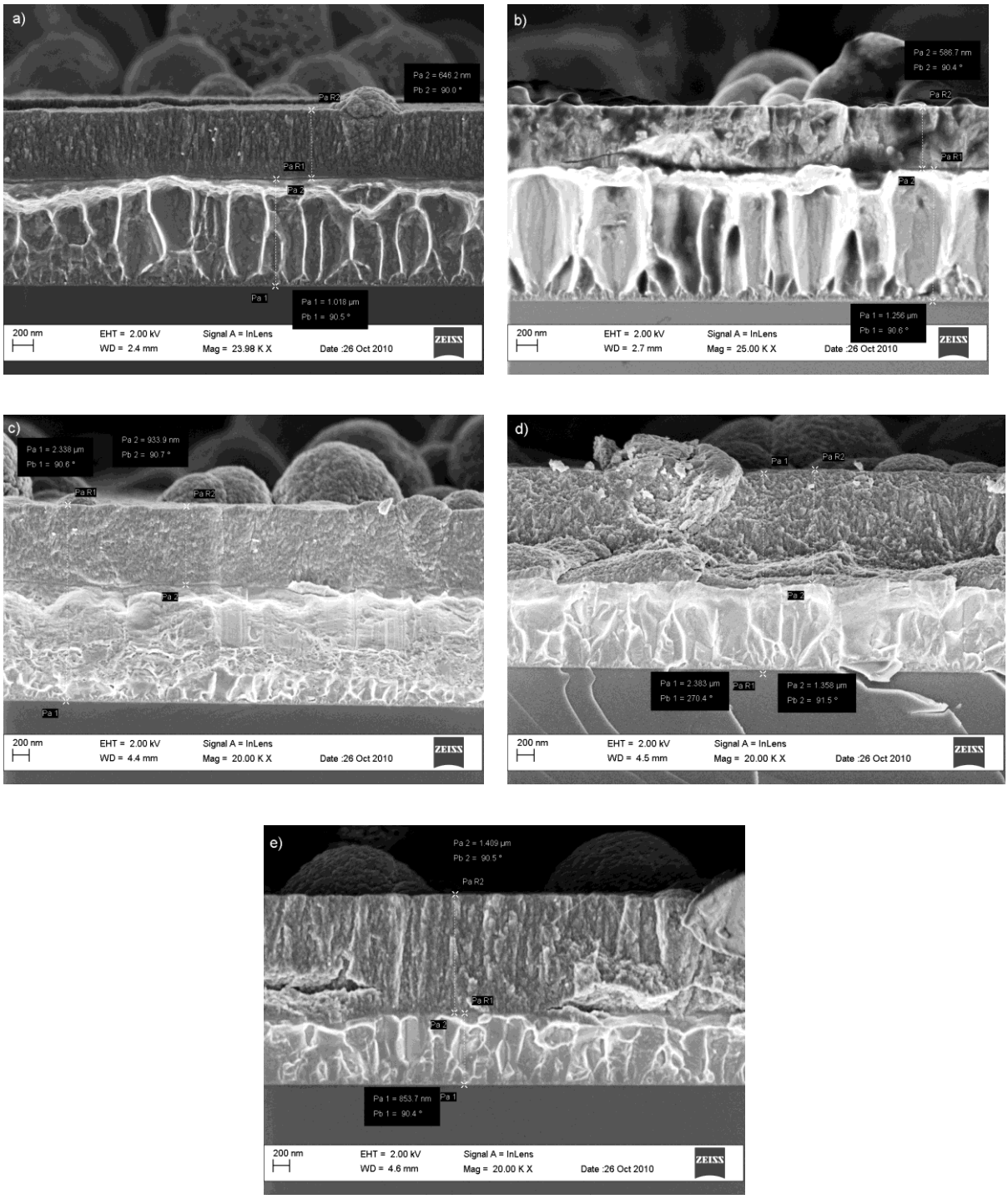

Fig. 6.1.2. SEM micrographies of coatings deposited on silicon substrate: a) C1, b) C2, c) C3, d) C4 and e) C5.

6.1.3.2. Raman Spectroscopy

The microstructure of the Ti-C-N coatings was analyzed by means of Raman spectroscopy (Fig. 6.1.3). The overall Raman intensity increases with the coating thickness and decreases with the Ti concentration measured by GD-OES. The Raman spectra show two strong bands at about 1380 and 1580 cm^{-1}. These are, respectively, the D and G bands typical of graphitic and amorphous carbon materials. The *G* band corresponds to a stretching vibrational mode of sp^2 bonded carbon. The D band is associated to disorder, and is related to a breathing mode of carbon rings[24]. The spectra were fitted in this region to two Gaussians, and a linear background (see Fig. 6.1.3 and Table 6.1.3 for a summary of the parameters). The position of the G band depends on the microstructure, and the laser wavelength. In this case, where the laser wavelength is 514 nm, the observed frequency is compatible with a material between nanocrystalline graphite (nc-G) and amorphous carbon (a-C) with a low content of sp^2 carbon. The relative intensity of the D band provides an indication of the disorder on the sp^2 layers, and the sp^3 content. For these samples, $I(D)/I(G) \approx 1$, which corresponds to a sp^3/sp^2 fraction of around 10%. This also discards other carbon species like ta-C (tetrahedral amorphous carbon) that have a much weaker D band. The observed values of the G band Full Width at Half Maximum (FWHM) of about 110–140 cm^{-1} indicate that the average size of the sp^2 flakes is of the order of 1 nm, which is below the size expected for microstructured graphite. All these facts confirm that the material is in the so-called stage 2 (between nc-G and a-C)[24].

[24] Ferrari, A. C.; Rodil, S. E.; Robertson, J., *Phys Rev B.* **2003**, 67, 155306-155325.

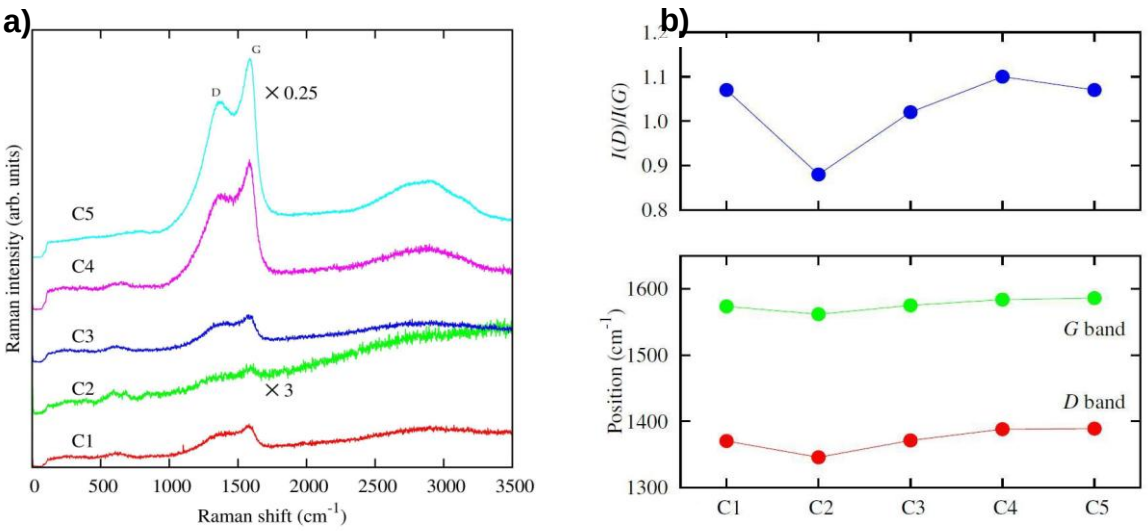

Fig. 6.1.3. a) Room temperature Raman spectra of the Ti-C-N samples (laser wavelength 514.5 nm). For clarity the intensity for C2 and C5 samples has been multiplied, respectively by 3 and 0.25, and spectra have been vertically offset. b) Plot of the I(D)/I(G) intensity ratio and the D and G band positions for the Ti-C-N samples as obtained from the fitting of the Raman spectra (Table 6.1.3).

Table 6.1.3.

Results of the fitting of the Raman spectra in the region of the D and G bands and the atomic percentage of chemical elements in the coating surface (ν̃, I and FWHM are the center wavenumber, the integrated area and the full width at half maximum of the obtained Gaussians, I(D)/I(G) is the radio of the integrated intensity for D and G Gaussians).

Sample	Ti	N	C	*D* band			*G* band			*I(D)/I(G)*
	At. %			ν̃ (cm^{-1})	*I*	FWHM (cm^{-1})	ν̃ (cm^{-1})	*I*	FWHM (cm^{-1})	
C1	20	25	55	1370	1.80	271.6	1574	0.86	138.6	1.07
C2	30	10	60	1346	1.83	198.3	1562	0.14	134.9	0.88
C3	20	10	70	1371	2.06	281.1	1575	0.95	132.5	1.02
C4	15	0	75	1388	8.70	316.9	1584	2.87	114.9	1.10
C5	15	15	70	1389	46.95	319.6	1586	15.43	112.4	1.07

Although the Raman spectra look very similar for all samples, with the exception of

the total intensity, the fitting shows that for sample C2 the I(D)/I(G) ratio is significantly smaller than for the other samples (see Fig. 3). For materials in stage 2, this decrease leads to the conclusion that the sample C2 has a larger sp^3/sp^2 fraction, thus explaining its elevated hardness (10 GPa). We also observe a decrease of the D and G band positions for sample C2. This shift for the D band could be related to the higher concentration of titanium or to a variation of residual stress due, for example, to the varying coating thickness.

The Raman spectra also show some weak bands in the range 200–800 cm^{-1}. They are related to the vibrational modes of TiC[25] and TiN[26] compounds. These bands therefore testify the alloying of the titanium with carbon atoms and titanium with nitrogen atoms with the carbon coating, and their intensity is relatively larger for samples C1, C2 and C3, which have the larger concentration of Ti or N atoms as obtained by GD-OES. They are also the thinnest where thermal diffusion of the ions to the whole coating thickness would be easier.

6.1.3.3. X-ray diffraction

XRD analysis (Fig. 6.1.4) is indicative of the presence of crystalline titanium as well as some C-specimens of the sp^2 type. In fact, up to three crystalline forms have been detected for titanium: two of them hexagonal ($P6_3/mmc$ and P6/mmm) and the third one cubic (I m-3m). In relation to the Ti-C-N, broad signals have been related to lignite (C), phase corresponding to an amorphous phase, and fullerite (C_{60}), with a higher contribution of sp^2 nanocrystalline graphite (nc-G) phase, which is related with the results obtained in Raman spectroscopy. With this technique the interfaces titanium adherence layer/substrate are analyzed.

[25] Klein, M. V.; Holy, J. A.; Williams, W. S., *Phys Rev B.* **1978**, 17, 1546-1556.
[26] Cheng, Y. H.; Tay, B. K.; Lau, S. P.; Kupfer, H.; Richter, F., *J Appl Phys.* **2002**, 92, 1845-1949.

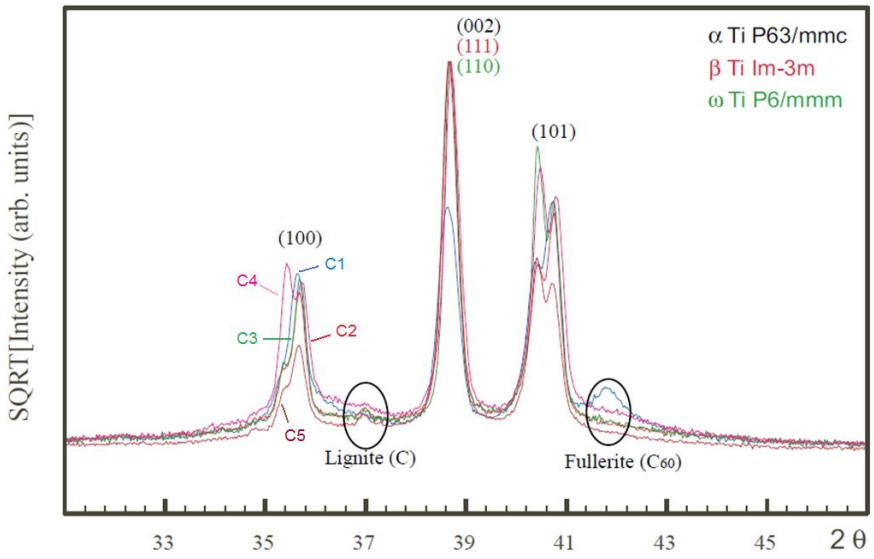

Fig. 6.1.4. XRD diffraction diagram of Ti-C-N coatings.

6.1.3.4. Fretting tests

Tribological study was carried out on Ti6Al4V substrate and Ti-C-N coatings under fretting conditions in the solution of FBS + EDTA + Sodium azide. The results of friction coefficient and wear scar analysis are listed in Table 6.1.4. All Ti-C-N coatings exhibit lower friction coefficients than Ti6Al4V substrate, being the C2 which presents the best tribological response. So it can be determined that, as expected[27], the Ti-C-N coatings improve effectively the fretting resistance of the Ti6Al4V substrate, reducing the friction coefficient and the wear. It seems that during sliding, the wear debris of the outer layers of Ti-C-N are transformed to graphite oriented with its basal plane parallel to the surface[28], generating a carbon-based coating as solid lubricant and reducing in this way friction and wear rates[6].

[27] Raman S, G. S.; Navaneethakrishnan, P.; Gnanamoorthy, R., *Proc Inst Mech Eng J J Eng Tribol.* **2009**, 223, 227-232.

Table 6.1.4.

Friction coefficients values and ball and disc wear scars measurements.

Sample	μ±SD	Disc Wear Scar, Maximum Depth (μm)
Ti6Al4V	0.86 ± 0.08	10(3)
C1	0.34 ± 0.01	Polishing effect
C2	0.24 ± 0.01	Polishing effect
C3	0.43 ± 0.01	Adhesions
C4	0.37 ± 0.02	Adhesions
C5	0.37 ± 0.01	Polishing effect

Among all Ti-C-N coatings, C1, C2 and C5 had very similar wear scars and only a smooth effect could be detected in the tested area. These coatings exhibit a better tribological behavior than others prepared by PA-CVD technique with similar columnar growth. This can be explained by the presence of metal in our coatings[29].

Al_2O_3 balls did not present significant wear scar in the tested surface. Only material transference from Ti-C-N surface to the alumina ball could be detected. This transfer film between sliding surfaces could be the reason of the reduction in the friction coefficient in all Ti-C-N coatings[12].

Analyzing the evolution of the friction coefficient in Fig. 6.1.5, it is observed that the uncoated Ti6Al4V sample has more unstable friction coefficient than the Ti-C-N coatings especially during the first half of the test. At the end of the test, an increase in the friction coefficient of C3 and C4 was also detected. This effect may be due to the material that has been removed from the coating and deposited again on the sliding surface (adhesions), which promotes an increase of the surface roughness, and hence, higher friction and wear on the samples. C1, C2 and C5 samples do not exhibit this phenomenon resulting in non failure of these coatings.

[28] Dearnaley, G.; Arps, J. H., *Surf Coat Tech.* **2005**, 200, 2518-2524.
[29] Österle, W.; Klaffke, D.; Griepentrog, M.; Gross, U.; Kranz, I.; Knabe, Ch., *Wear*. **2008**, 264, 505–517.

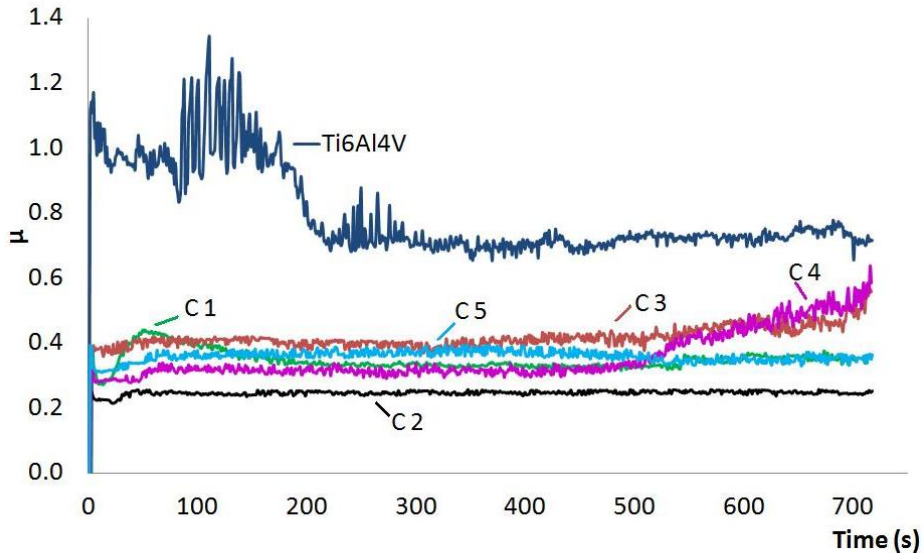

Fig. 6.1.5. Friction coefficient graph of fretting tests.

In Fig. 6.1.6 the wear profiles of each surface is represented. The reduction of the wear scar between uncoated Ti6Al4V and developed Ti-C-N coatings can be noticed. Effectively, the coatings C1, C2 and C5 show the best wear behavior with a polished track on the surface that reduces the roughness without causing wear (smooth effect). C3 and C4 coating profiles show also a better wear behavior than the substrate but the presence of adhesions in both cases can be confirmed, which explain the slight instability of friction coefficient at the end of the tests.

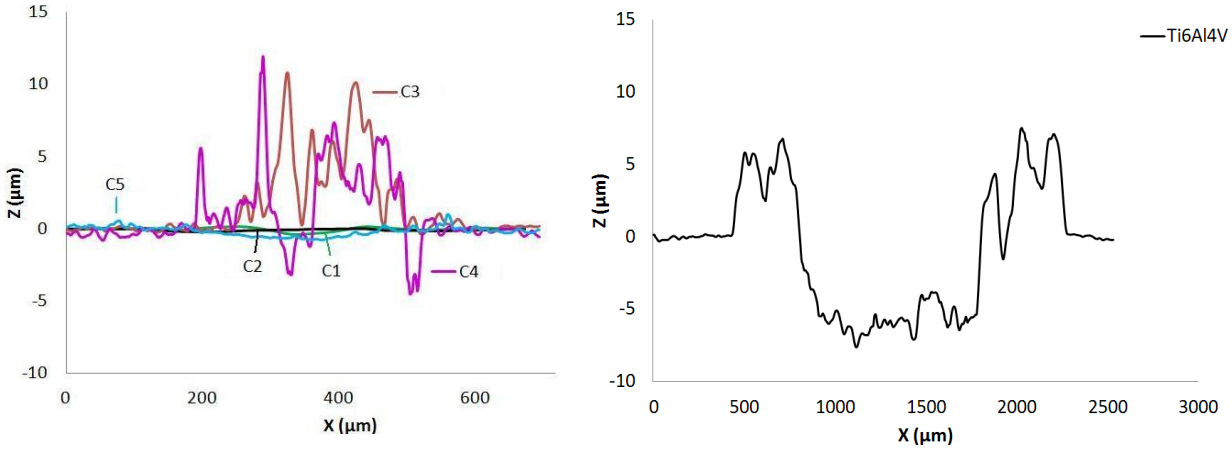

Fig. 6.1.6. Profiles of the wear tracks generated during fretting tests against alumina balls.

SEM micrographs (Fig. 6.1.7) show a detail of the scars produced on the surfaces during the fretting tests. The differences found on the wear scars and the magnitude of the damage produced on each sample can be observed.

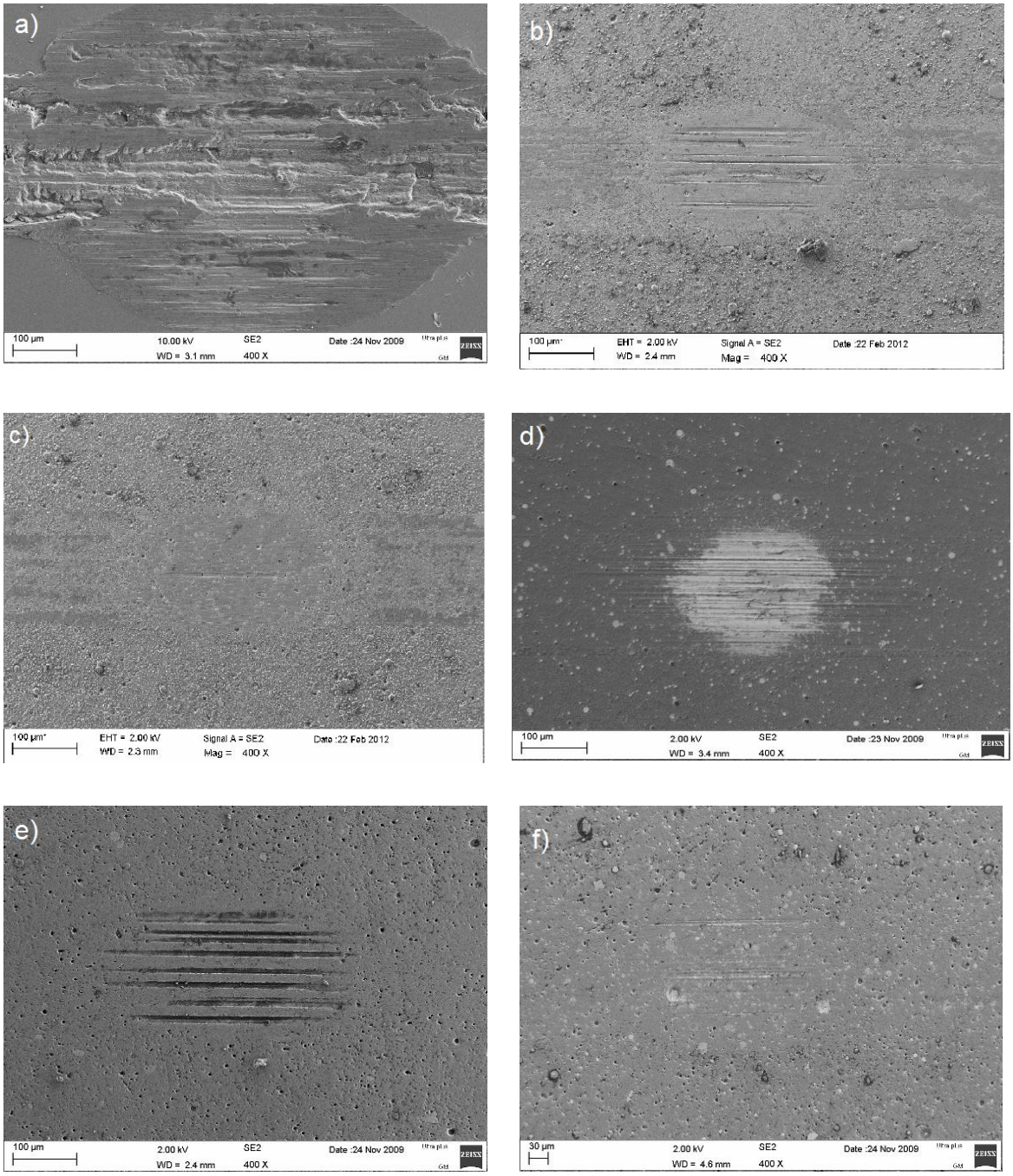

Fig. 6.1.7. SEM micrographs of the fretting tests wear scars. a) Ti6Al4V, b) C1, c) C2, d) C3, e) C4 and f) C5.

From the wear tracks morphology it can be observed that even if the friction coefficient of C3 and C4 are similar, the wear mechanism of both surfaces differs notably. Wear scratches for C4 are bigger than for C3. This could be related to the higher hardness of the wear particles produced during the fretting tests that act as abrasive agents when they are trapped between the alumina ball and the coating. The micrographs of C1, C2 and C5 show a smooth effect on the worn areas.

In general, it is noted that C2 coating exhibits the best tribological behavior. This Ti-C-N coating shows the lowest carbon content in the layer due to the lower acetylene concentration used during deposition process (see Table 6.1.1 and Fig. 6.1.1 b)). Additionally, this coating has a larger sp^3/sp^2 fraction, thus it could explain its better tribological properties with respect to the other samples, since it combines a relative higher hardness (10 GPa) due to sp^3 contribution on a predominantly sp^2 hybridation nanocrystalline graphite (nc-G) and amorphous carbon (a-C) structure.

6.1.4. Conclusions

All developed coatings consist of Ti-C-N layers. All coatings improved tribological properties of Ti6Al4V biomedical alloy commonly used in the manufacturing of artificial prosthesis. C2 coating exhibits the best tribological behavior with the lowest friction coefficient and negligible wear with only a polished effect in the sliding surface. This response of the coating could be related to the higher sp^3/sp^2 fraction which provides the necessary hardness (10 GPa) and the nanocrystalline graphite (nc-G) and amorphous carbon (a-C) structure that confers the best wear resistance to the coating. Additionally, it could also be due to the fact that, for the development of this Ti-C-N coating, the amount of acetylene employed in the deposition process has been the lowest. First trials have been done trying to correlate the tribological behavior of the coatings with their properties and microstructure, but more tests should be done in the future to reinforce these conclusions.

Contribution 2

Ti-C-N coatings developed by PVD technique: tribological and bacterial adhesion behavior of the selected coatings

Development of Ti-C-N coatings with improved tribological behaviour and antibacterial properties

Journal of the Mechanical Behavior of Biomedical Materials. **2015**, 55, 75-86

6.2.1. Introduction 104

6.2.2. Materials and Methods 107

6.2.2.1. Materials 107

6.2.2.2. Surface Characterization 108

6.2.2.3. Tribocorrosion tests 108

6.2.2.4. Surface hydrophilicity/hydrophobicity 110

6.2.2.5. Fretting tests 110

6.2.2.6. Bacterial adhesion 110

6.2.3. Results 112

6.2.3.1. Surface Characterization 112

6.2.3.2. Tribocorrosion tests 113

6.2.3.3. Surface hydrophilicity/hydrophobicity 118

6.2.3.4. Fretting tests 118

6.2.3.5. Bacterial adhesion 212

6.2.4. Discussion 124

6.2.4.1. Effect of Ti-C-N coatings in tribocorrosion response 124

6.2.4.2. Effect of Ti-C-N coatings in tribological behavior 124

6.2.4.3. Effect of Ti-C-N and silver coatings in bacterial adhesion 125

6.2.5. Conclusions 127

ABSTRACT

In artificial metallic joint implants, the failure is provoked by two effects in most of the cases: mass loss and wear debris removed due to tribological-corrosive effects on the implant alloy, and infections due to the presence of bacteria. In this work, several Ti-C-N corrosion and wear protective coatings were developed by Physical Vapour Deposition technology, and deposited on Ti6Al4V alloy. In order to provide the implant antibacterial properties, an additional silver top coating has been deposited. Tribological behavior was characterized through tribocorrosion and fretting tests. On the other hand, wettability tests were performed to study the grade of hydrophilicity/hydrophobia. Additionally, antibacterial properties were evaluated by means of bacterial adhesion tests. As a result of these characterization studies, the coating with the best performance was selected. The as-coated material includes excellent protection against tribocorrosion and fretting effects (in relation to the uncoated one) and the silver layer has been confirmed to exhibit antibacterial properties.

6.2.1. Introduction

In orthopedic applications, artificial joints (e.g., hip and knee prostheses) include bearing surfaces where the material is subjected to sliding wear. The surfaces in contact are immersed in the body fluid, and therefore, corrosion may also be a concern. Particles and metal ions generated from wear of prosthetic implants induce inflammatory reactions that provoke the release of inflammatory mediators from macrophages[1]. The concern of toxicity of high concentration of metal ions has generated a wide attention[2, 3, 4]. Therefore, for metallic artificial joint component, the improvement of tribocorrosion properties has become an important factor for their application in human body.

Tribocorrosion can be defined as a degradation phenomenon of material surfaces (wear, cracking, corrosion, etc.) subjected to the combined action of mechanical loading (friction, abrasion, erosion, etc.) and corrosion attack caused by the environment (chemical and/or electrochemical interaction)[5, 6]. This effect produces irreversible transformations on the material, as it involves numerous synergistic effects between mechanical and electrochemical phenomena, usually leading to an acceleration of material loss[7, 8, 9]. Tribocorrosion–involves numerous interaction effects between mechanical and chemical or electro-chemical phenomena[9]. The release of metallic ions due to corrosion and wear is of vital importance, since it can adversely affect the biocompatibility and mechanical integrity of implants[10]. The metal ions released into the surrounding tissue may induce the release of potentially osteolytic cytokines involved in implant loosening[11, 4].

Surface treatments are widely employed to improve wear and corrosion resistance as well as hardness of the surface of metallic alloys employed in orthopedic

[1] Sinnett-Jones, P. E.; Wharton, J. A.; Wood, R. J. K., *Wear.* **2005**, 59, 898-909.
[2] Brodner, W.; Bitzan, P.; Meisinger, V.; Kaider, A.; Gottsauner-wolf, F.; Kotz, R., *J Bone Joint Surg.* **1997**, 79, 316-321.
[3] Hallab, N.; Jacobs, J. J.; Black, J., *Biomaterials.* **2000**, 21, 1301-1314.
[4] Sargeant, A.; Goswami, T., *Mater Design.* **2007**, 28, 155-171.
[5] Mischler, S., *Tribol Int.* **2008**, 41, 573-583.
[6] Mischler, S.; Ponthiaux, P., *Wear.* **2001**, 428, 211-225.
[7] Diomidis, N.; Celis, J. P.; Ponthiaux, P.; Wenger, F., *Wear.* **2010**, 269, 93-103.
[8] Iwabuchi, A.; Lee, J. W.; Uchidate, M., *Wear.* **2007**, 236, 492-500.
[9] Landolt, D.; Mischler, S.; Stemp M.; Barril, S., *Wear.* **2004**, 256, 517-524.
[10] Vieira, A. C.; Ribeiro, A. R.; Rocha, L. A.; Celis, J. P., *Wear.* **2006**, 261, 994-1001.
[11] Rogers, S. D.; Howie, D. W.; Graves, S. E.; Pearcy, M. J.; Haynes, D. R., *J Bone Joint Surg.* **1997**, 79B, 311-315.

devices[12, 13, 14, 15]. In recent years, diamond-like-carbon (DLC) films have been the subject of extensive investigations due to their potential of attaining combination for highly desirable properties in the context of biomedical applications[16, 17, 18]. Their high hardness, low friction and wear, electrical insulation, chemical inertness and good biocompatibility make them ideal candidates as protective coatings in joints replacement[19]. These coatings are preferred since they improve resistance against wear and corrosion processes, especially on Ti6Al4V (the alloy most widely used for implant fabrication). The Ti6Al4V alloy has an excellent corrosion resistance, biocompatibility, high strength to weight ratio and also a high toughness[20]. However, the major disadvantage regarding the use of Ti6Al4V for bio-implant application is its low load-bearing capacity and poor wear resistance. Moreover, this alloy is not only subjected to wear but also to active corrosion, generated by breaking up of the protective passive oxide layer in sliding contact. The frictional movement in corrosive medium is continuous[21] which produces particles and ions that can result in adverse biological reactions[22, 4].

The present work is focused in total knee replacements, where two major problems can be presented: the first one is produced between the backside of the ultra-high molecular weight polyethylene (UHMWPE) patellar component and the tibial tray of fixed bearing tibial component made of Ti6Al4V where the fretting effect takes place, which is the responsible of the elimination of mounts of polyethylene and Ti6Al4V alloy debris[23]. In this case, the cause of failure in most cases is related with this wear debris elimination[24, 25]. The second problem is related to implant-

[12] Cheng, Y.; Zheng, Y.F., *Surf Coat Technol.* **2006**, 200, 4543-4548.
[13] Kaestner, P.; Olfe, J.; He, J. W.; Rie, K-T., *Surf Coat Tech.* **2001**, 142-144, 928-933.
[14] Yildiz, F.; Yetim, A. F.; Alsaran, A.; Çelik, A., *Surf Coat Tech.***2007**, 202, 2471-2476.
[15] Zhecheva, A.; Sha, W.; Malinov, S.; Long, A., *Surf Coat Tech.* **2005**, 200, 2192-2207.
[16] Martinu, L.; Raveh, A.; Domingue, A.; Bertrand, L.; Klemberg-Sapieha, J. E.; Gujrathi, S. C.; Wertheimer, M. R., *Thin solid Films.* **1992**, 208, 42-47.
[17] Raveh, A.; Martinu, L.; Gujrathi, S. C.; Klemberg-Sapieha, J. E.; Wertheimer, M. R., *Surf Coat Tech.* **1992**, 53, 275-282.
[18] Snyders, R.; Bousser, E.; Amireault, P.; Klemberg-Sapieha, J. E.; Park, E.; Taylor, K.; Casey, K.; Matinu, L., *Plasma Process Polym.* **2007**, 4, S640-S646.
[19] Bendavid, A.; Martin, P. J.; Comte, C.; Preston, E. W.; Haq, A. J.; Magdon Ismail, F. S.; Singh, R. K., *Diam Relat Mater.* **2007**, 16, 1616-1622.
[20] Xuanyong, L.; Paul, K. C.; Chuanxian, D., *Mat Sci Eng R.* **2004**, 47, 49-121.
[21] Arslan, E.; Totik, Y.; Efeoglu, I., *Prog Org Coat.* **2012**, 74, 768-771.
[22] Hodgson, A. W. E.; Mueller, Y.; Forster, D.; Virtanen, S., *Electrochim Acta.* **2002**, 47, 1913-1923.
[23] Billi, F.; Sangiorgio, S. N.; Aust, S.; Ebramzadeh, E., *J Biomech.* **2010**, 43, 1310-1315.
[24] Currier, J. H.; Bill, M. A.; Mayor, M. B., *J Biomech.* **2005**, 38, 367-375.
[25] Sharkey, P. F.; Hozack, W. J.; Rothman, R. H.; Shastri, S.; Jacoby, M., *Clin Orthop Relat R.*

associated infections. The presence of an implanted device results in an increased susceptibility to infection for the patient[26, 27]. Occurring at a rate of 5%, orthopedic implant infections remain one of the most devastating complications[28]. The diagnosis and treatment of prosthetic joint infections is further complicated by the development of a bacterial biofilm. This structure allows bacteria to resist antimicrobial agents and immune responses. Patients with this type of infection require a longer period of antibiotic therapy and repeated surgical procedures. These prosthetic-joint infections have severe consequences not only for patients but also for society[29, 30, 31, 32, 33, 34, 35, 36, 37, 38, 39]. Factors influencing the bacteria adherence to a biomaterial surface include chemical composition of the material, surface charge, hydrophobicity, as well as surface roughness and/or physical configuration. It would be desirable to develop biomedical coatings for implants which are repellent to bacteria to minimize the colonization of the implant surface with circulating planktonic bacteria that can lead to biofilm development[37, 40]. One of the strategies that is gaining renewed attention for combating the threat of bacterial infection is the use of an antibacterial noble metals[41].

Taking into consideration the above mentioned aspects, this work has been focused on the development of several Ti-C-N protective coatings for Ti6Al4V in order to improve the wear and corrosion resistance of the surfaces. Thus,

2001, 404, 7-13.
[26] Elek, S. D.; Conen, P. E., *Br J Exp Pathol.* **1957**, 38, 573-586.
[27] Guggenbichler, J.P.; Assadian, O.; Boeswald, M.; Kramer, A., Incidence and clinical implication of nosocomial infections associated with implantable biomaterials - catheters, ventilator-associated pneumonia, urinary tract infections. GMS Krankenhhyg Interdiszip. 6, Doc18, 2011.
[28] Gordon, O.; Vig Slenters, T.; Brunetto, P. S.; Villaruz, A. E.; Sturdevant, D. E.; Otto, M.; Landmann, R.; Fromm, K. M., *Antimicrob Agents Chemother.* **2010**, 54, 4208-4218.
[29] An, Y. H.; Friedman, R. J., *J Biomed Mater Res.* **1998**, 43, 338-348.
[30] Cordero, J.; Munuera, L.; Folgueira, M. D., *Injury.* **1996**, 27, SC34-7.
[31] Edwards, C.; Counsell, A.; Boulton, C.; Moran, C. G., *J Bone Joint Surg Br.* **2008**, 90, 770-777.
[32] Esteban, J.; Gomez-Barrena, E.; Cordero, J.; Martin-de-Hijas, N. Z.; Kinnari, T. J.; Fernandez-Roblas, R., *J Clin Microbiol.* **2008**, 46, 488-492.
[33] Garner, J. S.; Jarvis, W. R.; Emori, T. G.; Horan, T. C.; Hughes, J. M., *Am J Infect Control.* **1988**, 16, 128-140.
[34] Gristina, A.G., *Science.* **1987**, 237, 1588-1595.
[35] Harris, L. G.; Richards, R. G., *Injury.* **2006**, 37, S3-14.
[36] Katsikogianni, M.; Missirlis, Y. F., *Eur Cell Mater.* **2004**, 8, 37-57.
[37] Perez-Tanoira, R.; Perez-Jorge, C.; Endrino, J. L.; Gomez-Barrena, E.; Horwat, D.; Pierson, J. F.; Esteban, J., *J Biomed Mater Res A.* **2012**, 100, 1521-1528.
[38] Rochford, E. T.; Richards, R. G.; Moriarty, T. F., *Clin Microbiol Infect.* **2012**, 18, 1162-1167.
[39] Singhai, M.; Malik, A.; Shahid, M.; Malik, M. A.; Goyal, R., *J Glob Infect Dis.* **2012**, 4, 193-198.
[40] Perez-Tanoira, R.; Isea-Pena, M. C.; Celdran, A.; Garcia-Vasquez, C.; Esteban, J., *Surg Infect (Larchmt).* **2014**, 15, 90-93.

tribological behavior has been characterized through tribocorrosion and fretting tests. Additionally, the effect of the silver top film has been evaluated by means of a bacterial adhesion study. Finally, wettability tests have been performed in order to study the influence of the hydrophilicity/hydrophobicity grade in the bacterial adhesion.

6.2.2. Materials and methods

6.2.2.1. Materials

In a previous work carried out for some authors of this paper[42], five Ti-C-N coatings were developed on Ti6Al4V substrates by physical vapor deposition (PVD) cathodic arc method in order to improve the fretting resistance of the substrate. These coatings were characterized by analyzing their physical properties, thickness, hardness, adhesion and roughness. Microstructural characterization was assessed by means of X-ray diffraction (XRD), scanning electron microscope (SEM) and RAMAN spectroscopy techniques; chemical composition in depth was studied with Glow Discharge Optical Emission Spectroscopy (GD-OES) technique; and tribological behavior by means of fretting tests. This study allowed the selection of one coating (C2 coating) that could be a good alternative for protecting Ti6Al4V substrates from the tribological point of view, and has been codified in this work as Ti-C-N_1. Additionally, taking into account the superior tribocorrosion response characterized by R. Bayón in her thesis work[43], another coating was selected in this study: the Ti-C-N_2 coating (codified as C5 in Sáenz de Viteri et al.[42]). Thus, the details about Ti6Al4V samples preparation and coating deposition technique were reported elsewhere[42].

In table 6.2.1 the most significant results of selected coatings from the previous work are presented[42].

[41] Atiyeh, B. S.; Costagliola, M.; Hayek, S. N.; Dibo, S. A., *Burns*. **2007**, 33, 139-148.
[42] Sáenz de Viteri, V.; Barandika, M. G.; Ruiz de Gopegui, U.; Bayón, R.; Zubizarreta, C.; Fernández, X.; Igartua, A.; Agullo-Rueda, F., *J Inorg Biochem*. **2012**, 117, 359-366.
[43] Bayón, R., Corrosion-wear behaviour of novel surface coatings developed by means of advanced techniques. Doctoral thesis. University of Basque Country, **2011**.

Table 6.2.1.

Thickness, roughness, hardness, I(D)/I(G) and friction coefficient values of selected coatings.

Sample	Thickness (µm)	Roughness Ra, (µm)	Hardness (GPa)	I(D)/I(G)	Friction coefficient
Ti6Al4V	-	0.05	-	-	0.86 ± 0.08
Ti-C-N_1	2.40	0.36	10	0.88	0.24 ± 0.01
Ti-C-N_2	3.86	0.42	8	1.07	0.37 ± 0.01

I(D)/I(G) is the ratio of the integrated intensity for D and G Gaussians obtained by Raman spectroscopy. The G band corresponds to a stretching vibrational mode of sp^2 bonded carbon, and the D band is associated to disorder, and is related to a breathing mode of carbon rings.

With the aim of providing additional antibacterial properties, a thin silver film was deposited on the coatings with better properties from wear-corrosion tests. The Ag film was deposited by PVD in a vacuum chamber evacuated up to a pressure of 10^{-5} mbar. A DC-pulsed (250 KHz) ENI-RPG50 plasma source has been used to obtain the plasma. The Ag film was deposited with power density of 1.7 W/cm^2 and a deposition rate of 40 nm/min. During the deposition process, the argon flow was constant (45 sccm) and the pressure in the chamber during the deposition process was 0.4 Pa.

6.2.2.2. Surface characterization

Chemical composition of the new produced surface with Ag film was analyzed by GD-OES technique from Horiba Jobin Yvon. The measurement conditions were 650 Pa and 35 W, with a copper anode of 4 mm of diameter. Microstructural study was carried out by means of Scanning Electron Microscope (SEM), from OXFORD INCA Synergy.

6.2.2.3. Tribocorrosion tests

Tribocorrosion tests were carried out in order to study the synergistic effect of wear and corrosion following the experimental procedure defined by Celis and

Ponthiaux[44] and Ponthiaux[45] and explained below.

Prior to the wear tests, samples remained into the electrolyte for 60 minutes till reaching a stable open circuit potential (OCP). After this initial immersion time, an electrochemical impedance spectroscopy was performed to analyze the electrochemical state of the surfaces before the tribological test. The duration of the first mechanical tests was of 1000 cycles. During this stage, the open circuit potentials under sliding and friction coefficient were registered simultaneously. After this stage, a second sliding process of 3500 cycles was then performed under potentiostatic control by imposing to the system the previous potential measured during sliding. At the same time, a second electrochemical impedance spectroscopy was additionally performed during the sliding. After 3500 cycles, the samples were removed from the electrolyte, cleaned ultrasonically with alcohol for 5 min, and dried in warm air. The wear tracks were analyzed by confocal microscopy (Nykon Eclipse ME600 Confocal Microscopy) performing topographical measurements at different locations of the wear tracks.

The tests were performed by using a Microtest tribometer with rotatory movement under "ball on disc" configuration, assisted by an Autolab-Methrom potentiostat PGSTAT302N. The electrolyte used for simulating biological environment was a phosphate buffered saline (PBS) solution, composed by: 0.14 M NaCl, 1 mM KH_2PO_4, 3 mM KCl, and 10 mM Na_2HPO_4.

The applied load was 5 N, the rotational speed was 120 rpm and track radius 6 mm. The exposed area was, in all cases, 2.5 cm^2. Over the rotatory disc, an electrochemical cell with three electrodes was placed in order to perform electrochemical measurements simultaneously. The reference electrode employed to measure the potential was Ag/AgCl KCl 3M (0.207 V vs SHE) and the counter electrode was a platinum wire. As counterbodies, ceramic balls of alumina with 10 mm of diameter were chosen. Samples were previously polished until a final roughness of 0.03 µm, and then cleaned with distilled water and ethanol in an ultrasonic bath.

[44] Celis, J. P.; Ponthiaux, P., *Testing tribocorrosion of passivating materials supporting research and industrial innovation: Handbook EPC 62 Green Book*. Publishing Manley, London, UK, **2012**.
[45] Ponthiaux, P.; Bayón, R.; Wenger, F.; Celis, J. P., Testing protocol for the study of bio-tribocorrosion, in: Yan, Y. (Ed.), *Bio-tribocorrosion in Biomaterials and Medical Implants*, Woodhead Publishing Limited, Cambrigde, UK, **2013**.

After the tribocorrosion tests, the electrolytes (PBS) were collected and analyzed by inductively coupled plasma atomic emission spectroscopy (ICP-AES) in ULTIMA 2 HORIBA Jobin Yvon equipment for analyzing the presence of aluminum, vanadium and titanium released from the coating/substrate during tribocorrosion test. Each used electrolyte was then divided into two volumes. One was directly analyzed by ICP-AES after filtering at 0.45 µm in order to detect the dissolved elements, and the other one was firstly treated with H_2O:HNO_3 (1:1) and two droplets of HF in order to dissolve all the possible compounds. In this last measurement, total elements, dissolved and solids, were analyzed.

6.2.2.4. Surface hydrophilicity/hydrophobicity

The SURFTENS universal goniometer was used to investigate the wetting behavior of different samples, in order to evaluate the grade of hydrophilicity/hydrophobia. This evaluation is based on the measurement of the contact angle of a drop of distilled water on the surface to be investigated. This contact angle is measured by means of an optical camera, recording and calculating its value.

6.2.2.5. Fretting tests

Fretting tests were performed in SRV® tribometer under ball-on-disc configuration with the aim to try to reproduce as close as possible real working conditions. Balls of UHMWPE with a diameter of 10 mm were used as counterbody, trying to use the real materials. The stemmed tibial component is made of a titanium alloy and the patellar component is a UHMWPE. Tests were done under lubricated conditions by using fetal bovine serum (FBS) with sodium azide and ethylenediaminetetraacetic acid (EDTA), according to ASTM F732-00 standard. Tests were carried out at 37 ^{o}C during 60 minutes. Testing conditions applied were: a load of 30 MPa, a frequency of 210 Hz and a stroke of 150 µm.

6.2.2.6. Bacterial adhesion

Staphylococcal adhesion experiments

Coated Ti6Al4V samples were compared against controls of uncoated Ti6Al4V samples. Staphylococcal adhesion experiments were performed as described by

Kinnari et al.[46] and Perez-Tanoira et al.[37]. For the preliminary study of bacterial adhesion, the biofilm-forming collection strains *S. aureus* 15981[47], *S. epidermidis* ATCC 35984 and 6 clinical strain from S. aureus (p1...p6) and 6 other of *S. epidermidis* (p7...p12), isolated from patients with implant-related infection by sonication[32] were used. All strains were cultured overnight in tryptic soy broth (bioMérieux, Marcy l'Etoile, France) at 37ºC in 5% CO_2 atmosphere. It is worth mentioning that all patients were diagnosed articular infection based on clinical criteria[48]. The clinical Staphylococcus strains are positive for biofilm development[49].

After culture, bacteria were harvested by 10 minutes centrifugation at 3500 g at room temperature. Supernatant was discarded and the pellet was washed three times with sterile phosphate buffered saline (PBS). Bacteria were then suspended and diluted in PBS to 10^8 colony-forming units (CFU)/ml. The biomaterial discs were placed in the bacterial suspension and incubated for 90 min at 37 ºC. Afterwards, the biomaterial plates were rinsed three times with sterile PBS to remove any non-adherent bacteria[46].

The dried plates were stained for 15 min with a rapid fluorescence staining method using the Live/Dead® Bacterial Viability Kit (BacklightTM)[50] (Boulos et al., 1999). On each plate, 8 fields were viewed and photographed with a Nikon Coolpix 8400 (Nikon, Melville, NY) under a fluorescence microscope at 40x magnification. All experiments were performed in triplicate. The number of microphotographs studied was 24 for each material and bacterium. The surface area covered with adhered bacteria was calculated using the ImageJ software (National Institute of Health, Bethesda, MD).

Statistical analysis

For the statistical study, Mann-Whitney or Wilcoxon non parametric tests were employed. These tests were used for two samples while the Kruskal-Wallis test was

[46] Kinnari, T. J.; Soininen, A.; Esteban, J.; Zamora, N.; Alakoski, E.; Kouri, V. P.; Lappalainen, R.; Konttinen, Y. T.; Gomez-Barrena, E.; Tiainen, V. M., *J Biomed Mater Res A.* **2008**, 86, 760-768.
[47] Valle, J.; Toledo-Arana, A.; Berasain, C.; Ghigo, J. M.; Amorena, B.; Penadés, J. R.; Lasa, I., *Mol Microbiol.* **2003**, 48, 1075-1087.
[48] Cordero-Ampuero, J.; Esteban, J.; Garcia-Cimbrelo, E.; Munuera, L.; Escobar, R., *Acta Orthop.* **2007**, 78, 511-519.
[49] Esteban, J.; Molina-Manso, D.; Spiliopoulou, I.; Cordero-Ampuero, J.; Fernández-Roblas, R.; Foka, A.; Gómez-Barrena, E., *Acta Orthop.* **2010**, 81, 674-679
[50] Boulos, L.; Prevost, M.; Barbeau, B.; Coallier, J.; Desjardins, R., *J Microbiol Methods.* **1999**, 37, 77-89.

used for more than two samples. EPI-Info software version 3.5.1 (CDC, Atlanta, GA. USA) was used to perform the statistical studies.

6.2.3. Results

As previously mentioned, the surface characterization of Ti-C-N_1 and Ti-C-N_2 has been previously reported by the same authors[43, 42]. Thus, the aim of this study is the selection of the best coating for knee implants, the election being based on a pre-selection. With this aim, the first step was the study of the tribocorrosion behavior of both coatings, and the comparison with the substrate (Ti6Al4V). Taking into account the good tribocorrosion results, one of the coatings was selected (Ti-C-N_2) in order to continue with a more detailed study. As a further objective was the development of an antibacterial coating, Ti-C-N_2 film was coated with a film of silver, producing the coating Ti-C-N_2+Ag. This way, wettability, fretting and bacterial adhesion tests were carried out for Ti6Al4V and for Ti-C-N_2 and Ti-C-N_2+Ag coatings. Therefore, the surface characterization herein presented was performed just for the new coating Ti-C-N_2+Ag.

6.2.3.1. Surface characterization

A thin layer of 200 nm of silver was deposited on Ti-C-N_2 coating, and the analysis of the chemical composition was obtained by GD-OES technique (Fig. 6.2.1, left). The as-obtained profile gives a qualitative idea of the progression in depth of chemical composition. This measurement was carried out in a sample where the Ti-C-N_2 and Ag coatings where deposited onto silicon wafer. The presence of titanium layer can be detected on the top of silicon. The decrease of the amount of titanium is accompanied by the presence of C and N that appear gradually because the gases needed to deposit those elements were introduced into the chamber progressively. On the left hand side, it was observed that all elements related to the Ti-C-N coating disappeared, showing a top film layer of pure the silver, corresponding to the film. It should be noted the presence of oxygen in large part of the analysis and the nitrogen continuity once the coating has finished. It seems that the silver layer peeled due to a break in the vacuum allowing air introduction.

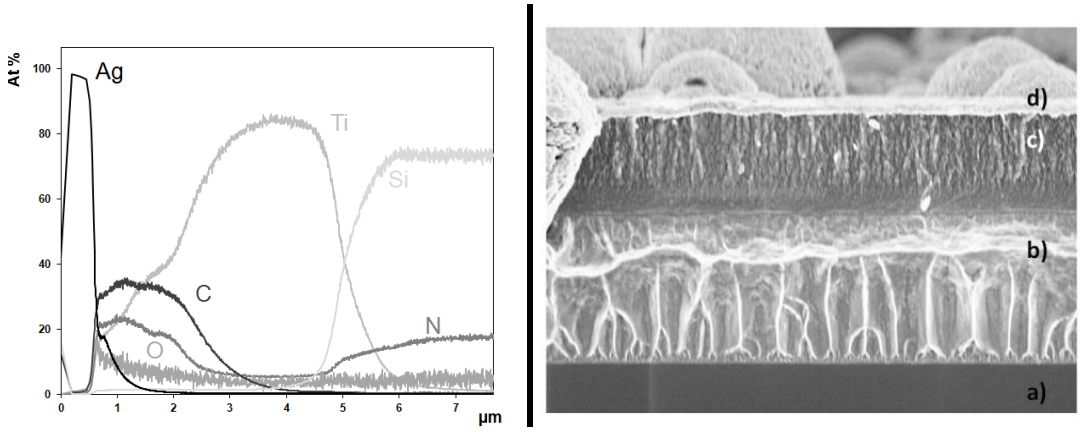

Fig. 6.2.1. (Left) Graded coating composition obtained by GD-OES, and (right) SEM micrograph for Ti-C-N_2+Ag coating.

Figure 6.2.1 right shows the SEM micrograph of transversal section obtained in a coated silicon wafer. All different coatings, seen by GD-OES analysis, can be also distinguished by SEM, first the silicon corresponding to the silicon wafer (a), second the pure titanium layer (b), afterwards the Ti-C-N coating (c), and finally the silver film (d). It can be detected the presence of droplets embedded in the film due to the deposition process itself. This effect was observed because the sample was not polished for the microstructure study. The different morphology between pure titanium layer and Ti-C-N coating is related to the process conditions and the influence of deposited elements[42].

6.2.3.2. Tribocorrosion tests

The first step in tribocorrosion testing procedure was the monitoring of the open circuit potential (OCP) of the surfaces immersed in PBS during 1 hour, until its stabilization. The OCP values for Ti6Al4V, Ti-C-N_1 and Ti-C-N_2 were -0.273 V, 0.063 V and 0.110 V, respectively. Once the OCP of the samples reached a stable value, an Electrochemical Impedance Spectroscopy (EIS) was registered in order to evaluate the corrosion resistance of the exposed surfaces before the sliding process. After the impedance measurement, the OCP was again registered during the first sliding process (Fig. 6.2.2). When the sliding process started, the potential decreased in all samples to more negative values as a consequence of an activation process on their track surface due to the effect of sliding. This decrease of the potential was related to the total or partial destruction of the passive film as a consequence of the mechanical contact imposed. In case of Ti6Al4V, the potential decreased to the lowest potential values in comparison to the Ti-C-N coatings. During sliding

process, the OCP for Ti6Al4V and Ti-C-N_1 fluctuated due to the constant removal and re-growth of their passive film as consequence of the sliding. In case of Ti-C-N_2 coating, the potential remained stable during rubbing process. Once the wear process was completed, the potential in all samples increased quickly to more positive values close to the initial ones, as a consequence of an immediate repassivation phenomenon on the worn area. The values of the samples at the end of the sliding, after a stabilization time were: -0.313 V (Ti6Al4V), -0.160 V (Ti-C-N_1) and -0.055 V (Ti-C-N_2). In any case, the potential didn't reach the initial value registered before the sliding due to the fact that the worn surface did not present the same electrochemical state as the unworn area

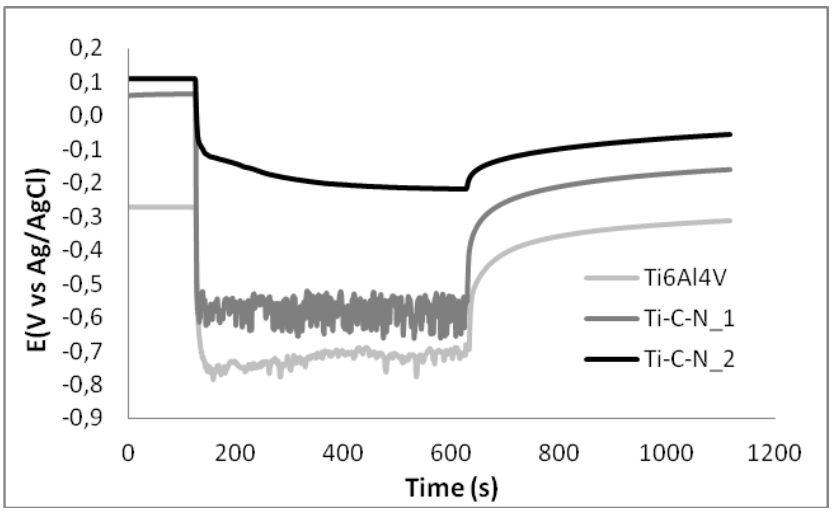

Fig. 6.2.2. Open circuit potential (OCP) during sliding process for TiAl4V,and Ti-C-N_1 and Ti-C-N_2 coatings.

Corrosion resistance before and during sliding process was evaluated from the experimental data registered during EIS measurements (Fig. 6.2.3).

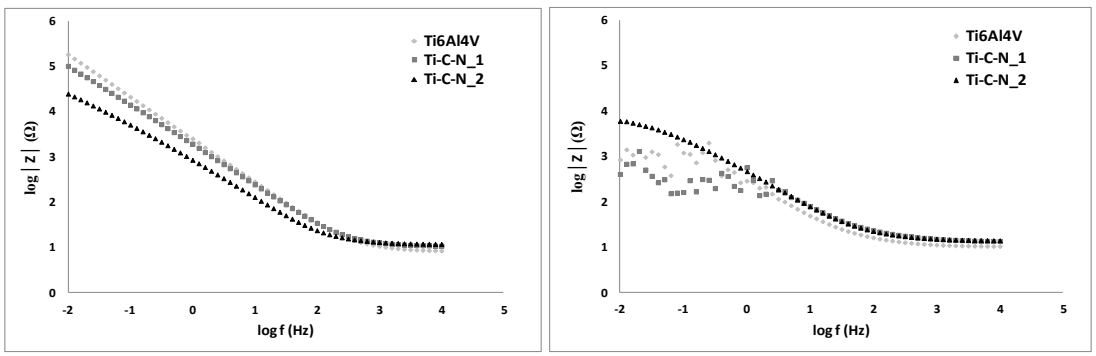

Fig. 6.2.3. Bode plots for TiAl4V, Ti-C-N_1 and Ti-C-N_2 coatings (left) before and (right) during siliding. (modulus IZI is the impedance modulus and f is the frequency).

As observed in figure 6.2.3, bode diagrams for Ti6Al4V, Ti-C-N_1 and Ti-C-N_2 coatings showed that the electrochemical state of the surfaces in all samples changed due to the wear, resulting in a reduction in their corrosion resistance. Ti-C-N_1 and Ti6Al4V samples showed similar values of corrosion resistance before sliding process, while Ti-C-N_2 presented slightly lower corrosion resistance after the first hour of inmersion in PBS. However, during sliding process, the corrosion behaviour of Ti6Al4V and Ti-C-N_1 coating was more significantly affected than in case of the Ti-C-N_2 coating. The reduction of the corrosion resistance in Ti-C-N_1 sample seems to be due to the fact that the protective Ti-C-N coating was completely removed in the sliding contact area and the bare substrate was exposed to the mechanical and electrochemical effect during some parts of the tribological test. The variation of the corrosion resistance before and during sliding process for the three samples was calculated by fitting the experimental data with appropriate equivalent circuits. The corrosion resistance in case of Ti6Al4V and Ti-C-N_1 was reduced 99.97% and 99.18%, respectively. Nevertheless, Ti-C-N_2 showed the lowest corrosion resistance variation with a reduction of 18.05 %. It must be pointed out that polarization resistance values obtained during the sliding process were calculated for the high-medium range of frequencies for all samples due to the instability of the system when measuring impedance at low frequencies. In case of the corrosion resistances before the sliding process, those values were obtained in the whole frequency range (10 kHz to 10 mHz).

In table 6.2.2, friction coefficients registered during sliding test are summarized as well as the total material loss in the wear track (W_{tr}), the percentage of material loss due to corrosion of active area in the wear track (W^{c}_{act}) and the percentage of material loss due to mechanical wear of active material in the wear track (W^{m}_{act}). As observed, the Ti-C-N_2 coating exhibits the lowest coefficient of friction and the best wear resistance with the lowest loss of material. The parameters obtained in case of Ti-C-N_1 coating are closed to the substrate ones, with higher friction coefficient and similar material loss. In all cases, the material loss due to corrosion is very low in comparison with the material loss due to mechanical effect, which is in all samples around 99.9%. In fact, the wear tracks produced for Ti6Al4V and Ti-C-N_1 exhibit similar depth and width, showing that the Ti-C-N_1 coating was completely removed during test, and the track depth reached the substrate. This explains the similar potential evolution during sliding observed for both samples. Additionally, it can be noticed that the wear depth of Ti-C-N_2 is very low in

comparison to Ti6Al4V and Ti-C-N_1, showing a polishing effect. The profile of the wear tracks produced after the tribocorrosion tests can be observed in figure 6.2.4.

Table 6.2.2.
Mean friction coefficient values and material loss of uncoated and Ti-C-N coated titanium alloy.

Sample	Friction coefficient (μ) ± SD	W_{tr} x10^4 (cm^3) ± SD	% W^c_{act}	% W^m_{act}
Ti6Al4V	0.41 ± 0.01	7.759 ± 0.172	0.07	99.93
Ti-C-N_1	0.38 ± 0.01	6.480 ± 0.169	0.06	99.94
Ti-C-N_2	0.15 ± 0.01	0.091 ± 0.011	0.10	99.90

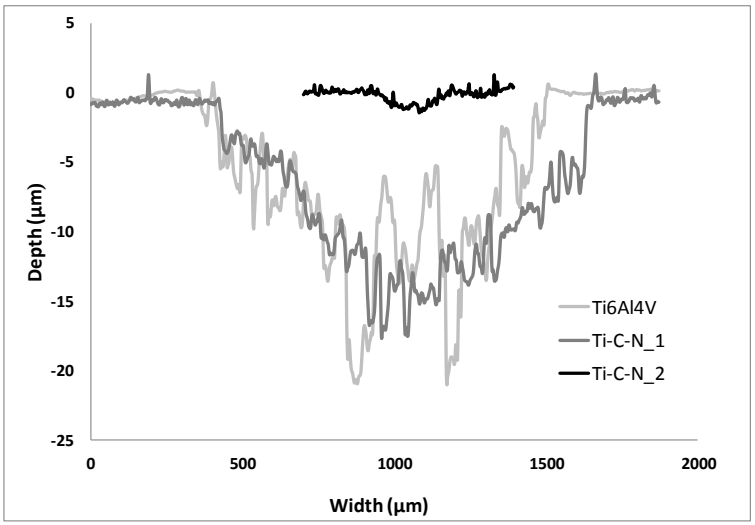

Fig. 6.2.4. Profiles of the wear scars.

In summary, the lowest friction coefficient, the better corrosion resistance and the lowest material loss produced during the tribocorrosion process in case of Ti-C-N_2 sample indicate that this coating is the best alternative in terms of tribocorrosion performance. In figure 6.2.5, the friction coefficient evolution during the sliding process in tribocorrosion tests is represented.

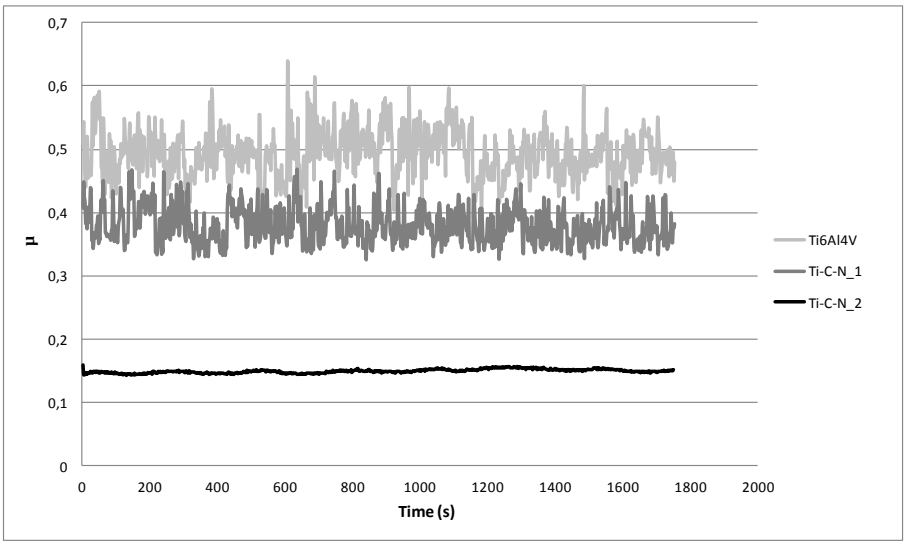

Fig. 6.2.5. Friction coefficient evolution in tribocorrosion tests.

In order to complete previous results, ICP technique was performed on the electrolyte used for tribocorrosion tests with the aim of studying the migration of elements from Ti6Al4V alloy due to the mechanical and electrochemical effect. In the first analysis, the results confirmed the absence of dissolved elements. However, after the chemical digestion (with HNO_3, H_2O and HF), Ti, Al and V elements were detected in electrolytes that were in contact with Ti6Al4V and Ti-C-N_1 samples during tribocorrosion tests. On the contrary, none of the cited elements were observed for the electrolyte in contact with Ti-C-N_2 sample, supporting that this coating was not removed at any time during tribocorrosion test and showing its good impermeability. Detailed information about elements detected in the electrolytes used in tribocorrosion tests by ICP measurements is presented in table 6.2.3.

Table 6.2.3.

Elements detected in the electrolytes after tribocorrosion tests.

	Dissolved elements (mg/l)			Total elements (mg/l)		
Sample	**Ti**	**Al**	**V**	**Ti**	**Al**	**V**
Reference (PBS)	‹0.01	‹0.01	‹0.01	‹0.01	‹0.01	‹0.01
Ti6Al4V	‹0.01	‹0.01	‹0.01	4.3	0.25	0.20
Ti-C-N_1	‹0.01	‹0.01	‹0.01	2.14	0.19	0.078
Ti-C-N_2	‹0.01	‹0.01	‹0.01	‹0.01	‹0.01	‹0.01

So-far showed results made us discard the Ti-C-N_1 coating for the rest of the study due to its poor tribological response. Therefore, next results will be referred to Ti6Al4V, Ti-C-N_2 and Ti-C-N_2+Ag.

6.2.3.3. Surface hydrophilicity/hydrophobicity

In order to study the hydrophilicity/hydrophobicity behavior of the samples, contact angles were measured after a stabilization period of 30 seconds. The results (Table 6.2.4) showed values lower than 65º, which indicates that all samples have a hydrophilic behavior. Additionally, contact angles point out that Ti6Al4V is the most hydrophilic surface, whereas Ti-C-N_2+Ag coating presented the highest value (63º).

Table 6.2.4.
Contact angle for TiAl4V, Ti-C-N_2 and Ti-C-N_2+Ag coatings.

Sample	Contact angle ± SD (°)
Ti6Al4V	48 ± 1
Ti-C-N_2	59 ± 3
Ti-C-N_2+Ag	63 ± 1

6.2.3.4. Fretting tests

Tribological behavior was analyzed by means of fretting tests. Mean friction coefficient values, and ball and disc wear scars are compiled in Table 6.2.5. As observed, Ti6Al4V and Ti-C-N_2 had similar tribological response with almost the same friction coefficient and without wear scar on their surface. The difference between both coatings was observed in the balls wear scars, where the ball tested against the Ti-C-N_2 samples suffered less wear. Ti-C-N_2+Ag presented the worst tribological behavior with the highest friction coefficient. Besides, the wear produced in the counterbody was higher in comparison with the other samples.

Table 6.2.5.
Friction coefficient values and ball and disc wear scar measurements.

Sample	μ ± SD	Ball wear scar (diameter, mm)	Disc wear scar
Ti6Al4V	0.21 ± 0.01	1.2 ± 0.1	No wear scar
Ti-C-N_2	0.23 ± 0.01	0.8 ± 0.1	No wear scar
Ti-C-N_2+Ag	0.32 ± 0.06	1.8 ± 0.4	Ag coating disappears

The evolution of friction coefficients (Fig. 6.2.6) clearly indicates that the presence of the silver film not only worsens the tribological response (increasing the friction coefficient) but it makes it more unstable over time. During the first 500 seconds, the friction coefficient increases, probably due to the removing of the silver layer. This generates the production of silver wear debris, resulting in the instability of the friction coefficient. In the last 1000 seconds, the friction coefficient becomes more stable, probably because a steady state regime is reached. The evolution of the friction coefficient for Ti6Al4V and Ti-C-N_2 coatings is more stable, becoming similar after the first 2000 seconds.

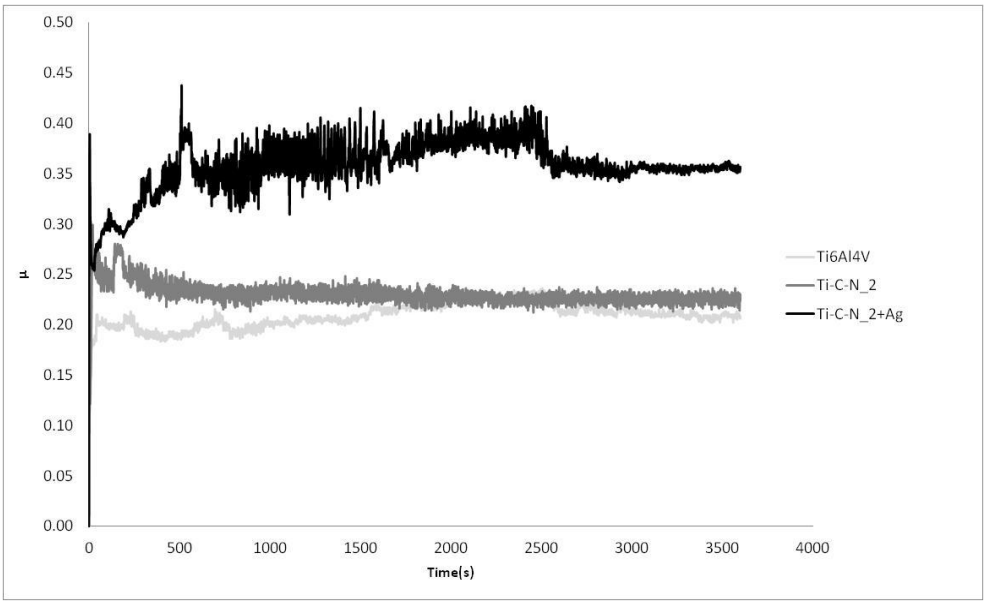

Fig. 6.2.6. Friction coefficient evolution in fretting tests

Wear scar of Ti-C-N_2+Ag disc was examined by optical microscope (Fig. 6.2.7 left) and confocal microscopy (Fig. 6.2.7 middle). The scar was evaluated by

topographical analysis and depth profile (Fig. 6.2.7 right). The depth of the scar in the sliding contact area was around 1.5 microns. Taking into account the thickness of the Ag coating and the depth of the wear scar, this indicates that all the silver film was removed in the sliding contact area during fretting tests. This was confirmed by SEM-EDS (electron discharge spectroscopy), where two measurements were carried out, one outside the sliding contact area, and the other one just in the wear scar. Thus, the absence of silver in the scar was confirmed. Further details about wear scars in UHMWPE balls and SEM-EDS analysis carried out in the sample Ti-C-N_2+Ag after fretting test can be found in figure 6.2.8 and figure 6.2.9, respectively.

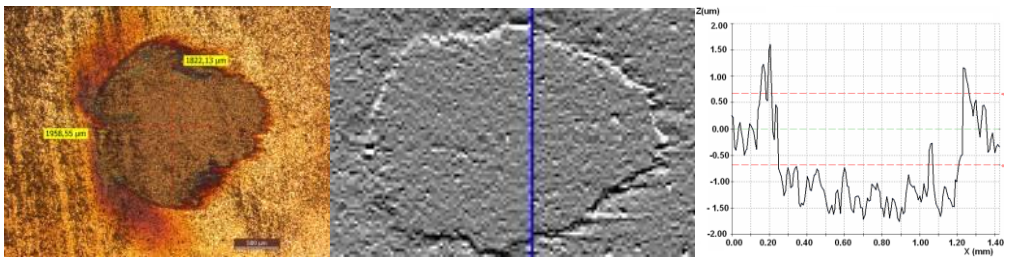

Fig. 6.2.7. (Left) Microscope image of Ti-C-N_2+Ag disc after fretting test against UHMWPE ball; (middle) topography; and (right) depth profile of Ti-C-N_2+Ag disc after fretting test against UHMWPE ball.

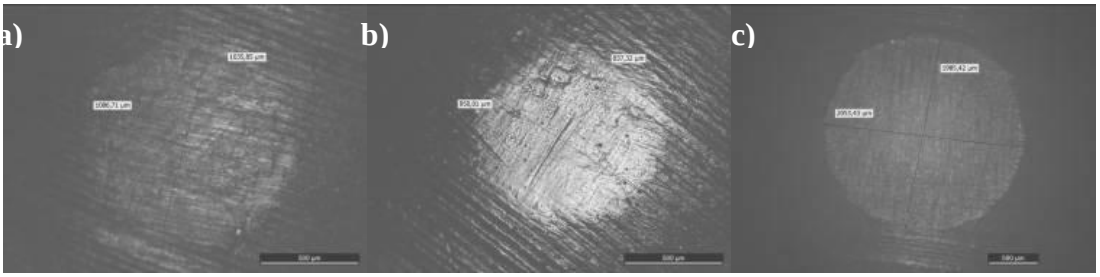

Fig. 6.2.8. Images obtained by optical microscope of wear scars in UHMWPE: a) Ti6Al4V, b) Ti-C-N_2, and c) Ti-C-N_2+Ag.

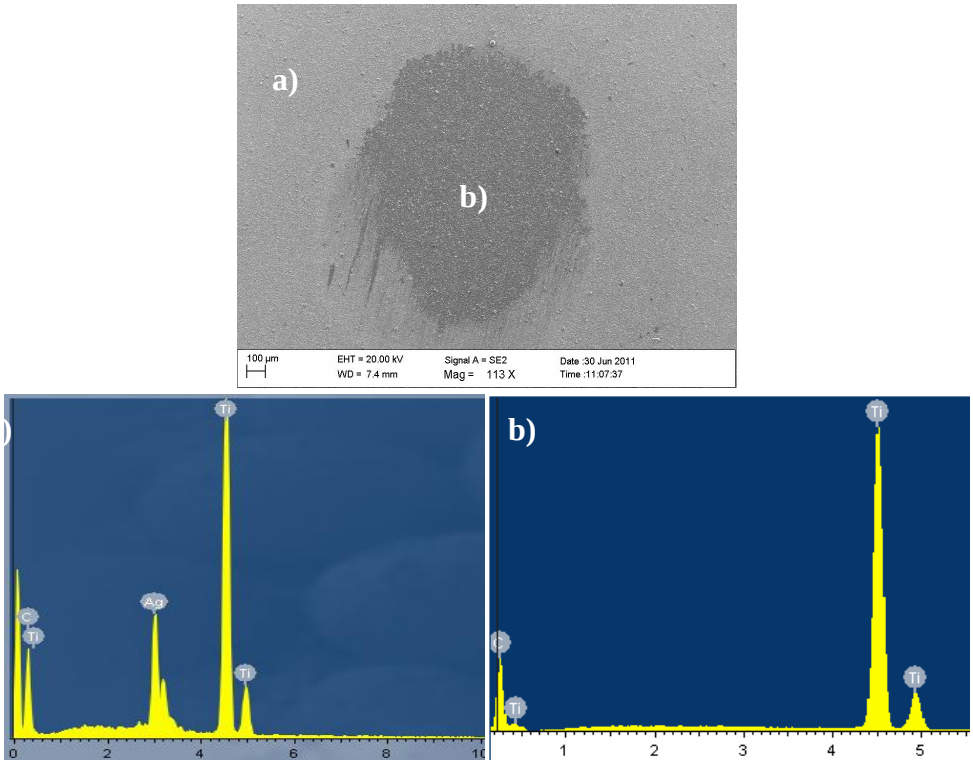

Fig. 6.2.9. Micrography and EDS spectrum of the wear scar in Ti-C-N_2+Ag after fretting test. a) EDS spectrum outside the sliding area, and b) EDS spectrum in the wear scar.

6.2.3.5. Bacterial adhesion

Results of bacterial adhesion for collection strains

Bacterial adhesion for collection strains, *S. aureus* and *S. epidermidis*, was analyzed by means of the percentage of surface covered by bacteria. Figure 6.2.10 shows that bacterial adherence to modified surface materials (Ti-C-N_2 and Ti-C-N_2+Ag) was lower than in the control material (Ti6Al4V) for both strains ($p<0.0001$, Kruskal-Wallis test).

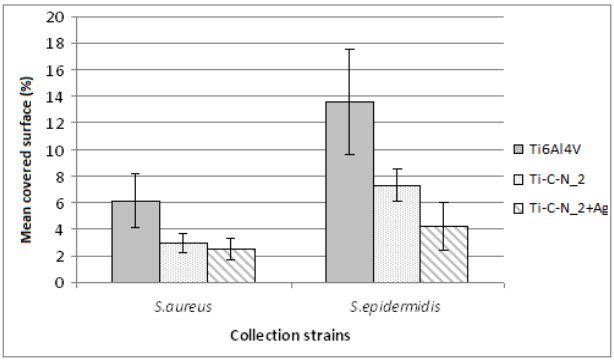

Fig. 6.2.10. Mean percentage of the surface of each biomaterial covered by the collection of *S. aureus* and *S. epidermidis* strains.

Taking into account the results obtained with the statistical analysis, it can be said that there were no statistical differences between both modified materials for *S. aureus* (p=0.1072, Kruskal-Wallis test), while such differences between both coated samples were statistically significant for *S. epidermidis* (p‹0.0001, Kruskal-Wallis test).

In figure 6.2.11, the efficiency of the silver coating is observed in the presence of very low concentration of living bacteria on the surface represented by the green color for collection strains. The images have been selected because of their quality but they cannot be used for quantitative comparisons.

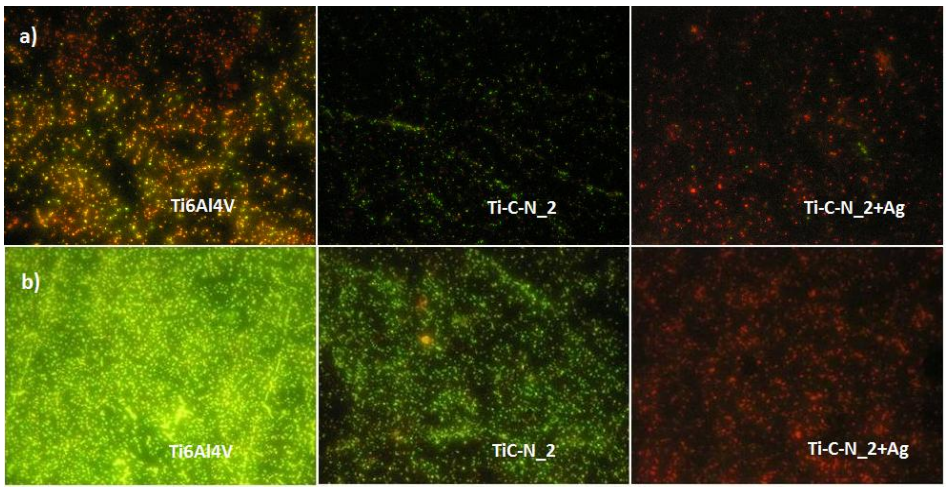

Fig.6.2.11. An example of the fluorescence microscope images for Ti6Al4V surface, Ti-C-N_2 surface and Ti-C-N_2+Ag surfaces covered by *S. aureus* (a) and *S.epidermidis* (b).

Results of bacterial adhesion for clinical strains

Bacterial adhesion for clinical strains, *S. aureus* and *S. epidermidis* obtained from patients was analyzed by means of the percentage of surface covered by bacteria. In figure 6.2.11, the results of adhesion of different clinical strain (p1...p12) for each material can be seen. As observed, Ti-C-N_2+Ag reduced the covered surface percentage except for p2, and in case of Ti-C-N_2 except for p1 and p2. Figure 6.2.13 shows an example of images obtained for clinical isolates of *S. aureus* (p18) and *S. epidermidis* (p33), where the efficacy against bacteria of Ti-C-N+Ag is observed.

After statistical analysis, the conclusion is that the differences between the surfaces of Ti6Al4V and Ti-C-N_2 were statistically significant for all isolates except for p5 and p6 (p = 0.1033 and 0.1032 respectively, Kruskal-Wallis). However, the

differences between the surfaces of Ti6Al4V and Ti-C-N_2+Ag were statistically significant for all isolates except p1 and p2 (p = 0.0564 and 0.1349 respectively, Kruskal-Wallis).

On the other hand, comparison of treated samples, Ti-C-N_2 and Ti_C_N_2+Ag, shows that the differences between both modified materials were statistically significant for all isolates except for p3 (p = 0.4272, Kruskal-Wallis).

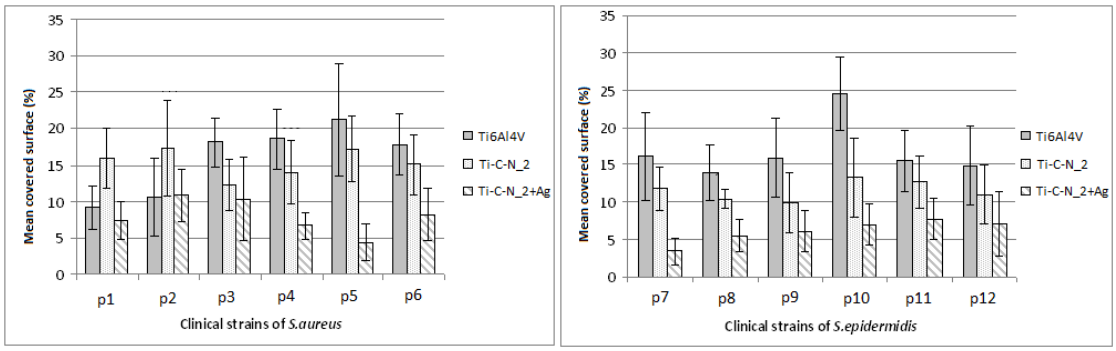

Fig. 6.2.12. Mean percentage of surface covered biomaterial with clinical strains for each material.

In figure. 6.2.13, similarly to figure 6.2.11, some representative images have been selected, but in this case with clinical strains.

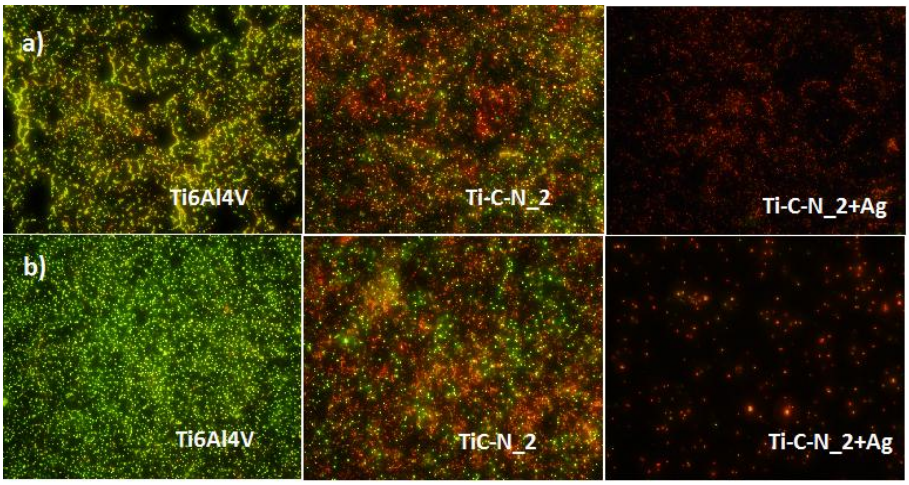

Fig. 6.2.13. (a) Example of images taken with a fluorescence microscope to the surface of Ti6Al4V, Ti-C-N_2 and Ti-C-N_2+Ag covered by the clinical strain p4 of *S. aureus*. (b) Example of images taken with a fluorescence microscope to the surface of Ti6Al4V, Ti-C-N_2 and Ti-C-N_2+Ag covered by the clinical strain p8 of *S. epidermidis*.

6.2.4. Discussion

6.2.4.1. Effect of Ti-C-N coatings in tribocorrosion response

Titanium implants inserted into the human body are usually surrounded with blood-rich tissue; this implies exposing the implant materials to a corrosive media. The release of vanadium and aluminum particles or metallic corrosion products may induce immune response in sensitive patients. Therefore, the assessment of a biomaterial or a coating able to avoid or reduce the tribocorrosion effect is required to ensure their safety in the corrosive environment of the human body.

In tribocorrosion tests performed in this work, it was observed that Ti-C-N_2 coating acts as a good barrier with a low friction coefficient and wear scar, and completely avoiding the releasing of elements from the substrate alloy to the electrolyte. This coating acts as a barrier able to protect the substrate from corrosion and wear processes avoiding the release of metallic ions and wear debris into the surrounding implant tissue as it was detected in a previous study of Cheng et al.[12, 8]

Concerning the corrosion resistance, it can be related to the microstructure of coatings. The initial lower corrosion resistance of Ti-C-N_2 compared with Ti-C-N_1 could be due to the columnar structure that presents the Ti-C-N_2 coating[42]. A columnar structure contains more open (through coating) porosity and straight grain species[51]. It seems that the coating is self-protected reducing the friction and wear under tribocorrosion conditions. The better tribological behaviour of Ti-C-N_2 also could be due to the higher quantity of C in the coating in comparison to Ti-C-N_1 coating[42]. The higher carbon content could lead to the formation of a carbon-rich tribo-layer during the sliding process and be transferred to the counterpart which would have self-lubricating properties[52, 53].

6.2.4.2. Effect of Ti-C-N coatings in tribological behavior

The results of the fretting tests are of specific interest since the fretting effect that takes places between the backside of the patellar component and the tibial tray of fixed bearing tibial component is the main cause that leads to the knee implant

[51] Liu, C.; Leyland, A.; Bi, Q.; Matthews, A., *Surf Coat Tech.* **2011**, 414, 164-174.
[52] Vitu, T.; Escudeiro, A.; Polcar, T.; Cavaleiro, A., *Surf Coat Tech.* **2014**, 258, 734-745.
[53] Wang, P.; Hirose, M.; Suzuki, Y.; Adachi, K., *Surf Coat Tech.* **2013**, 221, 163-173.

failure. The poor response of Ti-C-N_2+Ag sample obtained in fretting tests was expected due to the low hardness of silver in comparison with titanium and DLC, that is, 2.5-3, 6 and 9.5 Mohs hardness, respectively[54]. It was expected that Ti-C-N coating had lower friction coefficient due to its excellent tribological properties generated by its auto-lubricious property. However, the results showed a similar coefficient for Ti-C-N_2 sample than Ti6Al4V. Sheeja et al.[55] found that the wear resistance of UHMWPE sliding against DLC in simulated body fluid did not show any improvement over that of the untreated material. Though, analyzing the wear scars produced in the UHMWPE balls, the Ti-C-N_2 produced lower wear. This seems to indicate this coating is less aggressive than the Ti6Al4V. Alternatively, the presence of a carbon tribo-layer formed by the presence of carbon in the coating could reduce the wear in the UHMWPE balls.

Concerning the fast elimination of silver due to the friction process during the fretting test, this could have a positive effect in real applications, minimizing the risk of infection that could occur shortly after the implantation surgery process.

6.2.4.3. Effect of Ti-C-N and silver coating in bacterial adhesion

Implant devices are the most suitable to modification with the objective of preventing infection. Traditional surface-modifying preventive approaches have largely focused on antimicrobial coating of devices and resulted in variable clinical success in preventing device-associated infections[56]. The use of an antibacterial noble metal is one of the strategies to avoid bacterial adhesion. The incorporation of silver has produced a statistically significant decrease of adhesion with respect to the other materials for most of the strains. In general, all coated plates showed a decreased bacterial adherence for *S. aureus* and *S. epidermidis* collection strains and in most of the clinical strains in comparison to uncoated samples.

In this study, we evaluated the rough adherence of reference strains. These strains have a lower genetic load than clinical strains isolated from patients because they are laboratory-adapted strains which lose genes due to several passages on culture medium. Further experiments were performed to evaluate adherence using clinical

[54] Bhushan, B.; Gupta, B.K., *Handbook of Tribology: Materials, coatings, and surface treatments*, McGraw-Hill, New York, USA, **1991**.
[55] Sheeja, D.; Tay, B. K.; Lau, S. P.; Nung, L. N., *Surf Coat Tech.* **2001**, 146-147, 410-416
[56] Esteban, J.; Pérez-Tanoira, R.; Pérez-Jorge-Peremarch, C.; Gómez-Barrena, E., Bacterial adherence to biomaterials used in surgical procedures, in: Kon, K.; Rai, M., (Eds.),

strains isolated from patients with a diagnosis of prosthetic joint infection (which can show different properties than laboratory-adapted strains). These experiments showed slightly different behavior probably due to the different pathogenic properties of the strains.

Silver-based coatings have been studied in association with polymer and metal implants, particularly on external fixation pins. However, metallic silver mechanical properties are not adequate to constitute a load-bearing metal implant. So, the amount of silver deposited must be as low as possible in order to be useful in preventing implanted-related deep body infection caused in the first moments after surgery; and then keep the resistance against corrosion and wear from the Ti-C-N coating. Concerning the removed silver, it has been known to be eliminated via the renal system, and can be absorbed easily through the gastrointestinal system[57].

Silver particles (5–50 nm), has been tested and in vitro results have shown that it is effective against methicillin-resistant *S. aureus* and *S. epidermidis* and have indicated that it is not cytotoxic due to its higher porosity and active surface[58].

Furthermore, released silver ions act immediately, as shown by blockage of protein activities, which is beneficial for preventing local infections. Possibly the main indication for these compounds will be prevention of perioperative infections. The major effect on imported bacteria can occur immediately and vanishes relatively quickly. Thus, long-term bone damage and possible neutralization of silver effects by extracellular membrane components, which are deposited on implants, may be avoided.

Ti-C-N_2+Ag sample presented good bacterial anti-adhesive properties for both types of bacteria. K. Baba et al.[59] have studied the effect of different Ag-containing diamond-like carbon films in antibacterial activity. In their results, they just observed small variations depending on the Ag content. They also observed an increase in the contact angle as the concentration of silver in the coating is increased. In this study, the content of silver is stable but it has observed that the contact angle after a period of stabilization, in case of Ti-C-N_2+Ag is higher than in

Microbiology for Surgical Infections. Diagnosis, Prognosis and Treatment. Elsevier, USA, **2014**.
[57] Secinti, K. D.; Ozalp, H.; Attar, A.; Sargon, M. F., *J Clin Neurosci*. **2011**, 18, 391-395.
[58] Harris, L. G.; Richards, R. G., *Injury*. **2006**, 37, S3-14.
[59] Baba, K.; Hatada, R.; Flege, S.; Ensinger, W.; Shibata, Y.; Nakashima, J.; Sawase, T.; Morimura, T., *Vacuum*. **2013**, 89, 179-184.

the Ti-C-N_2 and substrate. There are several factors that influence the antibacterial behaviour, such as the chemical roughness, chemical composition, the structure and the surface free energy. The latter can be quantified by measuring the contact angle. The threshold of hydrophobicity is a contact angle greater than 65°; below this value it is considered hydrophilic[60]. In all analyzed samples, the contact angles values are lower than 65°, so that all samples are hydrophilic. As a general rule, high contact angles (low surface free energy) improve antibacterial properties decreasing the bacterial adhesion[61, 62]. This effect can be seen with all studied samples, confirming this theory. The Ti-C-N_2+Ag coating presented the highest contact angle and the bacterial adherence for *S. aureus* and *S. epidermidis* was the lowest one.

In this work it was also observed that silver-free coating, Ti-C-N_2, show antibacterial properties in comparison with Ti6Al4V sample. This effect was studied by Marciano et al.[63], where they investigate into the antibacterial property and bacterial adhesion of diamond-like carbon films.

6.2.5. Conclusions

The purpose of this work was to develop a coating with good tribological properties, higher corrosion resistance and antibacterial activity. The tribocorrosion behavior has been in depth studied for two preselected Ti-C-N coatings. Taking into account the tribocorrosion response, Ti-C-N_2 coating was selected due to its excellent wear and high corrosion resistance and because it acts as a protective barrier against the release of substrate elements to outside. For this reason, a thin layer of silver was deposited on this coating in order to provide antibacterial properties. Fretting tests did not show so much difference between Ti-C-N_2 coating and Ti6Al4V, with similar friction coefficient and wear. However, the wear produced in the UHMWPE balls was lower for Ti-C-N_2 sample probably due to the generation of a carbon rich tribo-layer during the sliding process. Bacterial

[60] Vogler, E. A., *Adv Colloid Interfac.* **1998**, 74, 69-117.
[61] Media, O.; Nocua, J.; Mendoza, F.; Gómez-Moreno, R.; Ávalos, J.; Rodríguez, C.; Morell, G., *Diam Relat Mater.* **2012**, 22, 77-81.
[62] Zhou, H.; Xu, L.; Ogino, A.; Nagatsu, M., *Diam Relat Mater.* **2008**, 17, 1416-1419.
[63] Marciano, F. R.; Bonetti, L. F.; Mangolin, J. F.; Da-Silva, N. S.; Corat, E. J.; Trava-Airoldi, V. J., *Vacuum.* **2001**, 85, 662-666.

adhesion tests exhibited that silver has broad-spectrum anti-adherence activity and low risk of resistance. Their low wear resistance makes the layer disappear during rubbing contact, then their application should be limited to the avoidance of infection during implant fixation. The inherent antimicrobial properties of the Ti-C-N_2 layer makes then still active avoiding infections during the life of the implant. Therefore, it can be concluded that developed Ti-C-N_2+Ag coating could be a promising alternative for orthopedic applications with excellent tribological behavior, corrosion resistance and antibacterial properties.

Contribution 3

TiO_2 coatings developed by PEO technique: tribocorrosion and bacterial adhesion characterization

Structure, tribocorrosion and biocide characterization of Ca, P ad I containing TiO_2 coatings developed by plasma electrolytic oxidation

Submitted to *Applied Surface Science*

Index

6.3.1. Introduction 138

6.3.2. Materials and Methods 142

6.3.2.1. Materials 142

6.3.2.2. Plasma Electrolytic Oxidation 142

6.3.2.3. Surface Characterization 142

6.3.2.4. Tribocorrosion tests 143

6.3.2.5. Bacterial adhesion 144

6.3.3. Results and discussion 144

6.3.3.1. Surface Characterization 144

6.3.3.2. X-ray diffraction 149

6.3.3.3. Tribocorrosion tests 150

6.3.3.4. Bacterial adhesion 156

6.3.4. Conclusions 158

ABSTRACT

In hip joint implants, in particular in the stems, wear-corrosion effects can accelerate the degradation of the biomaterial. The lack of osseointegration and the risk of contracting implant-associated infections may be other reasons for a premature failure of the implant. In this work, TiO_2 coatings have been developed by means of Plasma Electrolytic Oxidation (PEO) technique in order to achieve wear-resistant hard coatings with osseointegration ability and biocide characteristics. During the PEO process, elements that favor cell growth, like Ca and P, were introduced into the coating. With the purpose of providing the coating with antibacterial properties iodine was added like biocide agent. The microstructure and chemical composition of the developed coatings were analyzed in order to see if the surface of the films was suitable for the cell attachment. The effect of wear-corrosion synergy was studied by means of tribocorrosion tests. Finally, the biocide capacity of iodine against *S. aureus* and *S. epidermidis* was analyzed through bacterial adhesion tests. High wear and corrosion resistance was shown in one of the developed coatings. The achieved surface microstructures seem to be appropriate to improve the osseointegration with proper pore size and porosity index. The antibacterial capacity of iodine was confirmed for *S epidermidis*.

6.3.1. Introduction

According to the European Society of Biomaterial (ESB), a biomaterial is a material destined to interact with the biological systems to evaluate, treat, increase or replace some tissue, organ or body function. In the case of orthopedic implants, the main property required to a biomaterial to be compatible is to avoid an adverse reaction when placed into the body. As well, chemical stability, good mechanical properties, osseointegration, high corrosion resistance and excellent wear resistance are required. In this sense, titanium and its alloys have become the first choice for biocompatible orthopedic implant materials because of their high load strength bearing capacity, high strength to weight ratio, low toxicity, chemical stability, superior mechanical properties, excellent corrosion resistance and high biocompatibility[1, 2, 3]. Nevertheless, their poor tribological properties limit their use[4]. This tribological behavior is characterized by high coefficient of friction, severe adhesive wear with strong tendency to seizure and low abrasion resistance[5]. In the human body there are tribological contacts created as a consequence of locomotion that can contribute to the accelerated degradation of the material[6, 7, 8]. This can lead to crack initiation, excessive wear and release of wear debris from the implant into bloodstream or early fracture of the implant, as well as serious inflammatory reactions, allergies or osteolysis, which can significantly shorten the lifespan of the implanted device[9, 10, 11, 12]. On the other hand, the exposure of the biomaterial to the body fluids can induce corrosion damage on the material leading to irreversible material degradation process. This electrochemical process combined to the wear produced as a result of the relative contact movement of the

[1] Neupane, M. P.; Sankara, T. S. N.; Park, J. E.; Kim, Y. K.; Park, I. S.; Song, K. Y.; Bae, T. S.; Lee, H., *Worl Acad Sci Eng Technol.* **2012**, 6, 10-23.
[2] Durdu, S.; Usta, M., *Ceram Int.* **2014**, 40, 3627-3635.
[3] Alsaran, A.; Purcek, G.; Hacisalihoglu, I.; Vangolu, Y.; Bayrak, O.; Karaman, I.; Celik, A., *Surf Coat Technol.* **2011**, 205, S537-S542.
[4] Mabbouxa, F.; Ponsinnetb, L.; Morriera, J.; Jaffrezicb, N.; Barsottia, O., *Colloid Surface B.* **2004**, 39, 199-205.
[5] Yerokhin, A. L.; Niea, X.; Leyland, A.; Matthews, A., *Surf Coat Technol.* **2000**, 130, 195-206.
[6] Manhabosco, T. M.; Tamborim, S. M.; dos Santos, C. B.; Müller, I. L., *Corros Sci.* **2011**, 53, 1786-1793.
[7] Diomidis, N.; Mischler, S.; More, N. S.; Manish, R., *Acta Biomater.* **2012**, 8, 852-859.
[8] Niinomi, M., *J Mech Behav Biomed.* **2008**, 1, 30-42.
[9] Diomidis, N.; Mischler, S., *Tribol Int.* **2011**, 44, 1452-1460.
[10] Williams, S.; Tipper, J. L.; Ingham, E.; Stone, M. H.; Fisher, J., *P I Mech Eng H.* **2003**, 217, 155-163.
[11] Contu, F.; Elsener, B.; Böhni, H., *Electrochim Acta.* **2004**, 50, 33-41.
[12] Chandra, A.; Ryu, J. J.; Karra, P.; Shrotriya, P.; Tvergaard, V.; Gaisser, M.; Weik, T., *J Mech Behav Biomed.* **2011**, 4, 1990-2001.

implant, results in a process called tribocorrosion. This effect takes into account the synergistic interaction of wear and corrosion phenomena on surfaces subjected to a relative contact movement in biological environments[13].

On the other hand, from the biological point of view, two major complications may also be present in an implant: the lack of bone tissue integration of titanium and its alloys due to the lack of interface bioactivity and the post-operative infections from attached bacteria and following proliferation on the surfaces of implants[14].

After biomaterial implantation into the body, a complex series of reactions (mechanisms) take place on its surface[15]. The material osseointegration occurs in different steps, including the adsorption of proteins to the biomaterial surface, the contact and attachment of cells, and its subsequent surface diffusion[16, 17, 18]. Surface wettability, initially, may play a major role in adsorption of proteins onto the surface, as well as the later cell adhesion. Generally, hydrophobic surfaces are more prone to protein-absorption than hydrophilic ones, due to the stronger hydrophobic interactions[19]. Other studies have reported that surfaces with moderate hydrophilicity display improved cell growth and biocompatibility[20]. Nevertheless, cell adhesion can decrease as the material becomes too hydrophilic. Other factors that play an important role in the protein adsorption are the surface topography, where a high porosity may facilitate the contact with proteins, the chemical composition and surface heterogeneity.

Implant-associated infections generally result from bacterial adhesion to the surface of the implant and the following formation of the bio-film at the implant-tissue interface[21]. Sometimes, the outbreak of an infection mask the ongoing soreness of tissue inflammation process after surgery, and infection diagnosis

[13] Hailer, N. P.; Garellick, G.; Kärrholm, J., *Acta Orthop.* **2010**, 81, 34-41.
[14] Knetsch, M. L. W.; Koole, L. H., *Polymers.* **2011**, 3, 340-366.
[15] Kuzyk, P. R. T.; Schemitsch, E. H., *Indian J Orthop.* **2011**, 45, 108-115.
[16] Grinnell, F.; *Int Rev Cytol.* **1978**, 53, 65-144.
[17] Kulkarni, M.; Patil-Sen. Y.; Junkar, I.; Kulkarni, C. V.; Lorenzetti, M.; Iglic, A., *Colloid Surface B.* **2015**, 129, 47-53.
[18] Kulkarni, M.; Flasker, A.; Lokar, M.; Mrak-Poljsak, K.; Mazare, A.; Artenjak, A.; Cucnik, S.; Kralj, S.; Velikonja, A.; Schmuki, P.; Kralj-Iglic, V.; Sodin-Semrl, S.; Iglic, A., *Int J Nanomed.* **2015**, 10, 1359-1373.
[19] Xu, L. C.; Siedlecki, C. A., *Biomaterials.* **2007**, 28, 3273-3283.
[20] Application note 17: influence of topography and wettability on biocompatibility. ‹ http://www.biolinscientific.com/zafepress.php?url=%2Fpdf%2FAttension%2FApplication%20Notes%2FAT_AN_17_roughbio.pdf›.
[21] Zilberman, M.; Elsner, J. J., *J Control Release.* **2008**, 130, 202-215.

often occurs when a full-blown infection has already caused damage to tissue and host organism. This often involves the need for a second surgery to replace total or partially the infected device, leading to substantial patient health risk, involving additionally high medical costs[22]. The most common species that cause implant-associated infections are *Staphylococcus aureus, Staphylococcus epidermidis, Enterobacteriaceae, Pseudomonas aeruginosa and Candida fungus*[23].

A possible method to solve wear-corrosion problems, improve the osseontegration properties of a device and reduce the incidence of implant-related infections is to use surface treatments as Plasma Electrolytic Oxidation (PEO) technique. The PEO process consist of the modification of the growing anodic film by spark/arc micro-discharges in aqueous solutions, which are initiated at potentials above the breakdown voltage of the growing oxide film and move rapidly across the anode surface. The discharge leads locally to high temperature and high pressure plasma-chemical reactions, generating a porous coating. Developed coating usually contains constituent species derived from the substrate and the electrolyte. This character reveals that PEO coating has excellent bonding strength to the substrate due to its in situ growth process and apart from corrosion resistance, they exhibit high hardness and good wear resistance. Moreover, it is possible to adjust the composition of the used electrolyte, to introduce desired elements into the coating, producing functional films with osseointegration or biocide properties.

By PEO technique, it can be produced TiO_2 coatings in two crystallographic phases: anatase and rutile. Anatase exhibits poor corrosion resistance in contact with some acids and halide solutions, while rutile generally possesses much better protective characteristics. It has a high stability, good mechanical properties because of its higher hardness, and it is denser than anatase form. All these characteristics are responsible for the significance of the rutile in orthopedic implants. So it is of great interest that the developed TiO_2 layers are mainly rutile, allowing improving the tribological properties of the titanium alloy. Concerning the microstructure of TiO_2 layers obtained by this technology, they have a porous and rough surface which makes them appropriate for cell adhesion[24, 25, 26]. Additionally, the presence of Ca

[22] Vasilev, K.; Cook, J.; Griesser, H. J., *Expert Rev Med Devic.* **2009**, 6, 553-567.
[23] Temenoff, J. S.; Mikos, A. G., *Biomaterials: The Intersection of Biology and Materials Science*, Pearson Prentice Hall, New Jersey, USA, **2008**.
[24] Neoh, K. G.; Hu, X.; Zheng, D.; Tang Kang, E., *Biomaterials.* **2012**, 33, 2813-2822.
[25] Goriainov, V.; Cook, R.; Latham, J. M.; Dunlop, D. G.; Oreffo, R. O. C., *Acta Biomater.* **2014**, 10,

and P in the coating has been reported to be advantageous to cell growth[27, 28, 29, 30]. "In vivo" data showed that implant surfaces containing both Ca and P enhanced bone apposition of the implant surface[31].

In order to reduce the incidence of implant-related infections, antibacterial properties can be provided to the coatings, adding antimicrobial agents during the PEO process. Silver, cooper and fluoride have been the most common antimicrobial agents used until now in implants[22, 32, 33, 34]. Other antimicrobial agent that has been less studied for this application is the iodine. Iodine is the heaviest essential element needed by all living microorganism and is a component of thyroid hormones. Some studies indicate that iodine supported titanium has antibacterial activity, biocompatibility and no citotoxicity[35, 1]. However, iodine sublimes at room temperature, making it difficult to work with it.

The aim of this work is to develop TiO_2 coating with high wear-corrosion resistance, a proper surface morphology to promote the cells growth and antibacterial properties. The Ti6Al4V is the implant material of choice for use in hip joint stem implants. So, in this work, various TiO_2 layers have been developed on Ti6Al4V substrate by controlling the applied current intensity and processing time used in the plasma electrolytic oxidation (PEO) technology. Ca and P elements have been added to the electrolyte to generate a suitable surface for cell adhesion to improve the osseointegration. Also, addition of iodine to the electrolyte was carried out in order to provide the coating with antibacterial properties. To complete the

4043-4057.
[26] Ravanetti, F.; Borghetti, P.; De Angelis, E.; Chiesa, R.; Martini, F. M.; Gabbi, C.; Cacchioli, A., *Acta Biomater.* **2010**, 6, 1014-1024.
[27] Wang, H. Y.; Zhu, R. F.; Lu, Y. P.; Xiao, G. Y.; Zhao, X. C.; He, K.; Yuan, Y. F.; Li, Y.; Ma, X. N., *Mat Sci Eng C.* **2014**, 42, 657-664.
[28] Li, L. H.; Kong, Y. M.; Kim, H. W.; Kim, Y. W.; Kim, H. E.; Heo, S. J.; Koak, J. Y., *Biomaterials.* **2004**, 25, 2867-2875.
[29] Junker, R.; Dimakis, A.; Thoneick, M.; Jansen, *J. A., Clin Oral Implan Res.* **2009**, 20, 185-206.
[30] Maxian, S. H.; Zawadasky, J. P.; Dunnj, M. G., *J Biomed Mater Res.* **1994**, 28, 1311-1319.
[31] Basle, M. F.; Chappard, D.; Grizon, F.; Filmon, R.; Delecrin, J.; Daculsi, G.; Rebel, A., *Calcified Tissue Int.* **1993**, 53, 348-356.
[32] Kotharu, V.; Nagumothu, R.; Arumugam, C.B.; Veerappan, M.; Sankaran, S.; Davoodbasha, M. A.; Nooruddin, T., *Ceram Int.* **2012**, 38, 731-740.
[33] Arena, M. A.; Pérez-Jorge, C.; Conde, A.; Matykina, E.; Hernández-López, J. M.; Pérez-Tanoira, R.; de Damborenea, J. J.; Gómez-Barrena, E.; Esteban, J., *Colloid Surface B.* **2013**, 105, 106-112.
[34] Zhang, E.; Li, F.; Wang, H.; Liu, J.; Wang, C.; Li, M.; Yang, K., *Mat Sci Eng C.* **2013**, 33, 4280-4287.
[35] Shirai, T.; Shimizu, T.; Ohtani, K.; Zen, Y.; Takaya, M.; Tsuchiya, H., *Acta Biomater.* **2011**, 7, 1928-1933.

characterization, the thickness, roughness and porosity values were measured. The microstructure and chemical composition have been analyzed by means of XRD (X-Ray Diffraction), SEM (Scanning Electron Microscope), EDS (Energy Dispersive Spectroscopy) and XRF (X-Ray Fluorescence) techniques. Tribocorrosion tests have been performed to analyze the wear-corrosion synergy. And finally, the antibacterial efficacy has been evaluated studying the bacterial adherence.

6.3.2. Materials and methods

6.3.2.1. Materials

Ti6Al4V (grade 5) discs with dimensions of 24 mm diameter and 7.9 mm height were manufactured. Prior to PEO process, the surface of the Ti6Al4V specimens was ground by using 1200 grids SiC paper and then, submitted to a chemical attack being immersed for 10-15 seconds in a mixture of $HF:HNO_3:H_2O$. Finally, the samples were cleaned ultrasonically in distilled water, rinsed with alcohol and dried in warm air.

6.3.2.2. Plasma electrolytic oxidation

The titanium discs were subjected to PEO treatments in an aqueous electrolyte containing calcium acetate hydrate ($(CH_3COO)_2Ca{\cdot}H_2O$), beta-glycerophosphoric acid disodium salt pentahydrate ($C_3H_7Na_2O_6P{\cdot}5H_2O$) and sodium iodide (NaI) at different process conditions (PEO-1: 5 A/dm^2 during 19 minutes; PEO-2: 15 A/dm^2 during 5 minutes). The pH of the electrolyte was around 7.5. All experiments were carried out in a water-cooled bath with a stirring system that ensured an electrolyte temperature below 20ºC. A stainless steel mesh was used as the cathode, while titanium samples acted as anode. The total area of titanium exposed for each sample to electrolyte was 4.5 cm^2. After PEO process, the samples were immersed in a potassium iodide (KI) saturated solution for 24 hours. After some tests, it was observed that this last treatment seems to help to maintain the iodine into the coating avoiding its sublimation.

6.3.2.3. Surface characterization

The thickness of the PEO coatings was measured by using a Dual-Scope (Fischer)

probe. The average roughness was obtained by a profilometer (Perthometer M2, Mahr) at 10 randomly selected locations.

The microstructure of the specimens was evaluated by Scanning Electron Microscopy (SEM, Zeiss GEMINI®). The average pore size was calculated with the Graff-Snyder method and the pore percentage was analyzed by ImageJ software. The chemical composition of the samples was analyzed by Energy Dispersive Spectroscopy (EDS) and X-ray Fluorescence Spectroscopy (XRF) with S8 TIGER equipment, from BRUKER. The phase structure of the PEO coatings were detected by X-ray diffraction method (PHILIPS PW1710 powder diffractometer) using Cu-Kα radiation in steps of 0.02° over the 5–69.96° 2θ-angular range and a fixed-time counting of 1 s at 25 °C.

Hydrophilic/hydrophobia grade analyzed by means of wettability tests was carried out in the SURFTENS universal goniometer. The contact angle formed between a drop of distilled water and the surface under study was recorded by an optical camera and calculated with specialized software.

6.3.2.4. Tribocorrosion tests

Tribocorrosion tests were performed in a Microtest Tribometer, in rotating sliding conditions under ball on disc configuration. The rotating velocity was 20 rpm, the applied normal load 3 N and the radius track 5 mm. Tests were carried out during 200 cycles. The counterbody was an Al_2O_3 ball with 10 mm of diameter. The tests were done under lubricated conditions by using phosphate buffered saline (PBS) solution, consisting of 0.14 M NaCl, 1 mM KH_2PO_4, 3 mM KCl, and 10 mM Na_2HPO_4. The exposed area in all samples was 2.5 cm^2. Electrochemical measurements were assisted by an Autolab-Methrom potentiostat PGSTAT302N. A three-electrode system was used, corresponding as the working electrode the Ti6Al4V samples, as the counter electrode a platinum (Pt) wire and as the reference electrode Ag/AgCl KCl 3M (0.207 V vs SHE) electrode. Prior sliding tests, the open circuit potential (OCP) was monitored until achieving a stable value. During the sliding, OCP and friction coefficient were monitored. Once the wear process had been completed, OCP was recorded until new stabilization. Before and after the wear process, two electrochemical impedance spectroscopies (EIS) were registered. The sinusoidal wave was 10 mV of amplitude in the frequency range from 10^5 Hz to 10 mHz under OCP conditions. Completed the tribocorrosion test, samples were ultrasonically

cleaned in distilled water for 5 minutes and dried in warm air.

The morphology of wear tracks was analyzed by means of the scanning electron microscopy (SEM) and chemical composition in sliding area was analyzed by EDS. Topographical measurements were made using a confocal microscope (Nykon).

6.3.2.5. Bacterial adhesion

Staphylococcal adhesion experiments

Bacterial adhesion to a material surface is the first step in biofilm development. TiO_2 coatings were compared against control of untreated Ti6Al4V samples. Staphylococcal adhesion experiments were performed as described by Kinnari et al. and Perez-Tanoira et al.[36, 37].

For the preliminary study of bacterial adhesion, the biofilm-forming collection strains, *Staphylococcus aureus* 15981 (CITA) and *Staphylococcus epidermidis* ATCC 35984 have been used.

Statistical analysis

For the statistical study, non parametric tests were employed. Mann-Whitney or Wilcoxon were used for two samples and the Kruskal-Wallis test was used for more than two samples. EPI-Info software version 3.5.1 (CDC, Atlanta, GA. USA) was employed to perform the statistical studies.

6.3.3. Results and discussion

6.3.3.1. Surface characterization

The surface characterization related to mean thickness, roughness, pore size, porosity percentage and contact angle values of developed coatings are represented in Table 6.3.1.

[36] Kinnari, T. J.; Soininen, A.; Esteban, J.; Zamora, N.; Alakoski, E.; Kouri, V. P.; Lappalainen, R.; Konttinen, Y. T.; Gomez-Barrera, E.; Tiainen, V. M., *J Biomed Mater Res A.* **2008**, 86, 760-768.
[37] Pérez-Tanoira, R.; Pérez-Jorge, C.; Endrino, J. L.; Gómez-Barrena, E.; Horwat, D.; Pierson, J. F.; Esteban, J., *J Biomed Mater Res A.* **2012**, 100, 4208-4218.

Table 6.3.1.

Thickness, roughness, pore size and contact angle values.

Samples	Thickness (µm)	Roughness Ra, (µm)	Pore size (µm)	Porosity percentage (%)	Contact angle (°)
Ti6Al4V	-	0.26 ± 0.03	-	-	65 ± 2
PEO-1	3.31 ± 0.21	0.43 ± 0.04	5.39 ± 2.66	9	107 ± 2
PEO-2	4.49 ± 0.40	0.42 ± 0.05	7.25 ± 2.96	5	96 ± 5

The thickness of the coating increased when increasing the current density. The same effect was seen in a previous study carried out by Shin et al.[38], where they attributed this effect to the fact that at high current densities, the anodic reactions that take place at the interface with titanium substrate are induced with much more energy leading to a rapidly TiO_2 coating formation. Concerning the roughness of coatings, in both surfaces the roughness increased after the PEO process, without significant differences between them. This increase was influenced by both the pore size and porosity percentage, present in the surface[28, 39].

Figure 6.3.1 shows the surface morphology of the developed titanium oxide layers. SEM analysis exhibited the porous structure of coatings and the range of sizes. It seems that PEO-2 coating has a more homogeneous surface with better pore distribution. By SEM analysis and with the Graff-Snyder method the average pore size was calculated, obtaining for PEO-1 a pore size lower than for the PEO-2, that is, 5.39 µm and 7.25 µm, respectively. Concerning the pore percentage, it seems that increasing the current density in the process, apart from increase the pore size, the quantity of pore increase with a percentage of porosity in PEO-2 of 5%, whereas for PEO-1 was 9%. The bigger pores size obtained with the higher current density can be due to the large and long-lived discharges that take place in the surface and consequently form enlarged pores. In both coatings the pore size is within the suitable range of pore sizes for cell anchoring[40]. Cracks observed in the micrographs

[38] Shin, K. R.; Kim, Y. S.; Yan, H. W.; Ko, Y.G.; Shin, D. H., *Appl Surf Sci.* **2014**, 314, 221-227.
[39] Song, H. J.; Park, S. H.; Jeong, S. H.; Park, Y. J., *J Mater Process Technol.* **2009**, 209, 864-870.
[40] Buser, D.; Nydegger, T.; Oxland, T.; Cochran, D. L.; Schenk, R. K.; Hirt, H. P.; Snetivy, D.; Nolte, L. P., *J Biomed Mater Res.* **1999**, 45, 75-83.

in the surface of TiO_2 coating are attributed to thermal stresses[41].

Shin et al. found that TiO_2 surface with the smallest pore size (≈ 2 μm) and the highest porosity percentage showed the best results *in vitro* cell test, being the most suitable surface for cell anchoring[38]. Taking this fact into account, it can be concluded that PEO-1 could be the best coating to improve the osseointegration of stem. This coating has the smallest pore size and the highest quantity of pore.

Wettability tests showed that both coatings have a hydrophobic behavior with contact angles above 90°. Taking into consideration that hydrophobic surfaces are more suitable for protein adsorption[19], the PEO-1 coating seems to be the most promising selection to improve the osseointegration of the implants.

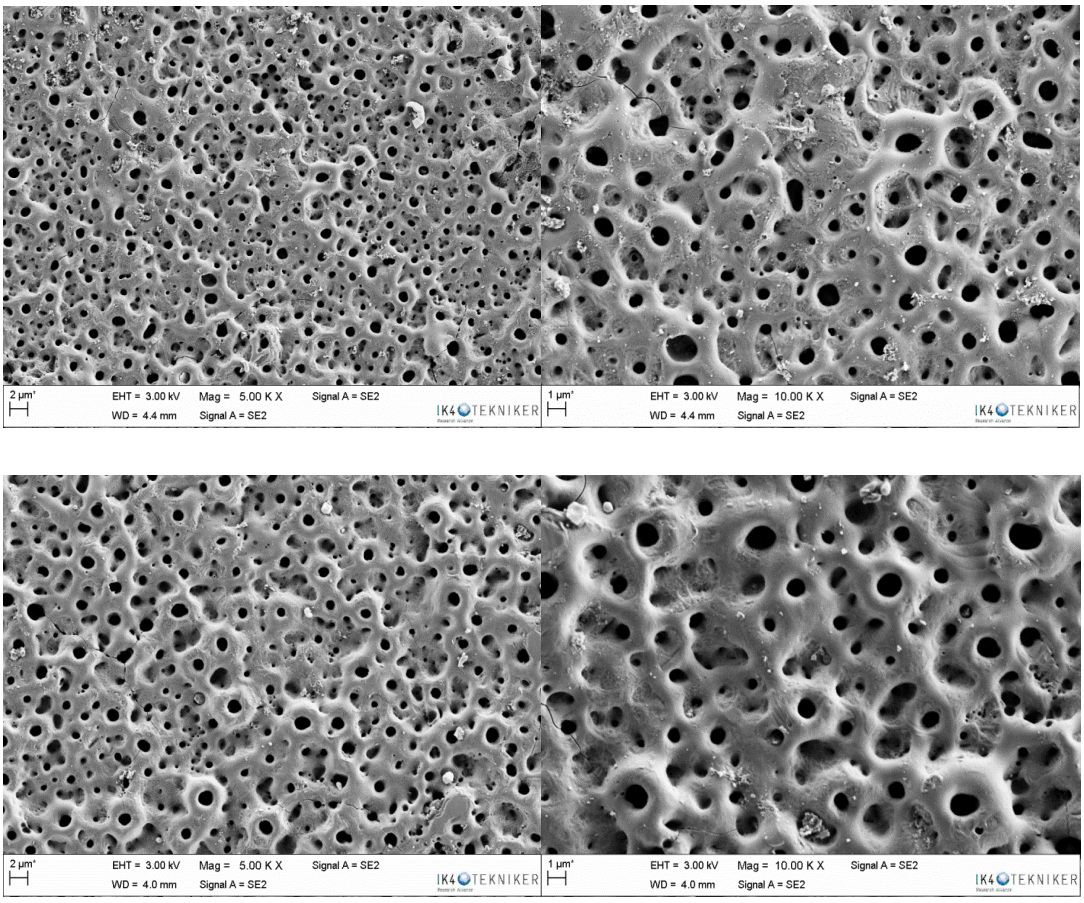

Fig. 6.3.1. SEM micrographs of the developed coatings.Top micrographs correspond to PEO-1 (left 5 KX and right 10 KX) and bottom micrographs correspond to PEO-2 (left 5 KX and right 10 KX).

Concerning the chemical composition, the EDS spectra of analysis carried out in

[41] Wang, H.; Liu, F.; Xiong, X.; Ke, S.; Zeng, X.; Lin, P., *Appl Surf Sci.* **2015**, 356, 1234-1243.

different areas of the developed coatings are shown in figure 6.3.2. In both cases, the elements from the substrate were detected, and those related to the developed electrolyte, Ca, P, Na. Also K from the saturated KI solution appeared. The presence of iodine in the coatings was also confirmed.

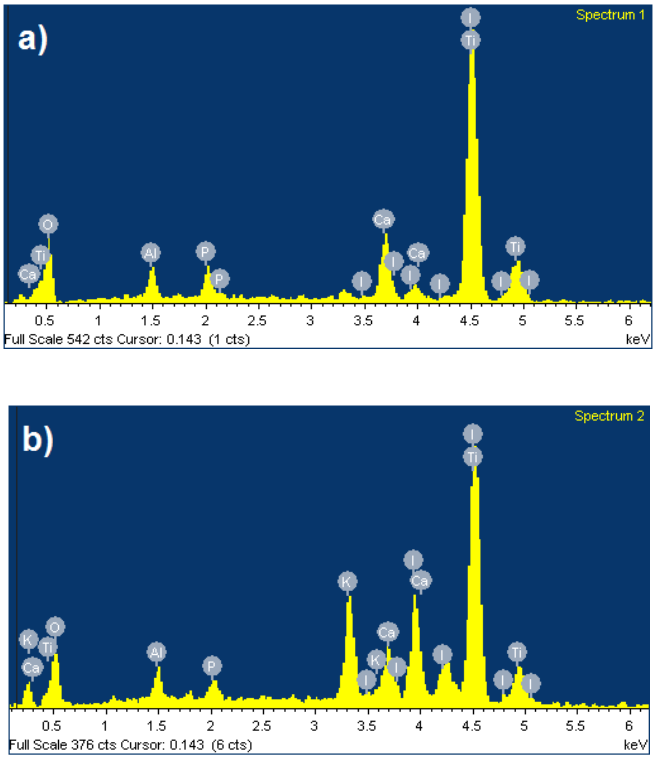

Fig. 6.3.2. EDS spectra of the PEO coatings: a) PEO-1 and b) PEO-2.

In order to get an idea of how similar the two developed coatings are in terms of chemical composition, XRF analysis was performed (Fig. 6.3.3). With this technology the analysis area is bigger than that studied by EDS. This study was carried out taking into account the count numbers. The intensity of peaks was compiled in table 6.3.2. The concentration of elements from the electrolyte increased with increasing the current in the PEO process while that of the substrate decreased. It seems to indicate that an increase in the voltage favors a greater insertion of elements from the substrate into the TiO_2 layer[28]. The presence of iodine was also confirmed by this technique.

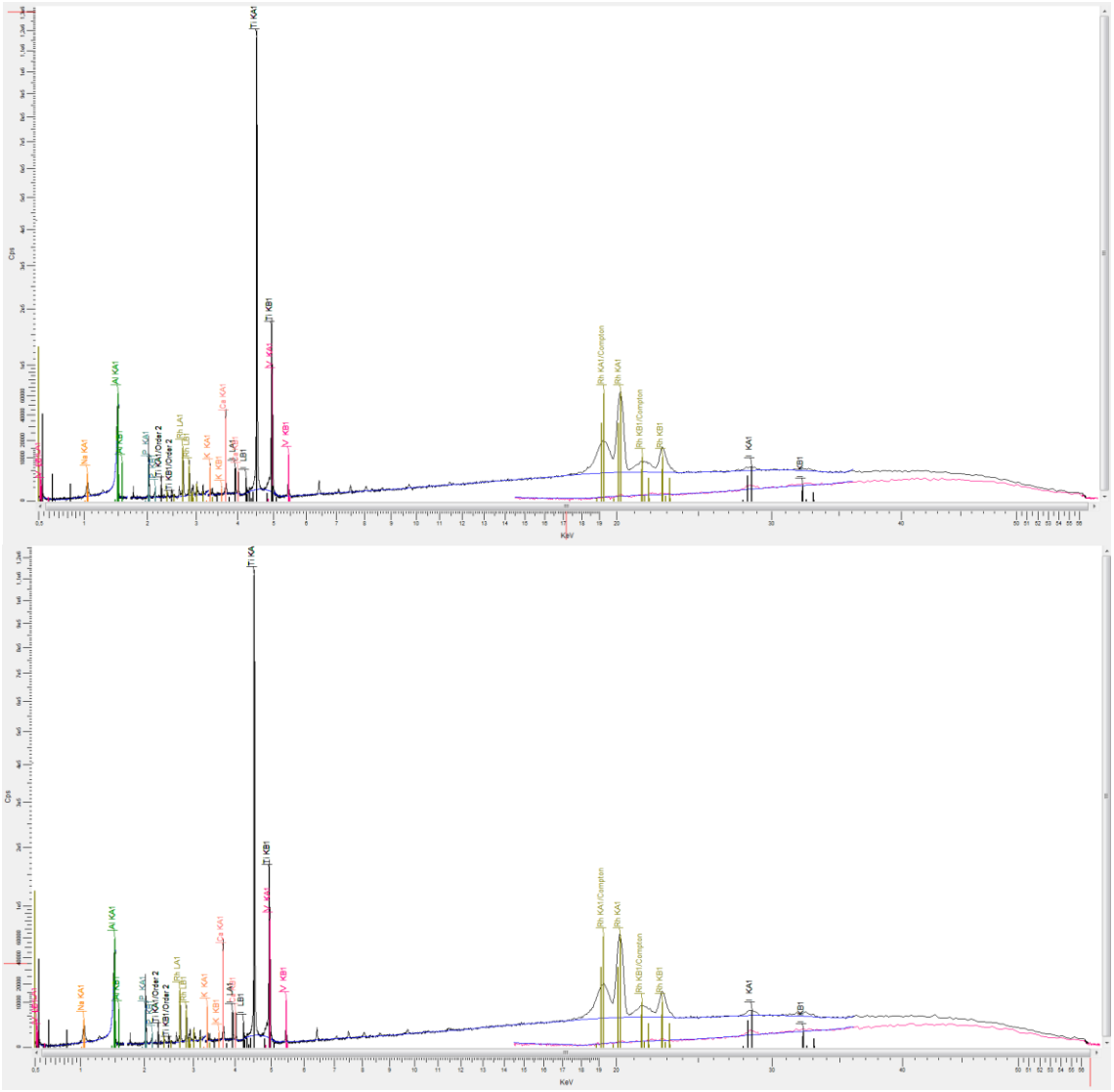

Fig. 6.3.3. XRF patterns of both developed coatings. PEO-1 (top) and PEO-2 (bottom).

Table 6.3.2.

Peaks intensity (KCps) of detected elements by XRF technology.

Samples	Ti	V	Al	Ca	P	Na	I	K
PEO-1	1192.6	81.2	21.3	46.0	23.4	1.8	1.2	7.1
PEO-2	1139.1	77.9	19.2	58.5	26.3	2.5	1.7	8.7

Chemical composition in depth obtained by means of GD-OES analysis showed a similar element´s distribution through the coatings (Fig. 6.3.4). In the right side of both graphs, the elements from the titanium alloy are observed. As the layer grows, a decrease of the elements from the substrate, the appearance of the elements belonging to the electrolyte and a significant presence of oxygen, due to the oxides formed during the PEO process, are observed. It can be noted that there are more

species from the electrolyte in the coating surface than near the substrate. There are studies which suggested that discharges that occur near the coating surface may incorporate more elements from the electrolyte[42, 43, 44]. In this analysis, no iodine was detected, since the equipment was not prepared to analyze this element.

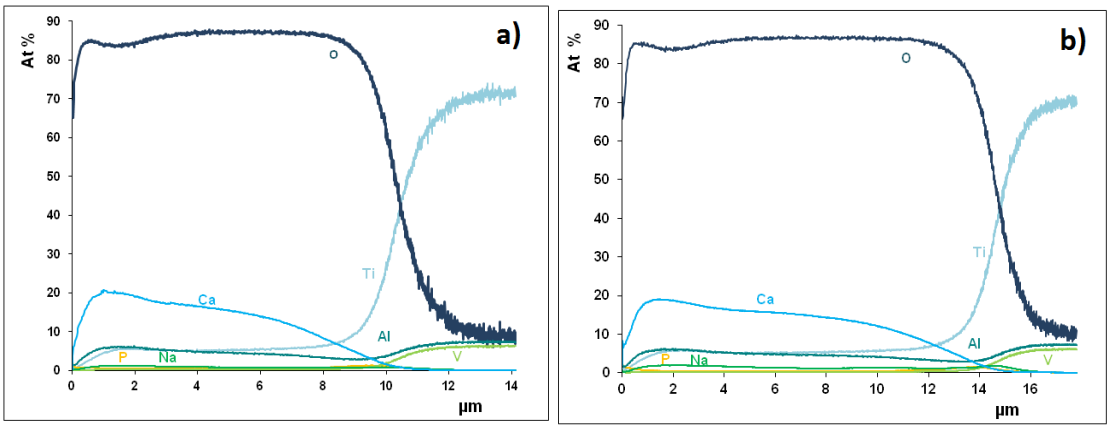

Fig. 6.3.4. Coating composition graphics obtained by GD-OES: a) PEO-1 and b) PEO-2.

6.3.3.2. X-ray diffraction

XRD analysis allowed establishing the relative rutile/anatase ratio in the coatings. This analysis was semiquantitative taking into account the diffraction peaks of the two phases. Thus, the anatase/rutile ratio for PEO-1 coating was 21/79 while for PEO-2 was 46/54. From the tribological point of view, it is of interest to have a higher rutile proportion because of its high stability and good mechanical properties. However, from the biological point of view, there are studies that show the biological effects of anatase, demonstrating that the bone growth is more evident with anatase phase[45, 46, 47]. This can lead to that a balance between the two phases could be the best option. No evidence of iodine was detected by this analysis due to that the small amount of this element in the coating. Neupane et al.[1]

[42] Jaspard-Mécuson, F.; Czerwiec, T.; Henrion, G.; Belmonte, T.; Dujardin, L.; Viola, A.; Beauvir, J., *Surf Coat Technol.* **2007**, 201, 8677-8682.
[43] Arrabal, R.; Matykina, E.; Hashimoto, T.; Skeldon, P.; Thompson, G. E., *Surf Coat Technol.* **2009**, 203, 2207-2220.
[44] Hussein, R. O.; Nie, X.; Northwood, D. O.; Yerokhin, A.; Matthews, A., *J Phys D: Appl Phys.* **2010**, 43, 105203-105216.
[45] Sollazzo, V.; Pezzetti, F.; Scarano, A.; Piattelli, A.; Massari, L.; Brunelli, G.; Carinci, F., *J Craniofac Surg.* **2007**, 18, 806-810.
[46] Uchida, M.; Kim, H. M.; Kokubo, T.; Fujibayashi S.; Nakamura, T., *J Biomed Mater Res.* **2003**, 64, 164-170.
[47] Segomotso, B.; Baozhy, T.; Feng, C.; Jinlong, Z., *Appl Surf Sci.* **2012**, 258, 3927-3935.

and Segomotso et al.[47] did not find iodine in their coatings either by this technique.

6.3.3.3. Tribocorrosion tests

In tribocorrosion tests, prior the sliding process, the samples were immersed in PBS and their open circuit potential values were monitored till they had stabilized. The OCP values for Ti6Al4V, PEO-1 and PEO-2 were -0.345 V, 0.009 V and 0.079 V, respectively. Once the open circuit potentials were stabilized, electrochemical impedance spectroscopy (EIS) measurements were carried out in order to see the corrosion resistance of each sample before the sliding process (Fig. 6.3.5). The next step was to record the OCP during 300 seconds and afterwards, start with the sliding process. This caused an immediate decrease of the potential in the bare Ti6Al4V sample, while the developed coatings did not suffer initially any variation. It indicated that in the Ti6Al4V, the spontaneous formed TiO_2 protective coating was removed due to the mechanical effect and the bare metal surface was exposed to the electrolyte. The fluctuation of the potential along the sliding process is related to the continuous de-passivation and re-passivation of the wear tracks[48]. In case of PEO-2 coating, approximately after the first 300 seconds, the potential started decreasing showing a partial or total removing of the protective coating. The PEO-1 sample did not exhibit significant variations in its potential. It indicates that the coating did not apparently suffer wear. Once the sliding tests had concluded, the potentials increased reaching values close to the initial ones. This effect is due to the re-passivation phenomenon. The OCP values were monitored for 10 minutes with the aim to stabilize. The recorded OCP values after the sliding were -0.357 V for Ti6Al4V, -0.001 V for PEO-1 and -0.025 V for PEO-2. The Ti6Al4V was re-passived with final OCP similar to initial one. In TiO_2 developed coatings the OCP after the sliding process were close to the obtained before.

[48] Kumar, S.; Sankara Narayanan, T. S. N.; Raman S, G. S.; Seshadri, S. K., *Mater Sci Eng C.* **2010**, 30, 921-927.

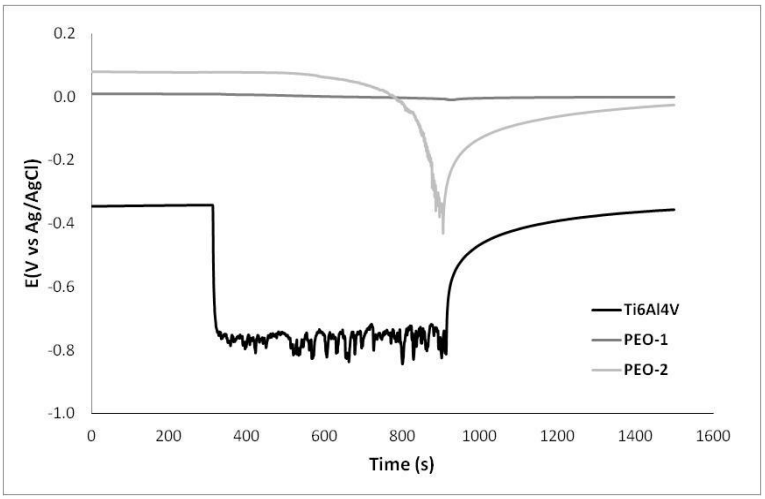

Fig. 6.3.5. Open circuit potential (OCP) during sliding process for TiAl4V, and PEO-1 and PEO-2 coatings.

Analyzing the bode impedance plots before and after the wear test (Fig. 6.3.6), no corrosion resistance variation has been observed. It seems that the electrochemical state has not been changed by the effect of the sliding process and the consequent wear produced on the surface of the samples. Anyway, it was noted that the corrosion resistance of developed TiO_2 coatings are similar but lower than that of Ti6Al4V. Similar results were obtained in the study of Fazel et al.[49], where at high frequencies the higher porosity of the outer layer produced the decreasing of the impedance values.

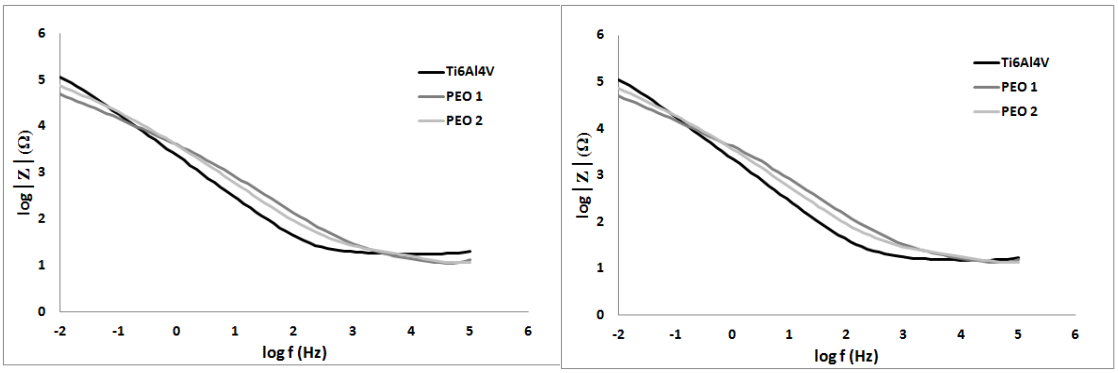

Fig. 6.3.6. Bode impedance plots for TiAl4V, PEO-1 and PEO-2 coatings (left) before and (right) after sliding. (modulus IZI is the impedance modulus and f is the frequency).

[49] Fazel, M.; Salimijazi, H. R.; Golozar, M. A.; Garsivaz jazi, M. R., *Appl Sur Sci.* **2015**, 324, 751-756.

During the sliding process against alumina counterbody, friction coefficients evolution was recorded (Fig. 6.3.7). It was noted that the friction coefficients of both developed TiO_2 coatings was higher than the substrate one. This can be related to the higher roughness of both coatings and the superior hardness of TiO_2 layer, due to its ceramic nature, in comparison to the Ti6Al4V. According to the website of ASM Aerospace Specification Metals INC, the hardness of Ti6Al4V alloy should be around 349 HV[50], while the hardness of TiO_2 coatings developed by PEO technology is around 400-600 HV. Mean friction coefficients and the total material loss in the wear track (W_{tr}) were calculated and compiled in Table 6.3.3. Similar friction coefficients were obtained for both layers, with a value of around 0.7. This tribological behavior is within the expected one[51, 52]. Regarding to the total material loss during the rubbing process, in PEO-1 coating it was not possible to calculate this value due to the low wear produced. PEO-2 coating suffered less material loss than Ti6Al4V sample.

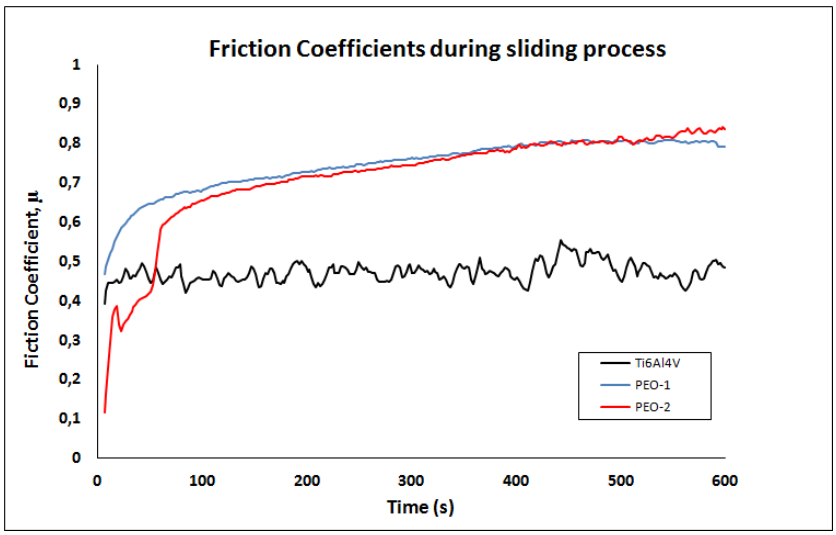

Fig. 6.3.7. Friction coefficient evolution during sliding process in tribocorrosion tests.

[50] "ASM Material Data Sheet". ASM. Web. 14 October 2015. http://asm.matweb.com/search/SpecificMaterial.asp?bassnum=MTP641.
[51] Khorasanian, M.; Dehghan, A.; Shariat, M. H.; Bahrololoom, M. E.; Javadpour, S., Surf *Coat Technol.* **2011**, 206, 1459-1502.
[52] Aliasghari, S.; Skeldon, P.; Thompson, G. E., *Appl Surf Sci.* **2014**, 316, 463-476.

Table 6.3.3.

Mean friction coefficient for Ti6Al4V substrate and both developed TiO_2 coatings.

Samples	Friction Coefficient ± STD	Wtr* (cm^3)
Ti6Al4V	0.472 ± 0.037	1.2 E^{-05}
PEO-1	0.744 ± 0.085	Not possible to measure
PEO-2	0.715 ± 0.134	1.62 E^{-06}

*approximate values are given due to the lack of wear track homogeneity.

Analyzing the wear scars by the confocal microscope (Fig. 6.3.8), it was seen that the TiO_2 coatings suffered lower wear during the rubbing conditions leading to irregular tracks. Analysis of the wear tracks profiles was carried out in order to ensure if the coatings were removed somewhere baring the substrate. The maximum wear track depth in PEO-1 was around 2 µm when the thickness of the coating was 3.31 µm (Fig. 6.3.9). This seems to indicate that the coating was not removed during the sliding. In case of PEO-2, the maximum wear track depth was around 4-5 µm whereas the thickness of the layer was 4.5 µm. In this sample, it can be concluded that in some areas of the wear track it has reached the substrate after the tribocorrosion test.

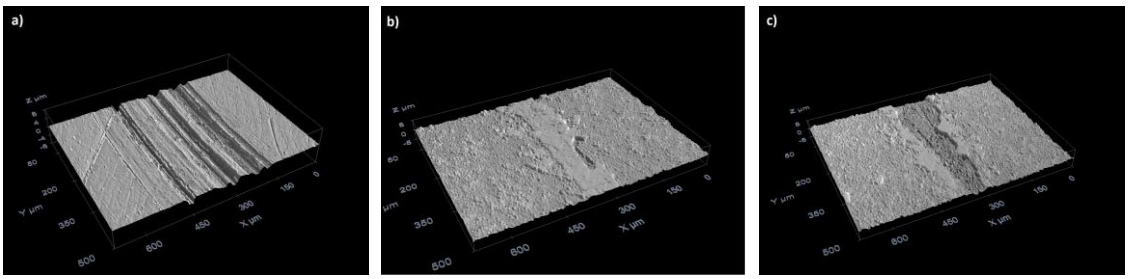

Fig. 6.3.8. Wear tracks topography: a) Ti6Al4V, b) PEO-1 and c) PEO-2.

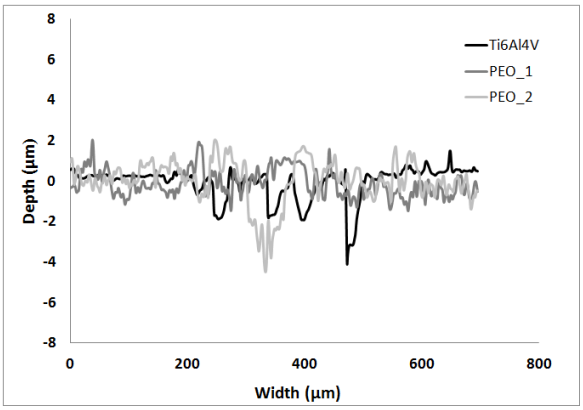

Fig. 6.3.9. Track profiles of uncoated and coated samples.

By EDS technology, the chemical composition of worn area of uncoated and coated samples was analyzed. As expected, in the wear track of Ti6Al4V sample only elements from the substrate were found (Fig. 6.3.10). Studying the wear scar in the confocal topography and SEM micrograph, it can be concluded that the wear mechanism for Ti6Al4V was abrasive type.

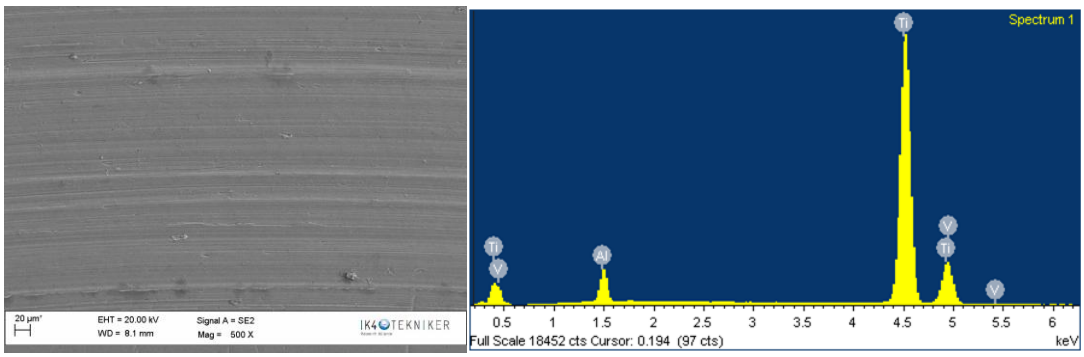

Fig. 6.3.10. SEM micrograph of Ti6Al4V (left) and corresponding spectrum form EDS analysis (right).

For the wear track of PEO-1 coating, three chemical analyses were performed in the affected area in order to ensure that the coating was not removed. In all analysis performed elements from the coating like calcium, phosphorus and potassium were detected, confirming that the coating acted as a protective layer against tribocorrosion conditions. In the micrograph it can be observed that part of the coating was removed during rubbing test and re-deposited generating a protective tribolayer, as a consequence of an adhesive wear (Fig. 6.3.11, point b).

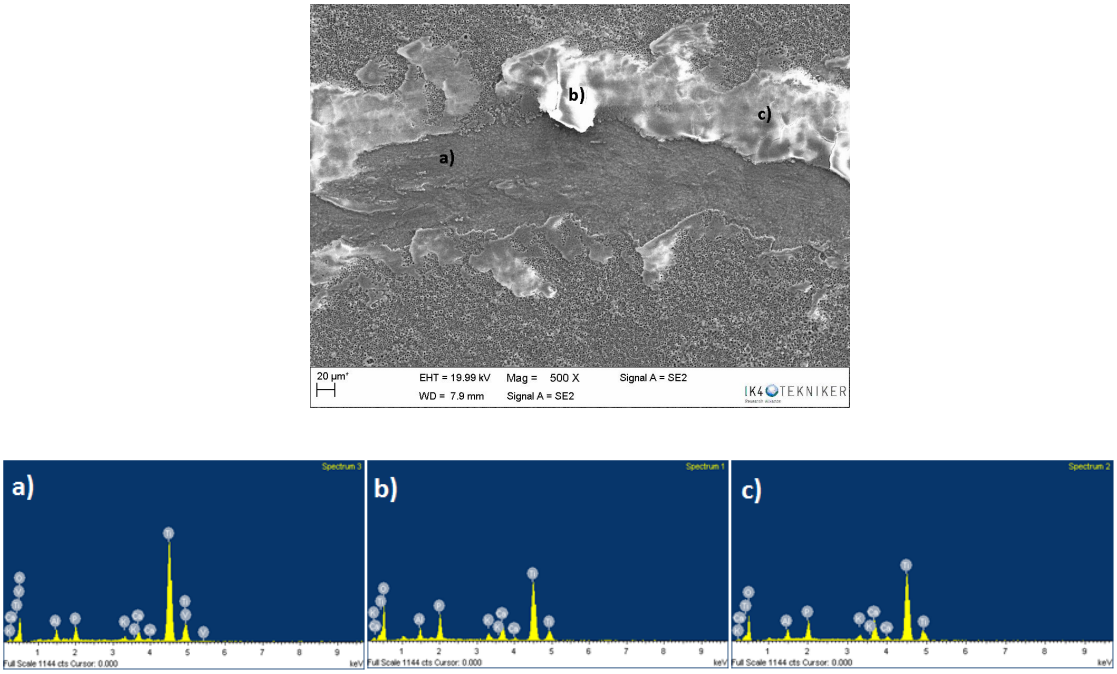

Fig. 6.3.11. SEM micrograph of PEO-1 coating (top) and corresponding spectra from EDS analysis (bottom).

Concerning the PEO-2 coating, chemical composition was also analyzed in different parts of the wear track by EDS technique (Fig. 6.3.12). It was noticed that in some areas of the track (in particular in a) spectrum), the substrate has been reached because elements from the coating were not detected, but only from the substrate, that is titanium, vanadium and aluminum. In this coating, the wear mechanism is dominantly an adhesive wear. Additionally, a polishing effect in some parts of the scar (point a in Figure 6.3.12) was detected.

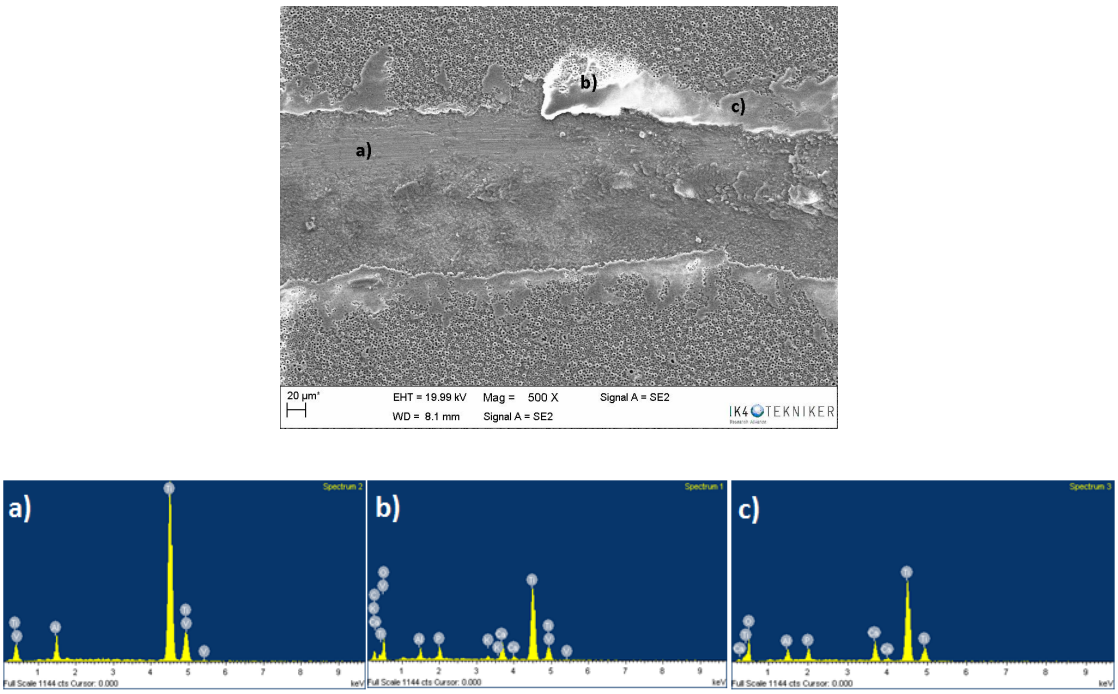

Fig. 6.3.12. SEM micrograph of PEO-2 coating (top) and corresponding spectra form EDS analysis (bottom).

6.3.3.4. Bacterial adhesion

Analyzing the biocide effect that the developed coatings showed against *Staphylococcus aureus* 15981, it was not observed improvement in the biocide effect of substrate (Fig. 6.3.13). There cannot be observed a statistically significant difference in the mean percentage of surface covered by bacteria compared to the control (Ti6Al4V), with the PEO-1 layer (P value= 0.0362, Kruskal-Wallis test). The same effect was observed with PEO-2 layer (P value= 0.1234, Kruskal-Wallis test).

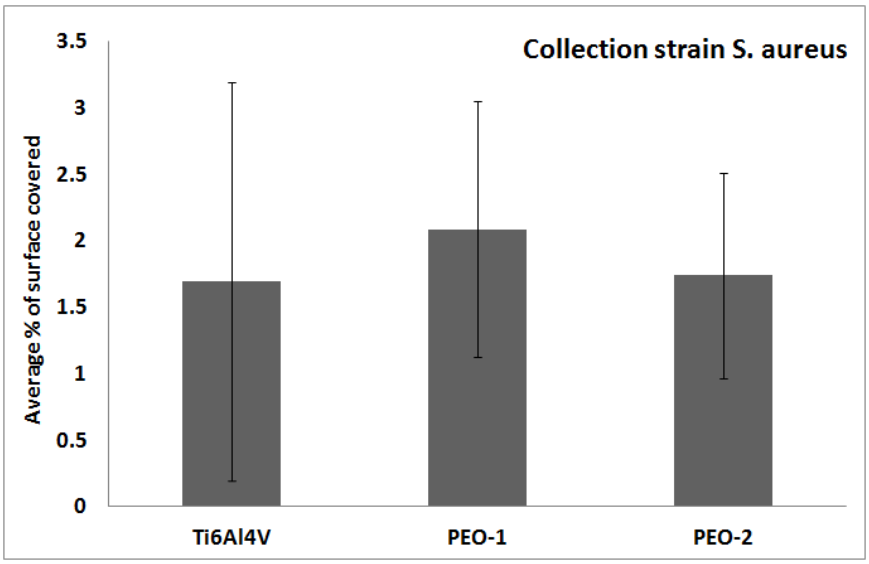

Fig. 6.3.13. Mean percentage of surface covered by *S. aureus*.

Concerning the *S. epidermidis* collection strains, developed TiO_2 coatings with iodine improved the antibacterial properties decreasing the percentage of surface covered by bacteria in comparison to the substrate (Fig. 6.3.14). There can be observed a statistically significant difference in the mean percentage of surface covered by bacteria compared to the control (Ti6Al4V), with the PEO-1 layer (P value= 0.0007, Kruskal-Wallis test). The same effect was observed with PEO-2 layer (P value= 0.0000, Kruskal-Wallis test).

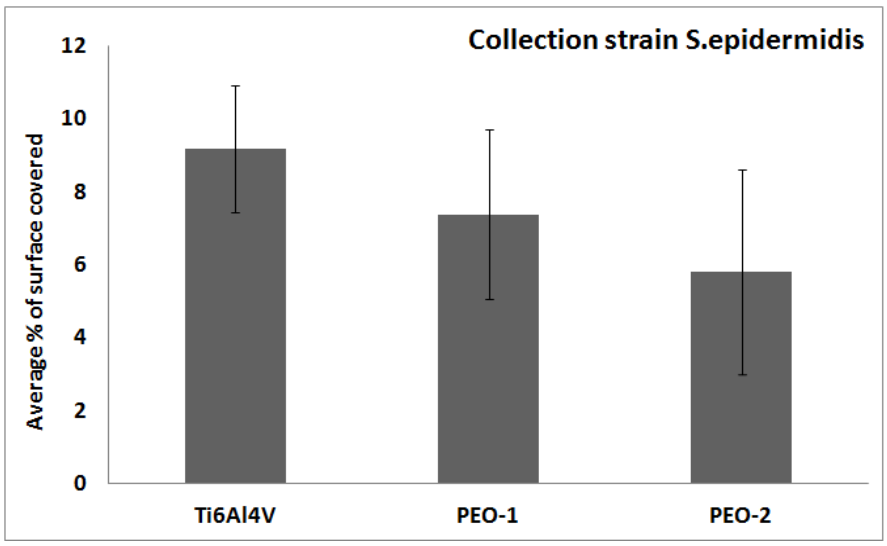

Fig. 6.3.14. Mean percentage of surface covered by *S. epidermidis*.

6.3.4. Conclusions

Among the developed coatings by PEO technology, PEO-1 coating seems to have the most suitable surface for cell growth. It is more hydrophobic than the substrate and PEO-2 coating. Besides, it has the highest pore percentage and the smaller average pore size. Additionally, osseointegration enhancing elements (Ca and P) have been introduced into the coating, with a higher concentration near the surface. Concerning the tribocorrosion tests, the corrosion resistance was kept in all the samples after the rubbing process. Noticeably, the wear resistance was increased in case of PEO-1 layer probably due to the high amount of rutile phase present in its microstructure. The friction coefficient was superior to bare Ti6Al4V because of the higher roughness in comparison to the substrate. The addition of iodine as biocide element improved the antibacterial features of Ti6Al4V alloy against *S. epidermidis*.

Chapter 7

CONCLUSIONS

- ✓ The behavior of Ti6Al4V has been improved for both, knee and hip orthopedic applications by means of the development of multifunctional coatings.
- ✓ The developed Ti-C-N coatings by Physical Vapor Deposition technique for knee implants improves the wear resistance of Ti6Al4V.
- ✓ The tribocorrosion response of Ti-C-N_2 shows a good corrosion resistance and low wear index in comparison to the substrate, behaving as a barrier that avoids the release of elements from the substrate.
- ✓ In fretting tests, the tribological behavior of Ti-C-N_2 and Ti6Al4V was similar, with very close friction coefficients and no wear on the surface. However, counterbody UHMWPE balls tested against Ti-C-N_2 shows lower wear.
- ✓ Ti-C-N_2+Ag exhibits excellent antibacterial properties against both *S. aureus* and *S. epidermidis* collection and clinical strains.
- ✓ The developed TiO_2 coatings by Plasma Electrolytic Oxidation for hip implants show a suitable surface for cell growth since they have osseointegration helpers (Ca and P), an appropriate porous size and porosity index, and because they are hydrophobic.
- ✓ The electrochemical behavior for TiO_2 coatings remains unaltered after the sliding process in tribocorrosion tests, and the wear resistance is better than the bare substrate, especially in PEO-1 coating.
- ✓ The biocide effect of iodine in TiO_2 has been confirmed against *S. epidermidis*.

Chapter 8

FUTURE PERSPECTIVES

The general conclusion of this thesis is that the behavior of Ti6Al4V alloy in orthopedic applications has been improved by developed coatings produced by different surface treatments.

The developed Ti-C-N_2 coating for knee implant has showed excellent tribocorrosion properties and a significant wear resistance. Besides, antibacterial properties have been conferred by the deposition of a top thin Ag film. So, the next step for this coating would be the characterization in real knee simulators in order to determine the effectiveness of the coating and the possible implementation at industrial scale in a future.

Concerning the selected TiO_2 coating (PEO-1) for hip implant, the tribological characterization carried out at laboratory scale exhibited a promising behavior consisting of high corrosion and wear resistance and an appropriate microstructural properties to promote the osseointegration. In this sense, cell proliferation analyses are intended to be performed. The first step should be the identification of the chemical specimen in which iodine is fixed in the TiO_2 matrix, in order to control the composition of the coating and then the biocide effect.

ANNEX A

Instrumental Techniques

A.1. Physical Vapor Deposition (PVD) techniques

A.1.1. Cathodic arc evaporation

The cathodic arc method is based on the arc discharge between an inert electrode (anode) and a target (cathode). The high current density generated in located points in the cathode (of the order of 10^{12} A m^{-2}) is associated to a high energy concentration (around 10^{12} W m^{2}) and is capable of melting and evaporating small quantities of material in the surface of the cathode.

The arc discharges require a low voltage and high current (around 100 A) power supply. The plasma generated in these conditions has an elevated density of ions (≈ 100 % of ionization), which implies that the material is evaporated in ions form. This allows the control of both, the path of evaporated material to the substrate and the energy of the ions by means of application of magnetic and electric fields with proper intensity. The ions energy adjustment turn allows the production of coatings with improved density, hardness and adherence properties. However, it is important to note that the evaporated material is not only formed by ions but also by small atomic cluster and particles, whose sizes are within the range of 0.1 – 10 µm, called "microparticles"[94].

If a reactive gas is introduced during the evaporation process, dissociation, ionization and excitation can occur during interaction with the ion flux, depositing a compound film on the substrate.

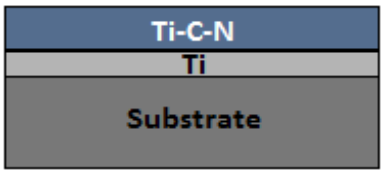

Fig. A.1. Different areas of a multifunctional layer for medical applications.

Figure 9.1., shows a titanium doped DLC coating. The first titanium layer was deposited in order to improve adhesion of the Ti-C-N coating to the substrate and relax internal stresses of the coating.

A.1.2. Magnetron Sputtering

The sputtering technique is based on the intensive ejection of a material by the ions

produced in an electrical discharge in plasma form. When the energy of incidental ions is sufficiently high, the interaction with the material surface (through the exchange of angular momentum) causes the atoms of the surface to be stripped, passing to vapor phase.

Concerning the electrical discharge in a sputtering system, the upper electrode acts as the cathode of the electric discharge, and is formed by the material to be evaporated. This cathode called sputtering target, is subjected to intense ejection from the positive ions of the discharge once they are accelerated by the plasma as a result of the potential fall associated to the electrical field. The ion bombardment produces, not only the effect of the target sputtering, but also the emission of secondary electrons that are accelerated towards the plasma.

The discharge gas is usually a noble gas of high mass in order to increase the transfer of angular momentum to the target atoms. The substrates to be coated are located on the anode, although they can be placed on an auxiliary support in front of the anode.

A.2. Plasma Electrolytic Oxidation (PEO)

The plasma electroxidation process involves the application of a modulated voltage to the component in an electrolytic bath agitated using compressed air and under temperature control. The sample acts as an anode while a stainless steel mesh acts as cathode. The voltage is sufficiently high to create intense plasma due to microarc generation at the component surface. This results in oxidation of the component surface (plasma electrolytic oxidation) as well as elemental co-deposition from the electrolyte solution, which creates a hard ceramic oxide layer on the substrate alloy (Fig. 9.2).

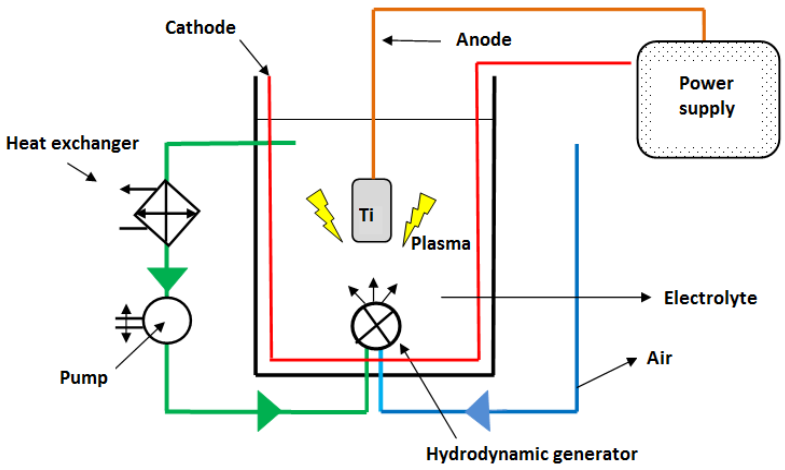

Fig. A.2. Illustration of plasma electrolytic oxidation.

A.3. Calotests

With this equipment the thickness of coatings can be measured. Coatings on substrates with plane, spherical or cylindrical faces can be considered (Fig. 9.3.).

Fig. A.3. Calotest equipment.

During the analysis, a hard steel ball turns on a coating until it achieves the substrate, causing a spherical crater (Fig. 9.4). Measuring its diameters with a microscope the thickness of the coating can be calculated. In order to accelerate the wear of the coating, the ball can be impregnated with grinding diamond paste.

The suitable thickness range goes from 0.2 to 10 µm.

The used balls have diameters of 10, 20 (the only one calibrated) and 30 mm.

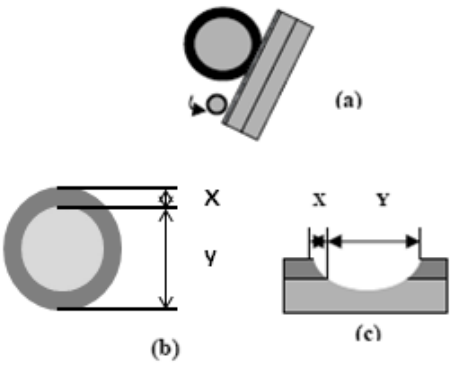

(a) The shaft rotates the pellet which in turn rotates on the sample.

(b) Top view of the crater and its dimensions.

(c) Cross section of the crater.

Fig. A.4. Diagram of the basic operation mechanism of a Calotest.

The coating thickness (e) calculation follows the next equation:

$$e = \frac{xy}{\emptyset}$$

where $\emptyset$ is the nominal diameter of the ball.

A.4. Fischer nanoindenter

FISCHERSCOPE H100 nanodurometer (Fig. 9.5) consists of a Vickers nanoindenter which measures the hardness corresponding to the first nanometers or microns of a material's surface. In this way, this equipment is suitable for measuring hardness of coatings and surface treatments, which cannot be measured with conventional durometers due to their minimum dimensions.

Fig. A.5. FISCHERSCOPE H100 nanodurometer.

The nanodurometer is controlled by a software in which all the indentation test values are registered. The gradual application of the indenter load can be indicated by the number of pulses needed, both to achieve the desired final load and to

remove the load after the indentation. In this way, plastic and elastic material properties can be measured.

An average of the different indentation tests can be calculated; several points over the same surface can be selected and plastic and elastic coefficients, differential hardness, plastic hardness, Young's modulus and penetration values depending on loads can be obtained. In the FISCHERSCOPE H-100 equipment the penetration depth under indenter load is measured, in contrast the Vickers hardness test, where the diagonal of the indentation trace is measured. The equivalence with Vickers hardness (expressed in Kg/mm^2) is obtained by applying the next conversion formula from the curves penetration depth versus applied load:

$$HV = 378{,}5 * \frac{P(mN) * h_r\ (\mu m)}{h_t^3(\mu m^3)(1-\frac{W_E}{W_T})}$$

where

- **P** = total applied load
- $\mathbf{W_E}$ = energy invested in the deformation and elastically recovered.
- $\mathbf{W_T}$ = total energy invested in the deformation (plastic + elastic)
- $\mathbf{h_r}$ = residual deep of the indentation
- $\mathbf{h_t}$ = maximum penetration deep under load.

Total indentation load can range between 4 and 1000 mN; the minimum indentation load is 0.4 mN. The indentation deep must not be higher than 10 % of the coating total thickness to consider the test valid. Because of this, the load used in the test will depend on the coating thickness.

The surface to be measured has to be flat and with a quite good finishing. This last characteristic depends on the loads to be applied; the lower the indentation load the lower surface roughness is required so that the possible surface anomalies do not affect the test.

A.5. Perthometer M2 profilometer

Surface roughness, often shortened to roughness, is a measure of the texture of a surface. The Perthometer M2 profilometer of Mahr (Fig. 9.6) is used to study the roughness of the surfaces.

The Tracing method is an inspection method for the two-dimensional tracing of the surface. It requires a surface pick-up to be traversed horizontally across the surface at constant speed. The Traced profile is the surface profile traced by the pick-up stylus. It is quantified by the vertical deviations of a real surface from its ideal form. If these deviations are large, the surface is rough; if they are small the surface is smooth.

Fig. A.6. Perthometer M2 profilometer of Mahr.

The Mahr Perthometer M2 is used to measure the roughness with a maximum measuring range of 150 µm. The maximum length of the cut off is 17.5 mm. Both for the selection of the evaluation length as for the evaluation protocol, it can be used several standards (ISO, JIS and CNOMO). To calculate the Ra values, the equipment has followed the DIN EN ISO 4288 and DIN EN ISO 4287 standards.

A.6. Rockwell tests

By means of Rockwell tests, measurement of the toughness of the coating can be carried out.

The test consists on making a Rockwell C indentation (with a load of 150 Kg) and examining the edges of the trace with the optical microscope: the higher the number of cracks and delaminations, the worse is the adhesion.

This is a qualitative measurement, and in order to have comparable results, the

substrates must be of similar material and have similar hardness.

A graphic table is used to establish the grade of adhesion (Fig. 9.7).

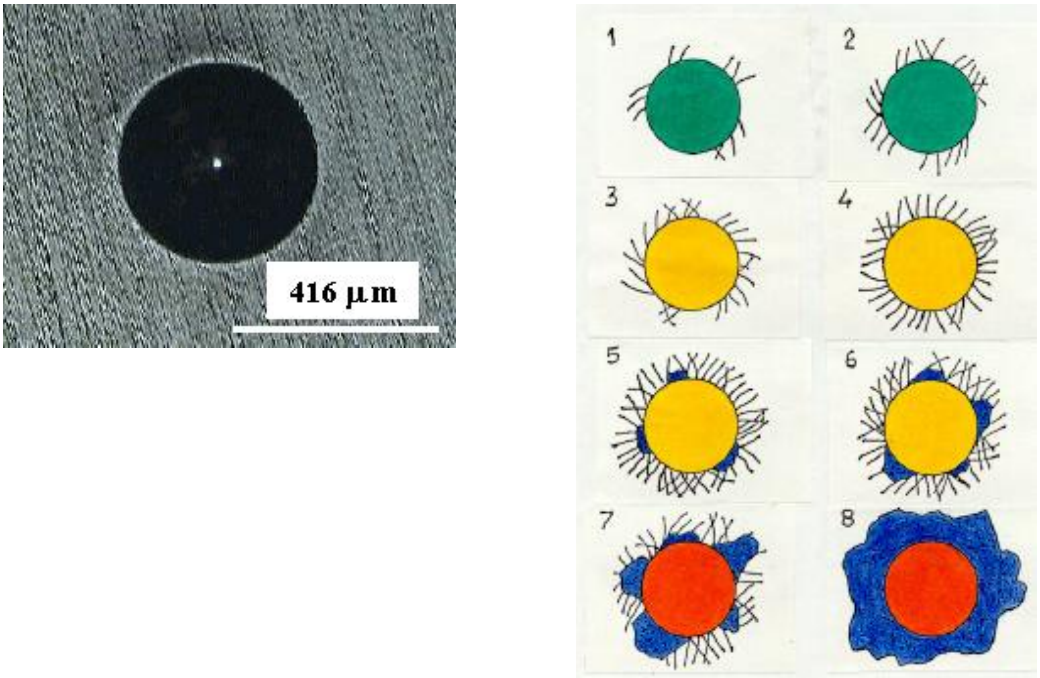

Fig. A.7. (left) trace obtained after the test and (right) graphic table for the evaluation.

A.7. Glow Discharge Optical Emission Spectroscopy (GD-OES)

The Glow Discharge Optical Emission Spectroscopy (Fig. 9.8.) allows obtaining profiles in depth detecting simultaneously the presence of different elements in the layers to be characterized.

Fig. A.8. GD-Profiler 2 equipment from Horiba Jobin Yvon

During the GD-OES analysis, the sample is eroded by the low energy (‹50 eV) Ar^+ ions bombardment, that come from a plasma form discharge. The eroded atoms are excited by the plasma, losing energy after the emission of photons with characteristics wavelengths allowing distinction of the different elements present in the sample (Fig. 9.9.). The analysis is performed from the outside to inside of the sample.

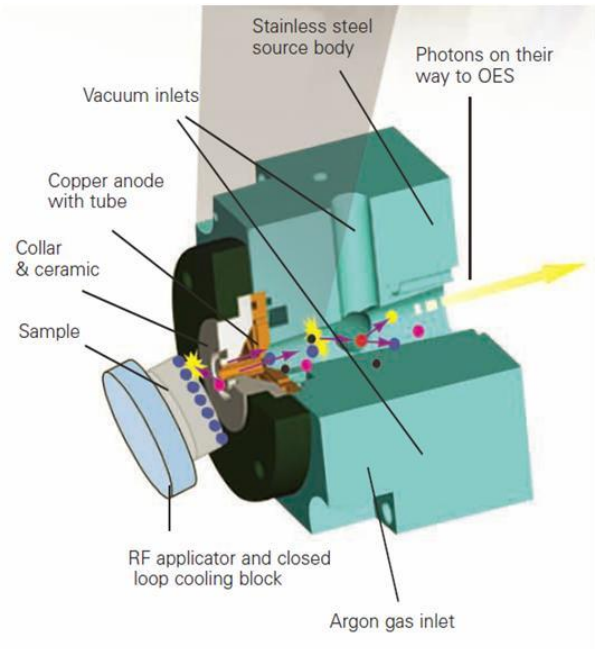

Fig. A.9. Details of the analysis area in a simple (glow discharge)

The equipment provides signal-time profiles, which can be semi-quantified in atomic or mass composition versus thickness profiles. This semi-quantification feature provides a characterization tool for comparative analysis of different samples.

Elements that can be analyzed: 38 (polychromator) + 1 (monochromator)

Polychromator elements: H, O, Mg, N, C, Nb, Cu, Ag, Zr, Ni, Co, P, Ta, Ti, Fe, Y, Sn, Mo, Ca, Al, Sr, V, Cr, W, Pb, In, Ce, Sb, Zn, Au, B, Mn, Pt, S, Hf, Si, Na, Bi.

Thickness range for the samples to be analyzed: 10 nm-100 µm.

Typical erosion speed: 3 µm/min.

A.8. Raman spectroscopy

Raman spectroscopy allows the identification of vibrational (phonon) states of molecules. As a result, Raman spectroscopy provides an invaluable analytical tool for molecular finger printing as well as monitoring changes in molecular bond structure (e.g. state changes and stresses & strains).

Raman spectroscopy is based on the light inelastic scattering (Raman effect), as observed in figure 9.10. The laser beam that is monochromatic and contains the light of a single frequency falls on the material. Most of the light scattered by this one has the same frequency. But, due to the interactions with the molecules vibrations of the material, a small fraction of light suffers displacements of frequency similar to the frequency of the normal modes of vibration in the material (inelastic scattering or Raman effect).

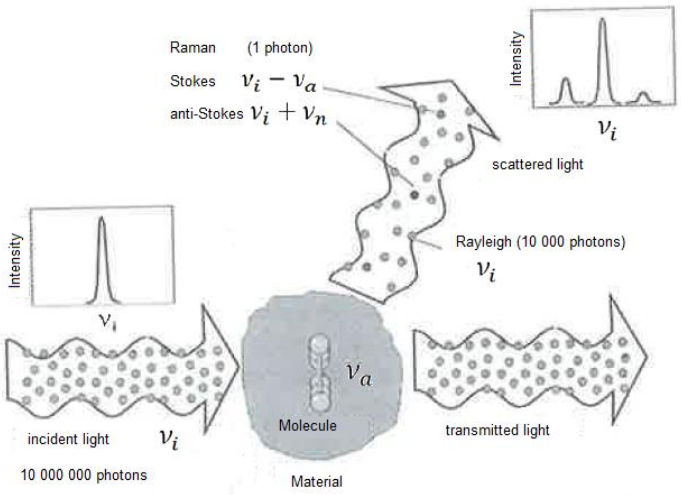

Fig. A.10. Schematic representation of the Raman effect.

In a Raman spectrum, the laser beam is focused on the sample with a lens or a microscope objective (Fig. 9.11). The scattered light is collected with other lens and goes through a holographic notch filter that removes the laser light and only allows passing the light with a frequency change (including Raman spectrum and luminescence). This light is spectrally analyzed with a diffraction grating monochromatic, and finally is collected with a detector, that can be a photomultiplier or a CCD (Charge Coupled Device, a solid state detector made from semiconductor materials)[1].

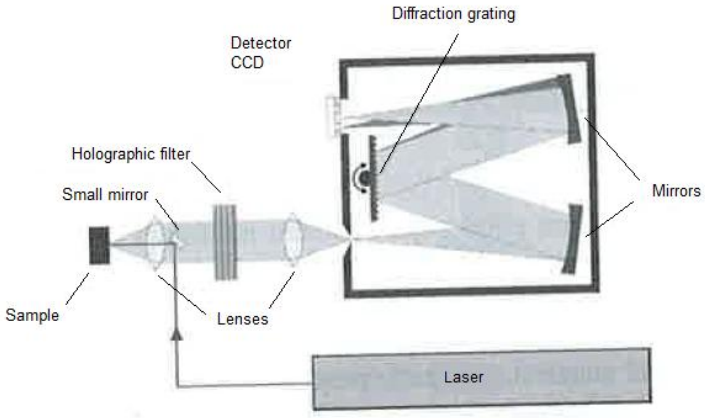

Fig. A.11. Raman spectrometer of one diffraction grating with holographic filter to block the elastically scattered light.

[1] Agulló-Rueda, F.; Serna, R., Métodos ópticos, in: Albella, J. M. (Ed.), *Láminas delgadas y recubrimientos: preparación, propiedades y aplicaciones*, CSIC, Madrid, Spain, **2003**.

A.9. X-ray diffraction

The X-rays are an electromagnetic radiation with a wavelength, λ, of the same order as the cell parameters of the crystals. This makes the crystalline substances are able to diffract X-rays. When this radiation strikes on the atoms electronic cloud of a crystal lattice, these become in on-time emitters of that radiation. The emitted radiation for each atom is expanded in the form of spherical wave and interferes with that created by the bordering atoms. This interference can be destructive or constructive. The directions in which the interference is constructive follow the Bragg´s Law:

$$n\lambda = 2d_{hkl}\sin$$

where n is a natural number, λ is the wavelength of the used X-rays, θ is the radiation incidence angle and d_{hkl} is the distance between two consecutive planes defined by a components vector hkl.

A.9.1. X-ray diffraction on polycrystalline sample

The X-ray diffraction on polycrystalline sample has been used, in general, for the qualitative analysis of the detected and presented phases in this memory. These tests have been useful for both the phase identification and its chemical purity determination, due to the fact that all crystalline solids have a characteristic difractograma.

A polycrystalline material is formed by a large number of small crystals randomly arranged, ones with respect to each others. A sample with these features, when irradiated with a beam of X-rays, always will present a certain number of crystallites that fulfill the Bragg´s law. The diffractometers allow the accurate determination the direction in which the diffraction occurs. The most common diffractometers geometry, and that have been used diffractometer in this work, is called Bragg-Brentano. In this type of geometry, the goniometer incorporates two coaxial rotations: one for the sample and the other one for the detector. These rotations are coupled, in such a way that if the sample is moved a θ angle, the detector moves, in the same time, a 2θ angle. The representation of the X radiation intensity that reaches to the detector with respect to the rotation 2θ angle is called

difractograma.

To obtain information from the difractogramas is necessary to analyze them, where it has to be taken into account the position of the maximum diffraction, its shape and intensity.

Used diffractometers belong to the General Services of X-rays: Rocks and Minerals (SGIker), from the Basque Country University (UPV/EHU). The difractogramas for the characterization of the phases have been registered in a Philips PW1710 diffractometer, with Bragg-Brentano geometry and copper anticathode (Cu-Kα radiation). Measurements have been carried out from 5 to 70º in 2θ, with a 0.02 step and a time counting of 1s. Difractogramas thus obtained for the studied phases were used to make the Pattern Maching from the same.

A.10. Scanning Electron Microscope (SEM)

The ULTRA *plus* Field Emission Scanning Electron Microscope with EDS and EBSD microanalysis from OXFORD INCA synergy was used to analyze the microstructure and the chemical composition (Fig. 9.12). The equipment is a scanning electron microscope with controlled field emission source with incorporated GEMINI® patented column, for high resolution and analysis from ZEISS Company. The detection system is formed by a SE Everhart-Thomley detector, an in-lens secondary integrated detector (SE) of high efficiency, a retrodispersed electron detector mounted on the microscope camera (AsB), a retrodispersed electron detector in the column, a specimen current detector (SCM) and an infrared TV camera to observed the inside of the sample chamber. Besides, the equipment incorporate an EDS microanalysis system with a high resolution X-ray detector with Peltier type refrigeration without liquid nitrogen, and a EBSD system for the acquisition and the indexed of retrodispersed electron diffraction patterns with a Nordlys detector. The equipment also has a high current/depth of field module (HC/DoF). The complete system is under vacuum, so it is free of oil.

Fig. A.12. Scanning Electron Microscope (SEM)

The equipment incorporated the charge balancing device in order to observe no-conductive samples at high resolution in high vacuum conditions.

A.11. Energy Dispersive Spectroscopy (EDS)

The energy dispersive X-ray spectroscopy (EDS) is a surface chemical composition characterization technique. A focused electron beam impact against the surface of the sample ejecting an electron from the inner layer of the atom. This electron leaves a hole in its origin level and is taken up by other electron from the upper layers of the same atom. By moving to a lower energy state, a photon is released whose energy is in the range of X-rays. This emitted energy is different for each atomic number, so, it allows determining the elemental composition of the sample but it does not have information about the bonds. The elemental chemical composition obtained in EDS belongs to the microvolume of the sample invaded by the incident electron beam of the microscope. This depends on its energy but it is generally 1x1x2 μm^3.

The EDS spectrometer is integrated in the scanning electron microscope[2].

A.12. X-Ray Fluorescence (XRF)

The purpose of X-ray fluorescence is to determine chemical elements both qualitatively and quantitatively by measuring their characteristic radiation. To do this, the chemical elements in a sample must emit X-rays. As characteristic X-rays only arise in the transition of atomic shell electrons to lower, vacant energy levels of the atom, a method must be applied that is suitable for releasing electrons from the innermost shell of an atom. This involves adding to the inner electrons amounts of energy that are higher than the energy bonding them to the atom.

Every element is clearly defined by its atomic number Z in the periodic system of elements or by the number of its electrons in a neutral state. The binding energies or the energy levels in every element are different and characteristic for every element as a result of the varying number of electrons (negative charges) or the number Z of the positive charges in the atomic nucleus (=atomic number).

If an electron of an inner shell is now separated from the atom by the irradiation of energy, an electron from a higher shell falls into this resultant "hole" which releases an amount of energy equivalent to the difference between the energy levels involved.

The energy being released can be either emitted in the form of an X-ray or be transferred to another atomic shell electron (Auger effect). The probability of an X-ray resulting from this process is called the *fluorescence yield* ω. This depends on the element´s atomic number and the shell in which the "hole" occurred. ω is very for light elements and almost reaches a value of 1 for the K-shell of heavier elements.

However, decisive is that the energy or wavelength of the X-ray is very characteristic for the element from which it is emitted; such radiation is called *characteristic X-rays*.

This provides the basis for determining chemical elements with the aid of *X-ray fluorescence analysis*.

[2] Martínez de Olcoz Sainz, L., Caracterización Física y Funcional de Recubrimientos en Capa Fina Depositados por PVD para Aplicaciones Avanzadas. Tesis. Universidad de Barcelona. **2014**.

Concerning the layer thickness analyzed, the more readily the radiation of an element in the sample material is absorbed, the smaller is the layer of the sample from which the measurable radiation comes. A K-alpha photon from the element molybdenum (Mo $K\alpha_1$, 17.5 keV) has a greater chance of being measured at a depth of 0.5 mm from the analysis surface of a steel sample than a photon from carbon (C $K\alpha_{1,2}$, 0.282 keV). As a consequence, a specific layer thickness is analyzed for each element which depends on the specific energy of the used element line. The analysis of very light elements e.g. in solids (such as Be, B, C..., for example) is comparable with a plain surface analysis as their radiation originates from few atomic layers. Practically all the radiation from deeper layers is fully absorbed within the sample.

X-ray fluorescence measurements have been carried out by means of the BRUKER, S8 TIGER equipment in order to analyze the chemical composition of TiO_2 coatings developed by Plasma Electrolytic Oxidation (PEO).

A.13. Goniometer

The SURFTENS universal goniometer (Fig. 9.13, left) is used to investigate the wetting behaviour of the samples, i. e., to evaluate the grade of hydrophilia/hydrophobia of surfaces.

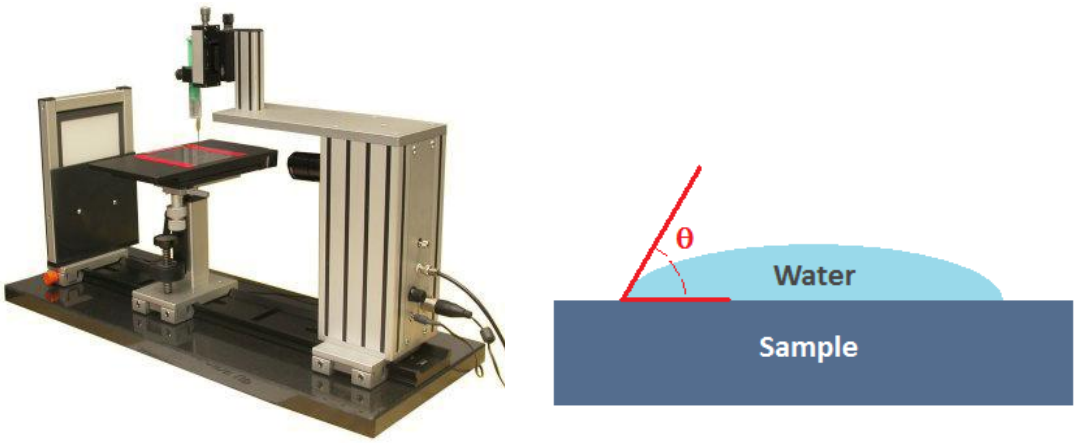

Fig. A.13. Goniometer for hydrophilia/hydrophobia measurements (left) and contact angle of a drop of water on a steel surface (right)

This evaluation is based in the measurement of the static contact angle of a drop of

water on the surface to be investigated (Fig. 9.13, right). This contact angle is measured by means of an optical system which calculates its value. The higher the contact angle, the higher the hydrophobia of the surface is.

A.14. Inductively coupled plasma optical emission spectroscopy (ICP-OES)

The Inductively Coupled Plasma (ICP) associated with the optical emission spectrometry is a multielement technique for the determination of 70 elements from the μg/l to the percent level without dilution.

The technique is based upon the spontaneous emission of photons from atoms and ions that have been excited in a RF discharge. Liquid and gas samples may be injected directly into the instrument, while solid samples require extraction or acid digestion so that the analytes will be present in a solution. The sample solution is converted to an aerosol and directed into the central channel of the plasma. At its core the inductively coupled plasma (ICP) sustains a temperature of approximately 10 000 K, so the aerosol is quickly vaporized. Analyte elements are liberated as free atoms in the gaseous state. Further collisional excitation within the plasma imparts additional energy to the atoms, promoting them to excited states. Sufficient energy is often available to convert the atoms to ions and subsequently promote the ions to excited states. Both the atomic and ionic excited state species may then relax to the ground state via the emission of a photon. These photons have characteristic energies that are determined by the quantized energy level structure for the atoms or ions. Thus the wavelength of the photons can be used to identify the elements from which they originated. The total number of photons is directly proportional to the concentration of the originating element in the sample.

The digestion of solid samples in this study has consisted of treating the sample (PBS) with H_2O:HNO_3 (1:1) and two droplets of HF.

The presence of elements from the substrate released to the PBS electrolyte during the tribocorrosion tests was analyzed with the ULTIMA 2 HORIBA Jobin Yvon equipment.

A.15. Fretting test

Fretting tests were carried out in the SRV test machine (Schwingung=Oscillation,

Reibung=Friction and Verschleiss= Wear) (Fig. 9.14).

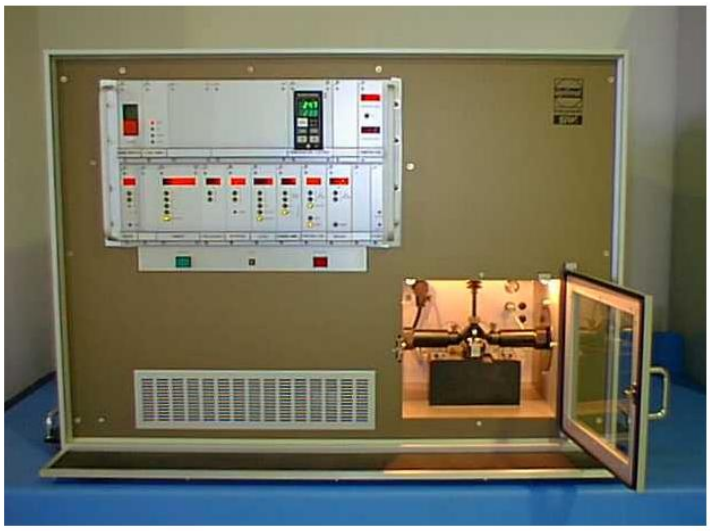

Fig. A.14. SRV tribometer

The Optimol SRV Friction and Wear Test Machine comprises a fixed bottom specimen support and a mobile, replaceable top specimen holder. The upper and lower specimens are pressed against each other by an adjustable force and are oscillated tangentially, employing an adequate frequency/stroke combination. The friction force is tranfered to the quartz force transducer by the specimens. The piezoelectric voltage of the quartz force transducer represents the measure of the friction coefficient (Fig. 9.15).

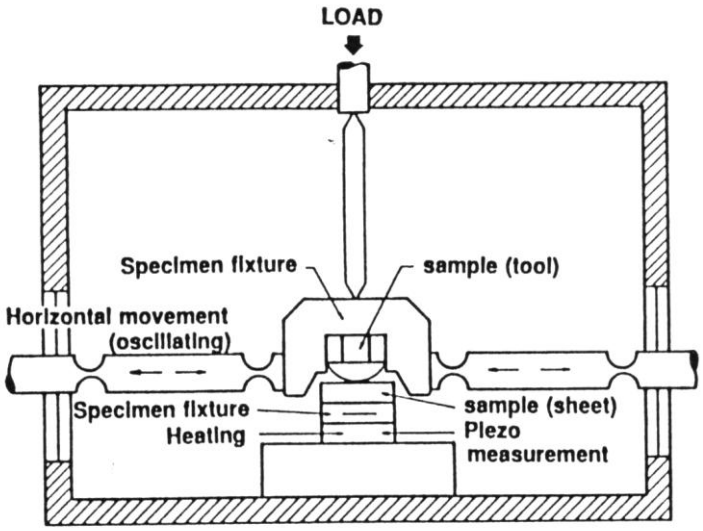

Fig. A.15. SRV friction and wear tester

The machine permitted ranges:

- Load: 1-2000N
- Time: 1 minuto-999 hours
- Frequency: 1-511 Hz*
- Stroke 0.1 - 4mm
- Linear speed 0.01-0.4 m/s
- Temperature
  - Standard range: ambient-290°C
  - Low temperature range: -35°C- 290°C
  - High temperature range: ambiente-900°C

The objective with SRV equipment has been to simulate real working conditions in implants related to produce micromovements. In fretting conditions, small amplitude oscillatory sliding motion takes place. For this reason, a stroke of 150 µm was selected to perform the tests under ball-on-disc configuration.

A.16. Tribocorrosion test

Tribocorrosion studies can be conducted by coupling electrochemical methods to tribology testing. For this, Microtester Tribometer and Autolab-Methrom potentiostat PGSTAT302N was used. In figure 9.14 the tribocorrosion set-up can be observed. It consists of a polytetrafluoroethylene cell mounted on a ball-on-disc tribometer. A loaded ceramic ball (the counterbody) slides against the specimen (the working electrode) while the tangential force is measured with a force sensor. The electrochemical potential of the specimen is controlled with respect to a platinum wire reference electrode (Fig. 9.16)[3].

[3] Takadoum, J.; Igartua, A., Phenomena of tribocorrosion in medical and industrial sectors, in: Celis, J. P.; Ponthiaus, P. (Ed.), *Testing tribocorrosion of passivating materials supporting research and industrial innovation: Handbook*. Maney Publishing, Leeds, UK, **2012**.

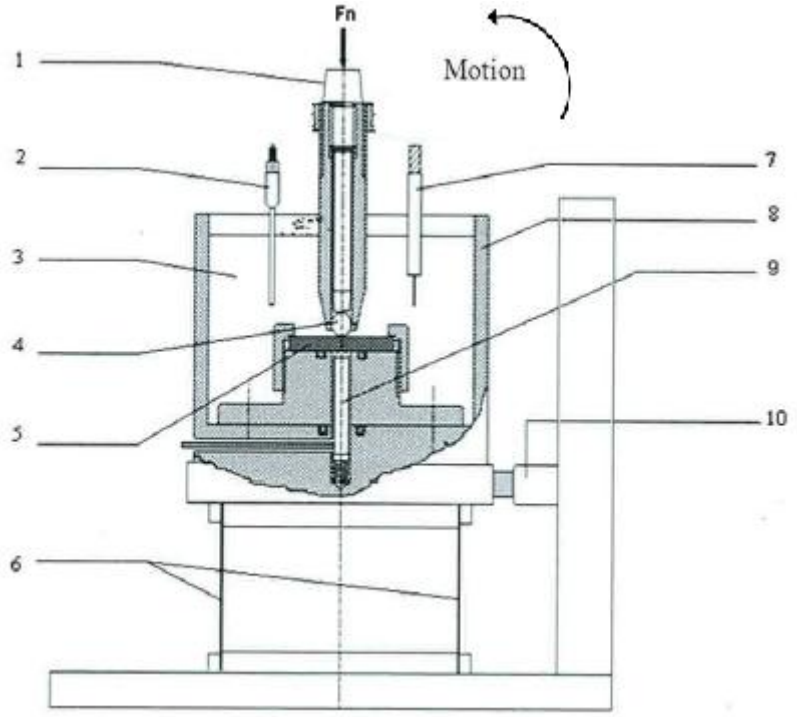

Fig. A.16. Tribocorrosion set-up: (1) normal load, Fn; (2) reference electrode; (3) electrolyte; (4) counterbody; (5) sample as working electrode; (6) spring plates; (7) counter electrode; (8) electrochemical cell; (9) connection of sample to potentiostat; (10) tangential force sensor[4]

Environment, mechanical properties, chemical composition and microstructure are the most important parameters that determine the material behavior in the case of tribocorrosion. Under tribocorrosion conditions, the interaction between the surface of a material and the electrolyte may lead to the formation of a new compound whose properties differ from those of the bare material. This lead to an enhanced or decreased surface resistance to friction, wear and corrosion.

Additionally, passivity of alloy is a phenomenon of major technical importance that permits protection of materials from general corrosion. Under tribocorrosion conditions, the integrity of the passive surface film can be affected by mechanical loading but can also be damaged by a local dissolution of the bare material.

In tribocorrosion tests, mechanical and electrochemical in situ measurements are needed to obtain information about the synergistic and antagonistic mechanism. The electrochemical methods used in this thesis work have been the open-circuit potential and electrochemical impedance measurements. From the mechanical

[4] Takadoum, J., *Corros Sci.* **1996**, 38, 643-654.

point of view, friction coefficient was recorded during the sliding process and once the tribocorrosion test was finished, the wear tracks were evaluated by means of the confocal microscope.

A.16.1. Open circuit potential measurements (OCP)

This method gives information about the balance between anodic and cathodic reactions in time. Under sliding conditions, a galvanic coupling between the material in the sliding track area (worn part) and the material outside the sliding track area (unworn part) on the disc sample may take place. Consequently, the open circuit potential will be determined by the following parameters:

- The respective intrinsic open circuit potentials of the materials in worn and unworn areas. These open circuit potentials are different because the electrochemical state of the metal is disturbed by wiping of the surface films that may consist of adsorbed species, passive films, or corrosion products, in the sliding contact, and by a mechanical straining of the metal.

- The ratio of worn to unworn areas. In particular, if the extent of the worn area increases, the open circuit potential of the disk will shift depending on the controlling electrochemical processes, being either the anodic (e.g., the dissolution of the metal) or the cathodic reaction (e.g., the reduction of hydrogen ions or protons and/or dissolved oxygen).

- The relative position of worn and unworn areas. As a result of the galvanic coupling, a current is flowing between anodic and cathodic areas. The ohmic drop in the test solution may induce a non-uniform distribution of potential and current density over the disc surface. The measured open circuit potential is thus an average value depending on that distribution.

- The mechanism and kinetics of the anodic and cathodic reactions in worn and unworn areas.

A.16.2. Electrochemical impedance measurements (EIS)

The Electrochemical Impedance Spectroscopy (EIS) is the most adequate method for a detailed analysis of electrochemical reactions mechanisms and kinetics. The measurement of the electrochemical impedance is made by superposing a

sinusoidal voltage signal with a very small amplitude (5-10 mV) to the open circuit potential (alternating current technique). This has the advantage of generating only a negligible perturbation of the electrochemical steady state of the tested material. Impedance diagrams give data on the elementary steps occurring in an electrochemical reaction and on their kinetics. The analysis of these diagrams allows a thorough study of the role of intermediate species adsorbed on the surface and of reaction mechanism, as well as a study of the properties of passive films. EIS measurements can be implemented under stationary electrochemical conditions, after and before the sliding process when the electrochemical state of the sample has been stabilized (method followed in chapter 6.2 and 6.3), and when a continuous sliding is applied on the surface of the tested material (method followed in chapter 6.2).

The controlling computer system measures the magnitude of the current induced by the potential and in addition the phase angle between the potential and current.

EIS data is commonly analyzed by fitting it to an equivalent electrical circuit model. By means of these equivalent circuits, the R_p (polarization resistance) can be obtained.

A.17. Confocal microscope

Confocal microscopy (Fig. 9.17) is an optical imaging technique used to increase optical resolution and contrast of a micrograph by using point illumination and a spatial pinhole to eliminate out-of-focus light in specimens that are thicker than the focal plane. It enables the reconstruction of three-dimensional structures from the obtained images (Fig.9.18).

Fig. A.17. Nikon Eclipse ME600 Confocal Microscopy

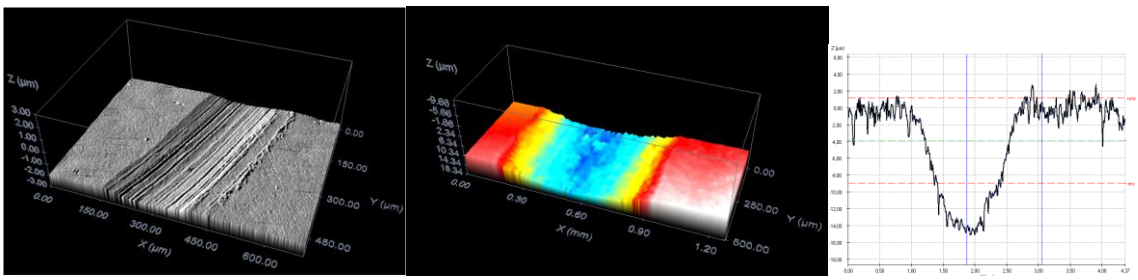

Fig. A.18. Images of topography (left and middle) and wear profile (right)

This microscope has been used to calculate the total volume loss due to tribocorrosion tests. For that, it was measured in different parts the width and the depth of the wear tracks in order to estimate the worn area (S). With the length of the track (L), and following the next equation, the total volume loss was obtained:

$$W_{tr} = S.L$$

In the total tribocorrosion wear (W_{tr}) it is assuming that this value is the sum of the material loss due to electrochemical effects (W^{c}_{act}) and material loss due to mechanical effects (W^{m}_{act}) in the wear track[5]. That is,

$$W^{m}_{act} = W_{tr} - W^{c}_{act}$$

The material loss due to electrochemical effects can be calculated by this

[5] Diomidis, N., Towards a standard test for the determination of synergism in tribocorrosion: Design of a protocol for passivating materials, in: Celis, J. P.; Ponthiaux, P. (Eds.), *Testing tribocorrosion of passivating materials supporting research and industrial innovation:*

expression:

$$W_{act}^{c} = i_{act} A_{act} \frac{M}{nFd} N t_{lat}$$

where,

i_{act} is the current density due to corrosion

A_{act} is the active area of the wear track

($A_{act}=2\pi(R_{ext}-R_{int})$)

M is the molecular weight

n is the number of electrons involved in the process

F is the Faraday constant (96485 C/mol)

d is the density of the sample[6, 7]

N is the number of cycles performed

t_{lat} is the period between two successive cycles or constant events (t_{lat}=1/frequency)

The current density due to corrosion (i_{act}) is obtained from equation:

$$i_{act}=B/r_{act}$$

where B is a constant which value for these tests is assumed as 24 mV, and r_{act} (specific polarization resistance of the active area) can be calculated from the following expression:

$$r_{act}=R_{act}.A_{act}$$

being R_{act} the polarization resistance in the active area of the track (A_{act}).

Taking into consideration that during tribocorrosion tests the exposed surface is divided in two differentiate areas, that is, the area of the wear track (A_{act}) and the area outside the wear track, the polarization resistance measured by EIS technique

Handbook. Manley Publishing, Leeds, UK, **2012**.
[6] Peng, Y.; Miao, H.; Peng, Z., *Int J Refract Met H.* **2013**, 39, 78-89.
[7] Sun, Y.; Lu, C.; Yu, H.; Tieu, A. K.; Su, L.; Zhao, Y.; Zhu, H.; Kong, C., *Mat Sci Eng A.* **2015**, 625, 56-64.

during sliding process (R_{ps}) is in fact the combination of two polarization resistances connected in parallel (applicable to chapter 6.2). The first one is related to the area of the wear track (R_{act}) and the second one, named R_{pass}, is related to the passive area outside the wear track (A_0-A_{act}). Being A_0 the total exposed area (2.5 cm^2).

In this way, the polarization resistance measured during the sliding process can be describes as:

$$\frac{1}{R_{ps}}=\frac{1}{R_{act}}+\frac{1}{R_{pass}}$$

From impedance measurements before sliding, it is possible to calculate r_p (specific polatization resistance of passive surface), where:

$$r_p=R_p.A_0$$

being R_p the polarization resistance and obtained from experimental data simulation. With this last parameter, it is possible to estimate the value of the polarization resistance of the passive area outside the wear track when sliding takes place (R_{pass}). In this sense, R_{pass} can be expressed as:

$$R_{pass}=\frac{r_p}{A_0-A_{act}}$$

Then, Rpass and Rps parameters are obtained directly from the impedance data analysis before and during sliding. After determination of these two values, the Ract parameter can be estimated by means of the following equation:

$$R_{act}=\frac{R_{ps}R_{pass}}{R_{pass}-R_{ps}}$$

Once the R_{act} is know, i_{act} can be estimated and used to calculate the material loss due to corrosion effects (W^c_{act}).

A.18. Bacterial adhesion study

Bacterial adhesion study was carried out in two steps:

A.18.1. Staphylococcal adhesion experiments

Staphylococcal adhesion experiments were performed as described by Kinnari et

al.[8] and Perez-Tanoira et al.[9]. For the preliminary study of bacterial adhesion, the biofilm-forming collection strains *S. aureus* 15981[10], *S. epidermidis* ATCC 35984 and 6 clinical strain from *S. aureus* (p1...p6) and 6 other of *S. epidermidis* (p7...p12), isolated from patients with implant-related infection by sonication[11] were used. All strains were cultured overnight in tryptic soy broth (bioMérieux, Marcy l'Etoile, France) at 37 ºC in 5% CO_2 atmosphere. It is worth mentioning that all patients were diagnosed articular infection based on clinical criteria[12]. The clinical Staphylococcus strains are positive for biofilm development[13].

After culture, bacteria were harvested by 10 minutes centrifugation at 3500 g at room temperature. Supernatant was discarded and the pellet was washed three times with sterile phosphate buffered saline (PBS). Bacteria were then suspended and diluted in PBS to 10^8 colony-forming units (CFU)/ml. The biomaterial discs were placed in the bacterial suspension and incubated for 90 min at 37 ºC. Afterwards, the biomaterial plates were rinsed three times with sterile PBS to remove any non-adherent bacteria[8].

The dried plates were stained for 15 min with a rapid fluorescence staining method using the Live/Dead® Bacterial Viability Kit (BacklightTM)[14]. On each plate, 8 fields were viewed and photographed with a Nikon Coolpix 8400 (Nikon, Melville, NY) under a fluorescence microscope at 40x magnification. All experiments were performed in triplicate. The number of microphotographs studied was 24 for each material and bacterium. The surface area covered with adhered bacteria was calculated using the ImageJ software (National Institute of Health, Bethesda, MD).

A.18.2. Statistical analysis

For the statistical study, Mann-Whitney or Wilcoxon non parametric tests were

[8] Kinnari, T. J.; Soininen, A.; Esteban, J.; Zamora, N.; Alakoski, E.; Kouri, V. P.; Lappalainen, R.; Konttinen, Y. T.; Gomez-Barrena, E.; Tiainen, V. M., *J Biomed Mater Res A.* **2008**, 86, 760-768.
[9] Perez-Jorge, C.; Conde, A.; Arenas, M. A.; Perez-Tanoira, R.; Matykina, E.; de Damborenea, J. J.; Gómez-Barrena, E.; Esteban, J., *J Biomed Mater Res A.* **2012**, 100, 1696-1705.
[10] Valle, J.; Toledo-Arana, A.; Berasain, C.; Ghigo, J. M.; Amorena, B.; Penadés, J. R; Lasa, I., *Mol Microbiol.* **2003**, 48, 1075-1087.
[11] Esteban, J.; Gomez-Barrena, E.; Cordero, J.; Martin-de-Hijas, N. Z.; Kinnari, T. J.; Fernandez-Roblas, R., *J Clin Microbiol.* **2008**, 46, 488-492.
[12] Cordero-Ampuero, J.; Esteban, J.; Garcia-Cimbrelo, E.; Munuera, L.; Escobar, R., *Acta Orthop.* **2007**, 78, 511-519.
[13] Esteban, J.; Molina-Manso, D.; Spiliopoulou, I.; Cordero-Ampuero, J.; Fernández-Roblas, R.; Foka, A.; Gómez-Barrena, E., *Acta Orthop.* **2010**, 81, 674-679.
[14] Boulos, L.; Prevost, M.; Barbeau, B.; Coallier, J.; Desjardins, R., *J Microbiol Methods.* **1999**, 37,

employed. These tests were used for two samples while the Kruskal-Wallis test was used for more than two samples. EPI-Info software version 3.5.1 (CDC, Atlanta, GA. USA) was used to perform the statistical studies.

77-89.

ANNEX B

Bibliography

"ASM Material Data Sheet". ASM. Web. 14 October 2015. http://asm.matweb.com/search/SpecificMaterial.asp?bassnum=MTP641.

Agulló-Rueda, F.; Serna, R., Métodos ópticos, in: Albella, J. M. (Ed.), *Láminas delgadas y recubrimientos: preparación, propiedades y aplicaciones*, CSIC, Madrid, Spain, **2003**.

Albella, J. M., Introducción: Ciencia y tecnología de capas delgadas, in: Albella, J. M. (Ed.), *Láminas delgadas y recubrimientos. Preparación, propiedades y aplicaciones*, CSIC, Madrid, **2003**.

Aliasghari, S.; Skeldon, P.; Thompson, G. E., *Appl Surf Sci*. **2014**, 316, 463-476.

Alsaran, A.; Purcek, G.; Hacisalihoglu, I.; Vangolu, Y.; Bayrak, O.; Karaman, I.; Celik, A., *Surf Coat Technol*. **2011**, 205, S537-S542.

An, Y. H.; Friedman, R. J., *J Biomed Mater Res*. **1998**, 43, 338-348.

Ando, Y.; Miyamoto, H.; Noda, I.; Sakurai, N.; Akiyama, T.; Yonekura, Y.; Shimazaki, T.; Miyazaki, M.; Mawatari, M.; Hotokebuchi, T., *Mater Sci Eng C*. **2010**, 30, 175-180.

Antunes, R. A.; Rodas, A. C. D.; Lima, N. B.; Higa, O. Z.; Costa, I., *Surf Coat Technol*. **2010**, 205, 2074-2081.

Application note 17: influence of topography and wettability on biocompatibility. ‹ http://www.biolinscientific.com/zafepress.php?url=%2Fpdf%2FAttension%2FApplication%20Notes%2FAT_AN_17_roughbio.pdf›.

Arena, M. A.; Pérez-Jorge, C.; Conde, A.; Matykina, E.; Hernández-López, J. M.; Pérez-Tanoira, R.; de Damborenea, J. J.; Gómez-Barrena, E.; Esteban, J., *Colloid Surface B*. **2013**, 105, 106-112.

Arrabal, R.; Matykina, E.; Hashimoto, T.; Skeldon, P.; Thompson, G. E., *Surf Coat Technol*. **2009**, 203, 2207-2220.

Arslan, E.; Totik, Y.; Efeoglu, I., *Prog Org Coat*. **2012**, 74, 768-771.

ASTM G40-13, Standard Terminology Relating to Wear and Erosion.

Atiyeh, B. S.; Costagliola, M.; Hayek, S. N.; Dibo, S. A., *Burns*. **2007**, 33, 139-148.

Azzi, M.; Klemberg-Sapieha, J. E., Tribocorrosion test protocols for sliding contacts, in: Landolt, D.; Mischler, S. (Eds.), *Tribocorrosion of Passive Metals and Coatings*, Woodhead Publishing Limited, Oxford, UK, **2011**.

Baba, K.; Hatada, R.; Flege, S.; Ensinger, W.; Shibata, Y.; Nakashima, J.; Sawase, T.; Morimura, T., *Vacuum*. **2013**, 89, 179-184.

Bania, P. J., Beta titanium alloys and their role in the titanium industry, in: Eylon, D.; Boyer, R. R.; Koss, D. A. (Eds), *Beta Titanium Alloys in the 1990´s*, The Minerals, Metals and Materials Society: Warrendale, Pennsylvania, USA, **1999**.

Basle, M. F.; Chappard, D.; Grizon, F.; Filmon, R.; Delecrin, J.; Daculsi, G.; Rebel, A., *Calcified Tissue Int*. **1993**, 53, 348-356.

Bayón, R., Corrosion-wear behaviour of novel surface coatings developed by means of advanced techniques. Doctoral thesis. University of Basque Country, **2011**.

Bendavid, A.; Martin, P. J.; Comte, C.; Preston, E. W.; Haq, A. J.; Magdon Ismail, F. S.; Singh, R. K., *Diam Relat Mater*. **2007**, 16, 1616-1622.

Bhushan, B.; Gupta, B. K., *Handbook of Tribology: Materials, coatings, and surface treatments*, McGraw-Hill, New York, USA, **1991**.

Billi, F.; Sangiorgio, S. N.; Aust, S.; Ebramzadeh, E., *J Biomech*. **2010**, 43, 1310-1315.

Black, J., *Orthopaedic Biomaterials in Research and Practice*, Churchill Livingstone, New York, USA, 1988.

Black, J.; Hastings, G. W., *Handbook of biomaterials propertie*, Champan and Hall, London, UK, **1998**.

Bociaga, D.; Komorowski, P.; Batory, D.; Szymanski, W.; Olejnik, A.; Jastrzebski, K.; Jakubowski, W., *Appl Surf Sci*. **2015**, 355, 388-397.

Boulos, L.; Prevost, M.; Barbeau, B.; Coallier, J.; Desjardins, R., *J Microbiol Methods*. **1999**, 37, 77-89.

Brodner, W.; Bitzan, P.; Meisinger, V.; Kaider, A.; Gottsauner-wolf, F.; Kotz, R., *J Bone Joint Surg*. **1997**, 79, 316-321.

Buser, D.; Nydegger, T.; Oxland, T.; Cochran, D. L.; Schenk, R. K.; Hirt, H. P.; Snetivy, D.; Nolte, L. P., *J Biomed Mater Res.* **1999**, 45, 75-83.

Canteli, J. A.; Cantero, J. L.; Marín, N. C.; Gómez, B.; Gordo, E.; Miguélez, M. H., *J Mater ProcessTechnol.* **2010**, 210, 122-128.

Carapeto, A. P.; Serro, A. P.; Nunes, B. M. F.; Martins, M. C. L.; Todorovic, S.; Duarte, M. T.; André, V.; Colaço, R.; Saramago, B., *Surf Coat Tech.* **2010**, 204, 3451-3458.

Carlsson, L. V.; Macdonald, W.; Magnus Jacobsson, C.; Albrektsson, T., Osseointegration Principles in Orthopedics: Basic Research and Clinical Applications, in: Yaszemski, M. J.; Trantolo, D. J.; Lewandrowski K-U.; Hasirci, V.; Altobelli D. E.; Wise, D. L. (Eds.), *Biomaterials in Orthopedics*, Marcel Dekker, New York, USA, **2004**.

Celis, J. P.; Ponthiaux, P., *Testing tribocorrosion of passivating materials supporting research and industrial innovation: Handbook EPC 62 Green Book*. Publishing Manley, London, UK, **2012**.

Chandra, A.; Ryu, J. J.; Karra, P.; Shrotriya, P.; Tvergaard, V.; Gaisser, M.; Weik, T., *J Mech Behav Biomed.* **2011**, 4, 1990-2001.

Chen, R.; Tu, J. P.; Liu, D. G.; Mai, Y. J.; Gu, C. D., *Surf Coat Technol.* **2011**,205, 5228-5234.

Cheng, Y. H.; Browne, T.; Heckerman, B.; Meletis, E. I., *Surf Coat Technol.* **2011**, 205, 4024-4029.

Cheng, Y. H.; Tay, B. K.; Lau, S. P.; Kupfer, H.; Richter, F., *J Appl Phys.* **2002**, 92, 1845-1949.

Cheng, Y.; Zheng, Y.F., *Surf Coat Technol.* **2006**, 200, 4543-4548.

Clark, R. K., *Anatomy and Physiology: Understanding the Human Body*, Jones and Bartlett Learning, Burlington, USA, **2005**.

Clavijo, D.; Orjuela, J.; Cardozo, C.; Torrado, A.; Covarrubias, A., *Rev Col Or Tra.* **2010**, 24, 168-177.

Collings, E. W., The physical metallurgy of titanium alloys, in: Gegel, H. L. (Ed), *ASM*

Series in Metal Processing, Edward Arnold Publications, Cleveland, Metal Park, OH, USA, **1984**.

Contu, F.; Elsener, B.; Böhni, H., *Electrochim Acta*, **2004**, 50, 33-41.

Cordero, J.; Munuera, L.; Folgueira, M. D., *Injury*. **1996**, 27, SC34-7.

Cordero-Ampuero, J.; Esteban, J.; Garcia-Cimbrelo, E.; Munuera, L.; Escobar, R., *Acta Orthop*. **2007**, 78, 511-519.

Cozza, R. C., *Surf Coat Technol*. **2013**, 215, 224-233.

Currier, J. H.; Bill, M. A.; Mayor, M. B., *J Biomech*. **2005**, 38, 367-375.

Czenuszka, J., *Mater World*. **1996**, 4, 452-453.

Dalmiglio, M.; Schaaff, P.; Holzwarth, V.; Chiesa, R.; Rondelli, G.; *J Biomed Mater Res A*. **2008**, 86B, 407-416.

Dearnaley, G.; Arps, J. H., *Surf Coat Tech*. **2005**, 200, 2518-2524.

Dee, K. C.; Puleo, D. A.; Bizios, R. P., Protein-surface interactions, in: Dee, K. C.; Puleo, D. A.; Bizios, R. P. (Eds.), *An introduction to tissue-biomaterial interactions*, John Wiley and Sons, Hoboken, NJ, USA, **2002**.

Deng, B.; Tao, Y.; Guo, D., *Appl Surf Sci*. **2012**, 258, 9080-9086.

Diomidis, N., Towards a standard test for the determination of synergism in tribocorrosion: Design of a protocol for passivating materials, in: Celis, J. P.; Ponthiaux, P. (Eds.), *Testing tribocorrosion of passivating materials supporting research and industrial innovation: Handbook*. Manley Publishing, Leeds, UK, **2012**.

Diomidis, N.; Celis, J. P.; Ponthiaux, P.; Wenger, F., *Wear*. **2010**, 269, 93-103.

Diomidis, N.; Mischler, S., *Tribol Int*. **2011**, 44, 1452-1460.

Diomidis, N.; Mischler, S.; More, N. S.; Manish, R., *Acta Biomater*. **2012**, 8, 852-859.

Dowling, D. P., *Diam Relat Mater*. **1997**, 6, 390-393.

Dunstan, E.; Ladon, D.; Whittingham-Jones, P.; Carrington, R.; Briggs, T. W., *J Bone*

Joint Surg (Am). **2008**, 90,517-522.

Durdu, S.; Usta, M., *Ceram Int*. **2014**, 40, 3627-3635.

Edwards, C.; Counsell, A.; Boulton, C.; Moran, C. G., *J Bone Joint Surg Br*. **2008**, 90, 770-777.

Elek, S. D.; Conen, P. E., *Br J Exp Pathol*. **1957**, 38, 573-586.

Eriksson, C.; Lausmaa, J.; Nygren, H., *Biomaterials*. **2001**, 22, 1987–1996.

Erturk, E.; Knotek, O.; Burgmer, W.; Prengel, H.G.; Heuvel, H.J.; Dederichs, H.G.; Stossel, C., *Surf Coat Technol*. **1991**, 46, 39-46.

Esteban, J.; Gomez-Barrena, E.; Cordero, J.; Martin-de-Hijas, N. Z.; Kinnari, T. J.; Fernandez-Roblas, R., *J Clin Microbiol*. **2008**, 46, 488-492.

Esteban, J.; Molina-Manso, D.; Spiliopoulou, I.; Cordero-Ampuero, J.; Fernández-Roblas, R.; Foka, A.; Gómez-Barrena, E., *Acta Orthop*. **2010**, 81, 674-679.

Esteban, J.; Pérez-Tanoira, R.; Pérez-Jorge-Peremarch, C.; Gómez-Barrena, E., Bacterial adherence to biomaterials used in surgical procedures, in: Kon, K.; Rai, M., (Eds.), *Microbiology for Surgical Infections. Diagnosis, Prognosis and Treatment*. Elsevier, USA, **2014**.

Everitt, N. M.; Ding, J.; Bandak, G.; Shipway, P. H.; Leen, S. B.; Williams, E.J., *Wear*. **2009**, 267, 283-291.

Farhat, Z. N.; King, Y.; Northwood, D. O.; Alpas, A. T., *Mater Sci Eng A*. **1996**, 206, 302-308.

Fazel, M.; Salimijazi, H. R.; Golozar, M. A.; Garsivaz jazi, M. R., *Appl Sur Sci*. **2015**, 324, 751-756.

Feng, W.; Zhou, H.; Yang, S., *Mater Sci Eng, A*. **2012**, 527, 4767-4770.

Ferrari, A. C.; Rodil, S. E.; Robertson, J., *Phys Rev B*. **2003**, 67, 155306-155325.

Fontaine, J.; Donnet, C.; Erdemir, A., *Fundamentals of the Tribology of DLC Coatings*, Springer, Berlin, Germany, **2008**.

Fraczek, T.; Olejnik, M.; Tokarz, A., *Metalurgija*. **2009**, 48, 83-86.

Freese, H. L.; Volas, M. G.; Wood, J. R., Metallurgy and technological properties of titanium and titanium alloys, in: Brunette, D. M.; Tengvall, P.; Textor, M.; Thomsen, P. (Eds.), *Titanium in Medicine: Material Science, Surface Science, Engineering, Biological Responses, and Medical Applications*, Springer, Berlin, Germany, **2001**.

Fukui, H., *Surf Coat Tech*. **2004**, 187, 70-76.

Garner, J. S.; Jarvis, W. R.; Emori, T. G.; Horan, T. C.; Hughes, J. M., *Am J Infect Control*. **1988**, 16, 128-140.

Geetha, M.; Singh, A. K.; Asokamani, R.; Gogia, A. K., *Prog Mater Sci*. **2009**, 54, 397-425.

George, L.; Wayne, D. K., *Mater Lett*. **1998**, 35, 344-350.

Gil, F. J.; Ginebra, M. P.; Planell, J. A., *Biomecánica*. **1999**, 13, 73-78.

Goikoetxea, J.; Ruiz de Gopegui, U.; Garmendia, K.; Delgado, A., *Arc evaporator and method for operating the evaporator*: Patent number WO2010072850 A1. Fundación Tekniker, **2010**.

Goodman, S. B.; Gómez Barrena, E.; Takagi, M.; Konttinen, Y. T., *J Biomed Mater Res A*. **2008**, 90A, 603-618.

Goosen, J. H.; Kums, A. J.; Kollen, B. J.; Verheyen, C. C., *Arch Orthop Trauma Surg*. **2008**, 129, 1165-1169.

Gordon, O.; Vig Slenters, T.; Brunetto, P. S.; Villaruz, A. E.; Sturdevant, D. E.; Otto, M.; Landmann, R.; Fromm, K. M., *Antimicrob Agents Chemother*. **2010**, 54, 4208-4218.

Goriainov, V.; Cook, R.; Latham, J. M.; Dunlop, D. G.; Oreffo, R. O. C., *Acta Biomater*. **2014**, 10, 4043-4057.

Grill, A.; Patel, V., *Diam Relat Mater*. **1993**, 2, 1519-1524.

Grill, A.; Patel, V., *Diamond Film Technol*. **1992**, *2, 25-29.*

Grinnell, F.; *Int Rev Cytol*. **1978**, 53, 65-144.

Gristina, A.G., *Science*. **1987**, 237, 1588-1595.

Guggenbichler, J.P.; Assadian, O.; Boeswald, M.; Kramer, A., Incidence and clinical implication of nosocomial infections associated with implantable biomaterials - catheters, ventilator-associated pneumonia, urinary tract infections. GMS Krankenhhyg Interdiszip. 6, Doc18, 2011.

Guoqing, L., *Thin Solid Films*. **2005**, 475, 279-282.

Hailer, N. P.; Garellick, G.; Kärrholm, J., *Acta Orthop*. **2010**, 81, 34-41.

Hallab, N. J.; Urban, R. M.; Jacobs, J. J., Corrosion and Biocompatibility of Orthopedic Implants, in: Yaszemski, M. J.; Trantolo, D. J.; Lewandrowski K-U.; Hasirci, V.; Altobelli D. E.; Wise, D. L. (Eds.), *Biomaterials in Orthopedics,* Marcel Dekker, New York, USA, **2004**.

Hallab, N.; Jacobs, J. J.; Black, J., *Biomaterials*. **2000**, 21, 1301-1314.

Han, I.; Choi, J. H.; Zhao, B. H.; Baik, H. K.; Lee, I., *Curr Appl Phys*, **2007**, 7S1, 23–27.

Han, Y.; Hong, S. H.; Xu, K. W., *Surf Coat Tec*. **2002**, 154, 314–318.

Harris, L. G.; Richards, R. G., *Injury*. **2006**, 37, S3-14.

Hauert, R., *Diamond Relat Mater*. **2003**, 12, 583-589.

Hauert, R.; Knoblauch-Meyer, L.; Francz, G.; Schroeder, A.; Wintermantel, E., *Surf Coat Technol*. **1999**, 120-121, 291-296.

Hodgson, A. W. E.; Mueller, Y.; Forster, D.; Virtanen, S., *Electrochim Acta*. **2002**, 47, 1913-1923.

Horbett, T. A., The role of adsorbed proteins in tissue response to biomaterials, in: Ratner, B. D.; Hoffman, A. S.; Schoen, F.J.; Lemons, J. E. (Eds.), *Biomaterials science*, Elsevier Academic Press, San Diego, USA, **2004**.

Hsieh, J. H.; Tan, A. L. K.; Zeng, X. T., *Surf Coat Technol*. **2006**, 201, 4094-4098.

http://www.doitpoms.ac.uk/tlplib/bones/structure.php.

http://www.hss.edu/conditions_arthritis-of-the-knee-total-knee-replacement.asp.

https://www.hss.edu/conditions_understanding-implants-in-knee-and-hip-replacement.asp.

Hussein, R. O.; Nie, X.; Northwood, D. O.; Yerokhin, A.; Matthews, A., *J Phys D: Appl Phys*. **2010**, 43, 105203-105216.

Iwabuchi, A.; Lee, J. W.; Uchidate, M., *Wear*. **2007**, 236, 492-500.

Jacobs, J. J.; Gilbert, J. L.; Urban, R. M., *J Bone Joint Surg [Am]*. **1998**, 80, 268-282.

Jacobs, J. J.; Goodman, S. B.; Sumner, D. R.; Hallab, N. J., Biologic response to orthopaedic implants, in: Buckwalter, J. A.; Einhorn, T. A.; Simon, S. R. (Eds.), *Orthopaedic Basic Science*, Rosemont, IL, American Academy of Orthopaedic Surgeons, **2000**.

Jämsen, E.; Furnes, O.; Engesaeter, L. B.; Konttinen, Y. T.; Odgaard, A.; Stefánsdóttir, A.; Lidgren L., *Acta Orhtop*. **2010**, 81, 660-666.

Jaspard-Mécuson, F.; Czerwiec, T.; Henrion, G.; Belmonte, T.; Dujardin, L.; Viola, A.; Beauvir, J., *Surf Coat Technol*. **2007**, 201, 8677-8682.

Junker, R.; Dimakis, A.; Thoneick, M.; Jansen, *J. A., Clin Oral Implan Res*. **2009**, 20, 185-206.

Kaestner, P.; Olfe, J.; He, J. W.; Rie, K-T., *Surf Coat Tech*. **2001**, 142-144, 928-933.

Kaplan, F. S.; Hayes, W.; Keaveny, T.; Boskey, A.; Einhorn, T.; Iannotti, J., Forma y función del hueso., in: Simon, S. R. (Ed.), *Ciencias básicas en ortopedia*, America Academy of Orthopaedic Surgeons, 135-191, **1997**.

Katsikogianni, M.; Missirlis, Y. F., *Eur Cell Mater*. **2004**, 8, 37-57.

Keller, J. C.; Stanford, C. M.; Wightman, J. P.; Draughn, R. A.; Zaharias, R., *J Biomed Mater Res*. **1994**, 28, 939–946.

Khorasanian, M.; Dehghan, A.; Shariat, M. H.; Bahrololoom, M. E.; Javadpour, S., Surf *Coat Technol*. **2011**, 206, 1459-1502.

Kieswetter, K.; Schwartz, Z.; Dean, D. D.; Boyan, B. D., *Crit Rev Oral Biol Med*. **1996**, 7, 329–345.

Kim, H. J.; Kim, S. H.; Kim, M. S.; Lee, E. J.; Oh, H. G.; Oh, W. M.; Park, S. W.; Kim, W. J.; Lee, G. J.; Choi, N. G.; Koh, J. T.; Dinh, D. B.; Hardin, R. R.; Johnson, K.; Sylvia, V. L.; Schmitz, J. P.; Dean. D. D., *J Biomed Mater Res A.* **2005**, 74, 366-373.

Kinnari, T. J.; Soininen, A.; Esteban, J.; Zamora, N.; Alakoski, E.; Kouri, V. P.; Lappalainen, R.; Konttinen, Y. T.; Gomez-Barrena, E.; Tiainen, V. M., *J Biomed Mater Res A.* **2008**, 86, 760-768.

Klein, J., *Science.* **2009**, 323, 47-48.

Klein, M. V.; Holy, J. A.; Williams, W. S., *Phys Rev B.* **1978**, 17, 1546-1556.

Knetsch, M. L. W.; Koole, L. H., *Polymers.* **2011**, 3, 340-366.

Kokubo, T.; Kim, H. M.; Miyaji, F.; Nakamura, T., *J Biomed Mater Res.* **1996**, 32, 409-417.

Korkusuz, P.; Korkusuz, F., Hard Tissue – Biomaterial Interactions, in: Yaszemski, M. J.; Trantolo, D. J.; Lewandrowski K-U.; Hasirci, V.; Altobelli D. E.; Wise, D. L. (Eds.), *Biomaterials in Orthopedics,* Marcel Dekker, New York, USA, **2004**.

Koskinen, J.; Hirvonen, J. P.; Levoska, J.; Torri, P., *Diam Relat Mater.* **1996**, 5, 669-673.

Kotharu, V.; Nagumothu, R.; Arumugam, C.B.; Veerappan, M.; Sankaran, S.; Davoodbasha, M. A.; Nooruddin, T., *Ceram Int.* **2012**, 38, 731-740.

Kulkarni, M.; Flasker, A.; Lokar, M.; Mrak-Poljsak, K.; Mazare, A.; Artenjak, A.; Cucnik, S.; Kralj, S.; Velikonja, A.; Schmuki, P.; Kralj-Iglic, V.; Sodin-Semrl, S.; Iglic, A., *Int J Nanomed.* **2015**, 10, 1359-1373.

Kulkarni, M.; Patil-Sen. Y.; Junkar, I.; Kulkarni, C. V.; Lorenzetti, M.; Iglic, A., *Colloid Surface B.* **2015**, 129, 47-53.

Kumar, S.; Sankara Narayanan, T. S. N.; Raman S, G. S.; Seshadri, S. K., *Mater Sci Eng C.* **2010**, 30, 921-927.

Kurtz, S.; Ong, K.; Jau, E.; Mowat F.; Halpem, M., *J Bone Joint Surg Am.* **2007**, 89, 780-785.

Kurze, P.; Dittrich, K. H.; Krysman, W.; Schneider, H. G., *Cryst Res Technol.* **1984**, 19,

93–99.

Kurze, P.; Krysman, W.; Dittrich, K. H.; Schneider, H. G., *Cryst Res Technol.* **1984**, 19, 973–979.

Kustas, F. M.; Misra, M. S., Friction and Wear of Titanium Alloys, in: Blau, P. J. (Ed.), *ASM Metals Handbook, Friction, Lubrication and Wear Technology*, ASM International, USA, **1992**.

Kuzyk, P. R. T.; Schemitsch, E. H., *Indian J Orthop.* **2011**, 45, 108-115.

Kyriacou, S. V.; Brownlow, W. J.; Xu, X. H., *Biochemistry.* **2004**, 43, 140-147.

Lampin, M.; Warocquier-Clerout, R.; Legris, C.; Degrange, M.; Sigot-Luizard, M. F., *J Biomed Mater Res.* **1997**, 36, 99-108.

Landolt, D., *Corrosion and Surface Chemistry of Metals*, EPFL Press, Lausanne, Switzerland, **2007**.

Landolt, D.; Mischler, S.; Stemp M.; Barril, S., *Wear*. **2004**, 256, 517-524.

Lawrence Katz, J., *Nature*. **1980**, 283, 106-107.

Letic-Gavrilovic, A.; Scandurra, R.; Abe, K., *Dent Mater J*. **2000**, 19, 99–132.

Li, L. H.; Kong, Y. M.; Kim, H. W.; Kim, Y. W.; Kim, H. E.; Heo, S. J.; Koak, J. Y., *Biomaterials*. **2004**, 25, 2867-2875.

Lim, Y. J.; Oshida, Y.; Andres, C. J.; Barco, M. T., *Int J Oral Maxillofac Implants*. **2001**, 16, 333–342.

Lin, N.; Huang, X.; Zhang, X.; Fan, A.; Qin, L.; Tang, B., *Appl Surf Sci*. **2012**, 258, 7047-7051.

Liu, C.; Leyland, A.; Bi, Q.; Matthews, A., *Surf Coat Tech*. **2011**, 414, 164-174.

Liu, F.; Wang, F.; Shimizu, T.; Igarashi, K.; Zhao, L., *Surf Coat Tech*. **2005**, 199, 220-224.

Liu, X.; Chu, P. K.; Ding, C., *Mater Sci Eng R*. **2004**, 47, 49-121.

Long, M.; Rack, H. J., *Biomaterials*. **2008**, 19, 1621-1639.

Loubet, J. L.; Georges, J. M.; Meille, G., Vickers indentation curves of elastoplastic materials, in: Blau, P. J.; Lawn, B. R. (Eds.), *Microindentation techniques in materials science and engineering, ASTM STP 889*, American Society for Testing and Materials, Philadelphia, **1986**.

Luo, Y., Biotribology of Titanium Alloys, in: Davim, P. (Ed), *Biotribology*, John Wiley & Sons, Inc, Hoboken, NJ, USA, **2013**.

Ma, G.; Gong, S.; Lin, G.; Zhang, L.; Sun, G., *Appl Surf Sci*. **2012**, 258, 3045-3050.

Mabbouxa, F.; Ponsinnetb, L.; Morriera, J.; Jaffrezicb, N.; Barsottia, O., *Colloid Surface B*. **2004**, 39, 199-205.

Magaziner, R. S.; Jain, V.K.; Mall, S., *Wear*. **2009**, 267, 368-373.

Malchau, H.; Herberts, P., Revision and re-revision rate in THR: a revisión-risk study in 148.359 primary operations. Scientific exhibition. 65th annual meeting of the AAOS, New-Orlands, USA, **1998**.

Mändl, S.; Rauschenbach, B., *Surf Coat Technol*. **2002**, 156, 276-283.

Manhabosco, T. M.; Tamborim, S. M.; dos Santos, C. B.; Müller, I. L., *Corros Sci*. **2011**, 53, 1786-1793.

Marciano, F. R.; Bonetti, L. F.; Mangolin, J. F.; Da-Silva, N. S.; Corat, E. J.; Trava-Airoldi, V. J., *Vacuum*. **2001**, 85, 662-666.

Martínez de Olcoz Sainz, L., Caracterización Física y Funcional de Recubrimientos en Capa Fina Depositados por PVD para Aplicaciones Avanzadas. Tesis doctoral. Universidad de Barcelona. **2014**.

Martinu, L.; Raveh, A.; Domingue, A.; Bertrand, L.; Klemberg-Sapieha, J. E.; Gujrathi, S. C.; Wertheimer, M. R., *Thin solid Films*. **1992**, 208, 42-47.

Matykina, E.; Berkani, A.; Skeldon, P.; Thompson, G. E., *Electrochim Acta*. **2007**, 53, 1987–1994.

Maxian, S. H.; Zawadasky, J. P.; Dunnj, M. G., *J Biomed Mater Res*. **1994**, 28, 1311-1319.

Media, O.; Nocua, J.; Mendoza, F.; Gómez-Moreno, R.; Ávalos, J.; Rodríguez, C.; Morell,

G., *Diam Relat Mater*. **2012**, 22, 77-81.

Mischler, S., *Tribol Int*. **2008**, 41, 573-583.

Mischler, S.; Ponthiaux, P., *Wear*. **2001**, 428, 211-225.

Montanaro, L.; Campoccia, D.; Arciola, C. R., *Int J Artif Organs*. **2008**, 31, 771-776.

Necula, B. S.; Apachitei, I.; Tichelaar, F. D.; Fratila-Apachitei, L. E.; Duszczyk, J.,*Acta Biomater*. **2011**, 7, 2751-2757.

Necula, B. S.; Fratila-Apachitei, L. E.; Zaat, S. A. J.; Apachitei, I.; Duszczyk, J., *Acta Biomater*. **2009**, 5, 3573-3580.

Necula, B. S.; van Leeuwen, J. P. T. M.; Fratila-Apachitei, L. E.; Zaat, S. A. J.; Apachitei, I.; Duszczyk, J., *Acta Biomater*. **2012**, 8, 4191-4197.

Neoh, K. G.; Hu, X.; Zheng, D.; Tang Kang, E., *Biomaterials*. **2012**, 33, 2813-2822.

Neupane, M. P.; Sankara, T. S. N.; Park, J. E.; Kim, Y. K.; Park, I. S.; Song, K. Y.; Bae, T. S.; Lee, H., *Worl Acad Sci Eng Technol*. **2012**, 6, 10-23.

Niinomi, M., *J Mech Behav Biomed*. **2008**, 1, 30-42.

Oliver, W. C., Pharr, G. M., *J Mater Res*. **1992**, 7, 1564-1583.

Österle, W.; Klaffke, D.; Griepentrog, M.; Gross, U.; Kranz, I.; Knabe, Ch., *Wear*. **2008**, 264, 505–517.

Pajarinen, J.; Mackiewiez, Z.; Pöllänen, R.; Takagi, M.; Epstein, N. J.; Ma, T.; Goodman, S. B.; Konttinen, Y. T., *J Biomed Mater Res*. **2010**, 92A, 1528-1537.

Pandit, H.; Glyn-Jones, S.; McLardy-Smith, P.; Gundle, R.; Whitwell, E.; Gibbons, C. L. M.; Ostlere, S.; Athanasou, N.; Gill, H. S.; Murray, D., *J Bone Joint Surg Br*. **2008**, 90, 847-851.

Park, B. J.; Bronzino J. D., *Biomaterials: Principles and Applications*, CRC Press, Boca Raton, Florida, USA, **2002**.

Park, S.; Woo, T. G.; Lee, M. H.; Ahn, S. G.; Park, M. S.; Bae, T. S.; Seol, K. W., *Metals Mater. Int*. **2006**, 12, 505-511.

Payling, R.; Michler, J.; Aeberhard, M., *Surf Interface Anal.* **2002**, 33, 472-477.

Peng, Y.; Miao, H.; Peng, Z., *Int J Refract Met H.* **2013**, 39, 78-89.

Perez-Jorge, C.; Conde, A.; Arenas, M. A.; Perez-Tanoira, R.; Matykina, E.; de Damborenea, J. J.; Gómez-Barrena, E.; Esteban, J., *J Biomed Mater Res A.* **2012**, 100, 1696-1705.

Perez-Tanoira, R.; Isea-Pena, M. C.; Celdran, A.; Garcia-Vasquez, C.; Esteban, J., *Surg Infect (Larchmt).* **2014**, 15, 90-93.

Perez-Tanoira, R.; Perez-Jorge, C.; Endrino, J. L.; Gomez-Barrena, E.; Horwat, D.; Pierson, J. F.; Esteban, J., *J Biomed Mater Res A.* **2012**, 100, 1521-1528.

Pérez-Tanoira, R.; Pérez-Jorge, C.; Endrino, J. L.; Gómez-Barrena, E.; Horwat, D.; Pierson, J. F.; Esteban, J., *J Biomed Mater Res A.* **2012**, 100, 4208-4218.

Pilliar, R.M., *Orthop Clin North Am.* **2005**, 36, 113-119.

Polmear, J. J., *"Titanium alloys", in Light Alloys*, Edward Arnold Publications, London, UK, **1981**.

Ponthiaux, P.; Bayón, R.; Wenger, F.; Celis, J. P., Testing protocol for the study of bio-tribocorrosion, in: Yan, Y. (Ed.), *Bio-tribocorrosion in Biomaterials and Medical Implants*, Woodhead Publishing Limited, Cambrigde, UK, **2013**.

Pouilleau, J.; Devilliers, D.; Garrido, F.; Durand-Vidal, S.; Mahe, E., *Mater Sci Eng.* **1997**, B47, 235–243.

Pretucci, R. H.; Hardwood, W. S., *Química General: Principios y aplicaciones modernas*, PRENTICE HALL IBERIA, Madrid, Spain, **1999**.

Prioli, R.; Zanette, S. I.; Caride, A. O.; Franceschini, D. F.; Freire Jr., F. L., *J Vac Sci Technol A.* **1996**, 14, 2351-2355.

Raman S, G. S.; Navaneethakrishnan, P.; Gnanamoorthy, R., *Proc Inst Mech Eng J J Eng Tribol.* **2009**, 223, 227-232.

Ratner, J. B. B. D.; Hoffman, A. S.; Shoen, F. J.; Lemons, J. E., *Biomaterials Science: An Introduction to Materials in Medicine*, Academic Press, Altham, MA, USA, **1996**.

Ravanetti, F.; Borghetti, P.; De Angelis, E.; Chiesa, R.; Martini, F. M.; Gabbi, C.; Cacchioli, A., *Acta Biomater.* **2010**, 6, 1014-1024.

Raveh, A.; Martinu, L.; Gujrathi, S. C.; Klemberg-Sapieha, J. E.; Wertheimer, M. R., *Surf Coat Tech.* **1992**, 53, 275-282.

Rochford, E. T.; Richards, R. G.; Moriarty, T. F., *Clin Microbiol Infect.* **2012**, 18, 1162-1167.

Rogers, S. D.; Howie, D. W.; Graves, S. E.; Pearcy, M. J.; Haynes, D. R., *J Bone Joint Surg.* **1997**, 79B, 311-315.

Ronkainen, H.; Holmberg, K., *Environmental and Thermal Effects on the Tribological Performance of DLC Coatings*, Springer, Berlin, Germany, **2008**.

Sáenz de Viteri, V.; Barandika, M. G.; Ruiz de Gopegui, U.; Bayón, R.; Zubizarreta, C.; Fernández, X.; Igartua, A.; Agullo-Rueda, F., *J Inorg Biochem.* **2012**, 117, 359-366.

Sánchez-López, J. C.; Abad, M. D.; Carvalho, I.; Escobar Galindo, R.; Benito, N.; Ribeiro, S.; Henriques, M.; Cavaleiro, A.; Carvalho, S., *Surf Coat Technol.* **2012**, 206, 2192-2198.

Santavirta, S.; Gristina, A.; Konttinen, Y. T., *Acta Orthop Scand.* **1992**, 63, 225-232.

Sargeant, A.; Goswami, T., *Mater Design.* **2007**, 28, 155-171.

Schneider, J. M.; Voevodin, A.; Rebholz, C.; Matthews, A.; Hogg, J. H. C.; Lewis, D. B.; Ives, M., *Surf Coat Technol.* **1995**, 74-75,312-319.

Schutz, R. W., An overview of beta titanium alloy environmental behavior, in: Eylon, D.; Boyer, R. R.; Koss, D. A. (Eds), *Beta Titanium Alloys in the 1990´s*, The Minerals, Metals and Materials Society: Warrendale, Pennsylvania, USA, **1999**.

Secinti, K. D.; Ozalp, H.; Attar, A.; Sargon, M. F., *J Clin Neurosci.* **2011**, 18, 391-395.

Segomotso, B.; Baozhy, T.; Feng, C.; Jinlong, Z., *Appl Surf Sci.* **2012**, 258, 3927-3935.

Shan, L.; Wang, Y.; Li, J.; Li, H.; Wu, X.; Chen, J., *Surf Coat Techno*l. **2013**, 226, 40-50.

Sharkey, P. F.; Hozack, W. J.; Rothman, R. H.; Shastri, S.; Jacoby, M., *Clin Orthop Relat*

R. **2001**, 404, 7-13.

Sheeja, D.; Tay, B. K.; Lau, S. P.; Nung, L. N., *Surf Coat Tech.* **2001**, 146-147, 410-416

Shin, K. R.; Kim, Y. S.; Yan, H. W.; Ko, Y.G.; Shin, D. H., *Appl Surf Sci.* **2014**, 314, 221-227.

Shirai, T.; Shimizu, T.; Ohtani, K.; Zen, Y.; Takaya, M.; Tsuchiya, H., *Acta Biomater.* **2011**, 7, 1928-1933.

Shokuhfar, M.; Dehghanian, C.; Montazeri, M.; Baradaran, A., *Appl Surf Sci.* **2012**, 258, 2416-2423.

Shtansky, D. V.; Levashov, E.A.; Glushankova, N. A.; D´yakonova, N. B.; Kulinich, S. A.; Petrzhik, M. I.; Kiryukhantsev-korneev, F. V.; Rossi, F., *Surf Coat Technol.* **2004**, 182, 101-11.

Singhai, M.; Malik, A.; Shahid, M.; Malik, M. A.; Goyal, R., *J Glob Infect Dis.* **2012**, 4, 193-198.

Sinnett-Jones, P. E.; Wharton, J. A.; Wood, R. J. K., *Wear*. **2005**, 59, 898-909.

Snyders, R.; Bousser, E.; Amireault, P.; Klemberg-Sapieha, J. E.; Park, E.; Taylor, K.; Casey, K.; Matinu, L., *Plasma Process Polym.* **2007**, 4, S640-S646.

Sollazzo, V.; Pezzetti, F.; Scarano, A.; Piattelli, A.; Massari, L.; Brunelli, G.; Carinci, F., *J Craniofac Surg*. **2007**, 18, 806-810.

Song, H. J.; Park, S. H.; Jeong, S. H.; Park, Y. J., *J Mater Process Technol.* **2009**, 209, 864-870.

Stadlinger, B.; Ferguson, S. J.; Eckelt, U.; Mai, R.; Lode, A. T.; Loukota, R.; Sclotting, F., *Brit J Oral Max Surg*. **2012**, 50, 74-79.

Stephenson, D. A.; Agapiou, J. S., *Metal Cutting Theory and Practice*, CRC Press, Taylor & Francis Group, Boca Raton, Florida, USA, **2006**.

Subramani, K.; Mathew, R. T., Titanium Surface Modification. Techniques for Dental Implants – From Microscale to Nanoscale, in: Subramani, K.; Ahmed, W. (Eds.), *Emerging Nanotechnologies in Dentistry: Materials, Processes and Applications*,

William Andrew, Elsevier, Oxford, UK, **2012**.

Sun, Y.; Lu, C.; Yu, H.; Tieu, A. K.; Su, L.; Zhao, Y.; Zhu, H.; Kong, C., *Mat Sci Eng A*. **2015**, 625, 56-64.

Sylvestre, M.; Zaidi, H.; Rivière, J.P.; Eyidi, D.; Doyen, F., *Surf Coat Tech*. **2010**, 205, 1374-1380.

Takadoum, J., *Corros Sci*. **1996**, 38, 643-654.

Takadoum, J.; Igartua, A., Phenomena of tribocorrosion in medical and industrial sectors, in: Celis, J. P.; Ponthiaus, P. (Ed.), *Testing tribocorrosion of passivating materials supporting research and industrial innovation: Handbook*. Maney Publishing, Leeds, UK, **2012**.

Takakubo, Y.; Berce, A.; Trebse, R.; Tamaki, Y.; Milosev, I.; Al- Samadi, A.; Tiainen, V.M.; Konttinen, Y. T., Wear and corrosion in the loosening of total joint replacements (TJRs), in: Yan, Y. (Ed.), *Bio-tribocorrosion in biomaterials and medical implants*, Woodhead Publishing Limited, Oxford, UK, **2013**.

Temenoff, J. S.; Mikos, A. G., *Biomaterials: The Intersection of Biology and Materials Science*, Pearson Prentice Hall, New Jersey, USA, **2008**.

Textor, M.; Freese, H. L.; Volas, M. G.; Wood, J. R., Titanium and its alloys in biomedical engineering, in: Buschow, K. H. J.; Cahn, R. W.; Flemings, M. C.; Ilscher, B.; Kramer, E. J.; Mahajan, S. (Eds.), *Encyclopedia of Materials: Science and Technology*, Elsevier, Oxford, UK, **2001**.

Uchida, M.; Kim, H. M.; Kokubo, T.; Fujibayashi S.; Nakamura, T., *J Biomed Mater Res*. **2003**, 64, 164-170.

Valle, J.; Toledo-Arana, A.; Berasain, C.; Ghigo, J. M.; Amorena, B.; Penadés, J. R; Lasa, I., *Mol Microbiol*. **2003**, 48, 1075-1087.

Vallet Regí, M., *Qué sabemos de?: Biomateriales*, Los libros de la CATARATA, Madrid, Spain, **2013**.

Vasilev, K.; Cook, J.; Griesser, H. J., *Expert Rev Med Devic*. **2009**, 6, 553-567.

Venkateswarlu, K.; Rameshbabu, N.; Sreekanth, D.; Bose, A. C.; Muthupandi, V.;

Subramanian, S., *Ceram Int.* **2013**, 39, 801-812.

Viceconti, M.; Muccini, R.; Bemakiewicz, M.; Baleani, M.; Cristofolini, L., *J Biomech.* **2000**, 33, 1611-1618.

Vieira, A. C.; Ribeiro, A. R.; Rocha, L. A.; Celis, J. P., *Wear*. **2006**, 261, 994-1001.

Vitu, T.; Escudeiro, A.; Polcar, T.; Cavaleiro, A., *Surf Coat Tech*. **2014**, 258, 734-745.

Vlacic-Zischke, J.; Hamlet, S. M.; Friis, T.; Tonetti, M. S.; Ivanovski, S., *Biomaterials*. **2011**, 32, 665-671.

Vogler, E. A., *Adv Colloid Interfac*. **1998**, 74, 69-117.

Wang, C. T.; Gao, N.; Gee, M. G.; Wood, R. J. K.; Langdon, T. G., *J Mech Behav Biomed Mater*. **2013**, 17, 166-175.

Wang, H. Y.; Zhu, R. F.; Lu, Y. P.; Xiao, G. Y.; Zhao, X. C.; He, K.; Yuan, Y. F.; Li, Y.; Ma, X. N., *Mat Sci Eng C*. **2014**, 42, 657-664.

Wang, H.; Liu, F.; Xiong, X.; Ke, S.; Zeng, X.; Lin, P., *Appl Surf Sci*. **2015**, 356, 1234-1243.

Wang, K., *Mat Sci Eng A-Struct*. **1996**, 213, 134-137.

Wang, P.; Hirose, M.; Suzuki, Y.; Adachi, K., *Surf Coat Tech*. **2013**, 221, 163-173.

Wang, Y.; Lei, T.; Jiang, B.; Guo, L., *Appl Surf Sci*. **2004**, 233, 258–267.

Wei, C.; Lin, J. F.; Jiang, T. H.; Ai, C. F., *Thin Solid Films*. **2001**, 381, 104-118.

Wendler, B.G.; Pawlak, W.; Achiev, J., *Mater Manuf Eng*. **2008**, 26, 207-210.

Wennerberg, A., On surface roughness and implant incorporation. Göteborg, Sweden: Biomaterials/Handicap Research; Doctoral thesis, Institute of Surgical Sciences, Göteborgs Universitet, 1996.

Williams, D. F., *Biomaterials*. **2008**, 29, 2941-2953.

Williams, D.F., Titanium and titanium alloys, in: Williams, D.F. (Ed.), *Biocompatibility of clinical implant materials*, CRC Press, Boca Raton, Florida, USA, **1981**.

Williams, J. M.; Bucharan, R. A., *Mater Sci Eng*. **1985**, 69, 237-246.

Williams, S.; Tipper, J. L.; Ingham, E.; Stone, M. H.; Fisher, J., *P I Mech Eng H*. **2003**, 217, 155-163.

Wolford, L. M., Factors to consider in joint prosthesis systems, Proc (Bayl Univ Med Cent). **2006**, 19, 232-238.

Xu, L. C.; Siedlecki, C. A., *Biomaterials*. **2007**, 28, 3273-3283.

Xuanyong, L.; Paul, K. C.; Chuanxian, D., *Mat Sci Eng R*. **2004**, 47, 49-121.

Yerokhin, A. L.; Nie, X.; Leyland, A.; Matthews, A.; Dowey, S. J., *Surf Coat Technol*. **1999**, 122, 73-93.

Yerokhin, A. L.; Niea, X.; Leyland, A.; Matthew, A., *Surf Coat Technol*. **2000**, 130, 195-206.

Yetim, A. F.; Celik, A.; Alsaran, A., *Surf Coat Tech*. **2010**, 205, 320-324.

Yildiz, F.; Yetim, A. F.; Alsaran, A.; Çelik, A., *Surf Coat Tech*.**2007**, 202, 2471-2476.

Zabinski, J. S.; Veovodin, A. A., Ceramic and other hard coatings, in: Vizintin, J.; Kalin, M.; Dohda, K.; Jahanmir, S. (Eds.), *Tribology of Mechanical Systems: A Guide to Present and Future Technologies*, ASME Press, New York, USA, **2004**.

Zhang, E.; Li, F.; Wang, H.; Liu, J.; Wang, C.; Li, M.; Yang, K., *Mat Sci Eng C*. **2013**, 33, 4280-4287.

Zhang, G.; Li, B.; Jiang, B.; Yan, F.; Chen, D., *Appl Surf Sci*. **2009**, 255, 8788-8793.

Zhang, L.; Lv, P.; Huang, Z. Y.; Lin, S. P.; Chen, D. H.; Pan, S. R.; Chen, M., *Diam Relat Mater*. **2008**, 17, 1922.1926.

Zhecheva, A.; Sha, W.; Malinov, S.; Long, A., *Surf Coat Tech*. **2005**, 200, 2192-2207.

Zheng, Y.; Liu, D.; Liu, X.; Li, L., *Biomed Mater*. **2008**, 3, 44103-44109.

Zhou, H.; Xu, L.; Ogino, A.; Nagatsu, M., *Diam Relat Mater*. **2008**, 17, 1416-1419.

Zhu, W.; Zhang, Z.; Gu, B.; Sun, J.; Zhu, L., *J Mater Sci Technol*. **2013**, 29, 237-244.

Zhu, X.; Chen, J.; Scheideler, L. R.; Reichl, R.; Geis-Gerstorfer, J., *Biomaterials*, **2004**, 25, 4087-4103.

Zhu, Y.; Wang, W.; Jia, X.; Akasaka, T.; Liao, S.; Watari, F., *Appl Surf Sci*. **2012**, 262, 15-158.

Zilberman, M.; Elsner, J. J., *J Control Release*. **2008**, 130, 202-215.

Zimmerli, W.; Trampuz, A.; Ochsner, P. E., *N Engl J Med*. **2004**, 351, 1645-1654.

ANNEX C

Publiscations and Dissamination

Contributions:

Sáenz de Viteri, V.; Igartua, A.; Fuentes, E.; Martinetti, R.; Tomppo, L.; Tikkanen, A. M.; Lappalainen, R., Comparative Testing of Bones and Hydroxyapatite Scaffolds. COST 533 – Materials for improved wear resistance of total artificial joints. **2008**, 1, 153-165.

Fuentes, E.; Sáenz de Viteri, V.; Igartua, A.; Martinetti, R.; Dolcini, L.; Barandika, G., Structural characterization and mechanical performance of Ca/P scaffolds and natural bones: a comparative study. *J Appl Biomater Biomech.* **2010**, 8, 159-165.

Sáenz de Viteri, V.; Barandika, M. G.; Ruiz de Gopegui, U.; Bayón, R.; Zubizarreta, C.; Fernández, X.; Igartua, A.; Agulló-Rueda, F., Characterization of Ti-C-N coating deposite don Ti6Al4V for biomedical applications. *J Inor Biochem.* **2012**, 117, 359-366.

Sáenz de Viteri, V.; Fuentes, E., Titanium and Titanium alloys as Biomaterials, in: Gegner, J. (Ed.), *Tribology – Fundamentals and advancements*, Intech, Rijeka, Croatia, **2013**, 155-181.

Alves, S. A.; Bayón, R.; Igartua, A.; Sáenz de Viteri, V.; Rocha, L. A., Tribocorrosion behavior of anodic titanium oxide films produced by plasma electrolytic oxidation for dental implants. *Lubrication Science.* **2014**, 26, 500-513.

Alves, S. A.; Bayón, R.; Sáenz de Viteri, V.; Garcia, M. P.; Igartua, A.; Fernandes, M. H.; Rocha, L. A., Tribocorrosion behavior of calcium- and phosphorous-Enriched titanium oxide films and study of osteoblast interactions for dental implants. *J Bio Tribo Corro.* **2015**, 1:23.

Sáenz de Viteri, V.; Barandika, G.; Bayón, R.; Fernández, X.; Ciarsolo, I.; Igartua, A.; Pérez Tanoira, R.; Esteban Moreno, J.; Pérez-Jorge Peremarch, C., Development of Ti-C-N coatings with improved tribological behavior and antibacterial properties. *J Mech Behav Biomed.* **2015**, *55, 75-86.*

Conference papers:

Sáenz de Viteri, V.; Igartua, A.; Fuentes, E.; Mendoza, G., Screeing of mechanical properties from inserts to bones. COST Workshop Biotribology, (Groningen, The Netherlands), **2008**.

Sáenz de Viteri, V.; Igartua, A.; Fuentes, E.; Tomppo, L.; Tikkanen, A. M.; Lappalainen, R., Martinetti, R.; Barandika, M. G., Ensayos comparativos de propiedades mecánicas cristalográficas y microestructurales de huesos e injertos de hidroxiapatita carbonatada. Reunión Bienal Plenaria de Química Inorgánica y Estado Sólido, (Almuñécar, Spain), **2008**.

Barandika, G.; Sáenz de Viteri, V.; Igartua, A.; Fuentes, E.; Tomppo, L.; Tikkanen, A. M.; Lappalainen, R., Martinetti, R., Caracterización de hidroxiapatitas sintéticas y de tejido óseo de origen animal: influencia de la cristalinidad y la porosidad en las propiedades físicas y mecánicas. Reunión Bienal Plenaria de Química Inorgánica y Estado Sólido, (Almuñécar, Spain), **2008**.

Barandika, G.; Sáenz de Viteri, V.; Igartua, A.; Fuentes, E.; Martinetti, R., Hidroxiapatitas porosas deficientes en Ca para injertos óseos: caracterización microestructural y propiedades de biocerámicas y materiales híbridos. Reunión Científica Bioinorgánica, (Mallorca, Spain), **2009**.

Sáenz de Viteri, V.; Igartua, A.; Fuentes, E.; Tomppo, L.; Tikkanen, A. M.; Lappalainen, R.; Barandika, G.; Martinetti, R., Structural, chemical and mechanical characterization of synthetic scaffolds. COST 533 Biotribology Workshop, (Guimaraes, Portugal), **2009**.

Sáenz de Viteri, V.; Bayón, R.; Ruiz de Gopegui, U.; Zubizarreta, C.; Fernández, X., Tribocorrosion response of PVD-TiCN coatings on Ti6Al4V for artificial joints. European Conference of Nano Films (ECNF), (Liège, Belgium), **2010**.

Sáenz de Viteri, V.; Bayón, R.; Ruiz de Gopegui, U.; Zubizarreta, C.; Fernández, X.; Barandika, M. G., Tribocorrosion response of PVD-TiCN coatings on Ti6Al4V for artificial joints. Bio-Coat 2010, (Zaragoza, Spain), **2010**.

Sáenz de Viteri, V.; Bayón, R.; Igartua, A.; Zubizarreta, C.; Fernández, X.; Barandika, M. G., Corrosion, tribocorrosion and tribological characterization of PEO coatings on

Ti6Al4V. VII International Materials Symposium MATERIAIS 2011, (Guimaraes, Portugal), **2011**.

Igartua, A.; Sáenz de Viteri, V.; Fuentes, E.; Bayón, R., Biomaterials for biomedical implants. 11th International Symposium on Applied Bioinorganic Chemistry, (Barcelona, Spain), **2011**.

Sáenz de Viteri, V.; Bayón, R.; Igartua. A.; Barandika, G., The effect of plasma electrolytic oxidation on titanium in the microstructure, tribocorrosion behavior and citotoxicity. World Tribology Congress 2013, (Torino, Italy), **2013**.

Sáenz de Viteri, V.; Barandika, G.; Igartua, A., Desarrollo de capas de TiO_2 mediante electro oxidación por plasma para aplicaciones médicas. VIII Reunión Científica de Bioinorgánica, (Burgos, Spain), **2013**.

Igartua, A.; Sáenz de Viteri, V.; Fuentes, E., Tribological response of the cotton textile against human skin equivalents. The International Istanbul Textile Congress 2013, (Istanbul, Turkey), **2013**.

Sáenz de Viteri, V.; Bayón, R.; Barandika, G.; Igartua, A., Tribocorrosion and antibacterial behavior of TiO_2 coatings obtained by PEO technique. MeMeA 2014, (Lisbon, Portugal), **2014**.

Journal of Inorganic Biochemistry 117 (2012) 359–366

Contents lists available at SciVerse ScienceDirect

Journal of Inorganic Biochemistry

journal homepage: www.elsevier.com/locate/jinorgbio

Characterization of Ti-C-N coatings deposited on Ti6Al4V for biomedical applications

V. Sáenz de Viteri [a,*], M.G. Barandika [b], U. Ruiz de Gopegui [a], R. Bayón [a], C. Zubizarreta [a], X. Fernández [a], A. Igartua [a], F. Agullo-Rueda [c]

[a] IK4-Tekniker, Polo Tecnológico de Eibar, Calle Iñaki Goenaga, 5, 20600, Eibar, Spain
[b] Departamento de Química Inorgánica, Facultad de Farmacia, UPV/EHU, Paseo de la Universidad 7, 01006, Vitoria, Spain
[c] Instituto de Ciencia de Materiales de Madrid (ICMM-CSIC), Calle Sor Juana Inés de la Cruz, 3, Cantoblanco, 28049, Madrid, Spain

ARTICLE INFO

Article history:
Received 15 March 2012
Received in revised form 7 September 2012
Accepted 7 September 2012
Available online 16 September 2012

Keywords:
Ti6Al4V
Biomaterials
Ti-C-N
Fretting
Friction coefficient

ABSTRACT

Ti6Al4V alloy is the most commonly employed implant material for orthopedic replacements due to its good mechanical properties close to those of bones, biocompatibility and its good corrosion resistance in biological media. Nevertheless, it does not exhibit good wear resistance, showing friction and wear even with soft tissues. This latter feature can lead to a premature failure of the implant with the subsequent component replacement. Therefore, a system with good tribological resistance is required for several medical applications. One possible alternative to solve tribological problems consists of protecting the alloy surface by means of biocompatible Ti-C-N coatings. In this work, five types of metallic Ti-C-N coatings deposited by physical vapor deposition (PVD) cathodic arc method on Ti6Al4V substrate have been studied. Different deposition conditions have been analyzed, and the superficial properties of films have been characterized. Additionally, tribological response of these films have been determined and compared with the substrate one under fretting conditions in simulated body fluid. The results indicate that Ti-C-N coatings improve the general response of the biomaterial.

1. Introduction

In total joint replacements, the purpose of the artificial components is to restore the functionality and smooth articulation between the bones [1]. Among all biomaterials, the Ti6Al4V alloy is one of the most used material because, in addition to its excellent biocompatibility, it exhibits low elastic modulus (comparable with that of human bone), good corrosion resistance, high specific strength, and fatigue resistance [2–5]. In general, the orthopedic bearing is manufactured from highly polished metal alloys with extreme precision that articulate against a metal material (CoCrMo or stainless steel), ceramic material or against a polymeric material, mainly ultra high molecular weight polyethylene (UHMWPE), in case of knee joints.

Major drawback of Ti alloys is their relative low load-carrying capacity and their poor tribological properties as high friction coefficient during dry sliding against numerous important technical materials [6]. In implants, one type of common wear mechanism that takes place on contacting surfaces is named fretting. It occurs when two surfaces are subjected to small amplitude reciprocating motion of micro order. This phenomenon generated by vibration can significantly reduce the contact mechanism life [7]. Moreover, as a result of wear, metallic ions are released with high facility to enter in the bloodstream, leading to inflammation of the surrounding tissues and give rise to bone resorption (osteolyse), causing pain and aseptic loosening of the prosthesis [8,9]. The wear causes the degradation of the surface with the consequent loss of accuracy and implant failure [10]. Avoiding the failure of the prosthesis is, therefore, one of the goals for these types of materials, and one of the possible approaches consists of minimizing the wear on the surface of the biomaterial. To this purpose, the enhancement of the surface hardness is desired as well as the reduction of the friction coefficient between contacting surfaces. Cathodic arc evaporation deposited gradient Ti-C-N coatings exhibiting good adhesion to the Ti6Al4V substrate, and serve as hard intermediate layers between the Ti substrate and the top hard amorphous carbon (a-C) layer. Ti-C-N films are an attractive biomedical material due to their high hardness, low friction coefficient, good chemical stability and excellent hemocompatibility [11–14]. Thus, Ti-C-N coatings are becoming a successful approach to the improvement of wear resistance of the implant [15]. The purpose of this work is to investigate the potential benefits of protecting the Ti6Al4V medical alloy by means of Ti-C-N coatings. Therefore, we herein present our first results, including significant chemical and structural information. To this purpose, a set of five coated samples has been deeply analyzed. In fact, microstructural characterization has been carried out by means of XRD (X-ray diffraction), SEM (scanning electron microscope), GD-OES (glow discharge optical emission spectroscopy) and RAMAN Spectroscopy techniques. Thickness, hardness, adhesion and roughness of coatings have also been measured. Concerning to the tribological study, fretting tests were conducted in

* Corresponding author. Tel.: +34 943 206 744; fax: +34 943 202 757.
E-mail address: vsaenzdeviteri@tekniker.es (V.S. de Viteri).

0162-0134/$ – see front matter © 2012 Elsevier Inc. All rights reserved.
http://dx.doi.org/10.1016/j.jinorgbio.2012.09.012

fetal bovine serum (FBS) environment reproducing the characteristics of the biological fluids.

2. Experimental

2.1. Materials

Ti6Al4V ELI (extra low interstitial) was selected to be used as substrate. The mechanical properties and composition meet the ASTM F136-02 standard specification for wrought Titanium-6Aluminum-4Vanadium ELI alloy for surgical implant applications (UNS R56401).

Discs of Ti6Al4V with dimensions of 24 mm of diameter and 7.9 mm of height were manufactured. They were mirror polished up to a final roughness of 0.05 μm.

2.2. Coating deposition process

Ti-C-N coatings were deposited by physical vapor deposition (PVD) technique using cathodic arc evaporation (CAE) method in the industrial equipment MIDAS 775 designed and manufactured by Tekniker [16]. This system has 12 circular evaporators of 100 mm, working intensity range of 60–200 A, and a 45 kW pulsed DC bias power supply system consisting of two MDX II DC and one SPARC-VS pulsing unit from Advanced Energy.

Prior the coating deposition process, the samples were sprayed with a solvent product, cleaned in an alkaline detergent by means of ultrasounds method and finally rinsed with distilled water and alcohol before drying with hot air. The substrates were wrapped with aluminum foil so as to prevent particles of dirt and dust coming from the air on the surface of the parts. After loading the discs, the vacuum chamber was evacuated up to a pressure of 10^{-4} mbar. Then, they were heated by means of infrared radiant heaters up to a substrate temperature of 500 °C. After the heating process, a cleanliness step named Glow Discharge was applied to the samples. This process consists of an electrical pulsed DC discharge to create plasma around the samples by using a gas mixture of argon and hydrogen at a pressure of between 0.4 and 0.8 mbar. To ensure the necessary adhesion for the coating a very thin pure titanium layer (around 1 μm thickness) was deposited. This step needs a very high bias voltage up to 1000 V to get very high energy ions bombardment to the substrate. This promotes the adhesion in three ways. First of all, the high-energy-ion bombardment cleans the very top layers of the substrate. Secondly, it is an ion implantation of titanium in the substrate, and finally it is the beginning of the coating. Then, the Ti-C-N coating was completed by adding the necessary reactive gases, nitrogen and acetylene, with a gas flow of between 50 and 200 sccm (standard cm^3/min at a pressure of 1 bar). During this step the pressure in the chamber was set value in the range of $2–8\times10^{-3}$ mbar and the flow of the gases was controlled with a mass flow controller from Bronkhorst High Tech. The arc intensity of the titanium target was set between 70 and 140 A and the bias voltage between 400 and 30 V. Therefore, coatings were carried out in two steps for obtaining in this way two layers. The first one was a pure metallic titanium layer that worked as a stress relaxing for a better adhesion of the Ti-C-N coating. The second was the Ti-C-N layer that provided wear and corrosion resistance to the coated system. In this way, five different samples were prepared (C1 to C5) by varying the parameters of the coating process. During the deposition process, the argon flow was constant for all the samples (200 sccm), and the nitrogen flow was 50 sccm for all of them, with the exception of C4, that did not have any. An arc intensity of 100 A was applied for all the samples, with the exception of C5 (for which an intensity of 75 A was applied). Different flows of C_2H_2 were also tried: 100 sccm for C1, 50 sccm for C2, and 200 sccm for C3, C4, and C5. Table 1 shows the deposition parameters of the coating process for all samples.

Table 1
Deposition parameters of the coating process.

Sample	Ar sccm	N_2 sccm	C_2H_2 sccm	I_{arc} A
C1	200	50	100	100
C2	200	50	50	100
C3	200	50	200	100
C4	200	–	200	100
C5	200	50	200	75

In joint replacements, in areas in which two artificial components are in contact and movement takes place, it is necessary to have a very smooth surface to prevent or minimize friction, and therefore wear. A polish treatment was applied on the surfaces of the coated samples using 1 μm polishing diamond cloths in order to prepare the surface for the characterization process. The final roughness was lower than 0.2 μm, before performing tribological tests.

2.3. Coatings characterization

Coatings thickness measurement was made with Calotest equipment from CSEM.

For hardness measurements, Fischer nanoindenter equipment with Vickers indentor was employed, using the method of Oliver and Pharr [17–19]. A final load of 5 mN was applied in 20 steps to determine the coatings hardness profile versus depth.

The profiles of composition in depth were analyzed with GD-OES equipment from Horiba Jobin Yvon. The measurement conditions used were 650 Pa and 35 W, with a copper anode of 4 mm of diameter [20]. For this characterization, coatings deposited on Ti6Al4V samples were employed.

The adhesion of the coating to the substrates was measured by means of a Rockwell test and for discussion of the results the evaluation system employed in the VDI 3198 indentation test standard was followed. This test uses a standard Rockwell hardness tester fitted with a Rockwell "C"-type diamond cone indenter with an applied load of 150 kg. The result is obtained by using an optical microscope and classifying the adhesion as HF 1 to HF 6 according to the level of cracking or coating delamination around the indent. Only indents classified as HF 1 and HF 2 correspond to adequate adhesion. This method provides results rapidly with a minimum of effort.

The roughness measurements were performed according to ISO 4287 and ISO 4288 standards specifications with Mahr Perthometer M2 equipment. Obtained values correspond to the roughness before the polishing process.

Raman spectra were obtained with a Renishaw Ramascope 2000 microspectrometer and an ion argon laser (emission wavelength 514.5 nm) as the excitation light source. A 100× microscope objective was used to focus the laser on the sample and to collect the scattered light. Laser power on the sample was about 3 mW.

X-ray powder diffraction data were collected on a PHILIPS PW1710 powder diffractometer with Cu-Kα radiation in steps of 0.02° over the 5–69.96° 2θ-angular range and a fixed-time counting of 1 s at 25 °C.

Table 2
Coatings characterization. Physical properties.

Sample	Thickness μm	Hardness GPa	Carbon content C_2H_2 sccm	Roughness μm	Adhesion HF
C1	2.00	7	100	0.36	HF 1
C2	2.40	10	50	0.36	HF 1
C3	3.28	3	200	0.40	HF 1
C4	3.05	22	200	0.60	HF 1
C5	3.86	8	200	0.42	HF 1

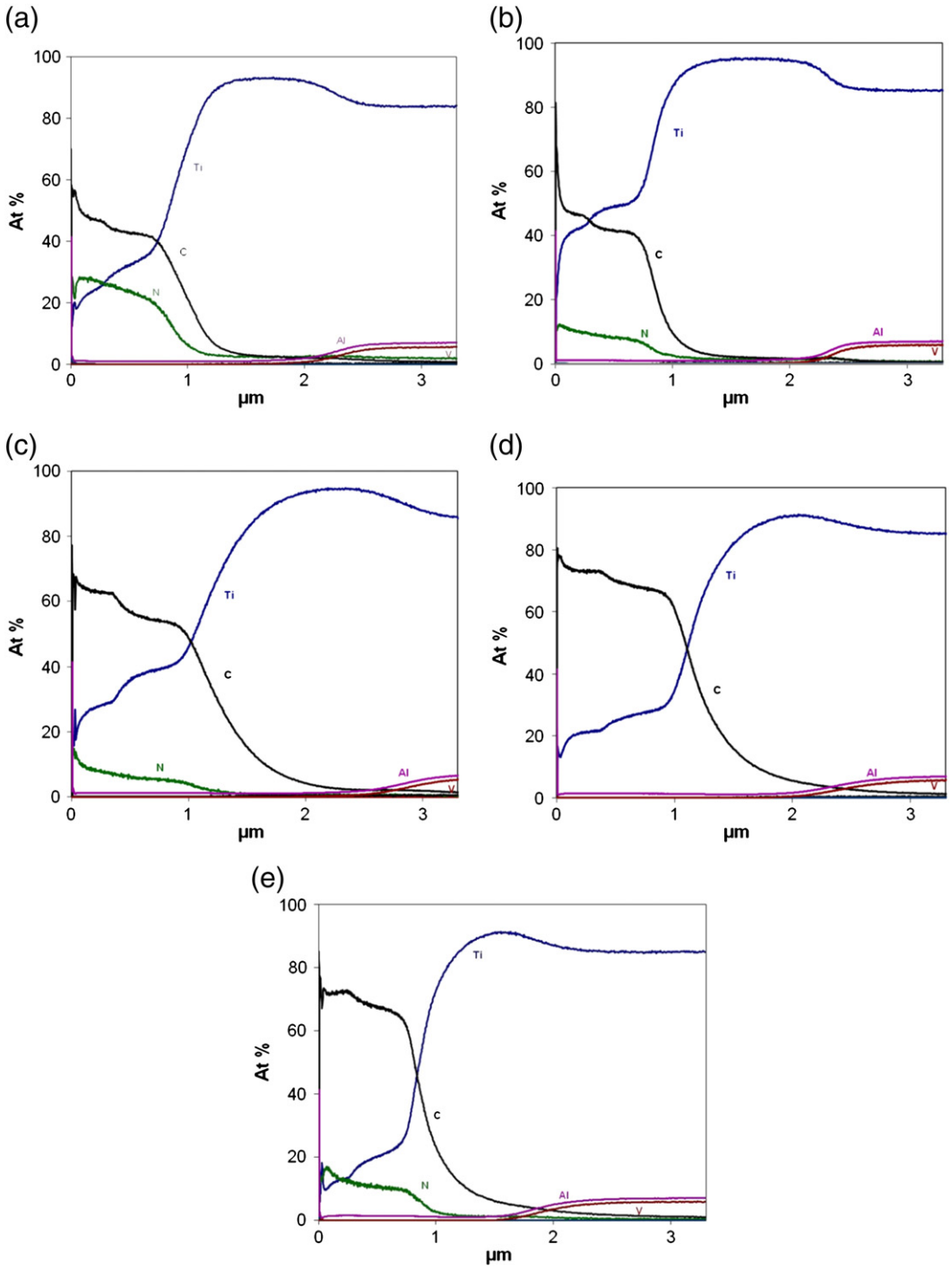

Fig. 1. Coating composition graphics obtained by GD-OES. a) C1, b) C2, c) C3, d) C4 and e) C5.

2.4. Fretting tests

For the fretting tests SRV tribometer with ball-on-disc configuration was selected. As counterbody balls of Al_2O_3 with a diameter of 10 mm were used. All tests were conducted at a load of 50 MPa, a frequency of 2 Hz (0.6 mm/s) and a stroke of 150 µm. Tests were carried out at 37 °C during 12 min (3 tests per sample). Tests were done under lubricated conditions by using fetal bovine serum (FBS) with sodium azide and EDTA, according to ASTM F732-00 standard. Friction and wear response of uncoated and Ti-C-N coated Ti6Al4V alloy were studied and compared.

3. Results and discussion

3.1. Chemical and structural characterization

Ti-C-N coatings developed had a thickness between 2.00 and 3.86 µm. The hardness values registered lie among the typical ones for this kind of coatings (up to 25 GPa) [21,22] and are displayed in Table 2. It must be pointed out that the highest hardness has been found for C4 (22 GPa) which does not present nitrogen. This could cause a higher sp^3/sp^2 fraction for the carbon that leads to a higher hardness values [23].

Almost all coatings show similar values of the roughness (higher than 0.3 μm), except the C4 in which is approximately twice. These high values of roughness are due to the droplets generated during arc deposition, promoting irregularities on the surface and increasing the roughness. Therefore, all samples should require post-deposition treatment for the rest of the characterization tests. Adhesion measurements indicated that, according to the Rockwell test, all the coatings are classified as HF 1. Therefore, all of them exhibit adequate adherence to the substrate (Table 2).

By means of GD-OES technique, the chemical composition profiles in depth are obtained (Fig. 1). It must be said that the profiles are accurate in thickness but they give us a qualitative idea of the progression in chemical composition. On the right of the graphs, the chemical composition of Ti6Al4V substrate can be seen, and afterwards an increase of the titanium concentration is appreciated due to the first titanium layer. The decrease of titanium accompanied by the presence of nitrogen and carbon indicates that the area corresponds to the Ti-C-N layer. In C3, C4 and C5 the increase of carbon observed is due to the increase of acetylene flow during the coating deposition process. This increase of carbon content, moreover, goes along with the increase of coating thickness, which can be verified with the measurement of thickness done by Calotest equipment, where C3, C4 and C5 are then samples exhibiting the highest thickness.

SEM micrographies of the transversal section of films deposited onto silicon wafer were taken (Fig. 2). All coatings showed pure titanium layer and Ti-C-N layer well defined. In all cases the coatings are dense. In the micrographies of C1, C2 and C5, a columnar growth of the layers can be seen. The presence of droplets embedded in the film while it grows can be also observed. This is due to the fact that for the study of the microstructure by the SEM, the samples were not previously polished.

3.2. Raman spectroscopy

The microstructure of the Ti-C-N coatings was analyzed with means of Raman spectroscopy (Fig. 3). The overall Raman intensity increases

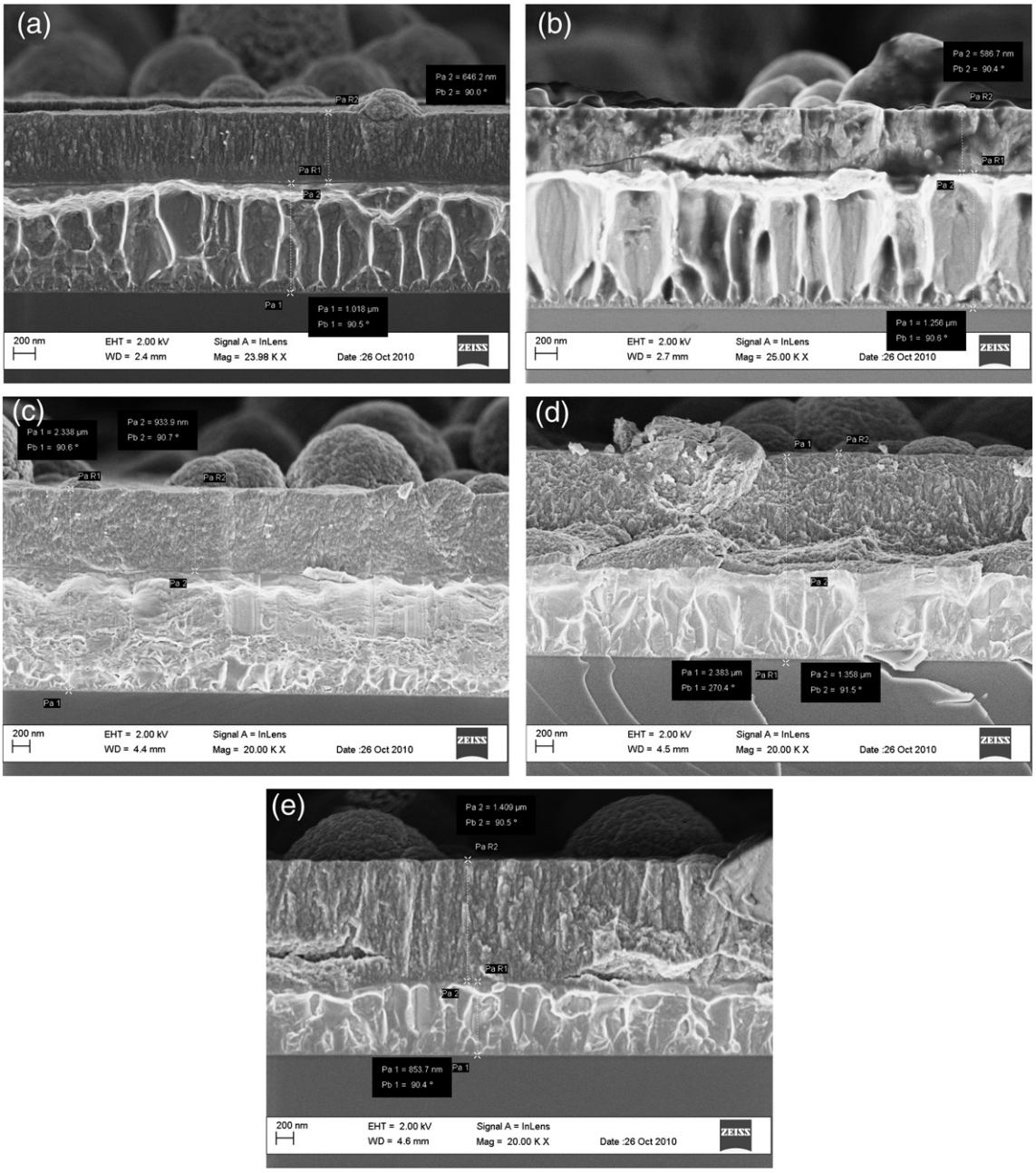

Fig. 2. SEM micrographies of coatings deposited on silicon substrate: a) C1, b) C2, c) C3, d) C4 and e) C5.

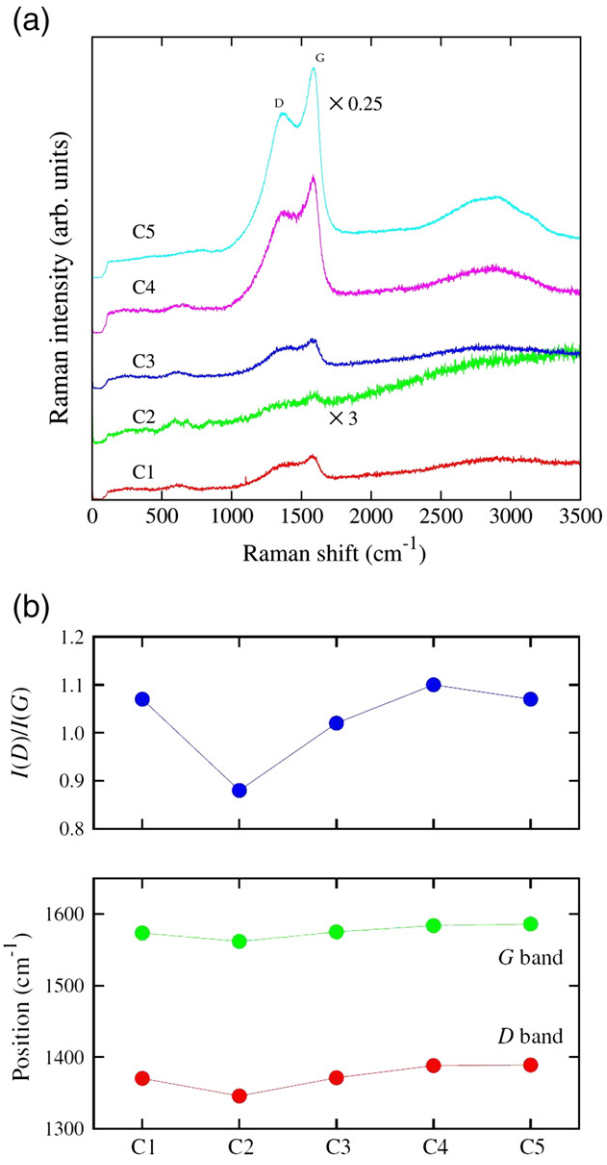

Fig. 3. a) Room temperature Raman spectra of the Ti-C-N samples (laser wavelength 514.5 nm). For clarity the intensity for C2 and C5 samples has been multiplied, respectively by 3 and 0.25, and spectra have been vertically offset. b) Plot of the I(D)/I(G) intensity ratio and the D and G band positions for the Ti-C-N samples as obtained from the fitting of the Raman spectra (Table 3).

with the coating thickness and decreases with the Ti concentration measured by GD-OES. The Raman spectra show two strong bands at about 1380 and 1580 cm^{-1}. These are, respectively, the D and G bands typical of graphitic and amorphous carbon materials. The *G* band corresponds to a stretching vibrational mode of sp^2 bonded carbon. The D band is associated to disorder, and is related to a breathing mode of carbon rings [24]. The spectra were fitted in this region to two Gaussians, and a linear background (see Fig. 3 and Table 3 for a summary of the parameters). The position of the G band depends on the microstructure, and the laser wavelength. In this case, where the laser wavelength is 514 nm, the observed frequency is compatible with a material between nanocrystalline graphite (nc-G) and amorphous carbon (a-C) with a low content of sp^2 carbon. The relative intensity of the D band provides an indication of the disorder on the sp^2 layers, and the sp^3 content. For these samples, $I(D)/I(G) \approx 1$, which corresponds to a sp^3/sp^2 fraction of around 10%. This also discards other carbon species like ta-C (tetrahedral amorphous carbon) that have a much weaker D band. The observed values of the G band Full Width at Half Maximum (FWHM) of about 110–140 cm^{-1} indicate that the average size of the sp^2 flakes is of the order of 1 nm, which is below the size expected for microstructured graphite. All these facts confirm that the material is in the so-called stage 2 (between nc-G and a-C) [24].

Although the Raman spectra look very similar for all samples, with the exception of the total intensity, the fitting shows that for sample C2 the I(D)/I(G) ratio is significantly smaller than for the other samples (see Fig. 3). For materials in stage 2, this decrease leads to the conclusion that the sample C2 has a larger sp^3/sp^2 fraction, thus explaining its elevated hardness (10 GPa). We also observe a decrease of the D and G band positions for sample C2. This shift for the D band could be related to the higher concentration of titanium or to a variation of residual stress due, for example, to the varying coating thickness.

The Raman spectra also show some weak bands in the range 200–800 cm^{-1}. They are related to the vibrational modes of TiC [25] and TiN [26] compounds. These bands therefore testify the alloying of the titanium with carbon atoms and titanium with nitrogen atoms with the carbon coating, and their intensity is relatively larger for samples C1, C2 and C3, which have the larger concentration of Ti or N atoms as obtained by GD-OES. They are also the thinnest where thermal diffusion of the ions to the whole coating thickness would be easier.

3.3. X-ray diffraction

XRD analysis (Fig. 4) is indicative of the presence of crystalline titanium as well as some C-specimens of the sp^2 type. In fact, up to three crystalline forms have been detected for titanium: two of them hexagonal ($P6_3/mmc$ and P6/mmm) and the third one cubic (I m-3 m). In relation to the Ti-C-N, broad signals have been related to lignite (C), phase corresponding to an amorphous phase, and fullerite (C_{60}), with a higher contribution of sp^2 nanocrystalline graphite (nc-G) phase, which is related with the results obtained in Raman spectroscopy. With this technique the interfaces titanium adherence layer/substrate are analyzed.

3.4. Fretting tests

Tribological study was carried out on Ti6Al4V substrate and Ti-C-N coatings under fretting conditions in the solution of FBS + EDTA + Sodium azide. The results of friction coefficient and wear scar analysis are listed in Table 4. All Ti-C-N coatings exhibit lower friction coefficients than Ti6Al4V substrate, being the C2 which presents the

Table 3
Results of the fitting of the Raman spectra in the region of the D and G bands and the atomic percentage of chemical elements in the coating surface ($\tilde{\nu}$, I and FWHM are the center wavenumber, the integrated area and the full width at half maximum of the obtained Gaussians, I(D)/I(G) is the ratio of the integrated intensity for D and G Gaussians).

Sample	Ti	N	C	*D* band			*G* band			I(D)/I(G)
	at. %			$\tilde{\nu}$ (cm^{-1})	I	FWHM (cm^{-1})	$\tilde{\nu}$ (cm^{-1})	I	FWHM (cm^{-1})	
C1	20	25	55	1370	1.80	271.6	1574	0.86	138.6	1.07
C2	30	10	60	1346	1.83	198.3	1562	0.14	134.9	0.88
C3	20	10	70	1371	2.06	281.1	1575	0.95	132.5	1.02
C4	15	0	75	1388	8.70	316.9	1584	2.87	114.9	1.10
C5	15	15	70	1389	46.95	319.6	1586	15.43	112.4	1.07

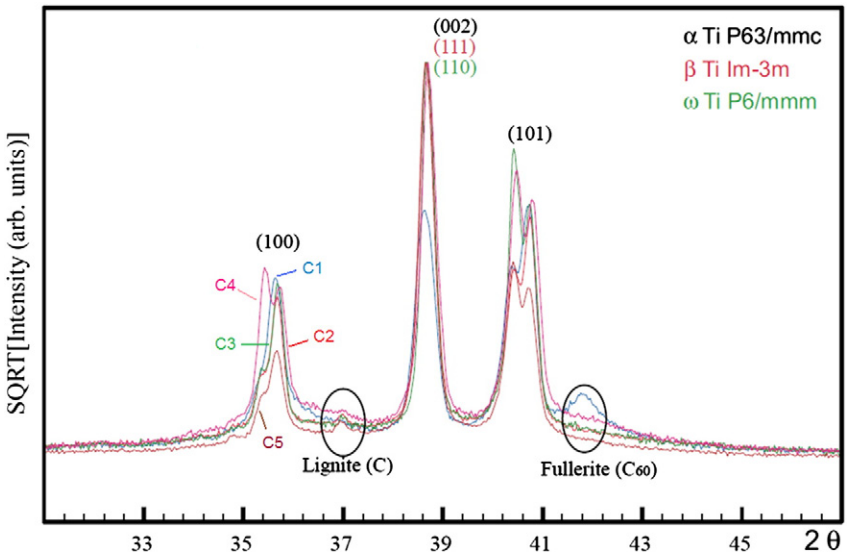

Fig. 4. XRD diffraction diagram of Ti-C-N coatings.

best tribological response. So it can be determined that, as expected [27], the Ti-C-N coatings improve effectively the fretting resistance of the Ti6Al4V substrate, reducing the friction coefficient and the wear. It seems that during sliding, the wear debris of the outer layers of Ti-C-N are transformed to graphite oriented with its basal plane parallel to the surface [28], generating a carbon-based coating as solid lubricant and reducing in this way friction and wear rates [6].

Among all Ti-C-N coatings, C1, C2 and C5 had very similar wear scars and only a smooth effect could be detected in the tested area. These coatings exhibit a better tribological behaviour than others prepared by PA-CVD technique with similar columnar growth. This can be explained by the presence of metal in our coatings [29] .

Al_2O_3 balls did not present significant wear scar in the tested surface. Only material transference from Ti-C-N surface to the alumina ball could be detected. This transfer film between sliding surfaces could be the reason of the reduction in the friction coefficient in all Ti-C-N coatings [12].

Analyzing the evolution of the friction coefficient in Fig. 5, it is observed that the uncoated Ti6Al4V sample has more unstable friction coefficient than the Ti-C-N coatings especially during the first half of the test. At the end of the test, an increase in the friction coefficient of C3 and C4 was also detected. This effect may be due to the material that has been removed from the coating and deposited again on the sliding surface (adhesions), which promotes an increase of the surface roughness, and hence, higher friction and wear on the samples. C1, C2 and C5 samples do not exhibit this phenomenon resulting in non failure of these coatings.

In Fig. 6 the wear profiles of each surface is represented. The reduction of the wear scar between uncoated Ti6Al4V and developed Ti-C-N coatings can be noticed. Effectively, the coatings C1, C2 and C5 show the best wear behaviour with a polished track on the surface that reduces the roughness without causing wear (smooth effect). C3 and C4 coating profiles show also a better wear behaviour than the substrate but the presence of adhesions in both cases can be confirmed, which explain the slight instability of friction coefficient at the end of the tests.

SEM micrographies (Fig. 7) show a detail of the scars produced on the surfaces during the fretting tests. The differences found on the wear scars and the magnitude of the damage produced on each sample can be observed.

From the wear tracks morphologies it can be observed that even if the friction coefficient of C3 and C4 are similar, the wear mechanism of both surfaces differs notably. Wear scratches for C4 are bigger than for C3. This could be related to the higher hardness of the wear particles produced during the fretting tests that act as abrasive agents when they are trapped between the alumina ball and the coating. The micrographs of C1, C2 and C5 show a smooth effect on the worn areas.

In general, it is noted that C2 coating exhibits the best tribological behaviour. This Ti-C-N coating shows the lowest carbon content in the layer due to the lower acetylene concentration used during deposition process (see Table 1 and Fig. 1 b)). Additionally, this coating has a larger sp^3/sp^2 fraction, thus it could explain its better tribological properties with respect to the other samples, since it combines a higher relative hardness (10 GPa) due to sp^3 contribution on a predominantly sp^2 hybridation nanocrystalline graphite (nc-G) and amorphous carbon (a-C) structure.

Table 4
Friction coefficients values and ball and disc wear scars measurements.

Sample	μ ± SD	Disc wear scar, maximum depth (μm)
Ti6Al4V	0.86 ± 0.08	10(3)
C1	0.34 ± 0.01	Polishing effect
C2	0.24 ± 0.01	Polishing effect
C3	0.43 ± 0.01	Adhesions
C4	0.37 ± 0.02	Adhesions
C5	0.37 ± 0.01	Polishing effect

4. Conclusions

All developed coatings consist of Ti-C-N layers. All coatings improved tribological properties of Ti6Al4V biomedical alloy commonly used in the manufacturing of artificial prosthesis. C2 coating exhibits the best tribological behaviour with the lowest friction coefficient and negligible wear with only a polished effect in the sliding surface. This response of the coating could be related to the higher sp^3/sp^2 fraction which provides the necessary hardness (10 GPa) and the nanocrystalline graphite (nc-G) and amorphous carbon (a-C) structure that confers the best wear resistance to the coating. Additionally, it could also be due to the fact that, for the development of this Ti-C-N coating, the amount of acetylene employed in the deposition process has been the lowest. First trials have been done trying to correlate the tribological behaviour of the coatings with their properties and microstructure, but more tests should be done in the future to reinforce these conclusions.

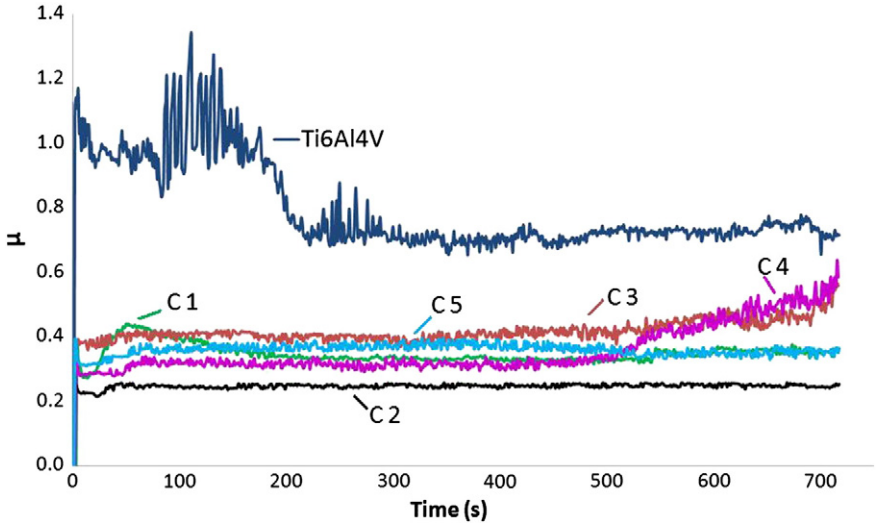

Fig. 5. Friction coefficient graph of fretting tests.

Abbreviations

PVD	Physical Vapor Deposition
XRD	X-Ray Diffraction
SEM	Scanning Electron Microscope
GD-OES	Glow Discharge Optical Emission Spectroscopy
ELI	Extra Low Interstitial
FBS	Fetal Bovine Serum
FWHM	Full Width at Half Maximum

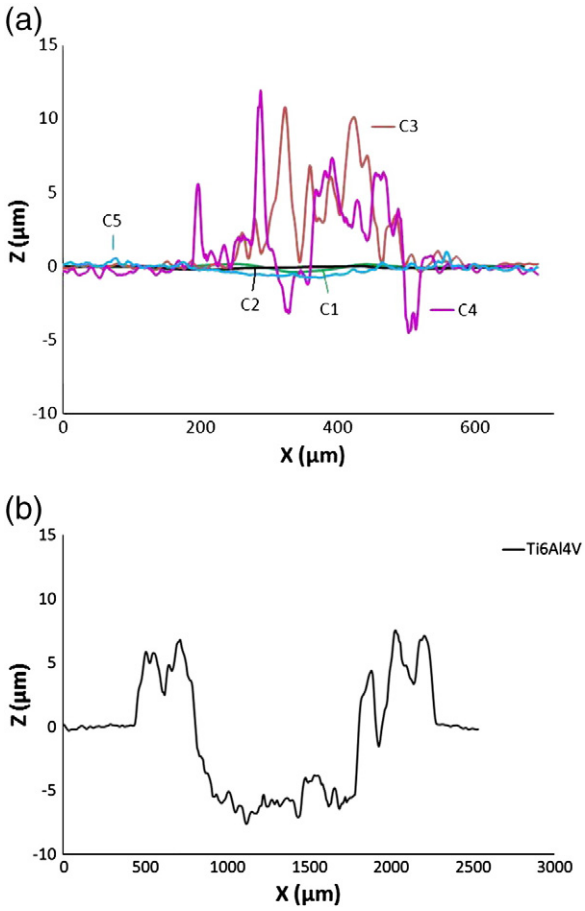

Fig. 6. Profiles of the wear tracks generated during fretting tests against alumina balls.

Acknowledgements

The authors acknowledge financial support from the Spanish Ministry of Science and Innovation obtained in the project: CSD2008-00023 FUNCOAT (in frames of the CONSOLIDER INGENIO-2010 program).

G. B. thanks the "Ministerio de Ciencia e Innovación" (MAT2010-15375) and the "Gobierno Vasco" (Basque University System Research Groups, IT-177-07) for their financial support. SGIker technical support (MEC, GV/EJ, European Social Fund) is also gratefully acknowledged.

References

[1] J. Klein, Repair or Replacement – A Joint Perspective, Science 232 (2009).
[2] J.M. Williams, R.A. Bucharan, Mater. Sci. Eng. 69 (1985) 237–246.
[3] R.S. Magaziner, V.K. Jain, S. Mall, Wear 267 (2009) 368–373.
[4] N.M. Everitt, J. Ding, G. Bandak, P.H. Shipway, S.B. Leen, E.J. Williams, Wear 267 (2009) 283–291.
[5] M. Dalmiglio, P. Schaaff, U. Holzwarth, R. Chiesa, G. Rondelli, J. Biomed. Mater. Res-A 86B (2008) 407–416.
[6] B.G. Wendler, W. Pawlak, J. Achiev. Mater. Manuf. Eng. 26 (2008) 207–210.
[7] M. Sylvestre, H. Zaidi, J.P. Rivière, D. Eyidi, F. Doyen, Surf. Coat. Tech. 205 (2010) 1374–1380.
[8] A. Chandra, J.J. Ryu, P. Karra, P. Shrotriya, V. Tvergaard, M. Gaisser, T. Weik, J. Mech. Behav. Biomed. 4 (2011) 1990–2001.
[9] M. Larry, Wolford, Proc. (Bayl. Univ. Med. Cent.) 19 (2006) 232–238.
[10] Stuart B. Goodman, Enrique Gómez Barrena, Michiaki Takagi, Yrjo T. Konttinen, J. Biomed. Mater. Res. A (2008).
[11] Yufeng Zheng, Dong Liu, Xiliang Liu, Biomed. Mater. 3 (2008) 044103–044109.
[12] D.P. Dowling, Diam. Relat. Mater. 6 (1997) 390–393.
[13] L. Zhang, P. Lv, Z.Y. Huang, S.P. Lin, D.H. Chen, S.R. Pan, M. Chen, Diam. Relat. Mater. 17 (2008) 1922–1926.
[14] Guojia Ma, Shuili Gong, Guoqiang Lin, Lin Zhang, Gang Sun, Appl. Surf. Sci. 258 (2012) 3045–3050.
[15] A.F. Yetim, A. Celik, A. Alsaran, Surf. Coat. Tech. 205 (2010) 320–324.
[16] "Arc evaporator and method for operating the evaporator": Patent number WO2010072850 (A1). FUNDACIÓN TEKNIKER.
[17] Z.N. Farhat, Y. King, D.O. Northwood, A.T. Alpas, Mater. Sci. Eng. A206 (1996) 302–308.
[18] J.L. Lubet, J.M. Georges, G. Meille, ASTM (1986) 72–89.
[19] W.C. Oliver, G.M. Pharr, J. Mater. Res. 7 (1992) 1564–1583.
[20] R. Payling, J. Michler, M. Aeberhard, Surf. Interface Anal. 33 (2002) 472–477.
[21] Haruyo Fukui, Surf. Coat. Tech. 187 (2004) 70–76.
[22] Geoffrey Dearnaley, Surf. Coat. Tech. 200 (2005) 2518–2524.
[23] L. Guoqing, Thin Solid Films 475 (2005) 279–282.
[24] A.C. Ferrari, S.E. Rodil, J. Robertson, Phys. Rev. B 67 (2003).
[25] M.V. Klein, J.A. Holy, W.S. Williams, Phys. Rev. B 17 (1978) 1546–1556.
[26] Y.H. Cheng, B.K. Tay, S.P. Lau, H. Kupfer, F. Richter, J. Appl. Phys. 92 (2002) 1845–1949.
[27] Ganesh Sundara S Raman, P. Navaneethakrishnan, R. Gnanamoorthy, P. I. Mech. Eng. J-J. Eng. 223 (2009) 227–231.
[28] Geoffrey Dearnaley, James H. Arps, Surf. Coat. Tech. 200 (2005) 2518–2524.
[29] W. Österle, D. Klaffke, M. Griepentrog, U. Gross, I. Kranz, Ch. Knabe, Wear 264 (2008) 505–517.

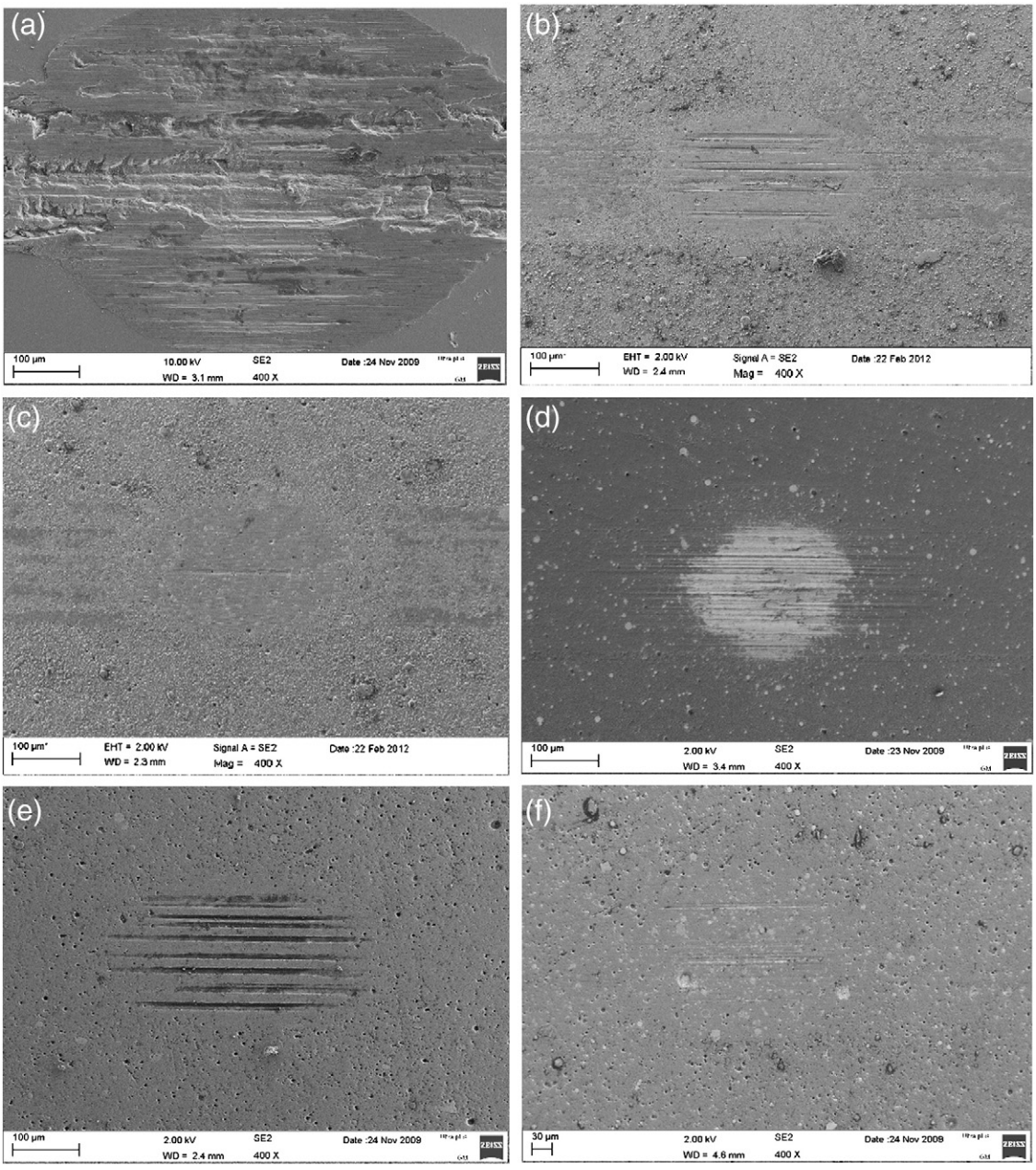

Fig. 7. SEM micrographies of the fretting tests wear scars. a) Ti6Al4V, b) C1, c) C2, d) C3, e) C4 and f) C5.

JOURNAL OF THE MECHANICAL BEHAVIOR OF BIOMEDICAL MATERIALS 55 (2015) 75–86

Available online at www.sciencedirect.com

ScienceDirect

www.elsevier.com/locate/jmbbm

Research paper

Development of Ti–C–N coatings with improved tribological behavior and antibacterial properties

Virginia Sáenz de Viteri[a,*], Gotzone Barandika[b], Raquel Bayón[a], Xana Fernández[a], Iñigo Ciarsolo[a], Amaya Igartua[a], Ramón Pérez Tanoira[c], Jaime Esteban Moreno[c], Conchita Pérez-Jorge Peremarch[c]

[a]IK4-Tekniker, Parke Teknologikoa, C/ Iñaki Goenaga, 5, 20600 Eibar, Gipuzkoa, Spain
[b]Departamento de Química Inorgánica, Facultad de Ciencia y Tecnología, Universidad del País Vasco, UPV/EHU, Apdo 644, 48080 Bilbao, Spain
[c]Department of Clinical Microbiology, IIS-Fundación Jiménez Díaz, Av. Reyes Católicos 2, Madrid 28040, Spain

ARTICLE INFO

Article history:
Received 15 July 2015
Received in revised form
1 October 2015
Accepted 23 October 2015
Available online 2 November 2015

Keywords:
Ti–C–N
Tribocorrosion
Fretting
Silver
Bacterial adhesion

ABSTRACT

In artificial metallic joint implants, the failure is provoked by two effects in most of the cases: mass loss and wear debris removed due to tribological-corrosive effects on the implant alloy, and infections due to the presence of bacteria. In this work, several Ti–C–N corrosion and wear protective coatings were developed by Physical Vapour Deposition technology, and deposited on Ti6Al4V alloy. In order to provide the implant antibacterial properties, an additional silver top coating has been deposited. Tribological behavior was characterized through tribocorrosion and fretting tests. On the other hand, wettability tests were performed to study the grade of hydrophilicity/hydrophobia. Additionally, antibacterial properties were evaluated by means of bacterial adhesion tests. As a result of these characterization studies, the coating with the best performance was selected. The as-coated material includes excellent protection against tribocorrosion and fretting effects (in relation to the uncoated one) and the silver layer has been confirmed to exhibit antibacterial properties.

1. Introduction

In orthopedic applications, artificial joints (e.g., hip and knee prostheses) include bearing surfaces where the material is subjected to sliding wear. The surfaces in contact are immersed in the body fluid, and therefore, corrosion may also be a concern. Particles and metal ions generated from wear of prosthetic implants induce inflammatory reactions that provoke the release of inflammatory mediators from macrophages (Sinnett-Jones et al., 2005). The concern of toxicity of high concentration of metal ions has generated a wide attention (Brodner et al., 1997; Hallab et al., 2000; Sargeant and Goswami, 2007). Therefore, for metallic artificial joint component, the improvement of tribocorrosion properties has become an important factor for their application in human body.

Tribocorrosion can be defined as a degradation phenomenon of material surfaces (wear, cracking, corrosion, etc.)

*Corresponding author. Tel.: +34 943 206744; fax: +34 943 72 42 08.
E-mail address: virginia.saenzdeviteri@tekniker.es (V. Sáenz de Viteri).

http://dx.doi.org/10.1016/j.jmbbm.2015.10.020
1751-6161/

subjected to the combined action of mechanical loading (friction, abrasion, erosion, etc.) and corrosion attack caused by the environment (chemical and/or electrochemical interaction) (Mischler, 2008; Mischler and Ponthiaux, 2001). This effect produces irreversible transformations on the material, as it involves numerous synergistic effects between mechanical and electrochemical phenomena, usually leading to an acceleration of material loss (Diomidis et al., 2010; Iwabuchi et al., 2007; Landolt et al., 2004). Tribocorrosion involves numerous interaction effects between mechanical and chemical or electro-chemical phenomena (Landolt et al., 2004). The release of metallic ions due to corrosion and wear is of vital importance, since it can adversely affect the biocompatibility and mechanical integrity of implants (Vieira et al., 2006). The metal ions released into the surrounding tissue may induce the release of potentially osteolytic cytokines involved in implant loosening (Rogers et al., 1997; Sargeant and Goswami, 2007).

Surface treatments are widely employed to improve wear and corrosion resistance as well as hardness of the surface of metallic alloys employed in orthopedic devices (Cheng and Zheng, 2006; Kaestner et al., 2001; Yildiz et al., 2007; Zhecheva et al., 2005). In recent years, diamond-like-carbon (DLC) films have been the subject of extensive investigations due to their potential of attaining combination for highly desirable properties in the context of biomedical applications (Martinu et al., 1992; Raveh et al., 1992; Snyders et al., 2007). Their high hardness, low friction and wear, electrical insulation, chemical inertness and good biocompatibility make them ideal candidates as protective coatings in joints replacement (Bendavid et al., 2007). These coatings are preferred since they improve resistance against wear and corrosion processes, especially on Ti6Al4V (the alloy most widely used for implant fabrication). The Ti6Al4V alloy has an excellent corrosion resistance, biocompatibility, high strength to weight ratio and also a high toughness (Xuanyong et al., 2004). However, the major disadvantage regarding the use of Ti6Al4V for bio-implant application is its low load-bearing capacity and poor wear resistance. Moreover, this alloy is not only subjected to wear but also to active corrosion, generated by breaking up of the protective passive oxide layer in sliding contact. The frictional movement in corrosive medium is continuous (Arslan et al., 2012) which produces particles and ions that can result in adverse biological reactions (Hodgson et al., 2002; Sargeant and Goswami, 2007).

The present work is focused in total knee replacements, where two major problems can be presented: the first one is produced between the backside of the ultra-high molecular weight polyethylene (UHMWPE) patellar component and the tibial tray of fixed bearing tibial component made of Ti6Al4V where the fretting effect takes place, which is the responsible of the elimination of mounts of polyethylene and Ti6Al4V alloy debris (Billi et al., 2010). In this case, the cause of failure in most cases is related with this wear debris elimination (Currier et al., 2005; Sharkey et al., 2001). The second problem is related to implant-associated infections. The presence of an implanted device results in an increased susceptibility to infection for the patient (Elek and Conen, 1957; Guggenbichler et al., 2011). Occurring at a rate of 5%, orthopedic implant infections remain one of the most devastating complications (Gordon et al., 2010). The diagnosis and treatment of prosthetic joint infections is further complicated by the development of a bacterial biofilm. This structure allows bacteria to resist antimicrobial agents and immune responses. Patients with this type of infection require a longer period of antibiotic therapy and repeated surgical procedures. These prosthetic-joint infections have severe consequences not only for patients but also for society (An and Friedman, 1998; Cordero et al., 1996; Edwards et al., 2008; Esteban et al., 2008; Garner et al., 1988; Gristina, 1987; Harris and Richards, 2006; Katsikogianni and Missirlis, 2004; Perez-Tanoira et al., 2012; Rochford et al., 2012; Singhai et al., 2012). Factors influencing the bacteria adherence to a biomaterial surface include chemical composition of the material, surface charge, hydrophobicity, as well as surface roughness and/or physical configuration. It would be desirable to develop biomedical coatings for implants which are repellent to bacteria to minimize the colonization of the implant surface with circulating planktonic bacteria that can lead to biofilm development (Perez-Jorge et al., 2012; Perez-Tanoira et al., 2014). One of the strategies that is gaining renewed attention for combating the threat of bacterial infection is the use of an antibacterial noble metals (Atiyeh et al., 2007).

Taking into consideration the above mentioned aspects, this work has been focused on the development of several Ti–C–N protective coatings for Ti6Al4V in order to improve the wear and corrosion resistance of the surfaces. Thus, tribological behavior has been characterized through tribocorrosion and fretting tests. Additionally, the effect of the silver top film has been evaluated by means of a bacterial adhesion study. Finally, wettability tests have been performed in order to study the influence of the hydrophilicity/hydrophobicity grade in the bacterial adhesion.

2. Materials and methods

2.1. *Materials*

In a previous work carried out for some authors of this paper (Sáenz de Viteri et al., 2012), five Ti–C–N coatings were developed on Ti6Al4V substrates by physical vapor deposition (PVD) cathodic arc method in order to improve the fretting resistance of the substrate. These coatings were characterized by analyzing their physical properties, thickness, hardness, adhesion and roughness. Microstructural characterization was assessed by means of X-ray diffraction (XRD), scanning electron microscope (SEM) and RAMAN spectroscopy techniques; chemical composition in depth was studied with Glow Discharge Optical Emission Spectroscopy (GD-OES) technique; and tribological behavior by means of fretting tests. This study allowed the selection of one coating (C2 coating) that could be a good alternative for protecting Ti6Al4V substrates from the tribological point of view, and has been codified in this work as Ti–C–N_1. Additionally, taking into account the superior tribocorrosion response characterized by Bayón in her thesis work (Bayón, 2011), another coating was selected in this study: the Ti–C–N_02 coating (codified as C5 in Sáenz de Viteri et al., 2012). Thus, the details about Ti6Al4V samples preparation and

Table 1 – Thickness, roughness, hardness, *I*(D)/*I*(G) and friction coefficient values of selected coatings.

Sample	Thickness (μm)	Roughness (μm)	Hardness (GPa)	*I*(D)/*I*(G)	Friction coefficient
Ti6Al4V	–	0.05	–	–	0.86±0.08
Ti–C–N_1	2.40	0.36	10	0.88	0.24±0.01
Ti–C–N_2	3.86	0.42	8	1.07	0.37±0.01

I(D)/*I*(G) is the ratio of the integrated intensity for D and G Gaussians obtained by Raman spectroscopy. The G band corresponds to a stretching vibrational mode of sp^2 bonded carbon, and the D band is associated to disorder, and is related to a breathing mode of carbon rings.

coating deposition technique were reported elsewhere (Sáenz de Viteri et al., 2012).

In Table 1 the most significant results of selected coatings from the previous work are presented (Sáenz de Viteri et al., 2012).

With the aim of providing additional antibacterial properties, a thin silver film was deposited on the coatings with better properties from wear-corrosion tests. The Ag film was deposited by PVD in a vacuum chamber evacuated up to a pressure of 10^{-5} mbar. A DC-pulsed (250 KHz) ENI-RPG50 plasma source has been used to obtain the plasma. The Ag film was deposited with power density of 1.07 W/cm^2 and a deposition rate of 40 nm/min. During the deposition process, the argon flow was constant (45 sccm) and the pressure in the chamber during the deposition process was 0.04 Pa.

2.2. *Surface characterization*

Chemical composition of the new produced surface with Ag film was analyzed by GD-OES technique from Horiba Jobin Yvon. The measurement conditions were 650 Pa and 35 W, with a copper anode of 4 mm of diameter. Microstructural study was carried out by means of Scanning Electron Microscope (SEM), from OXFORD INCA Synergy.

2.3. *Tribocorrosion tests*

Tribocorrosion tests were carried out in order to study the synergistic effect of wear and corrosion following the experimental procedure defined by Celis and Ponthiaux (2012) and Ponthiaux et al. (2013) (further explanations can be found as Supplementary material, under Protocol S1). The tests were performed by using a Microtest tribometer with rotatory movement under "ball on disc" configuration, assisted by an Autolab-Methrom potentiostat PGSTAT302N. The electrolyte used for simulating biological environment was a phosphate buffered saline (PBS) solution, composed by: 0.14 M NaCl, 1 mM KH_2PO_4, 3 mM KCl, and 10 mM Na_2HPO_4.

The applied load was 5 N, the rotational speed was 120 rpm and track radius 6 mm. The exposed area was, in all cases, 2.5 cm^2. Over the rotatory disc, an electrochemical cell with three electrodes was placed in order to perform electrochemical measurements simultaneously. The reference electrode employed to measure the potential was Ag/AgCl KCl 3M (0.207 V vs SHE) and the counter electrode was a platinum wire. As counter bodies, ceramic balls of alumina with 10 mm of diameter were chosen. Samples were previously polished until a final roughness of 0.03 μm, and then cleaned with distilled water and ethanol in an ultrasonic bath.

After the tribocorrosion tests, the electrolytes (PBS) were collected and analyzed by inductively coupled plasma atomic emission spectroscopy (ICP-AES) in ULTIMA 2 HORIBA Jobin Yvon equipment for analyzing the presence of aluminum, vanadium and titanium released from the coating/substrate during tribocorrosion test. Each used electrolyte was then divided into two volumes. One was directly analyzed by ICP-AES after filtering at 0.45 μm in order to detect the dissolved elements, and the other one was firstly treated with H_2O:HNO_3 (1:1) and two droplets of HF in order to dissolve all the possible compounds. In this last measurement, total elements, dissolved and solids, were analyzed.

2.4. *Surface hydrophilicity/hydrophobicity*

The SURFTENS universal goniometer was used to investigate the wetting behavior of different samples, in order to evaluate the grade of hydrophilicity/hydrophobia. This evaluation is based on the measurement of the contact angle of a drop of distilled water on the surface to be investigated. This contact angle is measured by means of an optical camera, recording and calculating its value.

2.5. *Fretting tests*

Fretting tests were performed in SRV® tribometer under ball-on-disc configuration with the aim to try to reproduce as close as possible real working conditions. Balls of UHMWPE with a diameter of 10 mm were used as counterbody, trying to use the real materials. The stemmed tibial component is made of a titanium alloy and the patellar component is a UHMWPE. Tests were done under lubricated conditions by using fetal bovine serum (FBS) with sodium azide and ethylenediaminetetraacetic acid (EDTA), according to ASTM F732-00 standard. Tests were carried out at 37 °C during 60 min. Testing conditions applied were: a load of 30 MPa, a frequency of 210 Hz and a stroke of 150 μm.

2.6. *Bacterial adhesion*

2.6.1. *Staphylococcal adhesion experiments*

Coated Ti6Al4V samples were compared against controls of uncoated Ti6Al4V samples. Staphylococcal adhesion experiments were performed as described by Kinnari et al. (2008) and Perez-Tanoira et al. (2012). For the preliminary study of bacterial adhesion, the biofilm-forming collection strains *S. aureus* 15981 (Valle et al., 2003), *S. epidermidis* ATCC 35984 and 6 clinical strain from *S. aureus* (p1…p6) and 6 other of *S. epidermidis* (p7…p12), isolated from patients with implant-related infection by sonication (Esteban et al., 2008) were

used. All strains were cultured overnight in tryptic soy broth (bioMérieux, Marcy l'Etoile, France) at 37 °C in 5% CO_2 atmosphere. It is worth mentioning that all patients were diagnosed articular infection based on clinical criteria (Cordero-Ampuero et al., 2007). The clinical Staphylococcus strains are positive for biofilm development (Esteban et al., 2010).

After culture, bacteria were harvested by 10 min centrifugation at 3500 g at room temperature. Supernatant was discarded and the pellet was washed three times with sterile phosphate buffered saline (PBS). Bacteria were then suspended and diluted in PBS to 10^8 colony-forming units (CFU)/ml. The biomaterial discs were placed in the bacterial suspension and incubated for 90 min at 37 °C. Afterwards, the biomaterial plates were rinsed three times with sterile PBS to remove any non-adherent bacteria (Kinnari et al., 2008).

The dried plates were stained for 15 min with a rapid fluorescence staining method using the Live/Dead® Bacterial Viability Kit (BacklightTM) (Boulos et al., 1999). On each plate, 8 fields were viewed and photographed with a Nikon Coolpix 8400 (Nikon, Melville, NY) under a fluorescence microscope at 40 × magnification. All experiments were performed in triplicate. The number of microphotographs studied was 24 for each material and bacterium. The surface area covered with adhered bacteria was calculated using the ImageJ software (National Institute of Health, Bethesda, MD).

2.6.2. *Statistical analysis*

For the statistical study, Mann–Whitney or Wilcoxon non parametric tests were employed. These tests were used for two samples while the Kruskal–Wallis test was used for more than two samples. EPI-Info software version 3.5.1 (CDC, Atlanta, GA. USA) was used to perform the statistical studies.

3. Results

As previously mentioned, the surface characterization of Ti–C–N_1 and Ti–C–N_2 has been previously reported by the same authors (Bayón, 2011; Sáenz de Viteri et al., 2012). Thus, the aim of this study is the selection of the best coating for knee implants, the election being based on a pre-selection. With this aim, the first step was the study of the tribocorrosion behavior of both coatings, and the comparison with the substrate (Ti6Al4V). Taking into account the good tribocorrosion results, one of the coatings was selected (Ti–C–N_2) in order to continue with a more detailed study. As a further objective was the development of an antibacterial coating, Ti–C–N_2 film was coated with a film of silver, producing the coating Ti–C–N_2+Ag. This way, wettability, fretting and bacterial adhesion tests were carried out for Ti6Al4V and for Ti–C–N_2 and Ti–C–N_2+Ag coatings. Therefore, the surface characterization herein presented was performed just for the new coating Ti–C–N_2+Ag.

3.1. *Surface characterization*

A thin layer of 200 nm of silver was deposited on Ti–C–N_2 coating, and the analysis of the chemical composition was obtained by GD-OES technique (Fig. 1, left). The as-obtained profile gives a qualitative idea of the progression in depth of chemical composition. This measurement was carried out in a sample where the Ti–C–N_2 and Ag coatings where deposited onto silicon wafer. The presence of titanium layer can be detected on the top of silicon. The decrease of the amount of titanium is accompanied by the presence of C and N that appear gradually because the gases needed to deposit those elements were introduced into the chamber progressively. On the left hand side, it was observed that all elements related to the Ti–C–N coating disappeared, showing a top film layer of pure the silver, corresponding to the film. It should be noted the presence of oxygen in large part of the analysis and the nitrogen continuity once the coating has finished. It seems that the silver layer peeled due to a break in the vacuum allowing air introduction.

Fig. 1 right shows the SEM micrograph of transversal section obtained in a coated silicon wafer. All different coatings, seen by GD-OES analysis, can be also distinguished by SEM, first the silicon corresponding to the silicon wafer (a), second the pure titanium layer (b), afterwards the Ti–C–N coating (c), and finally the silver film (d). It can be detected the presence of droplets embedded in the film due to the deposition process itself. This effect was observed because the sample was not polished for the microstructure study. The different morphology between pure titanium layer and

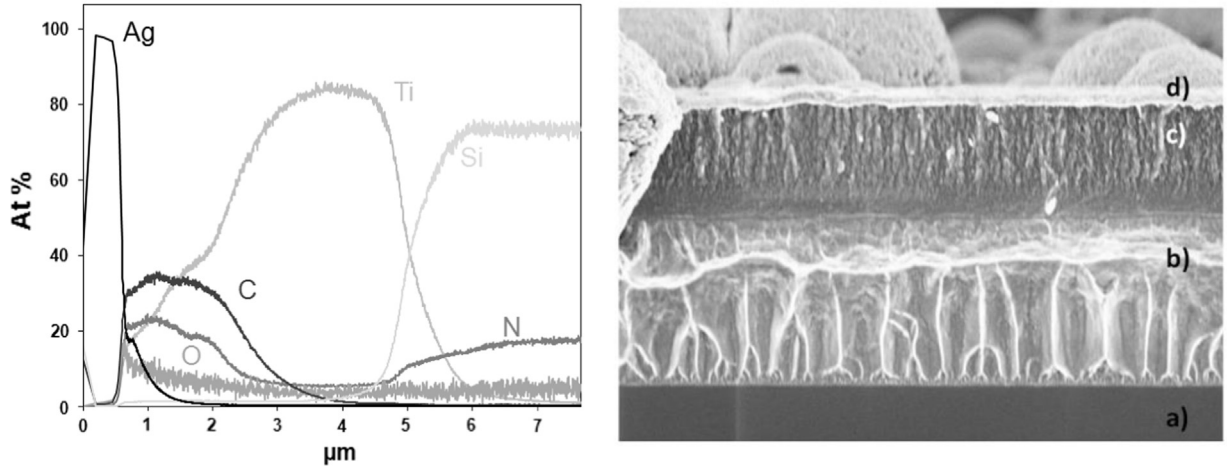

Fig. 1 – (Left) Graded coating composition obtained by GD-OES, and (right) SEM micrograph for Ti–C–N_2+Ag coating.

Ti–C–N coating is related to the process conditions and the influence of deposited elements (Sáenz de Viteri et al., 2012).

3.2. *Tribocorrosion tests*

The first step in tribocorrosion testing procedure was the monitoring of the open circuit potential (OCP) of the surfaces immersed in PBS during 1 h, until its stabilization. The OCP values for Ti6Al4V, Ti–C–N_1 and Ti–C–N_2 were −0.273 V, 0.063 V and 0.110 V, respectively. Once the OCP of the samples reached a stable value, an Electrochemical Impedance Spectroscopy (EIS) was registered in order to evaluate the corrosion resistance of the exposed surfaces before the sliding process. After the impedance measurement, the OCP was again registered during the first sliding process (Fig. 2). When the sliding process started, the potential decreased in all samples to more negative values as a consequence of an activation process on their track surface due to the effect of sliding. This decrease of the potential was related to the total or partial destruction of the passive film as a consequence of the mechanical contact imposed. In case of Ti6Al4V, the potential decreased to the lowest potential values in comparison to the Ti–C–N coatings. During sliding process, the OCP for Ti6Al4V and Ti–C–N_1 fluctuated due to the constant removal and re-growth of their passive film as consequence of the sliding. In case of Ti–C–N_2 coating, the potential remained stable during rubbing process. Once the wear process was completed, the potential in all samples increased quickly to more positive values close to the initial ones, as a consequence of an immediate repassivation phenomenon on the worn area. The values of the samples at the end of the sliding, after a stabilization time were: −0.313 V (Ti6Al4V), −0.160 V (Ti–C–N_1) and −0.055 V (Ti–C–N_2). In any case, the potential did not reach the initial value registered before the sliding due to the fact that the worn surface did not present the same electrochemical state as the unworn area.

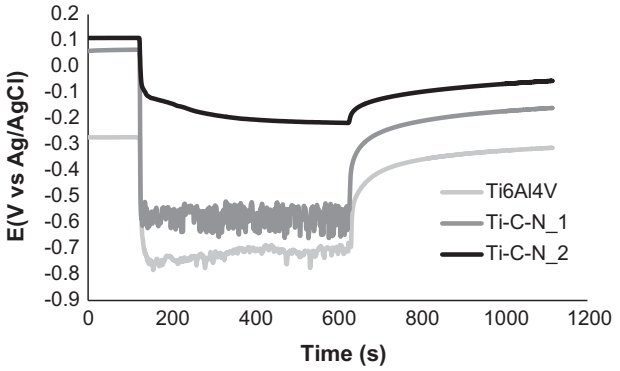

Fig. 2 – Open circuit potential (OCP) during sliding process for TiAl4V, and Ti–C–N_1 and Ti–C–N_2 coatings.

Corrosion resistance before and during sliding process was evaluated from the experimental data registered during EIS measurements (Fig. 3).

As observed in Fig. 3, bode diagrams for Ti6Al4V, Ti–C–N_1 and Ti–C–N_2 coatings showed that the electrochemical state of the surfaces in all samples changed due to the wear, resulting in a reduction in their corrosion resistance. Ti–C–N_1 and Ti6Al4V samples showed similar values of corrosion resistance before sliding process, while Ti–C–N_2 presented slightly lower corrosion resistance after the first hour of inmersion in PBS. However, during sliding process, the corrosion behavior of Ti6Al4V and Ti–C–N_1 coating was more significantly affected than in case of the Ti–C–N_2 coating. The reduction of the corrosion resistance in Ti–C–N_1 sample seems to be due to the fact that the protective Ti–C–N coating was completely removed in the sliding contact area and the bare substrate was exposed to the mechanical and electrochemical effect during some parts of the tribological test. The variation of the corrosion resistance before and during sliding process for the three samples was calculated by fitting the experimental data with appropriate equivalent circuits. The corrosion resistance in case of Ti6Al4V and Ti–C–N_1 was reduced 99.97% and 99.18%, respectively. Nevertheless, Ti–C–N_2 showed the lowest corrosion resistance variation with a reduction of 18.05%. It must be pointed out that polarization resistance values obtained during the sliding process were calculated for the high-medium range of frequencies for all samples due to the instability of the system when measuring impedance at low frequencies. In case of the corrosion resistances before the sliding process, those values were obtained in the whole frequency range (10 kHz to 10 mHz).

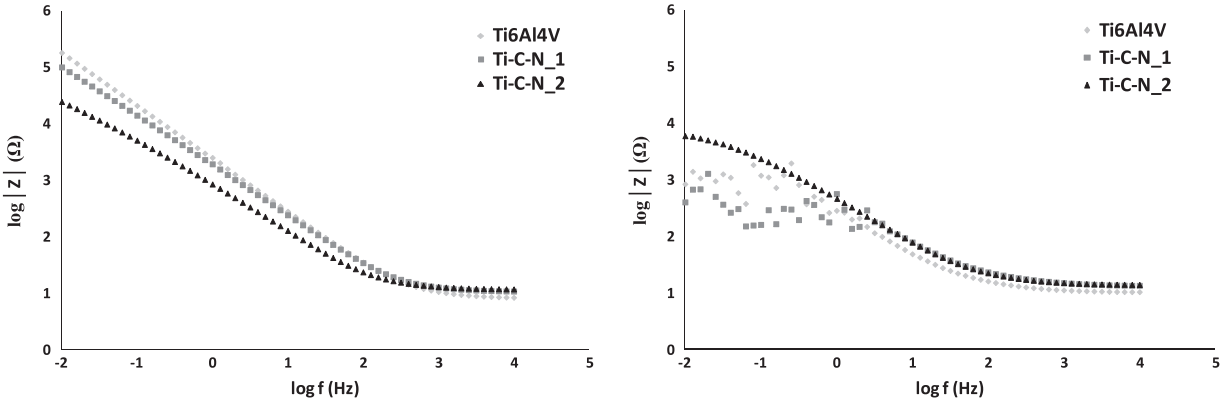

Fig. 3 – Bode plots for TiAl4V, Ti–C–N_1 and Ti–C–N_2 coatings (left) before and (right) during siliding. (Modulus IZI is the impedance modulus and *f* is the frequency).

Table 2 – Mean friction coefficient values and material loss of uncoated and Ti–C–N coated titanium alloy.

Sample	Friction coefficient (μ) ± SD	$W_{tr} \times 10^4$ (cm^3) ± SD	% W^c_{act}	% W^m_{act}
Ti6Al4V	0.41 ± 0.01	7.759 ± 0.172	0.07	99.93
Ti–C–N_1	0.38 ± 0.01	6.480 ± 0.169	0.06	99.94
Ti–C–N_2	0.15 ± 0.01	0.091 ± 0.011	0.10	99.90

Table 3 – Contact angle for TiAl4V, Ti–C–N_2 and Ti–C–N_2+Ag coatings.

Sample	Contact angle ± SD (°)
Ti6Al4V	48 ± 1
Ti–C–N_2	59 ± 3
Ti–C–N_2+Ag	63 ± 1

In table 2, friction coefficients registered during sliding test are summarized as well as the total material loss in the wear track (W_{tr}), the percentage of material loss due to corrosion of active area in the wear track (% W^c_{act}) and the percentage of material loss due to mechanical wear of active material in the wear track (W^m_{act}). As observed, the Ti–C–N_2 coating exhibits the lowest coefficient of friction and the best wear resistance with the lowest loss of material. The parameters obtained in case of Ti–C–N_1 coating are closed to the substrate ones, with higher friction coefficient and similar material loss. In all cases, the material loss due to corrosion is very low in comparison with the material loss due to mechanical effect, which is in all samples around 99.9%. In fact, the wear tracks produced for Ti6Al4V and Ti–C–N_1 exhibit similar depth and width, showing that the Ti–C–N_1 coating was completely removed during test, and the track depth reached the substrate. This explains the similar potential evolution during sliding observed for both samples. Additionally, it can be noticed that the wear depth of Ti–C–N_2 is very low in comparison to Ti6Al4V and Ti–C–N_1, showing a polishing effect (profile of the wear tracks in Supplementary material as Fig. S2).

In summary, the lowest friction coefficient (friction coefficient evolution can be found as Supplementary material, Fig. S1), the better corrosion resistance and the lowest material loss produced during the tribocorrosion process in case of Ti–C–N_2 sample indicate that this coating is the best alternative in terms of tribocorrosion performance.

In order to complete previous results, ICP technique was performed on the electrolyte used for tribocorrosion tests with the aim of studying the migration of elements from Ti6Al4V alloy due to the mechanical and electrochemical effect. In the first analysis, the results confirmed the absence of dissolved elements. However, after the chemical digestion (with HNO_3, H_2O and HF), Ti, Al and V elements were detected in electrolytes that were in contact with Ti6Al4V and Ti–C–N_1 samples during tribocorrosion tests. On the contrary, none of the cited elements were observed for the electrolyte in contact with Ti–C–N_2 sample, supporting that this coating was not removed at any time during tribocorrosion test and showing its good permeability (detailed information about detected elements in Supplementary material as Table S1).

So-far showed results made us discard the Ti–C–N_1 coating for the rest of the study due to its poor tribological response. Therefore, next results will be referred to Ti6Al4V, Ti–C–N_2 and Ti–C–N_2+Ag.

Table 4 – Friction coefficient values and ball and disc wear scar measurements.

Sample	μ ± SD	Ball wear scar (diameter, mm)	Disc wear scar
Ti6Al4V	0.21 ± 0.01	1.2 ± 0.1	No wear scar
Ti–C–N_2	0.23 ± 0.01	0.8 ± 0.1	No wear scar
Ti–C–N_2+Ag	0.32 ± 0.06	1.8 ± 0.4	Ag coating disappears

3.3. *Surface hydrophilicity/hydrophobicity*

In order to study the hydrophilicity/hydrophobicity behavior of the samples, contact angles were measured after a stabilization period of 30 s. The results (Table 3) showed values lower than 65°, which indicates that all samples have a hydrophilic behavior. Additionally, contact angles point out that Ti6Al4V is the most hydrophilic surface, whereas Ti–C–N_2+Ag coating presented the highest value (63°).

3.4. *Fretting tests*

Tribological behavior was analyzed by means of fretting tests. Mean friction coefficient values, and ball and disc wear scars are compiled in Table 4. As observed, Ti6Al4V and Ti–C–N_2 had similar tribological response with almost the same friction coefficient and without wear scar on their surface. The difference between both coatings was observed in the balls wear scars, where the ball tested against the Ti–C–N_2 samples suffered less wear. Ti–C–N_2+Ag presented the worst tribological behavior with the highest friction coefficient. Besides, the wear produced in the counterbody was higher in comparison with the other samples.

The evolution of friction coefficients (this information can be found in Supplementary material as Fig. S3) clearly indicates that the presence of the silver film not only worsens the tribological response (increasing the friction coefficient) but it makes it more instable over time. During the first 500 s, the friction coefficient increases, probably due to the removing of the silver layer. This generates the production of silver wear debris, resulting in the instability of the friction coefficient. In the last 1000 s, the friction coefficient becomes more stable, probably because a steady state regime is reached. The evolution of the friction coefficient for Ti6Al4V and Ti–C–N_2 coatings is more stable, becoming similar after the first 2000 s.

Wear scar of Ti–C–N_2+Ag disc was examined by optical microscope (Fig. 4, left) and confocal microscopy (Fig. 4, middle). The scar was evaluated by topographical analysis

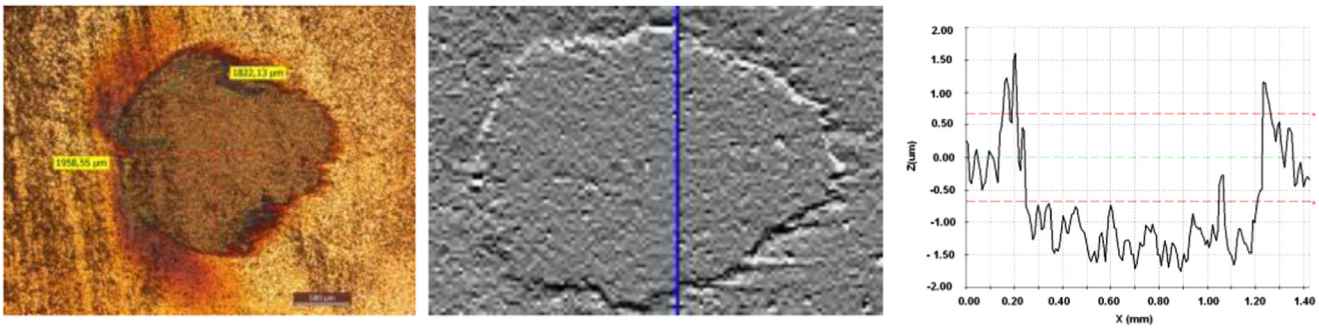

Fig. 4 – (Left) Microscope image of Ti–C–N_2+Ag disc after fretting test against UHMWPE ball; (middle) topography; and (right) depth profile of Ti–C–N_2+Ag disc after fretting test against UHMWPE ball.

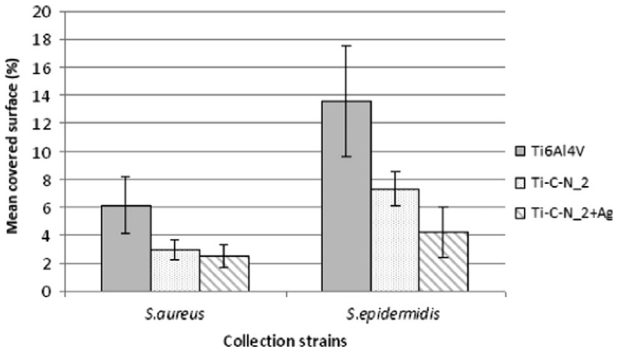

Fig. 5 – Mean percentage of the surface of each biomaterial covered by the collection of *S. aureus* and *S. epidermidis* strains.

and depth profile (Fig. 4, right). The depth of the scar in the sliding contact area was around 1.5 µm. Taking into account the thickness of the Ag coating and the depth of the wear scar, this indicates that all the silver film was removed in the sliding contact area during fretting tests. This was confirmed by SEM-EDS (electron discharge spectroscopy), where two measurements were carried out, one outside the sliding contact area, and the other one just in the wear scar. Thus, the absence of silver in the scar was confirmed. (Further details about wear scars in UHMWPE balls and SEM-EDS analysis carried out in the sample Ti–C–N_2+Ag after fretting test can be found in Supplementary material as Figs. S4 and S5, respectively).

3.5. *Bacterial adhesion*

3.5.1. *Results of bacterial adhesion for collection strains*

Bacterial adhesion for collection strains, *S. aureus* and *S. epidermidis*, was analyzed by means of the percentage of surface covered by bacteria. Fig. 5 shows that bacterial adherence to modified surface materials (Ti–C–N_2 and Ti–C–N_2+Ag) was lower than in the control material (Ti6Al4V) for both strains ($p<0.0001$, Kruskal–Wallis test).

Taking into account the results obtained with the statistical analysis, it can be said that there were no statistical differences between both modified materials for *S. aureus* ($p=0.1072$, Kruskal–Wallis test), while such differences between both coated samples were statistically significant for *S. epidermidis* ($p<0.0001$, Kruskal–Wallis test).

In Fig. 6 the efficiency of the silver coating is observed in the presence of very low concentration of living bacteria on the surface represented by the green color for collection strains. The images have been selected because of their quality but they cannot be used for quantitative comparisons.

3.5.2. *Results of bacterial adhesion for clinical strains*

Bacterial adhesion for clinical strains, *S. aureus* and *S. epidermidis* obtained from patients was analyzed by means of the percentage of surface covered by bacteria. In Fig. 7 the results of adhesion of different clinical strain (p1…p12) for each material can be seen. As observed, Ti–C–N_2+Ag reduced the covered surface percentage except for p2, and in case of Ti–C–N_2 except for p1 and p2. Fig. 8 shows an example of images obtained for clinical isolates of *S. aureus* (p18) and *S. epidermidis* (p33), where the efficacy against bacteria of Ti–C–N+Ag is observed.

After statistical analysis, the conclusion is that the differences between the surfaces of Ti6Al4V and Ti–C–N_2 were statistically significant for all isolates except for p5 and p6 ($p=0.1033$ and 0.1032 respectively, Kruskal–Wallis). However, the differences between the surfaces of Ti6Al4V and Ti–C–N_2+Ag were statistically significant for all isolates except p1 and p2 ($p=0.0564$ and 0.1349 respectively, Kruskal–Wallis).

On the other hand, comparison of treated samples, Ti–C–N_2 and Ti_C_N_2+Ag, shows that the differences between both modified materials were statistically significant for all isolates except for p3 ($p=0.4272$, Kruskal–Wallis).

In Fig. 8, similarly to Fig. 6, some representative images have been selected, but in this case with clinic strains.

4. Discussion

4.1. *Effect of Ti–C–N coatings in tribocorrosion response*

Titanium implants inserted into the human body are usually surrounded with blood-rich tissue; this implies exposing the implant materials to a corrosive media. The release of vanadium and aluminum particles or metallic corrosion products may induce immune response in sensitive patients. Therefore, the assessment of a biomaterial or a coating able to avoid or reduce the tribocorrosion effect is required to ensure their safety in the corrosive environment of the human body.

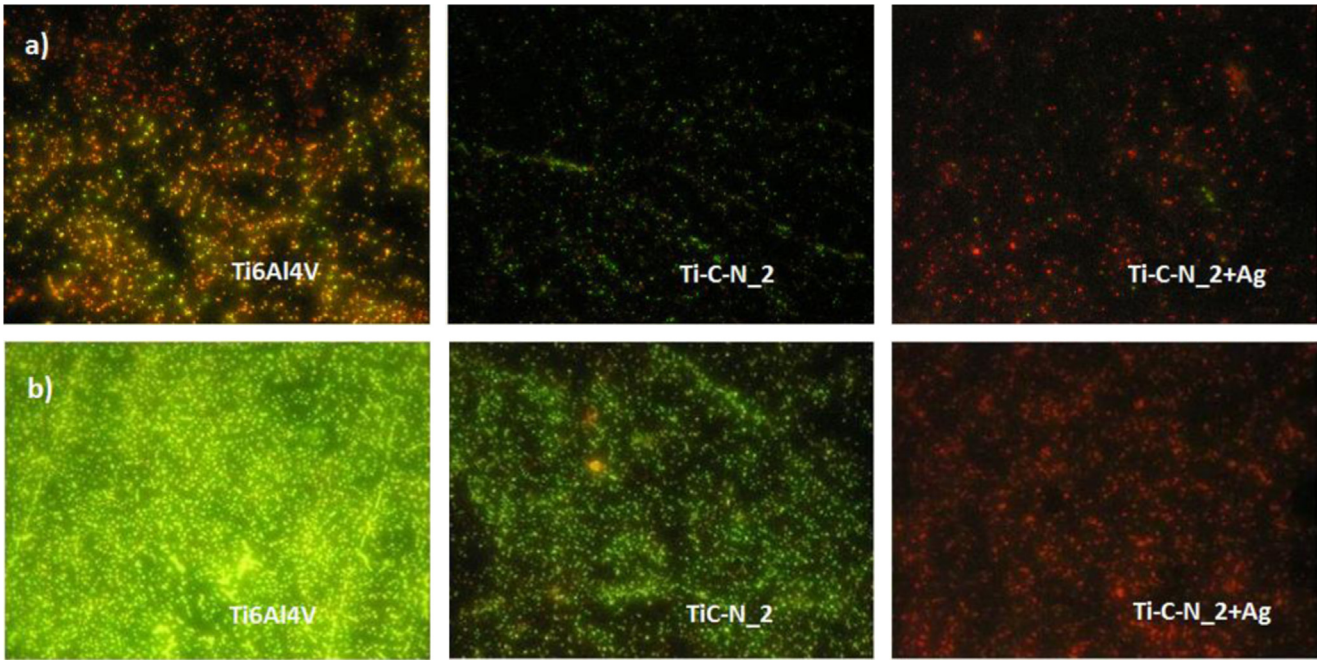

Fig. 6 – An example of the fluorescence microscope images for Ti6Al4V surface, Ti–C–N_2 surface and Ti–C–N_2+Ag surfaces covered by *S. aureus* (a) and *S.epidermidis* (b).

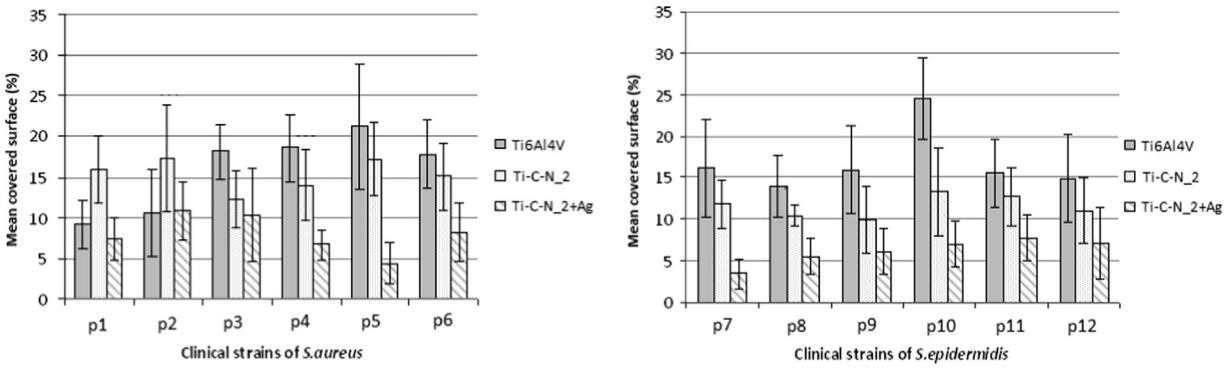

Fig. 7 – Mean percentage of surface covered biomaterial with clinical strains for each material.

In tribocorrosion tests performed in this work, it was observed that Ti–C–N_2 coating acts as a good barrier with a low friction coefficient and wear scar, and completely avoiding the releasing of elements from the substrate alloy to the electrolyte. This coating acts as a barrier able to protect the substrate from corrosion and wear processes avoiding the release of metallic ions and wear debris into the surrounding implant tissue as it was detected in a previous study of (Cheng and Zheng, 2006; Iwabuchi et al., 2007).

Concerning the corrosion resistance, it can be related to the microstructure of coatings. The initial lower corrosion resistance of Ti–C–N_2 compared with Ti–C–N_1 could be due to the columnar structure that presents the Ti–C–N_2 coating (Sáenz de Viteri et al., 2012). A columnar structure contains more open (through coating) porosity and straight grain species (Liu et al., 2011). It seems that the coating is self protected reducing the friction and wear under tribocorrosion conditions. The better tribological behavior of Ti–C–N_2 also could be due to the higher quantity of C in the coating in comparison to Ti–C–N_1 coating (Sáenz de Viteri et al., 2012). The higher carbon content could lead to the formation of a carbon-rich tribo-layer during the sliding process and be transferred to the counterpart which would have self-lubricating properties (Vitu et al., 2014; Wang et al., 2013).

4.2. *Effect of Ti–C–N coatings in tribological behavior*

The results of the fretting tests are of specific interest since the fretting effect that takes places between the backside of the patellar component and the tibial tray of fixed bearing tibial component is the main cause that leads to the knee implant failure. The poor response of Ti–C–N_2+Ag sample obtained in fretting tests was expected due to the low hardness of silver in comparison with titanium and DLC, that is, 2.5–3, 6 and 9.5 Mohs hardness, respectively (Bhushan and Gupta, 1991). It was expected that Ti–C–N coating had lower friction coefficient due to its excellent tribological properties generated by its auto-lubricious property. However, the

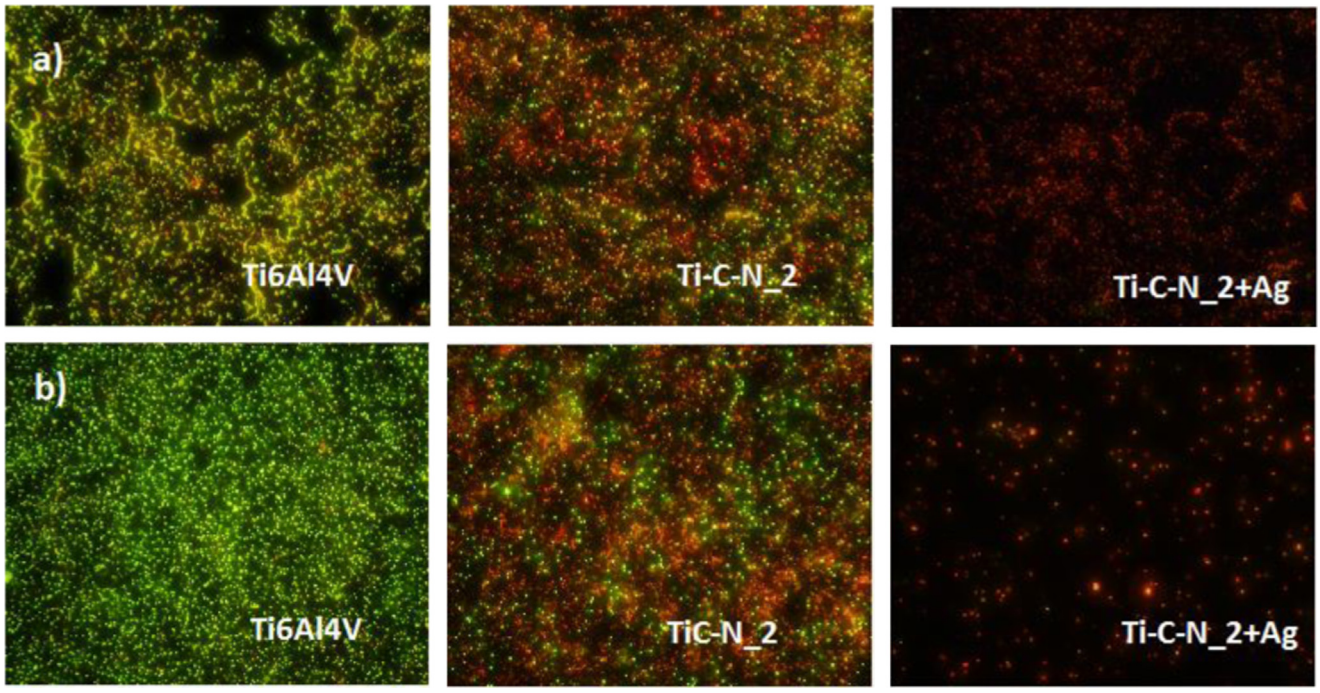

Fig. 8 – (a) Example of images taken with a fluorescence microscope to the surface of Ti6Al4V, Ti–C–N_2 and Ti–C–N_2+Ag covered by the clinical strain p4 of *S. aureus*. (b) Example of images taken with a fluorescence microscope to the surface of Ti6Al4V, Ti–C–N_2 and Ti–C–N_2+Ag covered by the clinical strain p8 of *S. epidermidis*.

results showed a similar coefficient for Ti–C–N_2 sample than Ti6Al4V. Sheeja et al. (2001) found that the wear resistance of UHMWPE sliding against DLC in simulated body fluid did not show any improvement over that of the untreated material. Though, analyzing the wear scars produced in the UHMWPE balls, the Ti–C–N_2 produced lower wear. This seems to indicate this coating is less aggressive than the Ti6Al4V. Alternatively, the presence of a carbon tribo-layer formed by the presence of carbon in the coating could reduce the wear in the UHMWPE balls.

Concerning the fast elimination of silver due to the friction process during the fretting test, this could have a positive effect in real applications, minimizing the risk of infection that could occur shortly after the implantation surgery process.

4.3. *Effect of Ti–C–N and silver coating in bacterial adhesion*

Implant devices are the most suitable to modification with the objective of preventing infection. Traditional surface-modifying preventive approaches have largely focused on antimicrobial coating of devices and resulted in variable clinical success in preventing device-associated infections (Esteban et al., 2014). The use of an antibacterial noble metal is one of the strategies to avoid bacterial adhesion. The incorporation of silver has produced a statistically significant decrease of adhesion with respect to the other materials for most of the strains. In general, all coated plates showed a decreased bacterial adherence for *S. aureus* and *S. epidermidis* collection strains and in most of the clinical strains in comparison to uncoated samples.

In this study, we evaluated the rough adherence of reference strains. These strains have a lower genetic load than clinical strains isolated from patients because they are laboratory-adapted strains which lose genes due to several passages on culture medium. Further experiments were performed to evaluate adherence using clinical strains isolated from patients with a diagnosis of prosthetic joint infection (which can show different properties than laboratory-adapted strains). These experiments showed slightly different behavior probably due to the different pathogenic properties of the strains.

Silver-based coatings have been studied in association with polymer and metal implants, particularly on external fixation pins. However, metallic silver mechanical properties are not adequate to constitute a load-bearing metal implant. So, the amount of silver deposited must be as low as possible in order to be useful in preventing implanted-related deep body infection caused in the first moments after surgery; and then keep the resistance against corrosion and wear from the Ti–C–N coating. Concerning the removed silver, it has been known to be eliminated via the renal system, and can be absorbed easily through the gastrointestinal system (Secinti et al., 2011).

Silver particles (5–50 nm), has been tested and in vitro results have shown that it is effective against methicillin-resistant *S. aureus* and *S. epidermidis* and have indicated that it is not cytotoxic due to its higher porosity and active surface (Harris and Richards, 2006).

Furthermore, released silver ions act immediately, as shown by blockage of protein activities, which is beneficial for preventing local infections. Possibly the main indication for these compounds will be prevention of perioperative

infections. The major effect on imported bacteria can occur immediately and vanishes relatively quickly. Thus, long-term bone damage and possible neutralization of silver effects by extracellular membrane components, which are deposited on implants, may be avoided.

Ti–C–N_2+Ag sample presented good bacterial anti-adhesive properties for both types of bacteria. Baba et al. (2013) have studied the effect of different Ag-containing diamond-like carbon films in antibacterial activity. In their results, they just observed small variations depending on the Ag content. They also observed an increase in the contact angle as the concentration of silver in the coating is increased. In this study, the content of silver is stable but it has observed that the contact angle after a period of stabilization, in case of Ti–C–N_2+Ag is higher than in the Ti–C–N_2 and substrate. There are several factors that influence the antibacterial behavior, such as the chemical roughness, chemical composition, the structure and the surface free energy. The latter can be quantified by measuring the contact angle. The threshold of hydrophobicity is a contact angle greater than 65° below this value it is considered hydrophilic (Vogler, 1998). In all analyzed samples, the contact angles values are lower than 65°, so that all samples are hydrophilic. As a general rule, high contact angles (low surface free energy) improve antibacterial properties decreasing the bacterial adhesion (Media et al., 2012; Zhou et al., 2008). This effect can be seen with all studied samples, confirming this theory. The Ti–C–N_2+Ag coating presented the highest contact angle and the bacterial adherence for *S. aureus* and *S. epidermidis* was the lowest one.

In this work it was also observed that silver-free coating, Ti–C–N_2, show antibacterial properties in comparison with Ti6Al4V sample. This effect was studied by Marciano et al. (2011) where they investigate into the antibacterial property and bacterial adhesion of diamond-like carbon films.

5. Conclusions

The purpose of this work was to develop a coating with good tribological properties, higher corrosion resistance and antibacterial activity. The tribocorrosion behavior has been in depth studied for two preselected Ti–C–N coatings. Taking into account the tribocorrosion response, Ti–C–N_2 coating was selected due to its excellent wear and high corrosion resistance and because it acts as a protective barrier against the release of substrate elements to outside. For this reason, a thin layer of silver was deposited on this coating in order to provide antibacterial properties. Fretting tests did not show so much difference between Ti–C–N_2 coating and Ti6Al4V, with similar friction coefficient and wear. However, the wear produced in the UHMWPE balls was lower for Ti–C–N_2 sample probably due to the generation of a carbon rich tribo-layer during the sliding process. Bacterial adhesion tests exhibited that silver has broad-spectrum anti-adherence activity and low risk of resistance. Their low wear resistance makes the layer disappear during rubbing contact, then their application should be limited to the avoidance of infection during implant fixation. The inherent antimicrobial properties of the Ti–C–N_2 layer makes then still active avoiding infections during the life of the implant. Therefore, it can be concluded that developed Ti–C–N_2+Ag coating could be a promising alternative for orthopedic applications with excellent tribological behavior, corrosion resistance and antibacterial properties.

Acknowledgment

The authors acknowledge FUNCOAT CONSOLIDER Project, financed by the Spanish Government, under contract CSD2008-00023 and to the Basque Country Government for the financing of EMAITEK project.

Appendix A. Supplementary material

Supplementary data associated with this article can be found in the online version at http://dx.doi:10.1016/j.jmbbm.2015.10.020.

REFERENCES

An, Y.H., Friedman, R.J., 1998. Concise review of mechanisms of bacterial adhesion to biomaterial surfaces. J. Biomed. Mater. Res. 43, 338–348.

Arslan, E., Totik, Y., Efeoglu, I., 2012. The investigation of the tribocorrosion properties of DLC coatings deposited on Ti6Al4V alloys by CFUBMS. Prog. Org. Coat. 74, 768–771.

Atiyeh, B.S., Costagliola, M., Hayek, S.N., Dibo, S.A., 2007. Effect of silver on burn wound infection control and healing: review of the literature. Burns 33, 139–148.

Baba, K., Hatada, R., Flege, S., Ensinger, W., Shibata, Y., Nakashima, J., Sawase, T., Morimura, T., 2013. Preparation and antibacterial properties of Ag-containing diamond-like carbon films prepared by a combination of magnetron sputtering and plasma source ion implantation. Vacuum 89, 179–184.

Bayón, R., 2011. Corrosion-Wear Behaviour of Novel Surface Coatings Developed by Means of Advanced Techniques (Ph.D. Thesis). University of Basque Country, Spain.

Bendavid, A., Martin, P.J., Comte, C., Preston, E.W., Haq, A.J., Magdon Ismail, F.S., Singh, R.K., 2007. The mechanical and biocompatibility properties of DLC-Si films prepared by pulsed DC plasma activated chemical vapor deposition. Diam. Relat. Mater. 16, 1616–1622.

Bhushan, B., Gupta, B.K., 1991. Handbook of Tribology: Materials, Coatings, and Surface Treatments. McGraw-Hill, New York.

Billi, F., Sangiorgio, S.N., Aust, S., Ebramzadeh, E., 2010. Material and surface factors influencing backside fretting wear in total knee replacement tibial components. J. Biomech. 43, 1310–1315.

Boulos, L., Prevost, M., Barbeau, B., Coallier, J., Desjardins, R., 1999. LIVE/DEAD BacLight: application of a new rapid staining method for direct enumeration of viable and total bacteria in drinking water. J. Microbiol. Methods 37, 77–89.

Brodner, W., Bitzan, P., Meisinger, V., Kaider, A., Gottsauner-wolf, F., Kotz, R., 1997. Elevated serum cobalt with metal-on-metal articulating surface. J. Bone Joint Surg. 79, 316–321.

Celis, J.P., Ponthiaux, P., 2012. Testing tribocorrosion of passivating materials supporting research and industrial innovation: Handbook EFC 62 Green Book. Publ. Manley, UK.

Cheng, Y., Zheng, Y.F., 2006. The corrosion behavior and hemocompatibility of TiNi alloys coated with DLC by plasma based ion implantation. Surf. Coat. Technol. 200, 4543–4548.
Cordero, J., Munuera, L., Folgueira, M.D., 1996. The influence of the chemical composition and surface of the implant on infection. Injury 27, SC34–SC37.
Cordero-Ampuero, J., Esteban, J., Garcia-Cimbrelo, E., Munuera, L., Escobar, R., 2007. Low relapse with oral antibiotics and two-stage exchange for late arthroplasty infections in 40 patients after 2–9 years. Acta Orthop. 78, 511–519.
Currier, J.H., Bill, M.A., Mayor, M.B., 2005. Analysis of wear asymmetry in a series of 94 retrieved polyethylene tibial bearing. J. Biomech. 38, 367–375.
Diomidis, N., Celis, J.P., Ponthiaux, P., Wenger, F., 2010. Tribocorrosion of stainless steel in sulfuric acid: identification of corrosion-wear components and effect of contact area. Wear 269, 93–103.
Edwards, C., Counsell, A., Boulton, C., Moran, C.G., 2008. Early infection after hip fracture surgery: risk factors, costs and outcome. J. Bone Joint Surg. Br. 90, 770–777.
Elek, S.D., Conen, P.E., 1957. The virulence of Staphylococcus pyogenes for man; a study of the problems of wound infection. Br. J. Exp. Pathol. 38, 573–586.
Esteban, J., Gomez-Barrena, E., Cordero, J., Martin-de-Hijas, N.Z., Kinnari, T.J., Fernandez-Roblas, R., 2008. Evaluation of quantitative analysis of cultures from sonicated retrieved orthopedic implants in diagnosis of orthopedic infection. J. Clin. Microbiol. 46, 488–492.
Esteban, J., Molina-Manso, D., Spiliopoulou, I., Cordero-Ampuero, J., Fernández-Roblas, R., Foka, A., Gómez-Barrena, E., 2010. Biofilm development by clinical isolates of *Staphylococcus* spp. from retrieved orthopedic prostheses. Acta Orthop. 81, 674–679.
Esteban, J., Pérez-Tanoira, R., Pérez-Jorge-Peremarch, C., Gómez-Barrena, E., 2014. Bacterial adherence to biomaterials used in surgical procedures. In: Kon, K., Rai, M. (Eds.), Microbiology for Surgical Infections. Diagnosis, Prognosis and Treatment. Elsevier, USA, pp. 41–60.
Garner, J.S., Jarvis, W.R., Emori, T.G., Horan, T.C., Hughes, J.M., 1988. CDC definitions for nosocomial infections. Am. J. Infect. Control 16, 128–140.
Gordon, O., Vig Slenters, T., Brunetto, P.S., Villaruz, A.E., Sturdevant, D.E., Otto, M., Landmann, R., Fromm, K.M., 2010. Silver coordination polymers for prevention of implant infection: thiol interaction, impact on respiratory chain enzymes, and hydroxyl radical induction. Antimicrob. Agents Chemother. 54, 4208–4218.
Gristina, A.G., 1987. Biomaterial-centered infection: microbial adhesion versus tissue integration. Science 237, 1588–1595.
Guggenbichler, J.P., Assadian, O., Boeswald, M., Kramer, A., 2011. Incidence and Clinical Implication of Nosocomial Infections Associated with Implantable Biomaterials-Catheters, Ventilator-Associated Pneumonia, Urinary Tract Infections. GMS Krankenhhyg Interdiszip, vol. 6, Doc18.
Hallab, N., Jacobs, J.J., Black, J., 2000. Hypersensitivity to metallic biomaterials: a review of leukocyte migration inhibition assays. Biomaterials 21, 1301–1314.
Harris, L.G., Richards, R.G., 2006. Staphylococci and implant surfaces: a review. Injury 37, S3–14.
Hodgson, A.W.E., Mueller, Y., Forster, D., Virtanen, S., 2002. Electrochemical characterization of passive films on Ti alloys under simulated biological conditions. Electrochim. Acta 47, 1913–1923.
Iwabuchi, A., Lee, J.W., Uchidate, M., 2007. Synergetic effects of fretting wear and sliding wear of Co-alloy and Ti-alloy in Hanks solution. Wear 236, 492–500.
Kaestner, P., Olfe, J., He, J.W., Rie, K.-T., 2001. Improvement in the load-bearing capacity and adhesion of TiC coatings on TiAl6V4 by duplex treatment. Surf. Coat. Technol. 142–144, 928–933.
Katsikogianni, M., Missirlis, Y.F., 2004. Concise review of mechanisms of bacterial adhesion to biomaterials and of techniques used in estimating bacteria-material interactions. Eur. Cells Mater. 8, 37–57.
Kinnari, T.J., Soininen, A., Esteban, J., Zamora, N., Alakoski, E., Kouri, V.P., Lappalainen, R., Konttinen, Y.T., Gomez-Barrena, E., Tiainen, V.M., 2008. Adhesion of staphylococcal and Caco-2 cells on diamond-like carbon polymer hybrid coating. J. Biomed. Mater. Res. A 86, 760–768.
Landolt, D., Mischler, S., Stemp, M., Barril, S., 2004. Third body effects and material fluxes in tribocorrosion systems involving a sliding contact. Wear 256, 517–524.
Liu, C., Leyland, A., Bi, Q., Matthews, A., 2011. Corrosion resistance of multi-layered PAPVD TiN and CrN coatings. Surf. Coat. Technol. 414, 164–174.
Marciano, F.R., Bonetti, L.F., Mangolin, J.F., Da-Silva, N.S., Corat, E.J., Trava-Airoldi, V.J., 2011. Investigation into the antibacterial property and antibacterial adhesion of diamond-like carbon films. Vacuum 85, 662–666.
Martinu, L., Raveh, A., Domingue, A., Bertrand, L., Klemberg-Sapieha, J.E., Gujrathi, S.C., Wertheimer, M.R., 1992. Hard carbon films deposited under high ion flux. Thin solid Films 208, 42–47.
Media, O., Nocua, J., Mendoza, F., Gómez-Moreno, R., Ávalos, J., Rodríguez, C., Morell, G., 2012. Bactericide and bacterial antiadhesive properties of the nanocrystalline diamond surface. Diam. Relat. Mater. 22, 77–81.
Mischler, S., 2008. Triboelectrochemical techniques and interpretation methods in tribocorrosion: a comparative evaluation. Tribol. Int. 41, 573–583.
Mischler, S., Ponthiaux, P., 2001. A round robin on combined electrochemical and friction tests on alumina/stainless steel contacts in sulphuric acid. Wear 428, 211–225.
Perez-Jorge, C., Conde, A., Arenas, M.A., Perez-Tanoira, R., Matykina, E., de Damborenea, J.J., Gómez-Barrena, E., Esteban, J., 2012. In vitro assessment of *Staphylococcus epidermidis* and *Staphylococcus aureus* adhesion on TiO(2) nanotubes on Ti–6Al–4V alloy. J. Biomed. Mater. Res. A 100, 1696–1705.
Perez-Tanoira, R., Isea-Pena, M.C., Celdran, A., Garcia-Vasquez, C., Esteban, J., 2014. Bacterial adherence to different meshes used in abdominal surgery. Surg. Infect. (Larchmt) 15, 90–93.
Perez-Tanoira, R., Perez-Jorge, C., Endrino, J.L., Gomez-Barrena, E., Horwat, D., Pierson, J.F., Esteban, J., 2012. Bacterial adhesion on biomedical surfaces covered by micrometric silver Islands. J. Biomed. Mater. Res. A 100, 1521–1528.
Ponthiaux, P., Bayón, R., Wenger, F., Celis, J.-P., 2013. Testing protocol for the study of bio-tribocorrosion. In: Yan, Y. (Ed.), Bio-tribocorrosion in Biomaterials and Medical Implants. Woodhead Publishing Limited, UK, pp. 372–394.
Raveh, A., Martinu, L., Gujrathi, S.C., Klemberg-Sapieha, J.E., Wertheimer, M.R., 1992. Structure-property relationship in dual-frequency plasma deposited hard a-C:H films. Surf. Coat. Technol. 53, 275–282.
Rochford, E.T., Richards, R.G., Moriarty, T.F., 2012. Influence of material on the development of device-associated infections. Clin. Microbiol. Infect. 18, 1162–1167.
Rogers, S.D., Howie, D.W., Graves, S.E., Pearcy, M.J., Haynes, D.R., 1997. In vitro human monocyte response to wear particles of titanium alloy containing vanadium or niobium. J. Bone Joint Surg. 79B, 311–315.
Sáenz de Viteri, V., Barandika, M.G., Ruiz de Gopegui, U., Bayón, R., Zubizarreta, C., Fernández, X., Igartua, A., Agullo-Rueda, F., 2012. Characterization of Ti–C–N coatings deposited on Ti6Al4V for biomedical applications. J. Inorg. Biochem. 117, 359–366.
Sargeant, A., Goswami, T., 2007. Hip implants – paper VI – ion concentrations. Mater. Des. 28, 155–171.

Secinti, K.D., Ozalp, H., Attar, A., Sargon, M.F., 2011. Nanoparticle silver ion coatings inhibit biofilm formation on titanium implants. J. Clin. Neurosci. 18, 391–395.

Sharkey, P.F., Hozack, W.J., Rothman, R.H., Shastri, S., Jacoby, M., 2001. Why are total knee arthroplasties failing today?. Clin. Orthop. Relat. Res. 404, 7–13.

Sheeja, D., Tay, B.K., Lau, S.P., Nung, L.N., 2001. Tribological characterization of diamond-like carbon coatings on Co–Cr–Mo alloy for orthopaedic applications. Surf. Coat. Technol. 146–147, 410–416.

Singhai, M., Malik, A., Shahid, M., Malik, M.A., Goyal, R., 2012. A study on device-related infections with special reference to biofilm production and antibiotic resistance. J. Glob. Infect. Dis. 4, 193–198.

Sinnett-Jones, P.E., Wharton, J.A., Wood, R.J.K., 2005. Micro-abrasion-corrosion of a CoCrMo alloy in simulated artificial hip joint environments. Wear 59, 898–909.

Snyders, R., Bousser, E., Amireault, P., Klemberg-Sapieha, J.E., Park, E., Taylor, K., Casey, K., Matinu, L., 2007. Tribo-mechanical properties of DLC coatings deposited on nitrided Biomedical Stainless Steel. Plasma Process. Polym. 4, S640–S646.

Valle, J., Toledo-Arana, A., Berasain, C., Ghigo, J.M., Amorena, B., Penadés, J.R., Lasa, I., 2003. SarA and not sigmaB is essential for biofilm development by *Staphylococcus aureus*. Mol. Microbiol. 48, 1075–1087.

Vieira, A.C., Ribeiro, A.R., Rocha, L.A., Celis, J.P., 2006. Influence of pH and corrosion inhibitors on the tribocorrosion of titanium in artificial saliva. Wear 261, 994–1001.

Vitu, T., Escudeiro, A., Polcar, T., Cavaleiro, A., 2014. Sliding properties of Zr-DLC coatings: the effect of tribolayer formation. Surf. Coat. Technol. 258, 734–745.

Vogler, E.A., 1998. Structure and reactivity of water at biomaterial surfaces. Adv. Colloid Interface Sci. 74, 69–117.

Wang, P., Hirose, M., Suzuki, Y., Adachi, K., 2013. Carbon tribolayer for super-low friction of amorphous carbon nitride coatings in inert gas environments. Surf. Coat. Technol. 221, 163–173.

Xuanyong, L., Paul, K.C., Chuanxian, D., 2004. Surface modification of titanium, titanium alloy, and related materials for biomedical applications. Mater. Sci. Eng. R 47, 49–121.

Yildiz, F., Yetim, A.F., Alsaran, A., Çelik, A., 2007. Plasma nitriding behavior of Ti6Al4V orthopaedic alloy. Surf. Coat. Technol. 202, 2471–2476.

Zhecheva, A., Sha, W., Malinov, S., Long, A., 2005. Enhancing the microstructure and properties of titanium alloys through nitriding and other surface engineering methods. Surf. Coat. Technol. 200, 2192–2207.

Zhou, H., Xu, L., Ogino, A., Nagatsu, M., 2008. Investigation into antibacterial property of carbon film. Diam. Relat. Mater. 17, 1416–1419.

Procedure S1. TRIBOCORROSION EXPERIMENTAL PROCEDURE

Prior to the wear tests, samples remained into the electrolyte for 60 minutes till reach a stable open circuit potential (OCP). After this initial immersion time, an electrochemical impedance spectroscopy was performed to analyze the electrochemical state of the surfaces before the tribological test. The duration of the first mechanical tests was of 1000 cycles. During this stage, the open circuit potential under sliding and friction coefficient were registered simultaneously. After this stage, a second sliding process of 3500 cycles was then performed under potentiostatic control by imposing to the system the previous potential measured during sliding. At the same time, a second electrochemical impedance spectroscopy was additionally performed during the sliding. After 3500 cycles, the samples were removed from the electrolyte, cleaned ultrasonically with alcohol for 5 min, and dried in warm air. The wear tracks were analyzed by confocal microscopy (Nykon Eclipse ME600 Confocal Microscopy) performing topographical measurements at different locations of the wear tracks.

Fig. S1. FRICTION COEFFICIENT EVOLUTION DURING SLIDING PROCESS IN TRIBOCORROSION TESTS

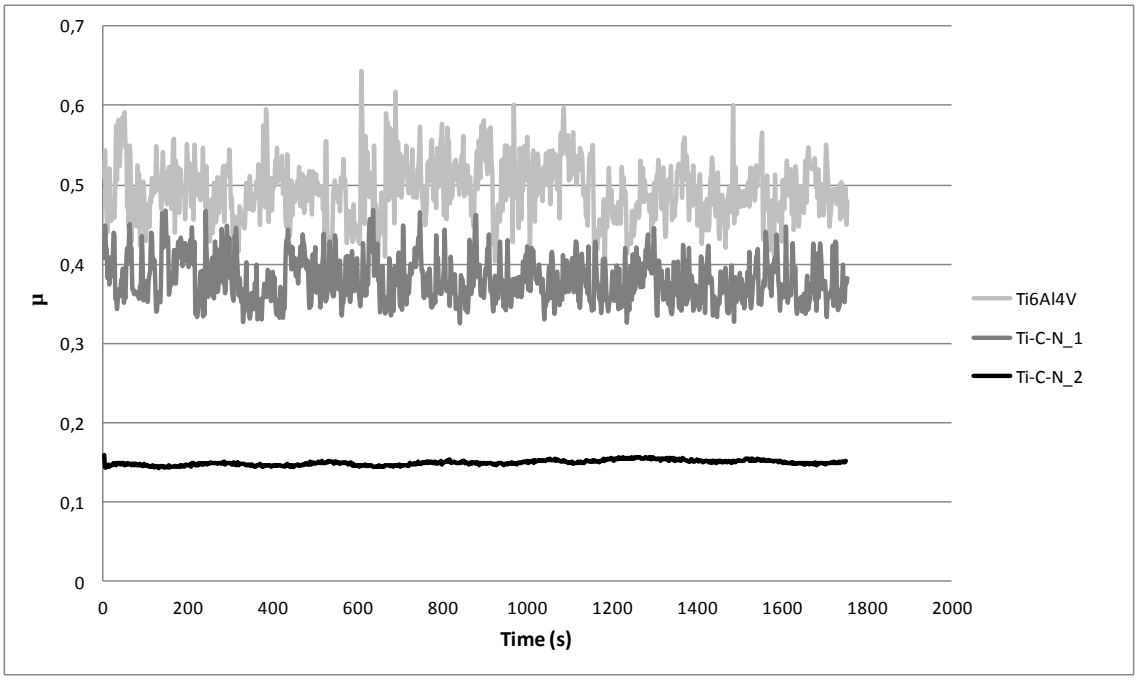

Fig. S2. PROFILES OF THE WEAR SCARS OBTAINED AFTER TRIBOCORROSION TESTS

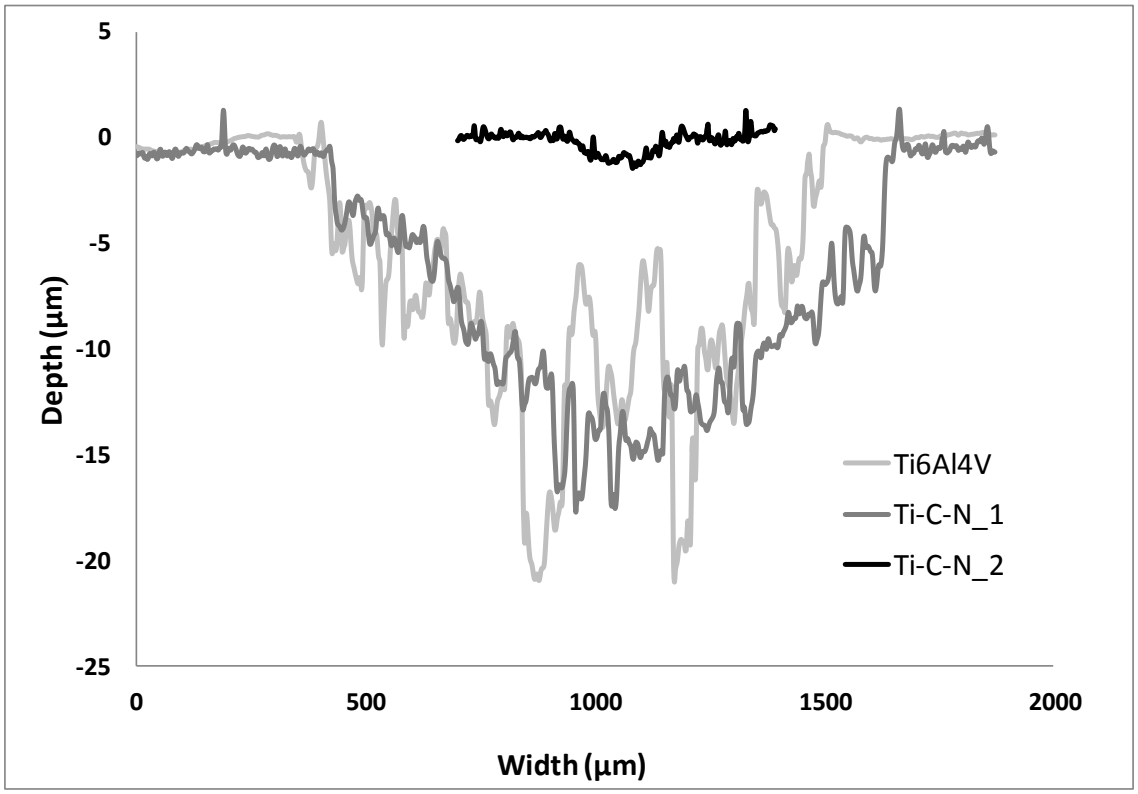

Table S1. ELEMENTS DETECTED BY ICP MEASUREMENTS IN THE ELECTROLYTES USED IN TRIBOCORROSION TESTS

	Dissolved elements (mg/l)			**Total elements (mg/l)**		
Sample	Ti	Al	V	Ti	Al	V
Reference (PBS)	<0.01	<0.01	<0.01	<0.01	<0.01	<0.01
Ti6Al4V	<0.01	<0.01	<0.01	4.3	0.25	0.20
Ti-C-N_1	<0.01	<0.01	<0.01	2.14	0.19	0.078
Ti-C-N_2	<0.01	<0.01	<0.01	<0.01	<0.01	<0.01

Fig. S3. FRICTION COEFFICIENT EVOLUTION IN FRETTING TESTS

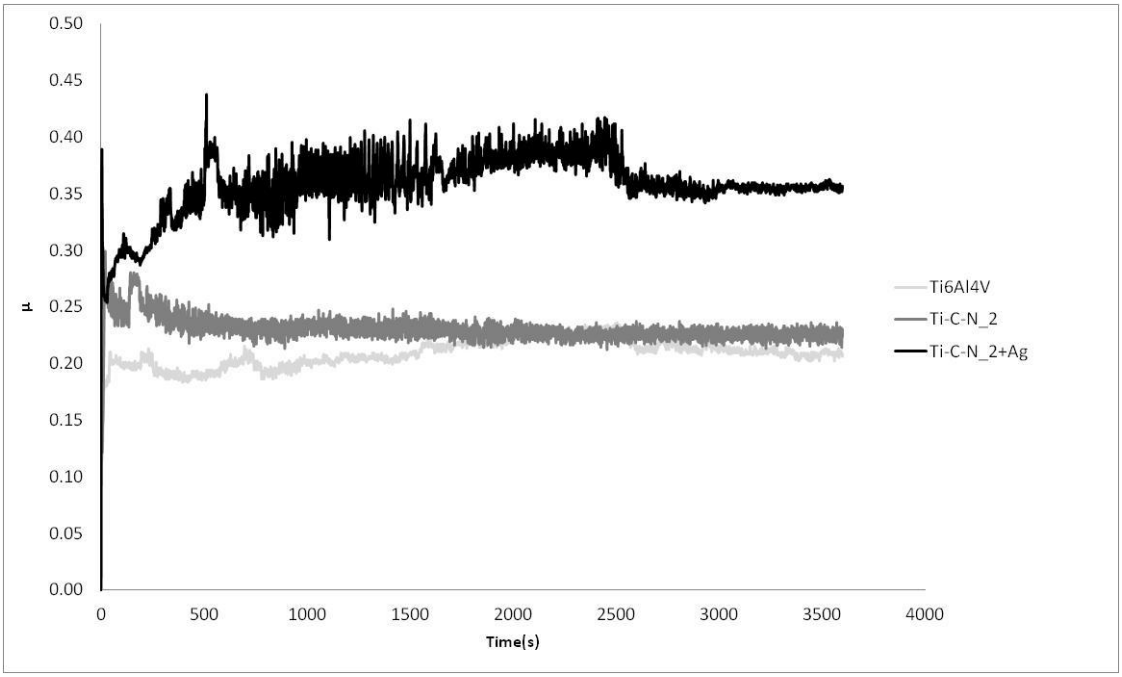

Fig. S4. IMAGES OBTAINED BY OPTICAL MICROSCOPE OF WEAR SCARS IN UHMWPE USED AS COUNTERBODY IN FRETTING TESTS AND TESTED AGAINTS: a) Ti6Al4V, b) Ti-C-N_2 and c) Ti-C-N_2+Ag

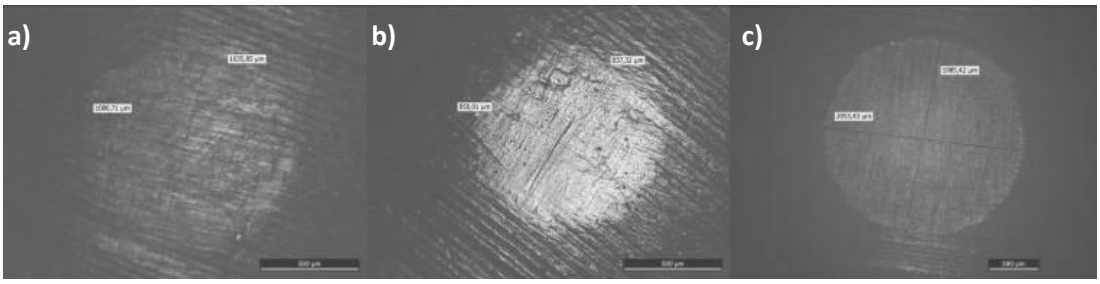

Fig. S5. MICROGRAPHY AND EDS SPECTRUM OF WEAR SCAR IN THE SAMPLE Ti-C-N_2+Ag AFTER FRETTING TEST AND WHERE IT CAN BE OBSERVED THE Ag WERE COMPLETELY REMOVED DURING SLIDING PROCESS (a) OUTSIDE THE SLIDING AREA AND b) IN THE WEAR SCAR

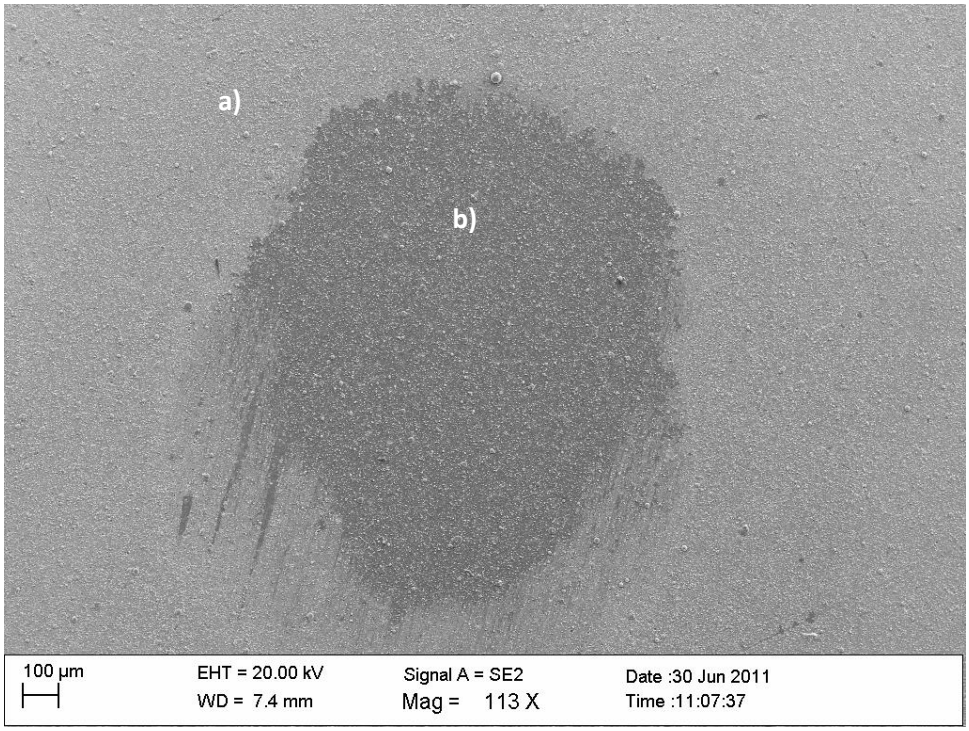
a)
b)
100 µm
EHT = 20.00 kV
WD = 7.4 mm
Signal A = SE2
Mag = 113 X
Date :30 Jun 2011
Time :11:07:37

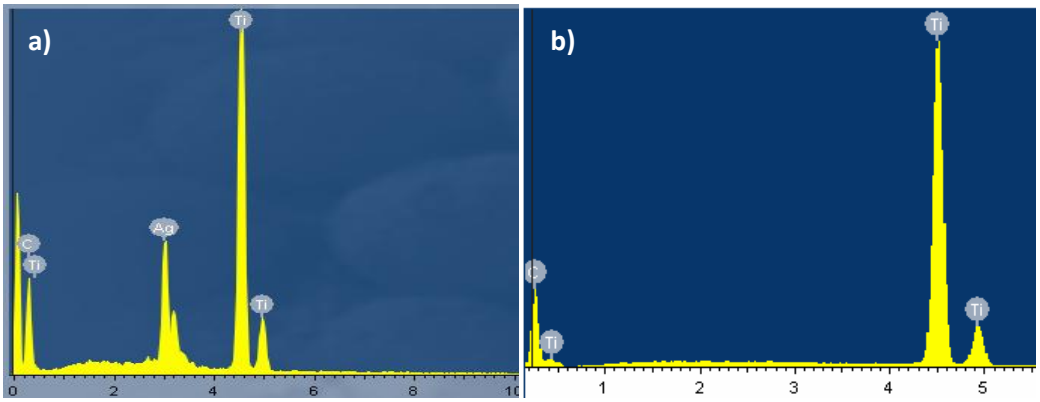
a)
C
Ti
Ag
Ti
Ti
0
2
4
6
8
b)
Ti
Ti
Ti
1
2
3
4
5

Structure, tribocorrosion and biocide characterization of Ca, P and I containing TiO_2 coatings developed by plasma electrolytic oxidation

V. Sáenz de Viteri[a], R. Bayón[a], A. Igartua[a], G. Barandika [b], J. Esteban Moreno[c], C. Pérez-Jorge Peremarch[c] and M. Martínez Pérez[c]

[a] IK4-Tekniker, Polo Tecnológico de Eibar, Calle Iñaki Goenaga, 5, 20600, Eibar, Spain
[b] Departamento de Química Inorgánica, Facultad de Ciencia y Tecnología, Universidad del País Vasco, UPV/EHU, Apartado 644, E-48080 Bilbao, Spain
[c] Department of Clinical Microbiology, IIS-Fundación Jiménez Díaz, Av. Reyes Católicos 2, Madrid 28040, Spain

Abstract

In hip joint implants, in particular in the stems, wear-corrosion effects can accelerate the degradation of the biomaterial. The lack of osseointegration and the risk of contracting implant-associated infections may be other reasons for a premature failure of the implant. In this work, TiO_2 coatings have been developed by means of Plasma Electrolytic Oxidation (PEO) technique in order to achieve wear-resistant hard coatings with osseointegration ability and biocide characteristics. During the PEO process, elements that favor cell growth, like Ca and P, were introduced into the coating. With the purpose of providing the coating with antibacterial properties iodine was added like biocide agent. The microstructure and chemical composition of the developed coatings were analyzed in order to see if the surface of the films was suitable for the cell attachment. The effect of wear-corrosion synergy was studied by means of tribocorrosion tests. Finally, the biocide capacity of iodine against *S. aureus* and *S. epidermidis* was analyzed through bacterial adhesion tests. High wear and corrosion resistance was shown in one of the developed coatings. The achieved surface microstructures seem to be appropriate to improve the osseointegration with proper pore size and porosity index. The antibacterial capacity of iodine was confirmed for *S epidermidis*.

1. Introduction

According to the European Society of Biomaterial (ESB), a biomaterial is a material destined to interact with the biological systems to evaluate, treat, increase or replace some tissue, organ or body function. In the case of orthopedic implants, the main property required to a biomaterial to be compatible is to avoid an adverse reaction when placed into the body. As well, chemical stability, good mechanical properties, osseointegration, high corrosion resistance and excellent wear resistance are required. In this sense, titanium and its alloys have become the premier choice for biocompatible orthopedic implant materials because of their high load strength bearing capacity, high strength to weight ratio, low toxicity, chemical stability, superior mechanical properties, excellent corrosion resistance and high biocompatibility [1][2][3]. Nevertheless, their poor tribological properties limit their use [4]. This tribological behavior is characterized by high coefficient of friction, severe adhesive wear with strong tendency to seizure and

low abrasion resistance [5]. In the human body there are tribological contacts created as a consequence of locomotion that can contribute to the accelerated degradation of the material [6][7][8]. This can lead to crack initiation, excessive wear and release of wear debris from the implant into bloodstream or early fracture of the implant, as well as serious inflammatory reactions, allergies or osteolysis, which can significantly shorten the lifespan of the implanted device [9][10][11][12]. On the other hand, the exposure of the biomaterial to the body fluids can induce corrosion damage on the material leading to irreversible material degradation process. This electrochemical process combined to the wear produced as a result of the relative contact movement of the implant, results in a process called tribocorrosion. This effect takes into account the synergistic interaction of wear and corrosion phenomena on surfaces subjected to a relative contact movement in biological environments [13].

On the other hand, from the biological point of view, two major complications may also be present in an implant: the lack of bone tissue integration of titanium and its alloys due to the lack of interface bioactivity and the post-operative infections from attached bacteria and following proliferation on the surfaces of implants [14].

After biomaterial implantation into the body, a complex series of reactions (mechanisms) take place on its surface [15]. The material osseointegration occurs in different steps, including the adsorption of proteins to the biomaterial surface, the contact and attachment of cells, and its subsequent surface diffusion [16][17][18]. Surface wettability, initially, may play a major role in adsorption of proteins onto the surface, as well as the later cell adhesion. Generally, hydrophobic surfaces are more prone to protein-absorption than hydrophilic ones, due to the stronger hydrophobic interactions [19]. Other studies have reported that surfaces with moderate hydrophilicity display improved cell growth and biocompatibility [20]. Nevertheless, cell adhesion can decrease as the material becomes too hydrophilic. Other factors that play an important role in the protein adsorption are the surface topography, where a high porosity may facilitate the contact with proteins, the chemical composition and surface heterogeneity.

Implant-associated infections generally result from bacterial adhesion to the surface of the implant and the following formation of the bio-film at the implant-tissue interface [21]. Sometimes, the outbreak of an infection mask the ongoing soreness of tissue inflammation process after surgery, and infection diagnosis often occurs when a full-blown infection has already caused damage to tissue and host organism. This often involves the need for a second surgery to replace total or partial the infected device, leading to substantial patient health risk, involving additionally high medical costs [22]. The most common species that cause implant-associated infections are *Staphylococcus aureus, Staphylococcus epidermidis, Enterobacteriaceae, Pseudomonas aeruginosa and Candida fungus [23]*.

A possible method to solve wear-corrosion problems, improve the osseontegration properties of a device and reduce the incidence of implant-related infections is to use surface treatments as Plasma Electrolytic Oxidation (PEO) technique. The PEO process consist of the modification of the growing anodic film by spark/arc micro-discharges in aqueous solutions, which are initiated at potentials above the breakdown voltage of the growing oxide film and move rapidly across the anode surface. The discharge leads locally to high temperature and high pressure plasma-chemical

reactions, generating a porous coating. Developed coating usually contains constituent species derived from the substrate and the electrolyte. This character reveals that PEO coating has excellent bonding strength to the substrate due to its in situ growth process and apart from corrosion resistance, they exhibit high hardness and good wear resistance. Moreover, it is possible to adjust the composition of the used electrolyte, to introduce desired elements into the coating, producing functional films with osseointegration or biocide properties.

By PEO technique, it can be produced TiO_2 coatings in two crystallographic phases: anatase and rutile. Anatase exhibits poor corrosion resistance in contact with some acids and halide solutions, while rutile generally possesses much better protective characteristics. It has a high stability, good mechanical properties because of its higher hardness and is denser than anatase form. All these characteristics are responsible for the significance of the rutile in orthopedic implants. So it is of great interest that the developed TiO_2 layers are mainly rutile, allowing improving the tribological properties of the titanium alloy. Concerning the microstructure of TiO_2 layers obtained by this technology, they have a porous and rough surface which makes them appropriate for cell adhesion [24][25][26]. Additionally, the presence of Ca and P in the coating has been reported to be advantageous to cell growth [27][28][29][30]. “In vivo” data showed implant surfaces containing both Ca and P enhanced bone apposition of the implant surface [31].

In order to reduce the incidence of implant-related infections, antibacterial properties can provide to the coatings, adding antimicrobial agents during the PEO process. Silver, cooper and fluoride have been the most common antimicrobial agents used until now in implants [22][32][33][34]. Other antimicrobial agent that has been less studied for this application is the iodine. Iodine is the heaviest essential element needed by all living microorganism and is a component of thyroid hormones. Some studies indicate that iodine supported titanium has antibacterial activity, biocompatibility and no citotoxicity [35][1]. However, iodine sublimes at room temperature, making it difficult to work with it.

The aim of this work is to develop TiO_2 coating with high wear-corrosion resistance, a proper surface morphology to promote the cells growth and antibacterial properties. The Ti6Al4V is the implant material of choice for use in hip joint stem implants. So, in this work, various TiO_2 layers have been developed on Ti6Al4V substrate by controlling the applied current intensity and processing time used in the plasma electrolytic oxidation (PEO) technology. Ca and P elements have been added to the electrolyte to generate a suitable surface for cell adhesion to improve the osseointegration. Also, addition of iodine to the electrolyte was carried out in order to provide the coating with antibacterial properties. To complete the characterization, the thickness, roughness and porosity values were measured. The microstructure and chemical composition have been analyzed by means of XRD (X-Ray Diffraction), SEM (Scanning Electron Microscope), EDS (Energy Dispersive Spectroscopy) and XRF (X-Ray Fluorescence) techniques. Tribocorrosion tests have been performed to analyze the wear-corrosion synergy. And finally, the antibacterial efficacy has been evaluated studying the bacterial adherence.

2. Materials and methods

2.1. Materials

Ti6Al4V (grade 5) discs with dimensions of 24 mm diameter and 7.9 mm height were manufactured. Prior to PEO process, the surface of the Ti6Al4V specimens was ground by using 1200 grids SiC paper and then, submitted to a chemical attack being immersed for 10-15 seconds in a mixture of $HF:HNO_3:H_2O$. Finally, the samples were cleaned ultrasonically in distilled water, rinsed with alcohol and dried in warm air.

2.2. Plasma electrolytic oxidation

The titanium discs were subjected to PEO treatments in an aqueous electrolyte containing calcium acetate hydrate ($(CH_3COO)_2Ca \cdot H_2O$), beta-glycerophosphoric acid disodium salt pentahydrate ($C_3H_7Na_2O_6P \cdot 5H_2O$) and sodium iodide (NaI) at different process conditions (PEO-1: 5 A/dm^2 during 19 minutes; PEO-2: 15 A/dm^2 during 5 minutes). The pH of the electrolyte was around 7.5. All experiments were carried out in a water-cooled bath with a stirring system that ensured an electrolyte temperature below 20ºC. A stainless steel mesh was used as the cathode, while titanium samples acted as anode. The total area of titanium exposed for each sample to electrolyte was 4.5 cm^2. After PEO process, the samples were immersed in a potassium iodide (KI) saturated solution for 24 hours. After some tests, it was observed that this last treatment seems to help to maintain the iodine into the coating avoiding its sublimation.

2.3. Surface characterization

The thickness of the PEO coatings was measured by using a Dual-Scope (Fischer) probe. The average roughness was obtained by a profilometer (Perthometer M2, Mahr) at 10 randomly selected locations.

The microstructure of the specimens was evaluated by Scanning Electron Microscopy (SEM, Zeiss GEMINI®). The average pore size was calculated with the Graff-Snyder method and the pore percentage was analyzed by ImageJ software. The chemical composition of the samples was analyzed by Energy Dispersive Spectroscopy (EDS) and X-ray Fluorescence Spectroscopy (XRF) with S8 TIGER equipment, from BRUKER. The phase structure of the PEO coatings were detected by X-ray diffraction method (PHILIPS PW1710 powder diffractometer) using Cu-Kα radiation in steps of 0.02° over the 5–69.96° 2θ-angular range and a fixed-time counting of 1 s at 25 °C.

Hydrophilic/hydrophobia grade analyzed by means of wettability tests was carried out in the SURFTENS universal goniometer. The contact angle formed between a drop of distilled water and the surface under study was recorded by an optical camera and calculated with specialized software.

2.4. Tribocorrosion tests

Tribocorrosion tests were performed in a Microtest Tribometer, in rotating sliding conditions under ball on disc configuration. The rotating velocity was 20 rpm, the applied normal load 3 N and the radius track 5 mm. Tests were carried out during 200 cycles. The counterbody was an Al_2O_3 ball with 10 mm of diameter. The tests were done under lubricated conditions by using phosphate buffered saline (PBS) solution,

consisting of 0.14 M NaCl, 1 mM KH_2PO_4, 3 mM KCl, and 10 mM Na_2HPO_4. The exposed area in all samples was 2.5 cm^2. Electrochemical measurements were assisted by an Autolab-Methrom potentiostat PGSTAT302N. A three-electrode system was used, corresponding as the working electrode the Ti6Al4V samples, as the counter electrode a platinum (Pt) wire and as the reference electrode Ag/AgCl KCl 3M (0.207 V vs SHE) electrode. Prior sliding tests, open circuit potential (OCP) was monitored until achieving a stable value. During the sliding, OCP and friction coefficient were monitored. Once the wear process had been completed, OCP was recorded until new stabilization. Before and after the wear process, two electrochemical impedance spectroscopies (EIS) were registered. The sinusoidal wave was 10 mV of amplitude in the frequency range from 10^5 Hz to 10 mHz under OCP conditions. Completed the tribocorrosion test, samples were ultrasonically cleaned in distilled water for 5 minutes and dried in warm air.

The morphology of wear tracks was analyzed by means of the scanning electron microscopy (SEM) and chemical composition in sliding area was analyzed by EDS. Topographical measurements were made using a confocal microscope (Nykon).

2.5. Bacterial adhesion

2.5.1. Staphylococcal adhesion experiments

Bacterial adhesion to a material surface is the first step in biofilm development. TiO_2 coatings were compared against control of untreated Ti6Al4V samples. Staphylococcal adhesion experiments were performed as described by Kinnari et al. and Perez-Tanoira et al. [36][37].

For the preliminary study of bacterial adhesion, the biofilm-forming collection strains, *Staphylococcus aureus* 15981 (CITA) and *Staphylococcus epidermidis* ATCC 35984 have been used.

2.5.2. Statistical analysis

For the statistical study, non parametric tests were employed. Mann-Whitney or Wilcoxon were used for two samples and the Kruskal-Wallis test was used for more than two samples. EPI-Info software version 3.5.1 (CDC, Atlanta, GA. USA) was employed to perform the statistical studies.

3. Results and discussion

3.1. Surface characterization

The surface characterization related to mean thickness, roughness, pore size, porosity percentage and contact angle values of developed coatings are represented in Table 1.

Table 1.
Thickness, roughness, pore size and contact angle values.

Samples	Thickness (µm)	Roughness Ra, (µm)	Pore size (µm)	Porosity percentage (%)	Contact angle (°)
Ti6Al4V	-	0.26 ± 0.03	-	-	65 ± 2
PEO-1	3.31 ± 0.21	0.43 ± 0.04	5.39 ± 2.66	9	107 ± 2
PEO-2	4.49 ± 0.40	0.42 ± 0.05	7.25 ± 2.96	5	96 ± 5

The thickness of the coating increased when increasing the current density. The same effect was seen in a previous study carried out by Shin et al. [38], where they attributed this effect to the fact that at high current densities, the anodic reactions that take place at the interface with titanium substrate are induced with much more energy leading to a rapidly TiO_2 coating formation. Concerning the roughness of coatings, in both surfaces the roughness increased after the PEO process, without significant differences between them. This increase was influenced by both the pore size and porosity percentage, present in the surface [28][39].

Figure 1 shows the surface morphology of the developed titanium oxide layers. SEM analysis exhibited the porous structure of coatings and the range of sizes. It seems that PEO-2 coating has a more homogeneous surface with better pore distribution. By SEM analysis and with the Graff-Snyder method the average pore size was calculated, obtaining for PEO-1 a pore size lower than for the PEO-2, that is, 5.39 µm and 7.25 µm, respectively. Concerning the pore percentage, it seems that increasing the current density in the process, apart from increase the pore size, the quantity of pore increase with a percentage of porosity in PEO-2 of 5%, whereas for PEO-1 was 9%. The bigger pores size obtained with the higher current density can be due to the large and long-lived discharges that take place in the surface and consequently form enlarged pores. In both coatings the pore size is within the suitable range of pore sizes for cell anchoring [40]. Cracks observed in the micrographs in the surface of TiO_2 coating are attributed to thermal stresses [41].

Shin et al. found that TiO_2 surface with the smallest pore size (≈ 2 µm) and the highest porosity percentage showed the best results *in vitro* cell test, being the most suitable surface for cell anchoring [38]. Taking this fact into account, it can be concluded that PEO-1 could be the best coating to improve the osseointegration of stem. This coating has the smallest pore size and the highest quantity of pore.

Wettability tests showed that both coatings have a hydrophobic behavior with contact angles above 90°. Taking into consideration that hydrophobic surfaces are more suitable for protein adsorption [19], the PEO-1 coating seems to be the most promising selection to improve the osseointegration of the implants.

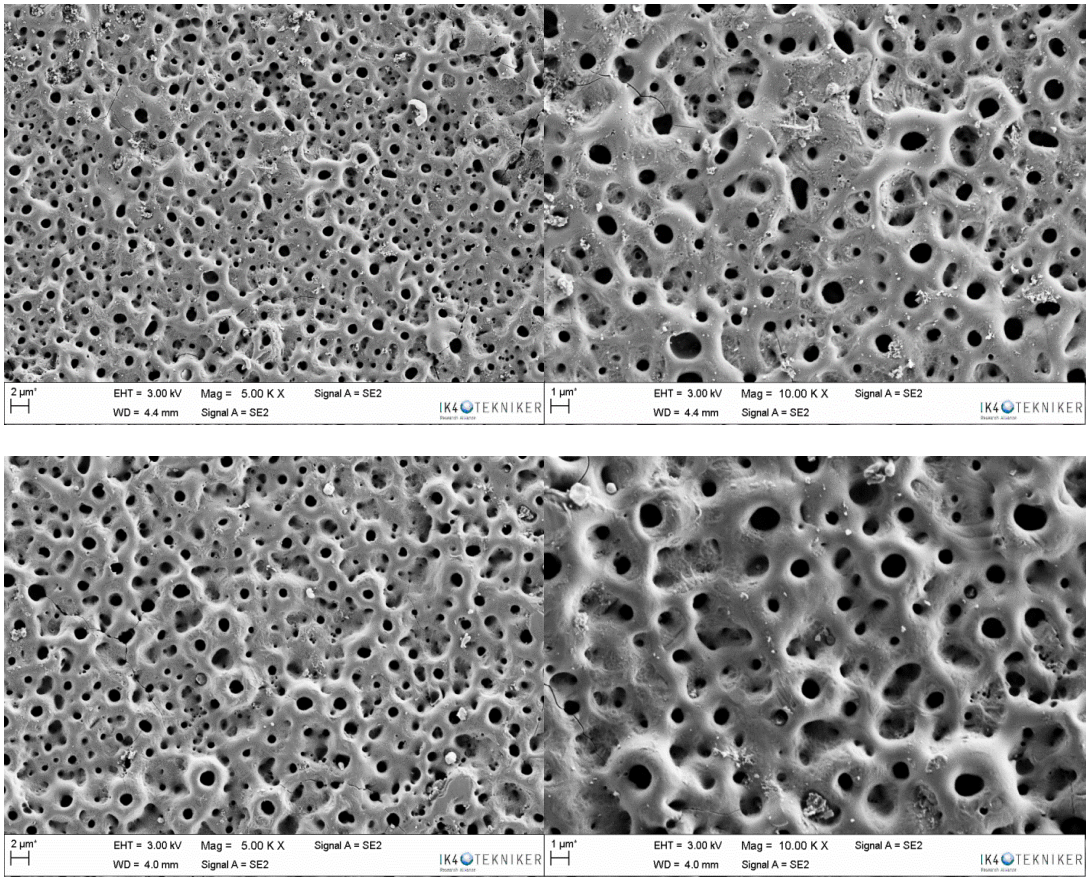

Fig. 1. SEM micrographs of the developed coatings.Top micrographs correspond to PEO-1 (left 5 KX and right 10 KX) and bottom micrographs correspond to PEO-2 (left 5 KX and right 10 KX).

Concerning the chemical composition, the EDS spectra of analysis carried out in different areas of the developed coatings are shown in figure 2. In both cases, the elements from the substrate were detected, and those related to the developed electrolyte, Ca, P, Na. Also K from the saturated KI solution appeared. The presence of iodine in the coatings was also confirmed.

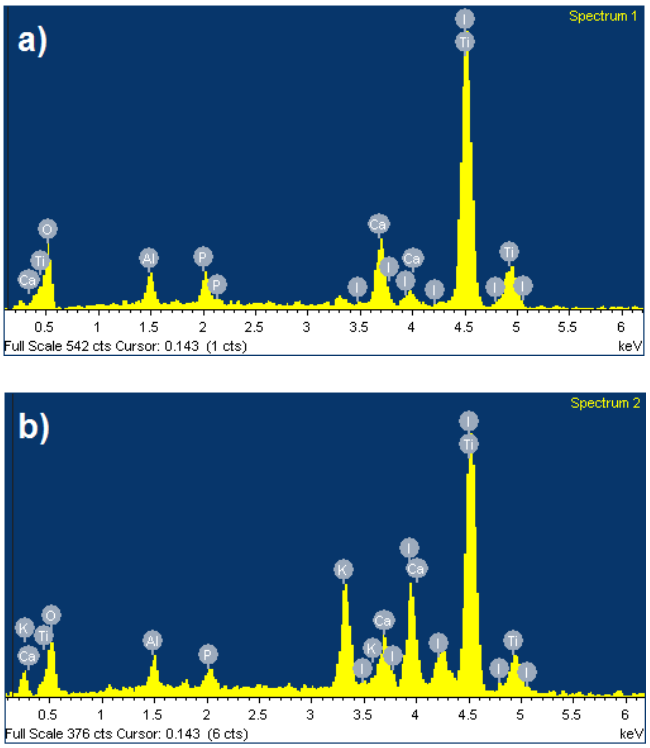

Fig. 2. EDS spectra of the PEO coatings: a) PEO-1 and b) PEO-2.

In order to get an idea of how similar the two developed coatings are in terms of chemical composition, XRF analysis was performed (XRF patterns in Figure S1 in supplementary material). With this technology the analysis area is bigger than that studied by EDS. This study was carried out taking into account the count numbers. The intensity of peaks was compiled in table S1 (Kcps in table S1 located in supplementary information). The concentration of elements from the electrolyte increased with increasing the current in the PEO process while that of the substrate decreased. It seems to indicate that an increase in the voltage favors a greater insertion of elements from the substrate into the TiO_2 layer [28]. The presence of iodine was also confirmed by this technique.

Chemical composition in depth obtained by means of GD-OES analysis showed a similar element´s distribution through the coatings (Fig. 3). In the right side of both graphs, the elements from the titanium alloy are observed. As the layer grows, a decrease of the elements from the substrate, the appearance of the elements belonging to the electrolyte and a significant presence of oxygen, due to the oxides formed during the PEO process, are observed. It can be noted that there are more species from the electrolyte in the coating surface than near the substrate. There are studies which suggested that discharges that occur near the coating surface may incorporate more elements from the electrolyte [42][43][44]. In this analysis, no iodine was detected, since the equipment was not prepared to analyze this element.

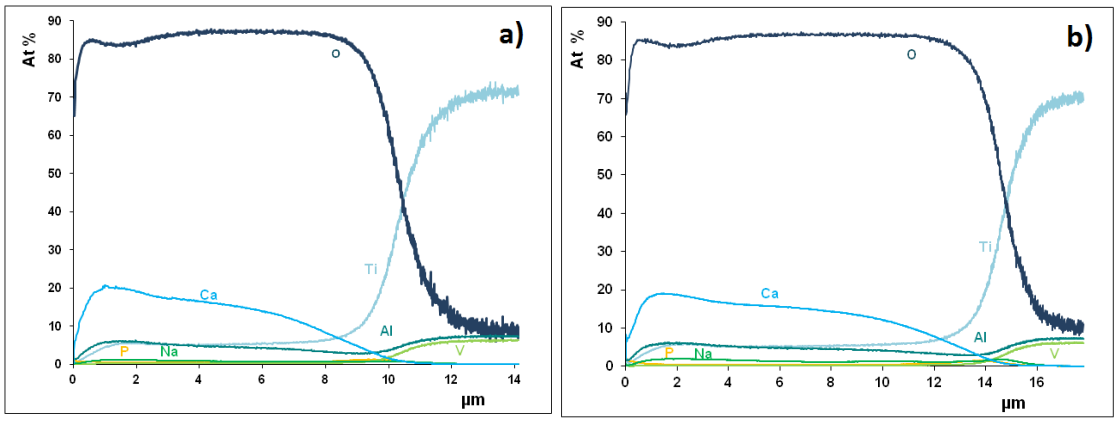

Fig. 3. Coating composition graphics obtained by GD-OES: a) PEO-1 and b) PEO-2.

3.2. X-Ray Diffraction

XRD analysis allowed establishing the relative rutile/anatase ratio in the coatings. This analysis was semiquantitative taking into account the diffraction peaks of the two phases. Thus, the anatase/rutile ratio for PEO-1 coating was 21/79 while for PEO-2 was 46/54. From the tribological point of view, it is of interest to have a higher rutile proportion because of its high stability and good mechanical properties. However, from the biological point of view, there are studies that show the biological effects of anatase, demonstrating that the bone growth is more evident with anatase phase [45][46][47]. This can lead to that a balance between the two phases could be the best option. No evidence of iodine was detected by this analysis due to that the small amount of this element in the coating. Neupane et al. [1] and Segomotso et al. [47] did not find iodine in their coatings either by this technique.

3.3. Tribocorrosion tests

In tribocorrosion tests, prior the sliding process, the samples were immersed in PBS and their open circuit potential values were monitored till they had stabilized. The OCP values for Ti6Al4V, PEO-1 and PEO-2 were -0.345 V, 0.009 V and 0.079 V, respectively. Once the open circuit potentials were stabilized, electrochemical impedance spectroscopy (EIS) measurements were carried out in order to see the corrosion resistance of each sample before the sliding process (Fig. 4). The next step was to record the OCP during 300 seconds and afterwards, start with the sliding process. This caused an immediate decrease of the potential in the bare Ti6Al4V sample, while the developed coatings did not suffer initially any variation. It indicated that in the Ti6Al4V, the spontaneous formed TiO_2 protective coating was removed due to the mechanical effect and the bare metal surface was exposed to the electrolyte. The fluctuation of the potential along the sliding process is related to the continuous de-passivation and re-passivation of the wear tracks [48]. In case of PEO-2 coating, approximately after the first 300 seconds, the potential started decreasing showing a partial or total removing of the protective coating. The PEO-1 sample did not exhibit significant variations in its potential. It indicates that the coating did not apparently suffer wear. Once the sliding tests had concluded, the potentials increased reaching values close to the initial ones. This effect is due to the re-passivation phenomenon. The OCP values were monitored for 10 minutes with the aim to stabilize. The recorded OCP values after the sliding were -0.357 V for Ti6Al4V, -0.001 V for PEO-1 and -0.025

V for PEO-2. The Ti6Al4V was re-passived with final OCP similar to initial one. In TiO_2 developed coatings the OCP after the sliding process were close to the obtained before.

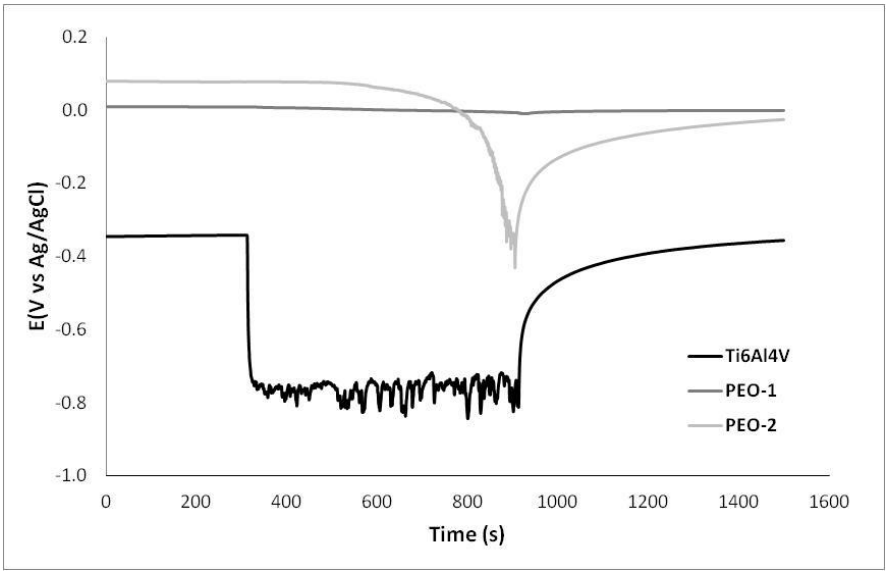

Fig. 4. Open circuit potential (OCP) during sliding process for TiAl4V, and PEO-1 and PEO-2 coatings.

Analyzing the bode impedance plots before and after the wear test (Fig. 5), no corrosion resistance variation has been observed. It seems that the electrochemical state has not been changed by the effect of the sliding process and the consequent wear produced on the surface of the samples. Anyway, it was noted that the corrosion resistance of developed TiO_2 coatings are similar but lower than that of Ti6Al4V. Similar results were obtained in the study of Fazel et al. [49], where at high frequencies the higher porosity of the outer layer produced the decreasing of the impedance values.

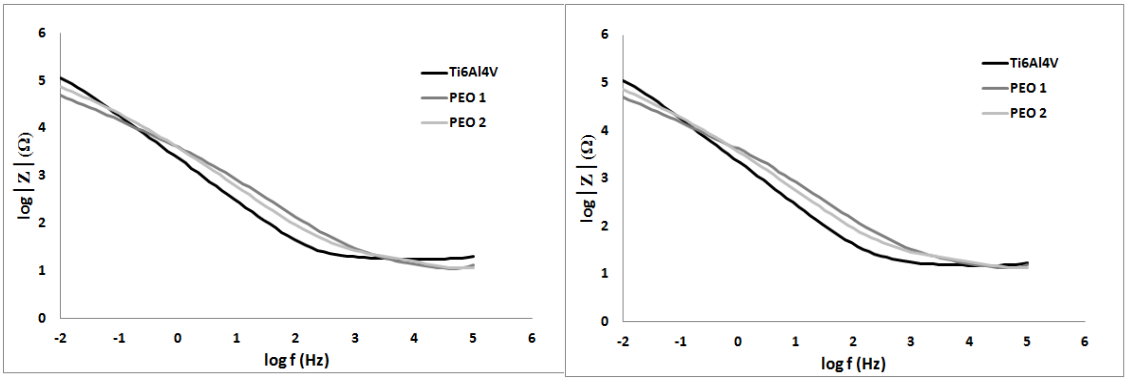

Fig. 5. Bode impedance plots for TiAl4V, PEO-1 and PEO-2 coatings (left) before and (right) after sliding. (modulus IZI is the impedance modulus and f is the frequency).

During the sliding process against alumina counterbody, friction coefficients evolution was recorded (Fig. 6). It was noted that the friction coefficients of both developed TiO_2 coatings was higher than the substrate one. This can be related to the higher roughness of both coatings and the superior hardness of TiO_2 layer, due to its ceramic

nature, in comparison to the Ti6Al4V. According to the website of ASM Aerospace Specification Metals INC, the hardness of Ti6Al4V alloy should be around 349 HV [50], while the hardness of TiO_2 coatings developed by PEO technology is around 400-600 HV. Mean friction coefficients and the total material loss in the wear track (W_{tr}) were calculated and compiled in Table 2. Similar friction coefficients were obtained for both layers, with a value of around 0.7. This tribological behavior is within the expected one [51][52]. Regarding to the total material loss during the rubbing process, in PEO-1 coating it was not possible to calculate this value due to the low wear produced. PEO-2 coating suffered less material loss than Ti6Al4V sample.

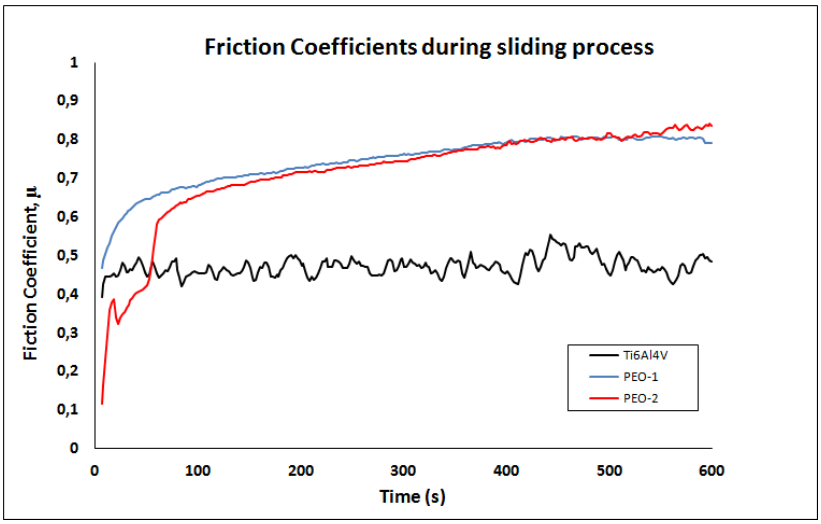

Fig. 6. Friction coefficient evolution during sliding process in tribocorrosion tests.

Table 2.
Mean friction coefficient for Ti6Al4V substrate and both developed TiO_2 coatings.

Samples	Friction Coefficient ± STD	Wtr* (cm^3)
Ti6Al4V	0.472 ± 0.037	1.2 E^{-05}
PEO-1	0.744 ± 0.085	Not possible to measure
PEO-2	0.715 ± 0.134	1.62 E^{-06}

*approximate values are given due to the lack of wear track homogeneity.

Analyzing the wear scars by the confocal microscope (Fig. 7), it was seen that the TiO_2 coatings suffered lower wear during the rubbing conditions leading to irregular tracks. Analysis of the wear tracks profiles was carried out in order to ensure if the coatings were removed somewhere baring the substrate. The maximum wear track depth in PEO-1 was around 2 µm when the thickness of the coating was 3.31 µm (Fig. S2 supplementary data). This seems to indicate that the coating was not removed during the sliding. In case of PEO-2, the maximum wear track depth was around 4-5 µm whereas the thickness of the layer was 4.5 µm. In this sample, it can be concluded that in some areas of the wear track it has reached the substrate after the tribocorrosion test.

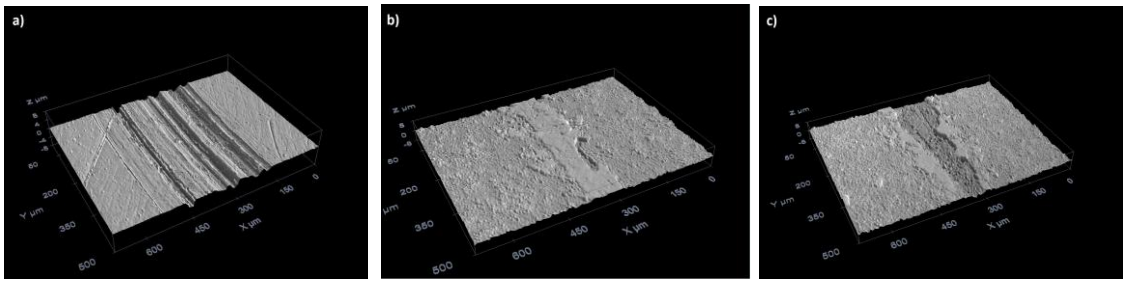

Fig. 7. Wear tracks topography: a) Ti6Al4V, b) PEO-1 and c) PEO-2.

By EDS technology, the chemical composition of worn area of uncoated and coated samples was analyzed. As expected, in the wear track of Ti6Al4V sample only elements from the substrate were found (Fig. 8). Studying the wear scar in the confocal topography and SEM micrograph, it can be concluded that the wear mechanism for Ti6Al4V was abrasive type.

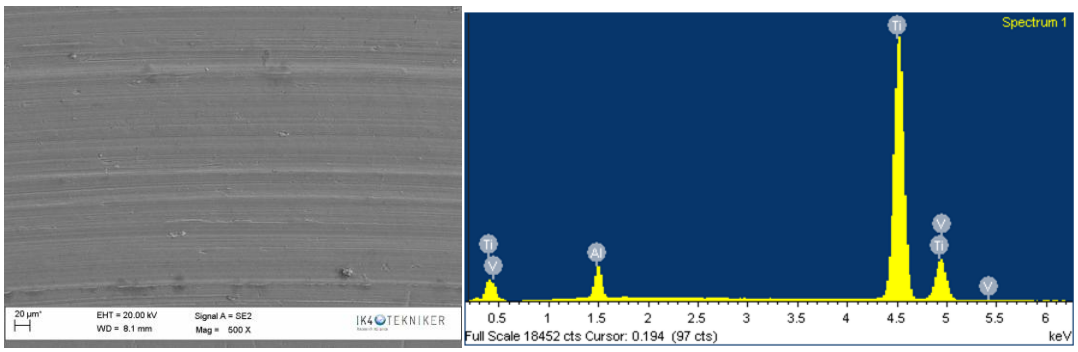

Fig. 8. SEM micrograph of Ti6Al4V (left) and corresponding spectrum form EDS analysis (right).

For the wear track of PEO-1 coating, three chemical analyses were performed in the affected area in order to ensure that the coating was not removed. In all analysis performed elements from the coating like calcium, phosphorus and potassium were detected, confirming that the coating acted as a protective layer against tribocorrosion conditions. In the micrograph it can be observed that part of the coating was removed during rubbing test and re-deposited generating a protective tribolayer, as a consequence of an adhesive wear (Fig. 9, point b).

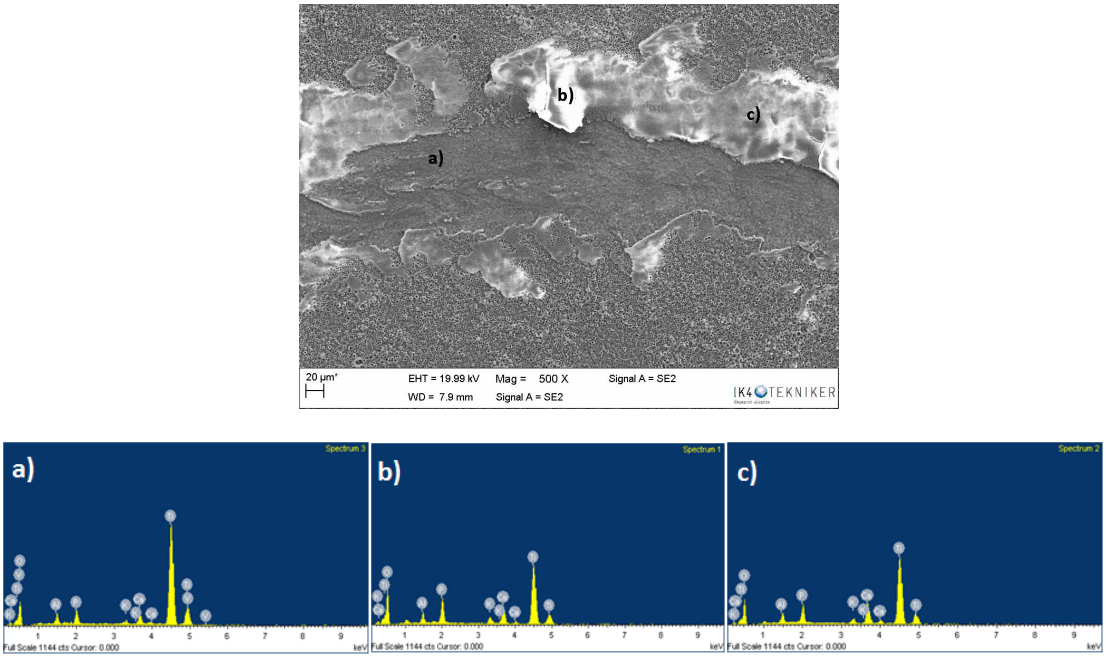

Fig. 9. SEM micrograph of PEO-1 coating (top) and corresponding spectra from EDS analysis (bottom).

Concerning the PEO-2 coating, chemical composition was also analyzed in different parts of the wear track by EDS technique (Fig. 10). It was noticed that in some areas of the track (in particular in a) spectrum), the substrate has been reached because elements from the coating were not detected, but only from the substrate, that is titanium, vanadium and aluminum. In this coating, the wear mechanism is dominantly an adhesive wear. Additionally, a polishing effect in some parts of the scar (point a in Figure 10) was detected.

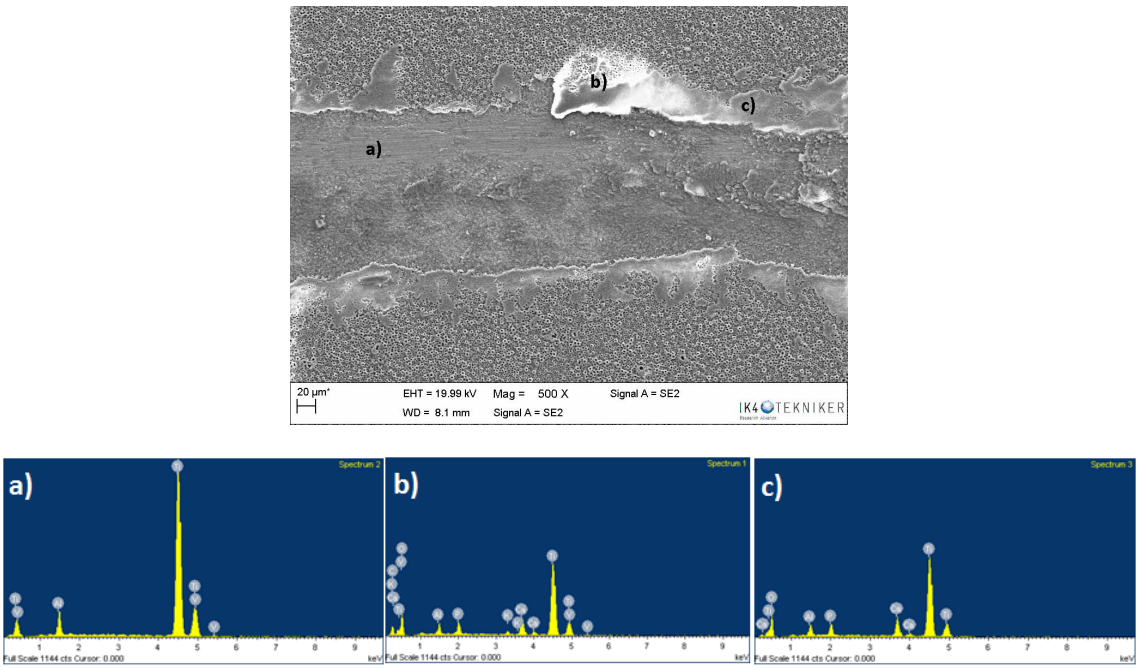

Fig. 10. SEM micrograph of PEO-2 coating (top) and corresponding spectra form EDS analysis (bottom).

3.4. Bacterial adhesion

Analyzing the biocide effect that the developed coatings showed against *Staphylococcus aureus* 15981, it was observed that in no case they improved the biocide effect of substrate (Fig. 11). There cannot be observed **a** statistically significant difference in the mean percentage of surface covered by bacteria compared to the control (Ti6Al4V), with the PEO-1 layer (P value= 0.0362, Kruskal-Wallis test). The same effect was observed with PEO-2 layer (P value= 0.1234, Kruskal-Wallis test).

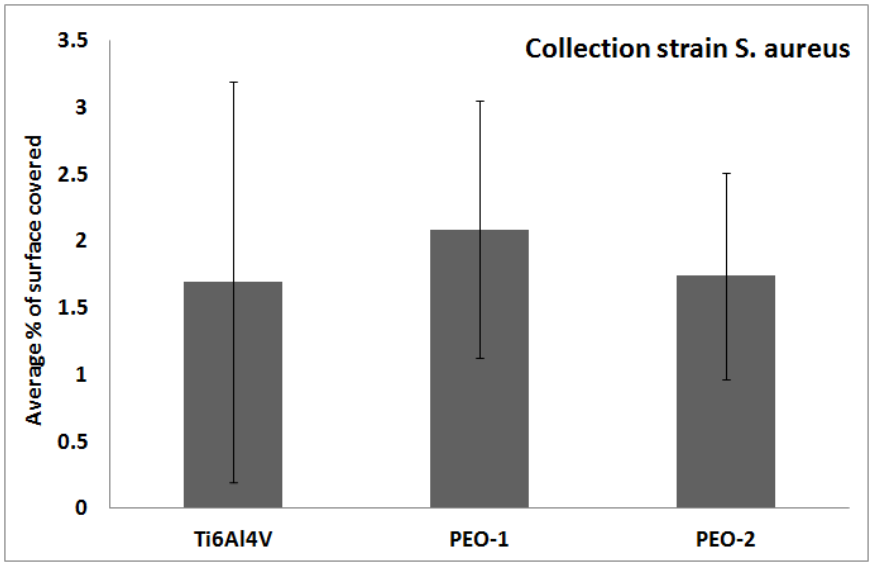

Fig. 11. Mean percentage of surface covered by *S. aureus*.

Concerning the S. epidermidis collection strains, developed TiO_2 coatings with iodine improved the antibacterial properties decreasing the percentage of surface covered by bacteria in comparison to the substrate (Fig. 12). There can be observed statistically significant difference in the mean percentage of surface covered by bacteria compared to the control (Ti6Al4V), with the PEO-1 layer (P value= 0.0007, Kruskal-Wallis test). The same effect was observed with PEO-2 layer (P value= 0.0000, Kruskal-Wallis test).

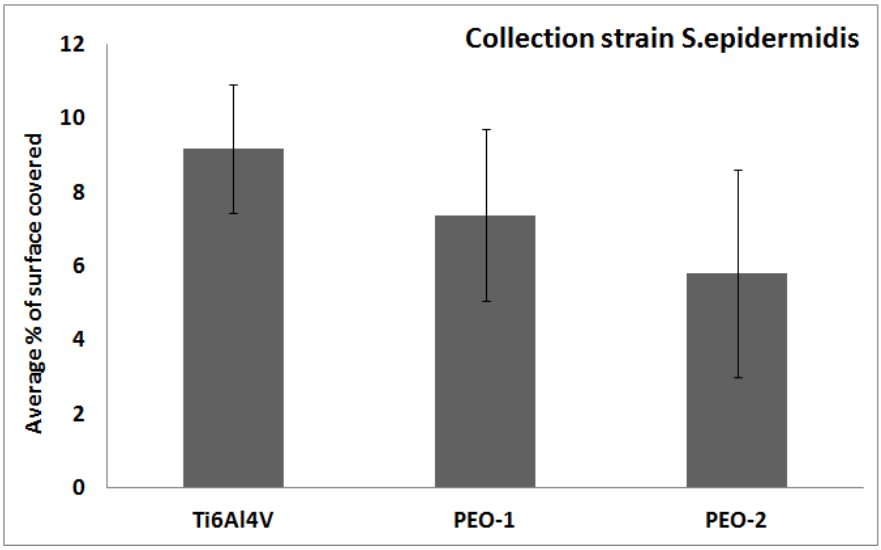

Fig. 12. Mean percentage of surface covered by *S. epidermidis*.

4. Conclusions

Among the developed coatings by PEO technology, PEO-1 coating seems to have the most suitable surface for cell growth. It is more hydrophobic than the substrate and PEO-2 coating. Besides, it has the highest pore percentage and the smaller average pore size. Additionally, osseointegration enhancing elements (Ca and P) have been introduced into the coating, with a higher concentration near the surface. Concerning the tribocorrosion tests, the corrosion resistance was kept in all the samples after the rubbing process. Noticeably, the wear resistance was increased in case of PEO-1 layer probably due to the high amount of rutile phase present in its microstructure. The friction coefficient was superior to bare Ti6Al4V because of the higher roughness in comparison to the substrate. The addition of iodine as biocide element improved the antibacterial features of Ti6Al4V alloy against *S. epidermidis*.

Acknowledgements

The authors want to acknowledge to the Basque Country for the financial support, to the Spanish Ministry of Science and Innovation for the financial of FUNCOAT (CSD2008-0023), the EMAITEK Project, CONSOLIDER Project, and to the SGIker technical support (MEC, GV/EJ, European Social Found). This work has also been financially supported by the ‘‘Ministerio de Economia y Competitividad” (MAT2013-42092-R).

References

[1] M.P. Neupane, T.S.N. Sankara, J.E. Park, Y.K. Kim, I.S. Park, K.Y. Song, T.S. Bae, H. Lee, Hydrothermal fabrication of iodine doped titanium oxide films on Ti substrate, World Acad. Sci, Eng. Technol. 6 (2012) 10-23.

[2] S. Durdu, M. Usta, The tribological properties of bioceramics coatings produced on Ti6Al4V alloy by plasma electrolytic oxidation, Ceram. Int. 40 (2014) 3627-3635.

[3] A. Alsaran, G. Purcek, I. Hacisalihoglu, Y. Vangolu, O. Bayrak, I. Karaman, A. Celik, Hydroxyapatite production on ultrafine-grained pure titanium by micro-arc oxidation and hydrothermal treatmen, Surf. Coat. Tech. 205 (2011) S537-S542.

[4] F. Mabbouxa, L. Ponsinnetb, J. Morriera, N. Jaffrezicb, O. Barsottia, Surface free energy and bacterial retention to saliva-coated dental implant materials-an in vivo study, Colloid Surface. B. 39 (2004) 199-205.

[5] A.L. Yerokhin, X. Niea, A. Leyland, A. Matthews, Characterization of oxide films produced by plasma electrolytic oxidation of a Ti-6Al-4V alloy Surf. Coat. Technol. 130 (2000) 195-205.

[6] T.M. Manhabosco, S.M. Tamborim, C.B. dos Santos, I.L. Müller, Tribological, electrochemical and tribo-electrochemical characterization of bare and nitrited Ti6Al4V in simulated body fluid solution, Corros. Sci. 53(5) (2011) 1786-1793.

[7] N. Diomidis, S. Mischler, N.S. More, R. Manish, Tribo-electrochemical characterization of metallic biomaterials for total joint replacement, Acta Biomater. 8(2) (2012) 852-859.

[8] M. Niinomi, Mechanical biocompatibilities of titanium alloys for biomedical applications, J. Mech. Behav. Biomed. 1(1) (2008) 30-42.

[9] N. Diomidis, S. Mischler, Third body effects on friction and wear during fretting of steel contacts, Tribol. Int. 44(11) (2011) 1452-1460.

[10] S. Williams, J.L. Tipper, E. Ingham, M.H. Stone, J. Fisher, In vitro analysis of wear, wear debris and biological activity of surface-engineered coatings for use in metal-on-metal total hip replacements, P. I. Mech. Eng. H. 217(3) (2003) 155-163.

[11] F. Contu, B. Elsener, H. Böhni, A study of the potentials achieved during mechanical abrasion and the repassivation rate of titanium and Ti6Al4V in inorganic buffer solutions and bovine serum, Electrochim. Acta. 50(1) 2004 33-41.

[12] A. Chandra, J.J. Ryu, P. Karra, P. Shrotriya, V. Tvergaard, M. Gaisser, T. Weik, Life expectancy of modular Ti6Al4V hip implants: Influence of stress and environment, J. Mech. Behav. Biomed. 4 (2011) 1990-2001.

[13] N.P. Hailer, G. Garellick, J. Kärrholm, Uncemented and cemented primary total hip arthroplasty in the Swedish Hip Arthroplasty Register, Evaluation of 170,413 operations, Acta Orthop. 81(1) (2010) 34-41.

[14] M.L.W. Knetsch, L.H. Koole, New strategies in the development of antimicrobial coatings: The example of increasing usage of silver and silver nanoparticles, Polymers. 3 (2011) 340-366.

[15] P.R.T. Kuzyk, E.H. Schemitsch, The basic science of peri-implant bone healing, Indian J. Orthop.45 (2011) 108-115.

[16] F. Grinnell, Cellular adhesiveness and extracellular substrata, Int. Rev. Cytol. 53 (1978) 65-144.

[17] M. Kulkarni, Y. Patil-Sen, I. Junkar, C.V. Kulkarni, M. Lorenzetti, A. Iglic, Wettability studies of topologically distinct titanium surfaces, Colloid Surface. B. 129 (2015) 47-53.

[18] M. Kulkarni, A. Flasker, M. Lokar, K. Mrak-Poljsak, A. Mazare, A. Artenjak, S. Cucnik, S. Kralj, A. Velikonja, P. Schmuki, V. Kralj-Iglic, S. Sodin-Semrl, A. Iglic, Binding of plasma proteins to titanium dioxide nanotubes with different diameters, Int. J. Nanomed. 10 (2015) 1359-1373.

[19] L.C. Xu, C.A. Siedlecki, Effects of surface wettability and contact time on protein adhesion to biomaterial surfaces, Biomaterials. 28 (2007) 3273-3283.

[20] Application note 17: influence of topography and wettability on biocompatibility. <
http://www.biolinscientific.com/zafepress.php?url=%2Fpdf%2FAttension%2FApplication%20Notes%2FAT_AN_17_roughbio.pdf >

[21] M. Zilberman, J.J. Elsner, Antibiotic-eluting medical devices for various applications, J. Control. Release. 130 (2008) 202-215.

[22] K. Vasilev, J. Cook, H.J. Griesser, Antibacterial surfaces for biomedical devices, Expert Rev. Med. Devic. 6(5) (2009) 553-567.

[23] J.S. Temenoff, A.G. Mikos, Biomaterials: The Intersection of Biology and Materials Science, ed., Pearson Prentice Hall, New Jersey, 2008.

[24] K.G. Neoh, X. Hu, D. Zheng, E. Tang Kang, Balancing osteoblast functions and bacterial adhesion on functionalized titanium surfaces, Biomaterials. 33 (2012) 2813-2822.

[25] V. Goriainov, R. Cook, J.M. Latham, D.G. Dunlop, R.O.C. Oreffo, Bone and metal: An orthopaedic perspective on osseointegration of metals, Acta Biomater. 10 (2014) 4043-4057.

[26] F. Ravanetti, P. Borghetti, E. De Angelis, R. Chiesa, F.M. Martini, C. Gabbi, A. Cacchioli, In vitro cellular response and in vivo primary osteointegration of electrochemically modified titanium, Acta Biomater. 6 (2010) 1014-1024.

[27] H.Y. Wang, R.F. Zhu, Y.P. Lu, G.Y. Xiao, X.C. Zhao, K. He, Y.F. Yuan, Y. Li, X.N. Ma, Preparation and properties of plasma electrolytic oxidation coating on sandblasted pure titanium by a combination treatment, Mat. Sci. Eng. C. 42 (2014) 657-664.

[28] L.H. Li, Y.M. Kong, H.W. Kim, Y.W. Kim, H.E. Kim, S.J. Heo, J.Y. Koak, Improved biological performance of Ti implants due to surface modification by micro-arc oxidation, Biomaterials. 25 (2004) 2867-2875.

[29] R. Junker, A. Dimakis, M. Thoneick, J.A. Jansen, Effects of implants surface coatings and composition on bone integration: a systematic review, Clin. Oral Implan. Res. 20 (2009) 185-206.

[30] S.H. Maxian, J.P. Zawadasky, M.G. Dunnj, Effect of Ca/P coating resorption and surgical fit on the bone/implant interface, J. Biomed. Mater. Res. 28 (1994) 1311-1319.

[31] M.F. Basle, D. Chappard, F. Grizon, R. Filmon, J. Delecrin, G. Daculsi, A. Rebel, Osteoclastic resorption of Ca-P biomaterials implanted in rabbit bone, Calcified Tissue Int. 53 (1993) 348-356.

[32] V. Kotharu, R. Nagumothu, C.B. Arumugam, M. Veerappan, S. Sankaran, M.A. Davoodbasha, T. Nooruddin, Fabrication of corrosion resistant, bioactive and antibacterial silver substituted hydroxyapatite/titania composite coating on Cp Ti, Ceram. Int. 38 (2012) 731-740

[33] M.A. Arena, C. Pérez-Jorge, A. Conde, E. Matykina, J.M. Hernández-López, R. Pérez-Tanoira, J.J. de Damborenea, E. Gómez-Barrena, J. Esteban, Doped TiO_2 anodic layers of enhanced antibacterial properties, Colloid Surface. B. 105 (2013) 106-112.

[34] E. Zhang, F. Li, H. Wang, J. Liu, C. Wang, M. Li, K. Yang, A new antibacterial titanium-copper sintered alloy: Preparation and antibacterial property, Mat. Sci. Eng. C. 33 (2013) 4280-4287.

[35] T. Shirai, T. Shimizu, K. Ohtani, Y. Zen, M. Takaya, H. Tsuchiya, Antibacterial iodine-supported titanium implants, Acta Biomater. 7 (2011) 1928-1933.

[36] T.J. Kinnari, A. Soininen, J. Esteban, N. Zamora, E. Alakoski, V.P. Kouri, R. Lappalainen, Y.T. Konttinen, E. Gomez-Barrera, V.M. Tiainen, Adhesion of staphylococcal and Caco-2 cells on diamond-like carbon polymer hybrid coating, J. Biomed. Mater. Res. A. 86 (2008) 760-768.

[37] R. Pérez- Tanoira, C. Pérez-Jorge, J.L. Endrino, E. Gómez-Barrena, D. Horwat, J.F. Pierson, J. Esteban, Bacterial adhesion on biomedical surfaces covered by micrometric silver islands. J. Biomed. Mater. Res. A. 100 (2012) 4208-4218.

[38] K.R. Shin, Y.S. Kim, H.W. Yan, Y.G. Ko, D.H. Shin, In vitro biological response to the oxide layer in pure titanium formed at different current densities by plasma electrolytic oxidation, Appl. Surf. Sci. 314 (2014) 221-227.

[39] H.J. Song, S.H. Park, S.H. Jeong, Y.J. Park, Surface characteristics and bioactivity of oxide films formed by anodic spark oxidation on titanium in different electrolytes, J. Mater. Process Technol. 209 (2009) 864–870.

[40] D. Buser, T. Nydegger, T. Oxland, D.L. Cochran, R.K. Schenk, H.P. Hirt, D. Snetivy, L.P. Nolte, Interface shear strength of titanium implants with a sandblasted

and acid-etched surface: a biomechanical study in the maxilla of miniature pigs, J. Biomed. Mater. Res. 45 (1999) 75–83.

[41] H. Wang, F. Liu, X. Xiong, S. Ke, X. Zeng, P. Lin, Structure, corrosion resistance and in vitro bioactivity of Ca and P containing TiO_2 coating fabricated on NiTi alloy by plasma electrolytic oxidation, Appl. Surf. Sci. 356 (2015) 1234-1243.

[42] F. Jaspard-Mécuson, T. Czerwiec, G. Henrion, T. Belmonte, L. Dujardin, A. Viola, J. Beauvir, Tailored aluminum oxide layers by bipolar current adjustment in the plasma electrolytic oxidation (PEO) process, Surf. Coat. Technol. 201 (2007) 8677–8682.

[43] R. Arrabal, E. Matykina, T. Hashimoto, P. Skeldon, G.E. Thompson, Characterization of AC PEO coatings on magnesium alloys, Surf. Coat. Technol. 203 (2009) 2207–2220.

[44] R.O. Hussein, X. Nie, D.O. Northwood, A. Yerokhin, A. Matthews, Spectroscopic study of electrolytic plasma and discharging behaviour during the plasma electrolytic oxidation (PEO) process, J. Phys. D: Appl. Phys. 43 (2010) 105203–105216.

[45] V. Sollazzo, F. Pezzetti, A. Scarano, A. Piattelli, L. Massari, G. Brunelli, F. Carinci, Anatase coating improves implant osseointegration in vivo, J. Craniofac. Surg. 18 (2007) 806-810.

[46] M. Uchida, H.M. Kim, T. Kokubo, S. Fujibayashi, T. Nakamura, Structural dependence of apatite formation on titania gels in simulated body fluid, J. Biomed. Mater. Res. 64 (2003) 164-170.

[47] B. Segomotso, T. Baozhy, C. Feng, Z. Jinlong, Synthesis, characterization and application of iodine modified titanium oxides in photocatalytical reactions under visible light irradiation, Appl. Surf. Sci. 258 (2012) 3927-3935.

[48] S. Kumar, T.S.N.Sankara Narayanan, S.Ganesh Sundara Raman, S.K. Seshadri, Surface modification of CP-Ti to improve the fretting-corrosion resistance: Thermal oxidation vs.anodizing, Mater. Sci. Eng. C 30 (2010) 921–927.

[49] M. Fazel, H.R. Salimijazi, M.A. Golozar, M.R. Garsivaz jazi, A comparison of corrosion, tribocorrosion and electrochemical impedance properties of pure Ti and Ti6Al4V alloy treated by micro-arc oxidation process, Appl. Surf. Sci. 324 (2015) 751-756.

[50] “ASM Material Data Sheet”. ASM. Web. 14 October 2015. http://asm.matweb.com/search/SpecificMaterial.asp?bassnum=MTP641.

[51] M. Khorasanian, A. Dehghan, M.H. Shariat, M.E. Bahrololoom, S. Javadpour, Microstructure and wear resistance of oxide coating on Ti-6Al-4V produced by plasma electrolytic oxidation in an inexpensive electrolyte, Surf. Coat. Technol. 206 (2011) 1495-1502.

[52] S. Aliasghari, P. Skeldon, G.E. Thompson, Plasma electrolytic oxidation of titanium in a phosphate/silicate electrolyte and tribological performance of the coatings, Appl. Surf. Sci. 316 (2014) 463-476.

Supplementary material

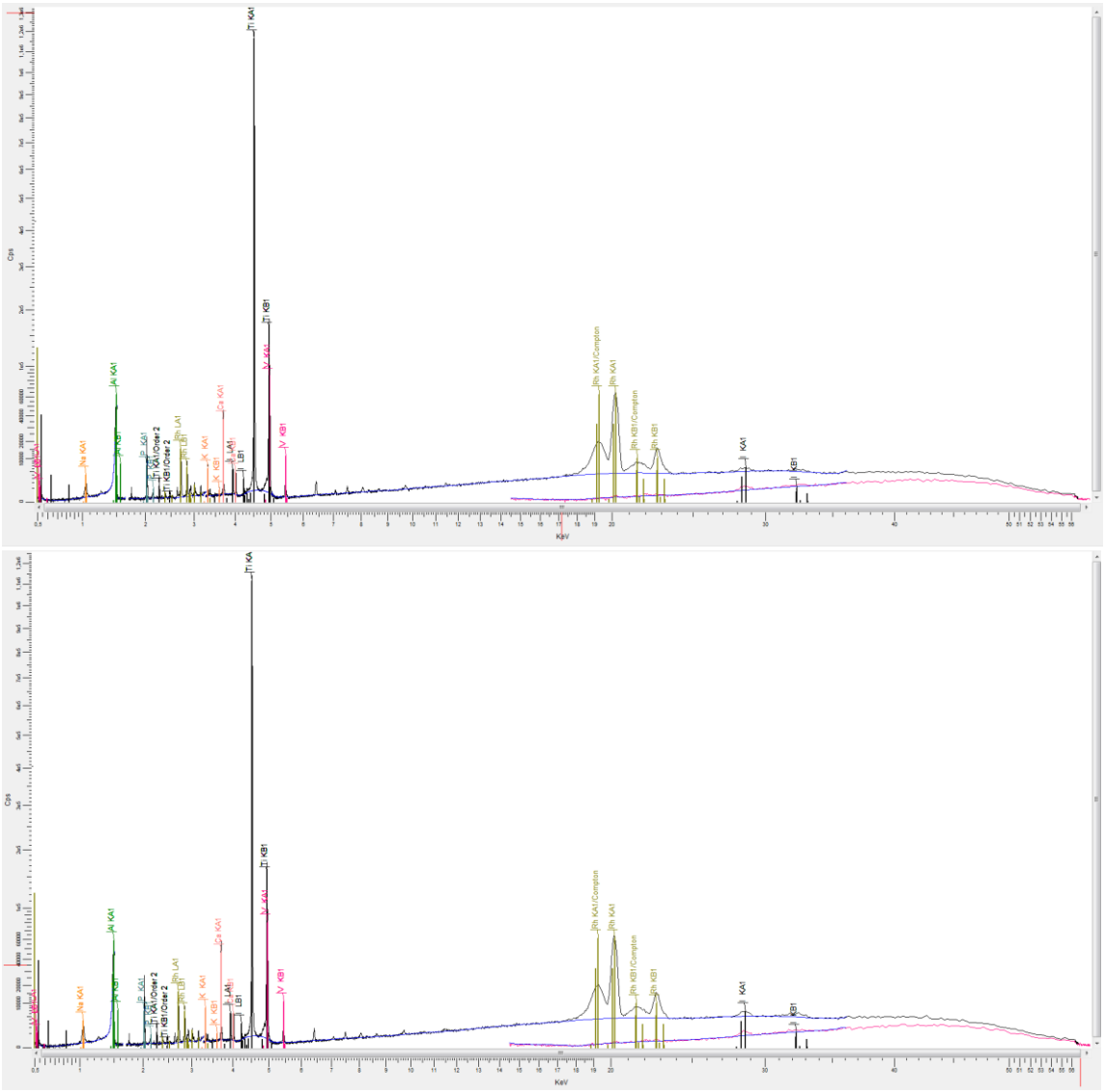

Fig. S1. XRF patterns of both developed coatings. PEO-1 (top) and PEO-2 (bottom).

Table S1.
Peaks intensity (KCps) of detected elements by XRF technology.

Samples	Ti	V	Al	Ca	P	Na	I	K
PEO-1	1192.6	81.2	21.3	46.0	23.4	1.8	1.2	7.1
PEO-2	1139.1	77.9	19.2	58.5	26.3	2.5	1.7	8.7

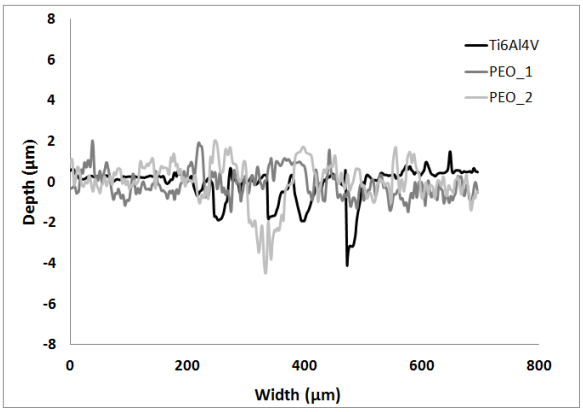

Fig. S2. Track profiles of uncoated and coated samples.

Chapter 5

Titanium and Titanium Alloys as Biomaterials

Virginia Sáenz de Viteri and Elena Fuentes

Additional information is available at the end of the chapter

http://dx.doi.org/10.5772/55860

1. Introduction

Bone and its several associated elements – cartilage, connective tissue, vascular elements and nervous components – act as a functional organ. They provide support and protection for soft tissues and act together with skeletal muscles to make body movements possible. Bones are relatively rigid structures and their shapes are closely related to their functions. Bone metabolism is mainly controlled by the endocrine, immune and neurovascular systems, and its metabolism and response to internal and external stimulations are still under assessment [1].

Long bones of the skeletal system are prone to injury, and internal or external fixation is a part of their treatment. Joint replacement is another major intervention where the bone is expected to host biomaterials. Response of the bone to biomaterial intervenes with the regeneration process. Materials implanted into the bone will, nevertheless, cause local and systemic biological responses even if they are known to be inert. Host responses with joint replacement and fixation materials will initiate an adaptive and reactive process [2].

The field of biomaterials is on a continuous increase due to the high demand of an aging population as well as the increasing average weight of people. Biomaterials are artificial or natural materials that are used to restore or replace the loss or failure of a biological structure to recover its form and function in order to improve the quality and longevity of human life. Biomaterials are used in different parts of the human body as artificial valves in the heart, stents in blood vessels, replacement implants in shoulders, knees, hips, elbows, ears and dental structures [3] [4] [5]. They are also employed as cardiac simulators and for urinary and digestive tract reconstructions. Among all of them, the highest number of implants is for spinal, hip and knee replacements. It is estimated that by the end of 2030, the number of total hip replacements will rise by 174% (572,000 procedures) and total knee arthroplasties are projected to grow by 673% from the present rate (3.48 million procedures) [6]. This is due to the fact that human joints suffer from degenerative diseases such as osteoarthritis (inflammation in the

bone joints), osteoporosis (weakening of the bones) and trauma leading to pain or loss in function. The degenerative diseases lead to degradation of the mechanical properties of the bone due to excessive loading or absence of normal biological self-healing process. Artificial biomaterials are the solutions to these problems and the surgical implantation of these artificial biomaterials of suitable shapes help restore the function of the otherwise functionally compromised structures. However, not only the replacement surgeries have increased, simultaneously the revision surgery of hip and knee implants have also increased. These revision surgeries which cause pain for the patient are very expensive and also their success rate is rather small. The target of present researches is developing implants that can serve for much longer period or until lifetime without failure or revision surgery [7]. Thus, development of appropriate material with high longevity, superior corrosion resistance in body environment, excellent combination of high strength and low Young´s modulus, high fatigue and wear resistance, high ductibility, excellent biocompatibility and be without citotoxicity is highly essential [8] [9].

In general, metallic biomaterials are used for load bearing applications and must have sufficient fatigue strength to endure the rigors of daily activity. Ceramic biomaterials are generally used for their hardness and wear resistance for applications such as articulating surfaces in joints and in teeth as well as bone bonding surfaces in implants. Polymeric materials are usually used for their flexibility and stability, but have also been used for low friction articulating surfaces. Titanium is becoming one of the most promising engineering materials and the interest in the application of titanium alloys to mechanical and tribological components is growing rapidly in the biomedical field [10], due to their excellent properties.

This chapter is focused on the use of titanium and its alloys as biomaterials from a tribological point of view. The main limitation of these materials is their poor tribological behavior characterized by high friction coefficient and severe adhesive wear. A number of different surface modification techniques have been recently applied to titanium alloys in order to improve their tribological performance as well as osseointegration. This chapter includes the most recent developments carried out in the field of surface treatments on titanium with very promising results.

2. Biomaterial properties

The main property required of a biomaterial is that it does not illicit an adverse reaction when placed into services, that means to be a biocompatible material. As well, good mechanical properties, osseointegration, high corrosion resistance and excellent wear resistance are required.

2.1. Biocompatibility

The materials used as implants are expected to be highly non toxic and should not cause any inflammatory or allergic reactions in the human body. The success of the biomaterials is mainly dependent on the reaction of the human body to the implant, and this measures the biocom-

http://dx.doi.org/10.5772/55860

patibility of a material [11]. The two main factors that influence the biocompatibility of a material are the host response induced by the material and the materials degradation in the body environment (Figure 1). According to the tissue reaction phenomena, the biocompatibility of orthopedic implant materials was classified into three categories by Heimke [12], such as "biotolerant", showing distant osteogenesis (bone formation with indirect contact to the material); "bioinert", showing contact osteogenesis (bone formation with direct contact to the material), and "bioactive", showing bonding osteogenesis (bone formation with chemical or biological bonding to the material).

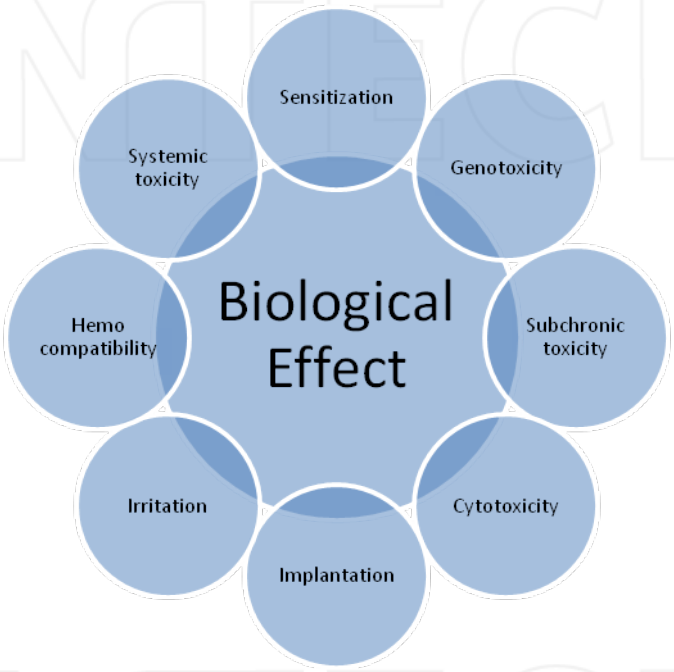

Figure 1. Biological effects of a biomaterial

When implants are exposed to human tissues and fluids, several reactions take place between the host and the implant material and these reactions dictate the acceptability of these materials by our system. The issues with regard to biocompatibility are (1) thrombosis, which involves blood coagulation and adhesion of blood platelets to biomaterial surface, and (2) the fibrous tissue encapsulation of biomaterials that are implanted in soft tissues.

2.2. Mechanical properties

The most important mechanical properties that help to decide the type of material are hardness, tensile strength, Young´s modulus and elongation. An implant fracture due to a mechanical failure is related to a biomechanical incompatibility. For this reason, it is expected that the

material employed to replace the bone has similar mechanical properties to that of bone. The bone Young´s modulus varies in a range of 4 to 30 GPa depending on the type of the bone and the direction of measurement [13] [14].

2.3. Osseointegration

The inability of an implant surface to integrate with the adjacent bone and other tissues due to micromotions, results in implant loosening [15]. Osseointegration (capacity for joining with bone and other tissue) is another important aspect of the use of metallic alloys in bone applications (Figure 2). A good integration of implant with the bone is essential to ensure the safety and efficacy of the implant over its useful life. It has been shown in previous studies [16], that enhancement of the bone response to implant surfaces can be achieved by increasing the roughness or by other surface treatments [17]. Although the precise molecular mechanisms are not well understood, it is clear that the chemical and physical properties of the surface play a major role in the implant – surface interactions through modulation of cell behavior, growth factor production and osteogenic gene expression [18] [19] [20].

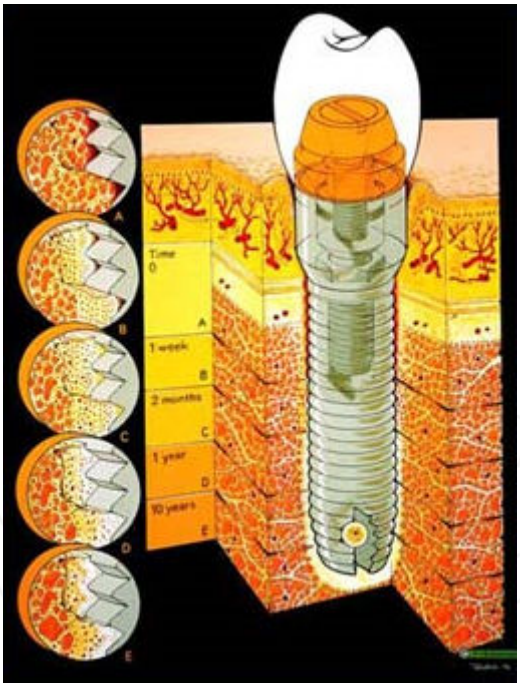

Figure 2. Schematic drawing of the principles of osseointegration [21]

Furthermore, it is known that even if initial implant stability is achieved, the bone may retreat from or be isolated from the implant because of different reasons or situations listed below:

1. Reaction of the implant with a foreign body as debris from implant component degradation or wear, or to toxic emissions from the implant [22]
2. Damage or lesion to the bone through mechanical trauma surgery
3. Imposition of abnormal or unphysiological conditions on the bone, such as fluid pressures or motion against implant components
4. Alteration to the mechanical signals encouraging bone densification; strain reductions or stress-shielding of replaced or adjacent bone.

2.4. High corrosion resistance

All metallic implants electrochemically corrode to some extent. This is disadvantageous for two main reasons: (1) the process of degradation reduces the structural integrity and (2) degradation products may react unfavorably with the host. Metallic implant degradation results from both electrochemical dissolution and wear, but most frequently occurs through a synergistic combination of the two [23] [24]. Electrochemical corrosion process includes both generalized dissolution uniformly affecting the entire surface and localized areas of a component.

Metal implant corrosion is controlled by (1) the extent of the thermodynamic driving forces which cause corrosion (oxidation/reduction reactions) and (2) physical barriers which limit the kinetics of corrosion. In practice these two parameters that mediate the corrosion of orthopedic biomaterials can be broken down into a number of variables: geometric variables (e.g., taper geometry in modular component hip prostheses), metallurgical variables (e.g., surface microstructure, oxide structure and composition), mechanical variables (e.g., stress and/or relative motion) and solution variables (e.g., pH, solution proteins and enzymes) [25].

The corrosion resistance of a surgically implanted alloy is an essential characteristic since the metal alloys are in contact with a very aggressive media such as the body fluid due to the presence of chloride ions and proteins. In the corrosion process, the metallic components of the alloy are oxidized to their ionic forms and dissolved oxygen is reduced to hydroxide ions.

The corrosion characteristics of an alloy are greatly influenced by the passive film formed on the surface of the alloy and the presence of the alloying elements.

2.5. Wear resistance

Wear always occurs in the articulation of artificial joints as a result of the mixed lubrication regime. The movement of an artificial hip joint produces billions of microscopic particles that are rubbed off cutting motions. These particles are trapped inside the tissues of the joint capsule and may lead to unwanted foreign body reactions. Histocytes and giant cells phagocytose and "digest" the released particles and form granulomas or granuloma-like tissues. At the boundary layer between the implant and bone, these interfere with the transformation process of the bone leading to osteolysis. Hence, the materials used to make the femoral head and cup play a significant role in the device performance. Since the advent of endoprosthetics, attempts

have been made to reduce wear by using a variety of different combinations of materials and surface treatments.

Nowadays, the materials used for biomedical applications are mainly metallic materials such as 316L stainless steel, cobalt chromium alloys (CoCrMo), titanium-based alloys (Ti-6Al-4V) and miscellaneous others (including tantalum, gold, dental amalgams and other "specialty" metals). Titanium alloys are fast emerging as the first choice for majority of applications due to the combination of their outstanding characteristics such as high strength, low density, high immunity to corrosion, complete inertness to body environment, enhanced compatibility, low Young´s modulus and high capacity to join with bone or other tissues. Their lower Young´s modulus, superior biocompatibility and better corrosion resistance in comparison with conventional stainless steels and cobalt-based alloys, make them an ideal choice for bio-applications [26]. Because of the mentioned desirable properties, titanium and titanium alloys are widely used as hard tissue replacements in artificial bones, joints and dental implants.

3. Titanium and titanium alloys

The elemental metal titanium was first discovered in England by William Gregor in 1790, but in 1795 Klaproth gave it the name of titanium. Combination of low density, high strength to weight ratio, good biocompatibility and improved corrosion resistance with good plasticity and mechanical properties determines the application of titanium and its alloys in such industries as aviation, automotive, power and shipbuilding industries or architecture as well as medicine and sports equipment.

Increased use of titanium and its alloys as biomaterials comes from their superior biocompatibility and excellent corrosion resistance because of the thin surface oxide layer, and good mechanical properties, as a certain elastic modulus and low density that make that these metals present a mechanical behaviour close to those of bones. Light, strong and totally biocompatible, titanium is one of the few materials that naturally match the requirements for implantation in the human body. Among all titanium and its alloys, the mainly used materials in biomedical field are the commercially pure titanium (cp Ti, grade 2) and Ti-6Al-4V (grade 5) alloy. They are widely used as hard tissue replacements in artificial bones, joints and dental implants. As a hard tissue replacement, the low elastic modulus of titanium and its alloys is generally viewed as a biomechanical advantage because the smaller elastic modulus can result in smaller stress shielding.

Other property that makes titanium and its alloys the most promising biomaterials for implants is that titanium-based materials in general rely on the formation of an extremely thin, adherent, protective titanium oxide film. The presence of this oxide film that forms spontaneously in the passivation or repassivation process is a major criterion for the excellent biocompatibility and corrosion resistance of titanium and its alloys.

Concerning the medical applications of these materials, the use of cp (commercially pure) Titanium is more limited to the dental implants because of its limited mechanical properties.

http://dx.doi.org/10.5772/55860

In cases where good mechanical characteristics are required as in hip implants, knee implants, bone screws, and plates, Ti-6Al-4V alloy is being used [27] [28]. One of the most common applications of titanium alloys is artificial hip joints that consist of an articulating bearing (femoral head and cup) and stem [24], where metallic cup and hip stem components are made of titanium. As well, they are also often used in knee joint replacements, which consist of a femoral and tibial component made of titanium and a polyethylene articulating surface.

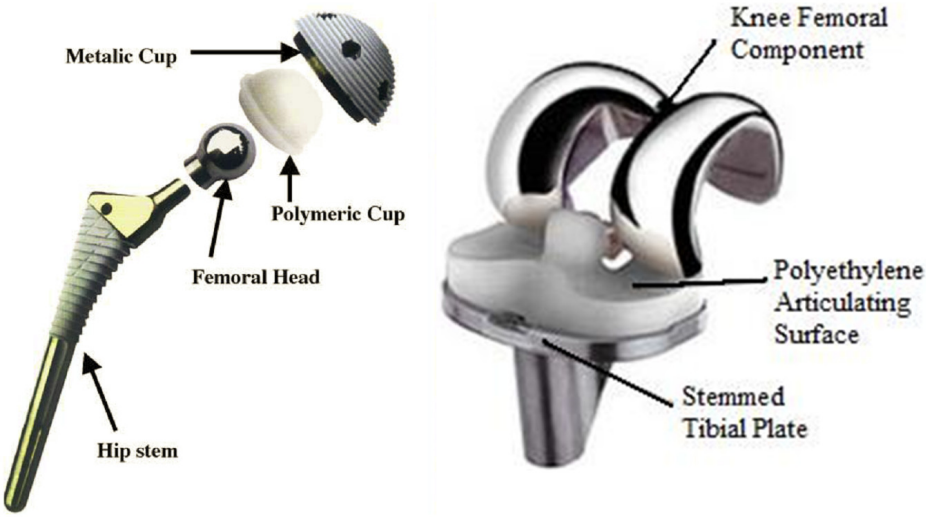

Figure 3. Schematic diagram of artificial hip joint (left) and knee implant [29] (right)

3.1. Wear problems in titanium and titanium alloys

The fundamental drawback of titanium and its alloys which limits wider use of these materials include their poor fretting fatigue resistance and poor tribological properties [30] [31], because of its low hardness [32]. Their poor tribological behavior is characterized by high coefficient of friction, severe adhesive wear with a strong tendency to seizing and low abrasion resistance [33]. Titanium tends to undergo severe wear when it is rubbed between itself or between other materials. Titanium has tendency for moving or sliding parts to gall and eventually seize. This causes a more intensive wear as a result of creation of adhesion couplings and mechanical instability of passive layer of oxides, particularly in presence of third bodies (Figure 4). Owing to this effect, in cases of total joint replacements made of titanium head and polymer cup, the 10%-20% of joints needs to be replaced within 15-20 years and the aseptic loosening accounts for approximately 80% of the revisions [34]. The reason for the failure of the implants is due to the high friction coefficient of these materials that can lead to the release of wear debris from the implant into the bloodstream that results in an inflammation of the surrounding tissue and gives rise to the bone resorption (osteolysis) [35] [36], which ultimately leads to loosening of the implant and hence the implant has to be replaced by a new one.

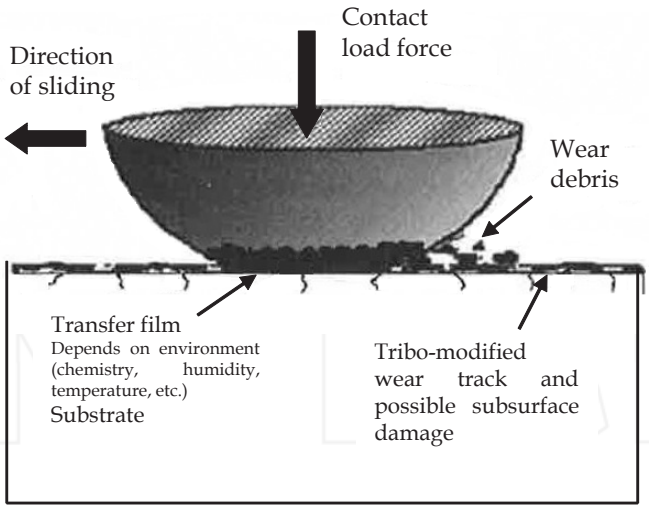

Figure 4. Schematic representation of a sliding tribological coating with the presence of third bodies [37]

3.2. Corrosion behaviour of titanium and titanium alloys

All metals and alloys are subjected to corrosion when in contact with body fluid as the body environment is very aggressive owing to the presence of chloride ions and proteins. A variety of chemical reactions occur on the surface of a surgically implanted alloy. The metallic components of the alloy are oxidized to their ionic forms and dissolved oxygen is reduced to hydroxide ions.

Most metals and alloys that resist well against corrosion are in the passive state. Metals in the passive state (passive metals) have a thin oxide layer (TiO_2 in case of titanium) on their surface, the passive film, which separates the metal from its environment [38]. Typically, the thickness of passive films formed on these metals is about 3-10 nm [39] and they consist of metal oxides (ceramic films). The natural oxide is amorphous and stoichiometrically defective. It is known that the protective and stable oxides on titanium surfaces (TiO_2) are able to provide favorable osseointegration. The stability of the oxide depends strongly on the composition structure and thickness of the film [40].

Because of the presence of an oxide film, the dissolution rate of a passive metal at a given potential is much lower than that of an active metal. It depends mostly on the properties of the passive film and its solubility in the environment. These films which form spontaneously on the surface of the metal prevent further transport of metallic ions and/or electrons across the film. To be effective barriers, the films must be compact and fully cover the metal surface; they must have an atomic structure that limits the migration of ions and/or electrons across the metal oxide–solution interface; and they must be able to remain on the surface of these alloys even with mechanical stressing or abrasion, expected with orthopedic devices [25].

http://dx.doi.org/10.5772/55860

The relatively poor tribological properties and possible corrosion problems have led to the development of surface treatments to effectively increase near-surface strength, improving the hardness and abrasive wear resistance thereby reducing the coefficient of friction as well as avoiding or reducing the transference of ions from the surface or bulk material to the surrounding tissue.

3.3. Osseointegration of titanium and titanium alloys

When an implant is surgically placed within bone there are numerous biological, physical, chemical, thermal and other factors functioning that determine whether or not osseointegration will occur.

Titanium and its alloys have been widely used for dental and orthopedic implants under load-bearing conditions because of their good biocompatibility coupled with high strength and fracture toughness. Despite reports of direct bonding to bone, they do not form a chemical bond with bone tissue. For the last decade, various coatings have been attempted to provide titanium and its alloys with bond-bonding ability, which spontaneously bond to living bone. Hydroxyapatite plasma spray coatings are widely used in cementless hip replacement surgery, but the hydroxyapatite coating, although exhibiting a very good biocompatibility, presents some disadvantages including delamination of the coating layer from the substrate, difficulties in controlling the composition of the coating layer and degradation of the coating layer itself, which can release debris becoming a source of third body wear [41].

A strong and durable bone to implant connection can be achieved by the formation of a stable bone tissue at the bone-implant interface by proper implant surface treatments, as can be electrochemical deposition, dipping and physical vapor deposition techniques [42].

3.4. Surface treatments of titanium and titanium alloys

Surface engineering can play a significant role in extending the performance of orthopedic devices made of titanium several times beyond its natural capability.

The main objectives of surface treatments mainly consist of the improvement of the tribological behaviour, corrosion resistance and osseointegration of the implant. There are coatings for enhanced wear and corrosion resistance by improving the surface hardness of the material that can be applied by different surface modifications techniques such as surface oxidation, physical deposition methods like ion implantation and plasma spray coatings, as well as thermo-chemical surface treatments such as nitriding, carburizing and boriding [43] [44].

Great efforts have been devoted to thickening and stabilizing surface oxides on titanium to achieve desired biological responses. The biological response to titanium depends on the surface chemical composition, and the ability of titanium oxides to absorb molecules and incorporate elements. Surface topography plays a fundamental role in regulating cell behavior, e.g. the shape, orientation and adhesion of cells.

One possible alternative to solve tribological problems and which is going to explain more detail consists of protecting the alloy surface by means of biocompatible Diamond-Like Carbon

(DLC) coatings. "Diamond-Like Carbon" is a generic term referring to amorphous carbon films, deposited by either Physical Vapor Deposition (PVD) or Plasma-Enhanced Chemical Vapor Deposition (PECVD). DLC coatings basically consist of a mixture of diamond (sp^3) and graphite (sp^2). The relative amounts of these two phases will determine much of the coating properties. They are thus metastable and mostly amorphous, "crystalline" clusters being too small or too defective to reach graphite or diamond structures. Both the mechanical and the tribological properties of DLC coatings have been studied for about 30 years, and several different types of DLC coatings can currently be found. DLC films are attractive biomedical materials due to their relatively high hardness, low friction coefficient, owing to the solid lubricant because of its graphite and amorphous carbon contents [31], good chemical stability and excellent bio and hemocompatibility [45] [44] [46] [47]. Cells are seen to grow well on these films coated on titanium and other materials without any cytotoxicity and inflammation.

Oxidation remains the most popular technique for the surface modification of Ti alloys; these oxide layers on titanium are commonly produced by either heat treatment [48] [49] [50] or electrolytic anodizing [51]. Thermal oxidation results in the formation of a 15-30 μm thick titanium dioxide layer of the rutile phase. However, due to their long-term high temperature action, thermal diffusion processes can also lead to the formation of a diffusion sub-layer consisting of an oxygen solid solution in α-Ti, and development of phase segregation and coalescence which may cause substrate embrittlement and worsened mechanical and/or corrosion performance.

Conventional anodic oxidation, which is carried out in various solutions providing passivation of the titanium surface, generates thin films of amorphous hydrated oxide or crystalline TiO_2 in the anatase form [52]. These films exhibit poor corrosion resistance in some reducing acids and halide solutions, while rutile generally possesses much better protective properties. However, recent developments in high voltage anodizing allow the production of crystalline rutile/anatase films at near to ambient temperature [53]. By anodic oxidation, elements such as Ca and P can be imported into the surface oxide on titanium and the micro-topography can be varied through regulating electrolyte and electrochemical conditions. The presence of Ca-ions has been reported to be advantageous to cell growth, and in vivo data show implant surfaces containing both Ca and P enhance bone apposition on the implant surface.

Furthermore, there are alternative methods to improve the biocompatibility such as biocompatible chemicals [54] and materials such as ceramics for coating. In some studies, titanium surfaces were modified using phosphoric acid in an "in vitro" study to improve the biocompatibility of dental implants. Results indicated that pretreatment of the implant with phosphoric acid caused no citotoxicity to the osteoblasts [55]. Micro arc oxidation method in phosphoric acid on titanium implants provided chemical bonding sites for calcium ions during mineralization [56].

Moreover, there have been developed coatings for high osseointegration. Hydroxyapatite (HA) coating is a proven method to improve the implants´ mechanical bonding [57] [58], biocompatibility and improve the osseointegration. The higher the degree of osseointegration, the higher is the mechanical stability and the probability of implant loosening becomes smaller. The process of osseointegration depends upon the surface properties such as surface chemis-

try, surface topography, surface roughness and mainly the surface energy. TiO_2, calcium phosphate, titania/hydroxiapatite composite and silica coating by the sol-gel method can be applied on the surface of the titanium and titanium alloys. Plasma Electrolytic Oxidation (PEO) or Micro-Arc Oxidation (MAO) technique is used for the synthesize TiO_2 layer. This technique is based on the modification of the growing anodic film by arc micro-discharges, which are initiated at potentials above the breakdown voltage of the growing oxide film and move rapidly across the anode surface. This technology provides a solution by transforming the surface into a dense layer of ceramic which not only prevents galling but also provides excellent dielectric insulation for contact metals, helping to protect them against aggressive galvanic corrosion. PEO process transforms the surface of titanium alloys into a complex ceramic matrix by passing a pulsed, bi-polar electrical current in a specific wave formation through a bath of low concentration aqueous solution. A plasma discharge is formed on the surface of the substrate, transforming it into a thin, protective layer of titanium oxide, without subjecting the substrate itself to damaging thermal exposure.

Among all the above mentioned surface treatments, Diamond-Like Carbon coating and Plasma Electrolytic Oxidation are the most promising ones applied on titanium surfaces. These two treatments are explained in more detail in the following sections.

3.4.1. Diamond-like carbon coatings

In some biomedical applications continuously sliding contact is required, subjecting the implant to aggressive situations. To achieve and maintain higher efficiency and durability under such increasingly more severe sliding conditions, protective and/or solid coatings are becoming prevalent.

These coatings can generally be divided in two broad categories [59] : “soft coatings”, which are usually good for solid lubrication and exhibit low friction coefficients, and “hard coatings”, which are usually good for protection against wear, and exhibit low wear rates and hence longer durability (Figure 5).

It would thus seem to be difficult to associate low friction and high wear resistance with all types of coating in most tribological contacts. Some trade-offs can be found in combining both hard and soft materials in composite or multilayer coatings, which require complex procedures and further optimization of the deposition process. Nevertheless, a diverse family of carbon-based materials seems to “naturally” combine the desired set of tribological properties, providing not only low friction but also high wear resistance. These materials are widely known as the diamond and Diamond-Like Carbon (DLC) coatings. They are usually harder than most metals and/or alloys, thus affording very high wear resistance and, at the same time, impressive friction coefficients generally in the range of 0.05-0.2 [60] [61] [62]. In some cases, friction values lower than 0.01 have been reported [63] [64], offering a sliding regime often referred to as “superlubricity”. These exceptional tribological abilities explain the increasing success of Diamond-Like Carbon coatings over the years, both in industrial applications and in the laboratory. The exceptional tribological behavior of Diamond-Like Carbon films appears to be due to a unique combination of surface chemical, physical, and mechanical interactions at their sliding interfaces [65].

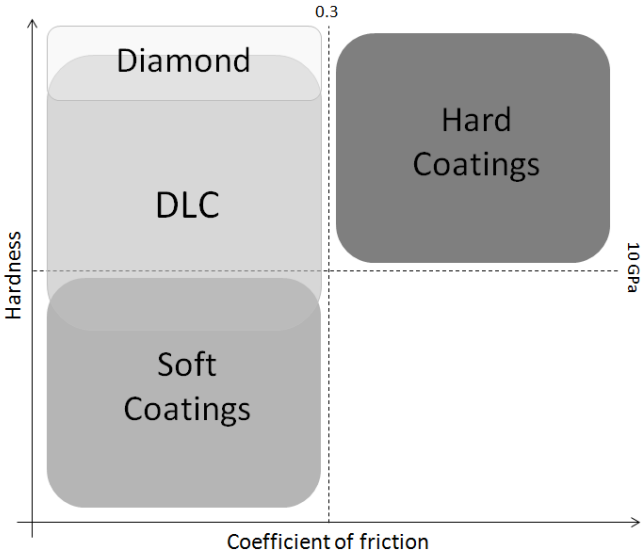

Figure 5. Classification of coatings with respect to hardness and coefficient of friction, highlighting the special case of carbon-based coatings

Since their initial discovery in the early 1950s, Diamond-Like Carbon coatings have attracted the most attention in recent years, mainly because they are cheap and easy to produce and offer exceptional properties for demanding engineering and medical applications. They can be used in invasive and implantable medical devices. These films are currently being evaluated for their durability and performance characteristics in certain biomedical implants including hip and knee joints and coronary stents.

Diamond-Like Carbon is the only coating that can provide both high hardness and low friction under dry sliding conditions. These films are metastable forms of carbon combining both sp2 and sp3 hybridizations, including hydrogen when a hydrocarbon precursor is used during deposition. The tribological behavior of Diamond-Like Carbon films requires a solid background on the chemical and structural nature of these films, which, in turn, depends on the deposition process and/or parameters. The chemical composition, such as the hydrogen and/or nitrogen content or the presence of other alloying elements, controls the mechanical and tribological properties of a sliding pair consisting of DLC on one or both sliding surfaces [66]. For example, DLC samples containing different concentrations of titanium (Figure 6) have also been examined "in vitro" to obtain a biocompatible surface that is hard, preventing abrasion and scratching [67].

It is well known that Diamond-Like Carbon films usually present smooth surfaces, except maybe in the case of films formed by unfiltered cathodic vacuum arc deposition (Figure 7). Roughness of the films on industrial surfaces will then be mainly controlled by the substrate roughness and can therefore be minimized.

http://dx.doi.org/10.5772/55860

Figure 6. Scheme of titanium doped DLC coating. In this case, the first titanium layer was deposited in order to improve adhesion of DLC coating to the substrate and relax stress of the coating

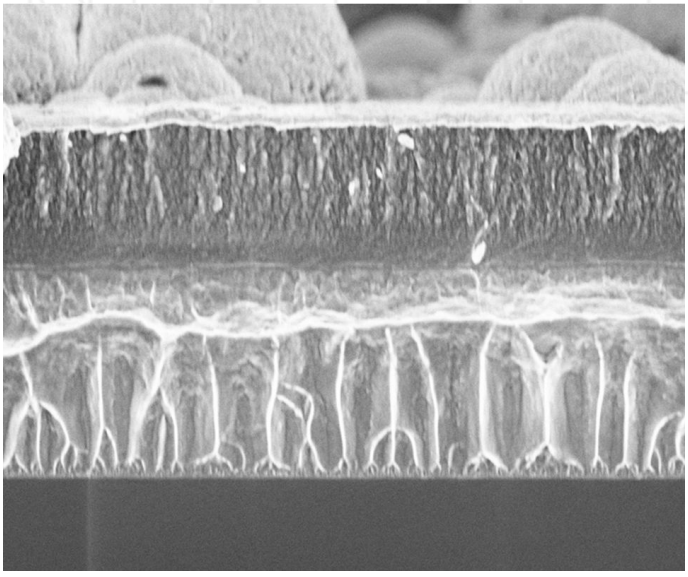

Figure 7. SEM (Scanning electron microscopy) micrograph of Ti-DLC coating deposited by physical vapour deposition technique using cathodic arc evaporation method

A frequently observed feature in tribological testing of Diamond-Like Carbon films is the formation of transfer layer. The formation of carbonous transfer layer on the sliding surface was observed to reduce the friction coefficient [68].

DLC coatings are usually applied by means of Cathodic Arc Evaporation Physical Vapor Deposition technology. An arc can be defined as a discharge of electricity between two electrodes. The arc evaporation process begins with the striking of a high current, low voltage arc on the surface of a cathode that gives rise to a small (usually a few microns wide) highly energetic emitting area known as a cathode spot. The localised temperature at the cathode spot is extremely high (around 15000 °C), which results in a high velocity (10 km/s) jet of vaporised cathode material, leaving a crater behind on the cathode surface.

The plasma jet intensity is greatest normal to the surface of the cathode and contains a high level of ionization (30%-100%) multiply charged ions, neutral particles, clusters and macro-particles (droplets). The metal is evaporated by the arc in a single step, and ionized and accelerated within an electric field. Theoretically the arc is a self-sustaining discharge capable of sustaining large currents through electron emission from the cathode surface and the re-bombardment of the surface by positive ions under high vacuum conditions.

If a reactive gas is introduced during the evaporation process dissociation, ionization and excitation can occur during interaction with the ion flux and a compound film will be deposited. Without the influence of an applied magnetic field the cathode spot moves around randomly evaporating microscopic asperities and creating craters. However if the cathode spot stays at one of these evaporative points for too long it can eject a large amount of macro-particles or droplets as seen above. These droplets are detrimental to the performance of the coating as they are poorly adhered and can extend through the coating.

A recent tribological study carried out about the effect of deposition of Diamond-Like Carbon coatings on a substrate of Ti-6Al-4V for knee implants has confirmed that these types of coating improve the tribological response of substrate decreasing the coefficient of friction (μ) (Table 1) and reducing the wear of the surface (Figure 8) [69]. For this study fretting tests were performed using alumina balls as counter body, bovine serum as lubricant and a continuous temperature of 37 ºC, trying to simulate real environment.

Sample	μ ± SD (standard deviation)	Disc Wear Scar, Maximum Depth (μm)
Ti-6Al-4V	0.86 ± 0.08	10 ± 3
Ti-DLC	0.24 ± 0.01	Polishing Effect

Table 1. Friction coefficients values and ball and disc wear scars measurements

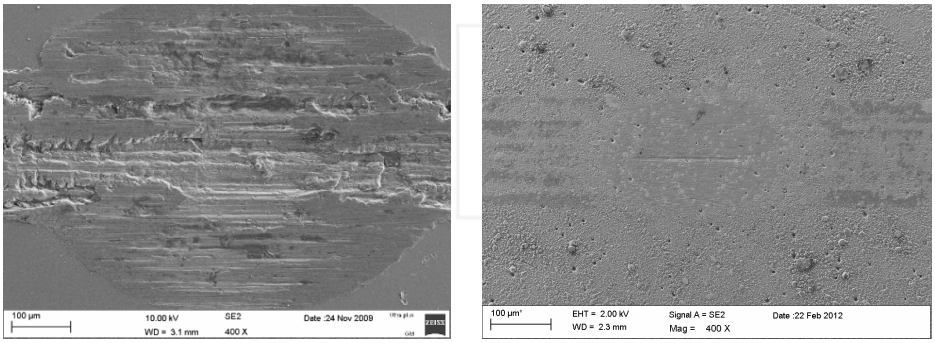

Figure 8. SEM micrographs of the fretting tests wear scars. Ti-6Al-4V (left), Ti-DLC (right)

3.4.2. Plasma electrolytic oxidation treatment

In biomedical application titanium is the most employed alloy due to its biocompatibility as an implant material, attributed to surface oxides spontaneously formed in air and/or physiological fluids [70]. Cellular behaviors, e.g. adhesion, morphologic change, functional alteration, proliferation and differentiation are greatly affected by surface properties, including composition, roughness, hydrophilicity, texture and morphology of the oxide on titanium [71] [72]. The natural oxide is thin (about 3–10nm in thickness [39]) amorphous and stoichiometrically defective. It is known that the protective and stable oxides on titanium surfaces are able to provide favorable osseointegration [73] [74]. The stability of the oxide depends strongly on the composition structure and thickness of the film [75].

On titanium and its alloys a thin oxide layer is formed naturally on the surface of titanium metal in exposure to air at room temperature [76] [77] [78]. Titania (TiO_2) exists in three polymorphic forms: rutile, anatase and brookite. Rutile, stable form of titania at ambient condition, possesses unique properties [79]. The metastable anatase and brookite phases convert to rutile upon heating. However, contact loads damage this thin native oxide film and cause galvanic and crevice corrosion as well as corrosion embrittlement. Moreover, the low wear resistance and high friction coefficient without applied protective coatings on the surface gravely limit its extensive applications. The most accepted technique for the surface modification of Ti alloys is oxidation. Anodizing produces anatase phase of titania that shows poor corrosion resistance in comparison with rutile phase. Recent developments in high voltage anodizing cause a crystalline rutile/anatase film at near to room temperature.

Attempts to improve surface properties of titanium and its alloys over the last few decades have led to development of Plasma Electrolytic Oxidation (PEO) technique by Kurze et al. [80] [81], which is a process to synthesize the ceramic-like oxide films at high voltages. This technique is based on the modification of the growing anodic film by spark/arc microdischarges in aqueous solutions (Figure 9), which are initiated at potentials above the breakdown voltage of the growing oxide film and move rapidly across the anode surface [53]. Since they rapidly develop and extinguish (within 10^{-4}-10^{-5} s), the discharges heat the metal substrate to less than 100-150 ºC. At the same time the local temperature and pressure inside the discharge channel can reach 10^{-3}-10^{-4} K and 10^{-2}-10^{-3} MPa, respectively, which is high enough to give rise to plasma thermo-chemical interactions between the substrate and the electrolyte. These interactions result in the formation of melt-quenched high-temperature oxides and complex compounds on the surface, composed of oxides of both the substrate material and electrolyte-borne modifying elements. The result is a porous oxide coating.

The PEO coating shows a significantly higher thickness (18 μm ± 4 μm) than PVD coatings and also a different morphology. The external part of the layer is porous (with pore diameter ranging from 3 to 8 μm) (Figure 10). The coating becomes increasingly compact on going towards the interface with the substrate. This kind of morphology leads to a relatively high surface roughness.

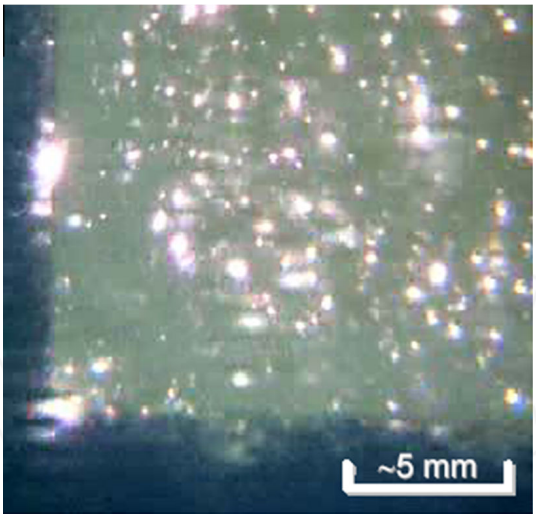

Figure 9. Photography of the arc micro-discharges in PEO process

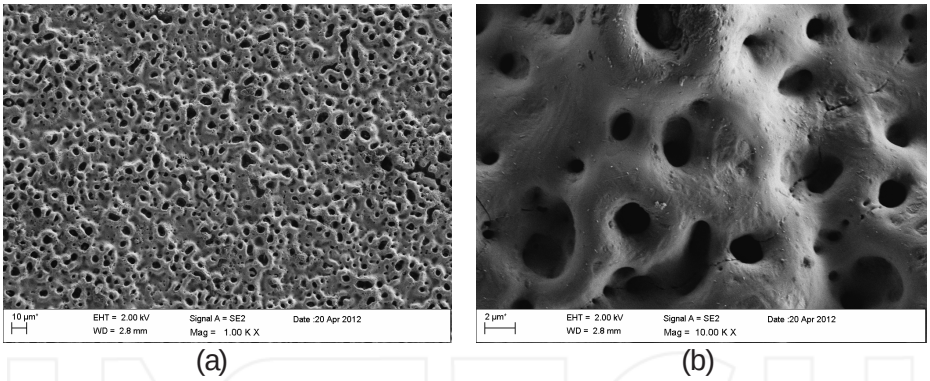

Figure 10. SEM micrographs of porosity of the external layer in PEO treatment. a) overview and b) detail

This method is characterized by the titanium surface, at near-to-ambient bulk temperature, into the high temperature titanium oxide (rutile) modified by other oxide constituents. Economic efficiency, ecological friendliness, corrosion resistance, high hardness, good wear resistance, and excellent bonding strength with the substrate are the other characteristics of this treatment [82] [83] [84].

The main conversion products formed by the PEO treatment are titanium oxides: rutile and anatase, typical anodic oxidation products of titanium. The structure and composition of anodic oxide films are known to be strongly dependent on film formation temperature and potential [85] [86]. In the case of PEO coatings, both the electrolyte composition and the current

density regime have an influence on the phase composition and morphology of the anodic oxide layer [87]. A higher spark voltage causes a higher level of discharge energy, which provides a larger pore [88].

The influence of electrolyte characteristics on the phase composition of PEO films on titanium has previously been studied [89] [90]. It has been shown that surface layers composed of rutile, anatase, rutile/anatase, as well as oxides of electrolyte elements (e.g. Al_2O_3, MgO, WO_3), their hydroxides and complex oxides (e.g. Al_2TiO_5, $AlPO_4$, $CaWO_4$, $BaTiO_3$, $MnTiO_3$, etc.) can be produced.

Surfaces containing Ca and/or P induce osteoinduction of new bones and become bioactive. Ca and P ions can be incorporated into the layer, controlling the electrolyte employed during the electro oxidation process, and they further transform it into hydroxyapatite by a hydrothermal treatment [41].

One technique that could show the effect of the electrolyte in the chemical composition of the coating could be the EDS (Energy Dispersive Spectroscopy) technique. In the following graphs a comparative study can be observed. The results of different samples, uncoated cp Ti, a coating obtained with a commercial electrolyte and a coating prepared in an aqueous electrolyte containing calcium phosphate and β-glycerophosphate, are showed in the following spectrums. The Ca- and P-containing titania coatings produced by PEO improve the bioactivity of the titanium-constructed orthopedic implant [91]. In Figure 11, in spectrum b) and c) can be observed the difference in the calcium quantity presented into the coating.

The biological response to titanium depends on the surface chemical composition and the ability of titanium oxides to absorb molecules and incorporate elements [92]. Surface topography plays a fundamental role in regulating cell behaviour, e.g. the shape, orientation and adhesion of cells [93] [94]. As a surface begins to contact with biological tissues, water molecules first reach the surface. Hence, surface wettability, initially, may play a major role in adsorption of proteins onto the surface, as well as cell adhesion. Cell adhesion is generally better on hydrophilic surfaces. It is known that changes in the physicochemical properties, which influence the hydrophilicity of Ti dioxide, will modulate the protein adsorption and further cell attachment [39]. By anodic oxidation, elements such as Ca and P can be imported into the surface oxide on titanium and the micro-topography can be varied through regulating electrolyte and electrochemical conditions. The presence of Ca-ions has been reported to be advantageous to cell growth, and "in vivo" data show implant surfaces containing both Ca and P enhance bone apposition on the implant surface.

Some experiments carried out to study the tribological behaviour of the PEO-treated Ti-6Al-4V by means of dry sliding tests against PS (plasma sprayed) Al_2O_3–TiO_2 and compared with that of thin PVD coatings showed that the best tribological behavior, both in terms of low coefficient of friction and high wear resistance (i.e. low wear damage) was displayed by the PEO treated samples. The highest wear resistance was displayed by the PEO-treated samples, with negligible wear loss even under the highest applied load of 35 N. This good tribological behavior should be mainly related to the superior thickness of this coating that can better support the applied load.

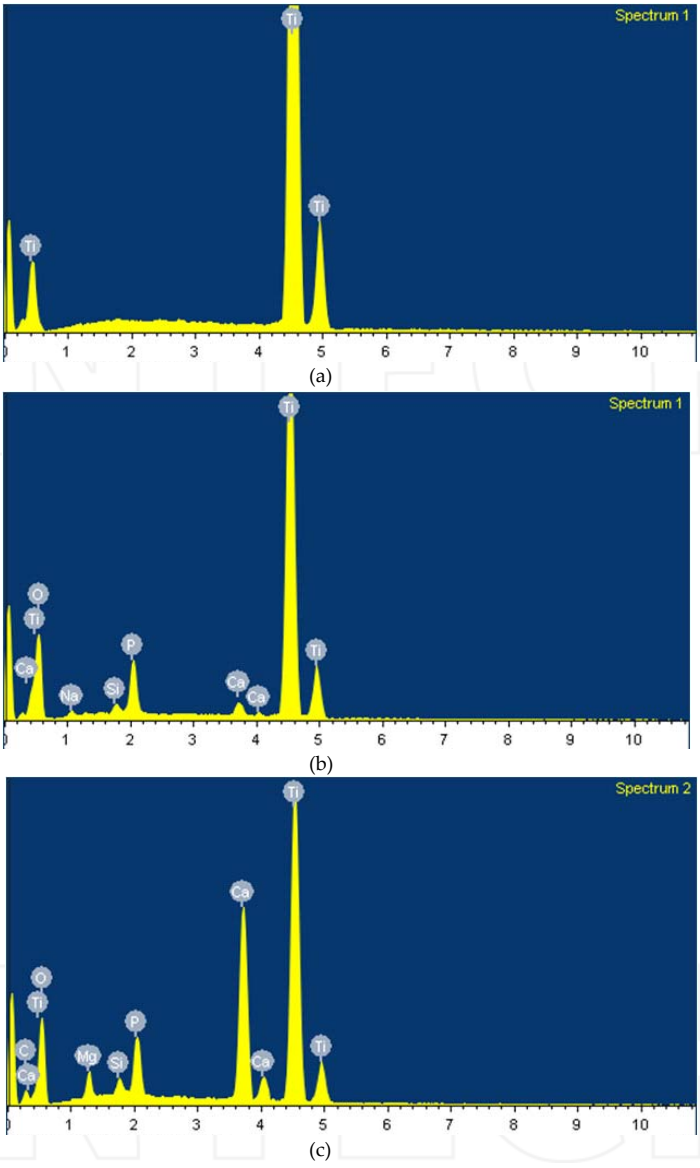

Figure 11. a) Microchemical analysis of cp Ti, b) microchemical analysis of coating prepared with commercial electrolyte, c) microchemical analysis of coating prepared with calcium phosphate and β-glycerophosphate electrolyte.

The PEO treatment leads to a very good tribological behavior, significantly reducing both wear and friction of the Ti-6Al-4V alloy, even under high applied loads (up to 35 N). This good tribological behaviour should be mainly related to the superior thickness of this coating, which

can better support the applied load. The main wear mechanism is micro-polishing and the coating thickness dictates its tribological life [95].

Last studies carried out have concluded that the PEO surface treatments enhance the biological response "in vitro", promoting early osteoblast adhesion, and the osseointegrative properties "in vivo", accelerating the primary osteogenic response, as they confirmed by the more extensive bone-implant contact reached after 2 weeks of study [94].

4. Conclusions

Titanium and its alloys are considered to be among the most promising engineering materials across a range of application sectors. Due to a unique combination of high strength-to-weight ratio, melting temperature and corrosion resistance, interest in the application of titanium alloys to mechanical and tribological components is growing rapidly in a wide range of industries, especially in biomedical field, also due to their excellent biocompatibility and good osseointegration. In such application, components made from Ti-alloys are often in tribological contact with different materials (metals, polymers or ceramics) and media, under stationary or dynamic loading and at various temperatures. These contact loads can cause damage of the thin native oxide film which passivates the titanium surface; and the metal can undergo intensive interactions with the counterface material and/or the surrounding environment. These interactions can generate various adverse effects on titanium components, such as high friction or even seizure (galvanic and crevice corrosion) as well as corrosion embrittlement, which lead to the premature failure of the implanted systems. The development of new specialized surface modification techniques for titanium and its alloys is therefore an increasingly critical requirement in order to control or prevent these effects and improve osseointegration, hence extending the lifetime of the implant.

Physical Vapour Deposition (PVD) technique allows develop Diamond-Like Carbon coatings that can be doped with different elements as titanium, tantalum, silver… which are biocompatible and increase the corrosion and wear resistance of the substrate, diminishing friction coefficient.

Plasma Electrolytic Oxidation (PEO) technique provides a possibility for the variation of composition and structure of the surface oxide film and attracts special interest for the corrosion protection and the optimization of friction and wear of titanium alloys as well as enhance the osseointegration.

Acknowledgements

The authors acknowledge financial support from the Spanish Ministry of Science and Innovation obtained in the project: CSD2008-00023 FUNCOAT (in the frame of the CONSOLIDER INGENIO-2010 program) and from the Basque Government.

Author details

Virginia Sáenz de Viteri* and Elena Fuentes

*Address all correspondence to: virginia.saenzdeviteri@tekniker.es

IK-Tekniker, Eibar, Spain

References

[1] Korkusuz, P. & Korkusuz, F. Hard Tissue – Biomaterial Interactions. In: Michael J. Yaszemski; Debra J. Trantolo; Kai-Uwe Lewandrowski; Vasif Hasirci, David E. Altobelli & Donald L. Wise. (ed.) Biomaterials in Orthopedics. United States of America: Marcel Dekker, Inc.; 2004. p1-40.

[2] Santavirta, S., Gristina, A. & Konttinen, YT. Cemented versus cementless hip arthroplasty: a review of prosthetic biocompatibility. Acta Orthopaedica Scandinavica 1992;63 225-232.

[3] Park, J.B. & Bronzino, L.D., (ed.) Biomaterials: principles and applications. Boca Raton, Florida: CC Press; 2003 p. 1-241.

[4] Ramakrishna, S., Mayer, J., Wintermantel, E. & Leong K. W. Biomedical applications of polymer-composite materials: A review. Composites Science and Technology 2001;61(9) 1189-1224.

[5] Wise, D.L. Biomaterials engineering and devices. Berlin: Human Press; 2000.

[6] Kurtz, S., Ong, K., Jau, E., Mowat, F. & Halpern, M. Projections of primary and revision hip and knee arthroplasty in the United States from 2005 to 2030. Journal of Bone and Joint Surgery – American Volume 2007;89 780-785.

[7] Geetha, M., Singh, A.K., Asokamani, R. & Gogia, A.K. Ti based biomaterials, the ultimate choice for orthopaedic implants- A review. Progress in Material Science 2009;54 397-425.

[8] Long, M. & Rack. H.J. Titanium alloys in total joint replacement – A materials science perspective. Biomaterials 1998;19 1621-1639.

[9] Wang, K. The use of titanium for medical applications in the USA. Materials Science and Engineering A - Structural Materials Properties Microstructure and Processing 1996;213 134-137.

[10] http://azom.com/article.aspx?ArticleID=108

[11] Williams, D.F. On the mechanisms of biocompatibility. Biomaterial 2008;29(20) 1941-2953.

[12] Heimke, G. & Stock, D. Clinical application of ceramic osseo – or soft tissue - integrated implant. Orthopedic Ceramic Implants 1984;4 1-19.

[13] Black, J. & Hastings G.W. Handbook of biomaterials properties. London UK: Chapman and Hall; 1998.

[14] Lawrence Katz, J. Anisotropy of Young´s modulus of bone. Nature 1980;283 106-107.

[15] Viceconti, M., Muccini, R., Bernakiewicz, M., Baleani M. & Cristofolini, L. Large-sliding contact elements accurately predict levels of bone-implant micromotion relevant to osseointegration. Journal of Biomechanics 2000;33 1611-1618.

[16] Wennerberg, A. On surface roughness and implant incorporation. Göteborg. Sweden: Biomaterials/Handicap Research; Institute of Surgical Sciences, Göteborgs Universitet, 1996.

[17] Calrsson, L.V., Macdonald, W., Magnus Jacobsson, C. &. Albrektsson T. Osseointegration Principles in Orthopedics: Basic Research and Clinical Applications. In: Michael J. Yaszemski; Debra J. Trantolo; Kai-Uwe Lewandrowski; Vasif Hasirci, David E. Altobelli & Donald L. Wise. (ed.) Biomaterials in Orthopedics. United States of America: Marcel Dekker, Inc.; 2004 p223-240.

[18] Junker, R., Dimakis, A., Thoneick, M. &. Jansen, J.A. Effects of implant surface coatings and composition on bone integration: a systematic review. Clinical Oral Implants Research 2009;20 185-206.

[19] Kim, H.J., Kim, S.H., Kim, M.S., LeeJ, E.J., Oh, H.G., Oh, W.M., et al. Varying Ti-6Al-4V surface roughness induces different early morphologic and molecular responses in MG63 osteoblast-like cells. Journal of Biomedical Materials Research 2005,74A 366-373.

[20] Vlacic-Zischke, J., Hamlet, S.M., Friis, T., Tonetti, M.S. & Ivanovski, S. The influence of surface microroughness and hydrophilicity of titanium on the up-regulation of TGFb/BMP signalling in osteoblasts. Biomaterials 2011;32 665-671.

[21] http://360oandp.com/Technology-Osseointegration.aspx

[22] Montanaro, L., Campoccia, D. & Arciola, C.R. Nanostructured materials for inhibition of bacterial adhesion in orthopedic implants: a minireview. International Journal of Artificial Organs 2008;31 771-776.

[23] Black. J. Othopaedic Biomaterials in Research and Practice. New York: Churchill Livingstone; 1988.

[24] Jacobs, J.J., Gilbert, J.L. & Urban, R.M. Corrosion of metal orthopaedic implants. Journal of Bone and Joint Surgery – American Volume 1998;80 268-282.

[25] Hallab, N.J., Urban, R. M. & Jacobs, J.J. (2004). Corrosion and Biocompatibility of Orthopedic Implants, In: Michael J. Yaszemski; Debra J. Trantolo; Kai-Uwe Lewan-

drowski; Vasif Hasirci, David E. Altobelli & Donald L. Wise. (ed.) Biomaterials in Orthopedics. United States of America: Marcel Dekker, Inc.; 2004 p63-92.

[26] Liu, X., Chu, P.K. & Ding C. (2004). Surface modification of titanium, titanium alloys, and related materials for biomedical applications. Mater Sci Eng, Vo. R 47, (2004), pp. 49-121.

[27] Stadlinger, B., Ferguson, S.J., Eckelt, U., Mai, R., Lode, A.T., Loukota, R. & Sclotting F. Biomechanical evaluation of a titanium implant surface conditioned by a hydroxide ion solution. British Journal of Oral & Maxillofacial Surgery 2012;50 74-79.

[28] Subramani, K. & Mathew, R.T. Titanium Surface Modification. Techniques for Dental Implants – From Microscale to Nanoscale. Emerging Nanotechnologies in Dentistry. DOI: 10.1016/B978-1-4557-7862-1.00006-7.

[29] http://hss.edu/conditions_arthritis-of-the-knee-total-knee-replacement.asp

[30] Fraczek, T., Olejnik, M. & Tokarz, A. Evaluations of plasma nitriding efficiency of titanium alloys for medical applications. Metalurgija 2009;48(2) 83-86.

[31] Kustas, F.M. & Misra, M.S. Friction and Wear of Titanium Alloys, In: Scott D. Henry (ed.) Volume 18, Friction, Lubrication and Wear Technology. United States of America: ASM International; 1992. p. 1585-1598.

[32] Freese, H., Volas, M.G. & Wood, J.R. (2001). In: Brunette D.M., Tengvall P., Textor M., Thomsen P. (eds.) Titanium in Medicine. Springer: Berlin; 2001. p25-51.

[33] Yerokhin, A.L., Niea, X., Leyland, A. & Matthews, A. Characterization of oxide films produced by plasma electrolytic oxidation of a Ti–6Al–4V alloy. Surface & Coating Technology 2000;130 195–206.

[34] Malchau, H. & Herberts, P. Revision and re-revision rate in THR: a revision-risk study of 148,359 primary operations. Scientific exhibition, 65th annual meeting of the AAOS, New-Orleans, 1998.

[35] Chandra, A., Ryu, J.J., Karra, P., Shrotriya, P., Tvergaard,V., Gaisser, M. & Weik, T. Life expectancy of modular Ti6Al4V hip implants: Influence of stress and environment. Journal of the Mechanical Behavior of Biomedical Materials 2011;4 1990-2001.

[36] Wolford, L.M. Factors to consider in joint prosthesis systems, Proceedings (Baylor University Medical Center) 2006;19 232-238.

[37] Zabinski, J.S. & Voevodin, A.A. Ceramic and other hard coatings, In: Joze Vizintin, Mitjan Kalin, Kuniaki Dohda & Said Jahanmir (eds) Trybology of Mechanical Systems: A Guide to Present and Future Technologies. United States of America: ASME Press; 2004 p157-182.

[38] Landolt, D. Corrosion and Surface Chemistry of Metals. Lausanne Switzerland: EPFL Press; 2007.

[39] Neoh, K.G., Hu, X., Zheng, D. & Tang Kang, E. Balancing osteoblast functions and bacterial adhesion on functionalized titanium surfaces. Biomaterials 2012;33 2813-2822.

[40] Zhu, X., Chen, J., Scheideler, L., R. Reichl, R. & Geis-Gerstorfer, J. Effects of topography and composition of titanium surface oxides on osteoblast responses. Biomaterials 2004;25 4087-4103.

[41] Liu, F., Wang, F., Shimizu, T., Igarashi, K. & Zhao, L. (2005). Formation of hydroxyapatite on Ti-6Al-4V alloy by microarc oxidation and hydrothermal treatment. Surface & Coatings Technology 2005;199 220-224.

[42] Kokubo, T., Kim, H-M., Miyaji, F. & Nakamura, T. Preparation of bioactive Ti and its alloys via simple chemical surface treatment. Journal of Biomedical Materials Research 1996;32 409-417.

[43] Carapeto, A.P., Serro, A.P., Nunes, B.M.F., Martins, M.C.L., Todorovic, S., Duarte, M.T., André, V., Colaço, R. & Saramago, B. Characterization of two DLC coatings for joint prosthesis: The role of albumin on the tribological behavior. Surface & Coatings Technology 2010;204 3451-3458.

[44] Ma, G., Gong, S., Lin, G., Zhang, L. & Sun, G. A study of structure and properties of Ti-doped DLC film by reactive magnetron sputtering with ion implantation. Applied Surface Science 2012;258 3045-3050.

[45] Dowling, D.P. Evaluation of diamond-like carbon coated orthopedic implants. Diamond and Related Materials 1997;6 390-393.

[46] Zhang, L., Lv, P., Huang, Z.Y., Lin, S.P., Chen, D.H., Pan, S.R. & Chen, M. Blood compatibility of La_2O_3 doped diamond-like carbon films. Diamond and Related Materials 2008;17 1922-1926.

[47] Zheng, Y., Liu, D., Liu, X. & Li, L. Ti-TiC-TiC/DLC gradient nano-composite film on a biomedical NiTi alloy. Biomedical Materials 2008;3 044103-044109.

[48] Han, Y., Hong, S.H. & Xu, K.W. Porous nanocrystalline titania films by plasma electrolytic oxidation. Surface & Coatings Technology 2002;154 314–318.

[49] Huang, P., Wang, F., Xu, K. & Han, Y. Mechanical properties of titania prepared by plasma electrolytic oxidation at different voltages. Surface & Coatings Technology 2007; 201 5168–5171.

[50] Lange, R., Lüthen, F., Beck, U., Rychly, J., Baumann, A. & Nebe, B. Cell-extracellular matrix interaction and physic-chemical characteristics of titanium surfaces depend on the roughness of the material. Biomolecular Engineering 2002;19 255-261.

[51] Huang, P., Xu, K-W. & Han, Y. Preparation and apatite layer formation of plasma electrolytic oxidation film on titanium for biomedical application. Materials Letters 2005;59 185-189.

[52] Cigada, A., Cabrini, M. & Pedferri, P. Increase of the corrosion resistance of Ti6Al4V alloy by high thickness anodic oxidation. Journal of Materials Science – Materials in Medicine 1992;3 408-412.

[53] Yerokhin, A.L., Nie, X., Leyland, A., Matthews, A. & Dowey, S.J. Surface & Coatings Technology 1999;116.

[54] Nanci, A., Wuest, J.D., Peru, L., Brunet, P., Sharma, V., Zalzal, S. & McKee, M.D. Chemical modification of titanium surfaces for covalent attachment of biological molecules. J Biomed Mater, Vol. 40, (1998), pp. 237-242.

[55] Viorney, C., Guenther, H.L., Aronsson, B.O., Pechy, P., Descouts, P. & Gratzel, M. (2002). Osteoblast culture on polished titanium disks modified with phosphoric acids. Journal of Biomedical Materials Research 2002;62 149-155.

[56] Sul, Y.T., Johansson, C.B., Kang, Y., Jeon, D.G., Kang, Y., Jeong, D.G. & Albrektsson, T. Bone reaction to oxidized titanium implants with electrochemical anion sulphuric acid and phosphoric acid incorporation. Clinical Implant Dentistry and Related Research 2002;4 78-87.

[57] Cook, S.D., Thomas, K.A., Kay, J.F. & Jarcho, M. Hydroxyapatite-coated porous titanium for use as an orthopedic biologic attachment system. Clinical Orthopaedic and Related Research 1988;230 303-312.

[58] Rashmir- Raven, M.A., Richardson, D.C., Aberman, H.M. & DeYoung, D.J. The response of cancellous and cortical canine bone to hydroxyapatite-coated and uncoated titanium rods. Journal of Applied Biomaterials 1995;6 237-242.

[59] Holmberg, K. & Matthews, A. Coatings Tribology – Properties, Techniques and Applications in Surface Engineering. Amsterdam, The Netherlands: Elsevier; 1994.

[60] Grill, A. Wear 1993;168(1-2) 143.

[61] Grill, A. Surface & Coatings Technology 1997;94-95(1-3) 507.

[62] Erdemir, A. & Donnet, C. Trybology of diamond, diamond-like carbon, and related films. In: B. Bhushan (ed.) Handbook of Modern Tribology, Vol. 2. Materials Coatings. Boca Raton, Florida: CRC Press; 2001.

[63] Donnet, C., Belin, M., Augé, J.C., Martin, J.M., Grill, A. & Patel, V. Surface & Coatings Technology 1994;68-69 626.

[64] Erdemir, A., Erylmaz, O.L. & Fenske, G. (2000). Journal of Vacuum Science of Technology A – Vacuum Surfaces and Films 2000;18(4) 1987.

[65] Fontaine, J., Donnet, C. & Erdemir, A. Fundamentals of the Tribology of DLC Coatings. In: Christophe Donnet & Ali Erdemir (ed.) Tribology of Diamond-Like Carbon Films. USA: Springer; 2008. p139-154.

[66] Donnet, C. & Erdemir, A. Diamond-like Carbon Films: A Historical Overview. In: Christophe Donnet & Ali Erdemir (ed.) Tribology of Diamond-Like Carbon Films. USA: Springer; 2008. p1-12.

[67] Hauert, R., Knoblauch-Meyer, L., Francz, G., Schroeder, A. & Wintermantel, E. Surface & Coatings Technology 1999;120-121 291-296.

[68] Ronkainen, H. & Holmberg, K. Environmental and Thermal Effects on the Tribological Performance of DLC Coatings. In: Christophe Donnet & Ali Erdemir (ed.) Tribology of Diamond-Like Carbon Films. USA: Springer; 2008. p155-200.

[69] Sáenz de Viteri, V., Barandika, M.G., Ruiz de Gopegui, U., Bayón, R., Zubizarreta, C., Fernández, X., Igartua, A. & Agullo-Rueda, F. Characterization of Ti-C-N coatings deposited on Ti6Al4V for biomedical applications. Journal of Inorganic Biochemistry 2012;117 359-366.

[70] Williams, D.F. Titanium and titanium alloys. In: Williams DF (ed.) Biocompatibility of clinical implant materials, Vol. I. Boca Raton, Florida: CRC Press, Inc; 1981. p. 9-44

[71] Lampin, M., Warocquier-Clerout, R., Legris, C., Degrange, M. & Sigot-Luizard, M.F. Correlation between substratum roughness and wettability, cell adhesion, and cell migration. Journal of Biomedical Materials Research 1997;36 99-108.

[72] Lim, Y.J., Oshida, Y., Andres, C.J. & Barco, M.T. Surface characterization of variously treated titanium materials. International Journal of Oral & Maxillofacial Implants 2001;16 333–342.

[73] Keller, J.C., Stanford, C.M., Wightman, J.P., Draughn, R.A. & Zaharias, R. Characterization of titanium implant surfaces. III. Journal of Biomedical Materials Research 1994;28 939–946.

[74] Kieswetter, K., Schwartz, Z., Dean, D.D. & Boyan, B.D. The role of implant surface characteristic in the healing of bone. Critical Reviews in Oral Biology & Medicine 1996;7 329–345.

[75] Pouilleau, J., Devilliers, D., Garrido, F., Durand-Vidal, S. & Mahe, E. Structure and composition of passive titanium oxide films. Materials Science and Engineering 1997;B47 235–243.

[76] Fei, C., Hai, Z., Chen, C. & Yangjian, X. Study on the tribological performance of ceramic coatings on titanium alloy surfaces obtained through microarc oxidation. Progress in Organic Coatings 2009;64 264–267.

[77] Kuromoto, N.K., Simão, R.A. & Soares, G.A. Titanium oxide films produced on commercially pure titanium by anodic oxidation with different voltages. Materials Characterization 2007;58 114–121.

[78] Wanga, Y., Jiang, B., Lei, T. & Guo, L. Dependence of growth features of microarc oxidation coatings of titanium alloy on control modes of alternate pulse. Materials Letters 2004;58 1907–1911.

[79] Han, Y., Hong, S. & Xu, K. Synthesis of nanocrystalline titania films by micro-arc oxidation. Materials Letters 2002;56 744–747.

[80] Kurze, P., Krysman, W., Dittrich, K.H. & Schneider, H.G. Process characteristics and parameters of anodic oxidation by spark deposition (ANOF). Crystal Research and Technology 1984;19 973–979.

[81] Kurze, P., Dittrich, K.H., Krysman, W. & Schneider, H.G. Structure and properties of ANOF layers. Crystal Research and Technology 1984;19 93–99.

[82] Han, I., Choi, J.H., Zhao, B.H., Baik, H.K. & Lee, I. Micro-arc oxidation in various concentration of KOH and structural change by different cut off potential. Current Applied Physics 2007;7S1 23–27.

[83] Matykina, E., Berkani, A., Skeldon, P. & Thompson, G.E. Real-time imaging of coating growth during plasma electrolytic oxidation of titanium. Electrochimica Acta 2007;53 1987–1994.

[84] Wang, Y., Lei, T., Jiang, B. & Guo, L. Growth, microstructure and mechanical properties of microarc oxidation coatings on titanium alloy in phosphate-containing solution. Applied Surface Science 2004;233 258–267.

[85] Shibata, T. & Zhu, Y. C., Corrosion Science 1995;37(1) 133–144.

[86] Shibata, T. & Zhu, Y. C., Corrosion Science 1995;37(2) 253–270.

[87] Yerokhin, A.L., Nie, X., Leyland, A., Matthews, A. & Dowey, S.J. (1999). Surface & Coatings Technolog 1999;122 73–93.

[88] Shokouhfar, M., Dehghanian, C., Montazeri, M. & Baradaran, A. Preparation of ceramic coating on Ti substrate by plasma electrolytic oxidation in different electrolytes and evaluation of its corrosion resistance: Part II. Applied Surface Science 2012;258 2416-2423.

[89] Amin, M.S., Randeniya, L.K., Bendavid, A., Martin, P.J. & Preston, E.W. Amorphous carbonated apatite formation on diamond-like carbon containing titanium oxide. Diamond and Related Materials 2009;18 1139-1144.

[90] Yang, B., Uchida, M., Kim, H-M., Zhang, X. & Kokubo, T. Preparation of bioactive titanium metal via anodic oxidation treatment. Biomaterials 2004;25 1003-1010.

[91] Han, Y., Sun, J. & Huang, X. Formation mechanism of HA-based coatings by microarc oxidation. Electrochemistry Communications 2008;10 510-513.

[92] Letic-Gavrilovic, A., Scandurra, R. & Abe, K. Genetic potential of interfacial guided osteogenesis in implant devices. Dental Materials Journal 2000;19 99–132.

[93] Eriksson, C., Lausmaa, J. & Nygren, H. Interactions between human whole blood and modified TiO2-surfaces: influence of surface topography and oxide thickness on leukocyte adhesion and activation. Biomaterials 2001;22 1987–1996.

[94] Ravanetti, F., Borghetti, P., De Angelis, E., Chiesa, R., Martini, F.M., Gabbi, C. & Cacchioli, A. (2010). In vitro cellular response and in vivo primary osteointegration of electrochemically modified titanium. Acta Biomaterialia 2010;6 1014-1024.

[95] Ceschini, L., Lanzoni, E., Martini, C., Prandstraller, D. & Sambogna, G. Comparison of dry sliding friction and wear of Ti6Al4V alloys treated by plasma electrolytic oxidation and PVD coating. Wear 2008;26 86-95.

INTECH


eman ta zabal zazu
Universidad del País Vasco
Euskal Herriko Unibertsitatea


ZTF-FCT


IK4 TEKNIKER
Research Alliance